Computational Predictions of Conjugated Polymer Properties for Photovoltaic Applications

Hedström, Svante

2015

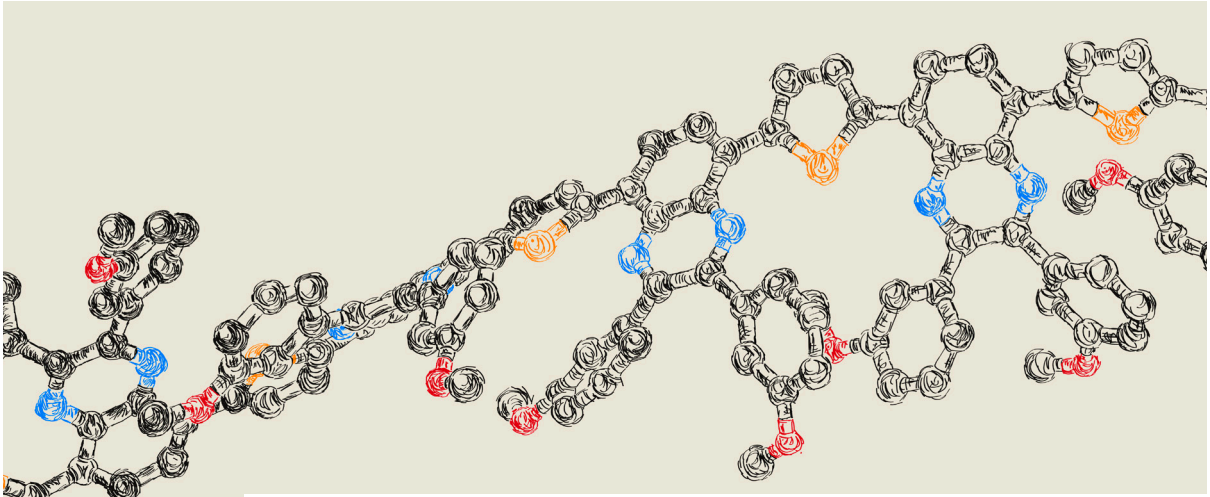

Computational Predictions of Conjugated Polymer Properties for Photovoltaic Applications

SVANTE HEDSTRÖM | DIVISION OF THEORETICAL CHEMISTRY | LUND UNIVERSITY

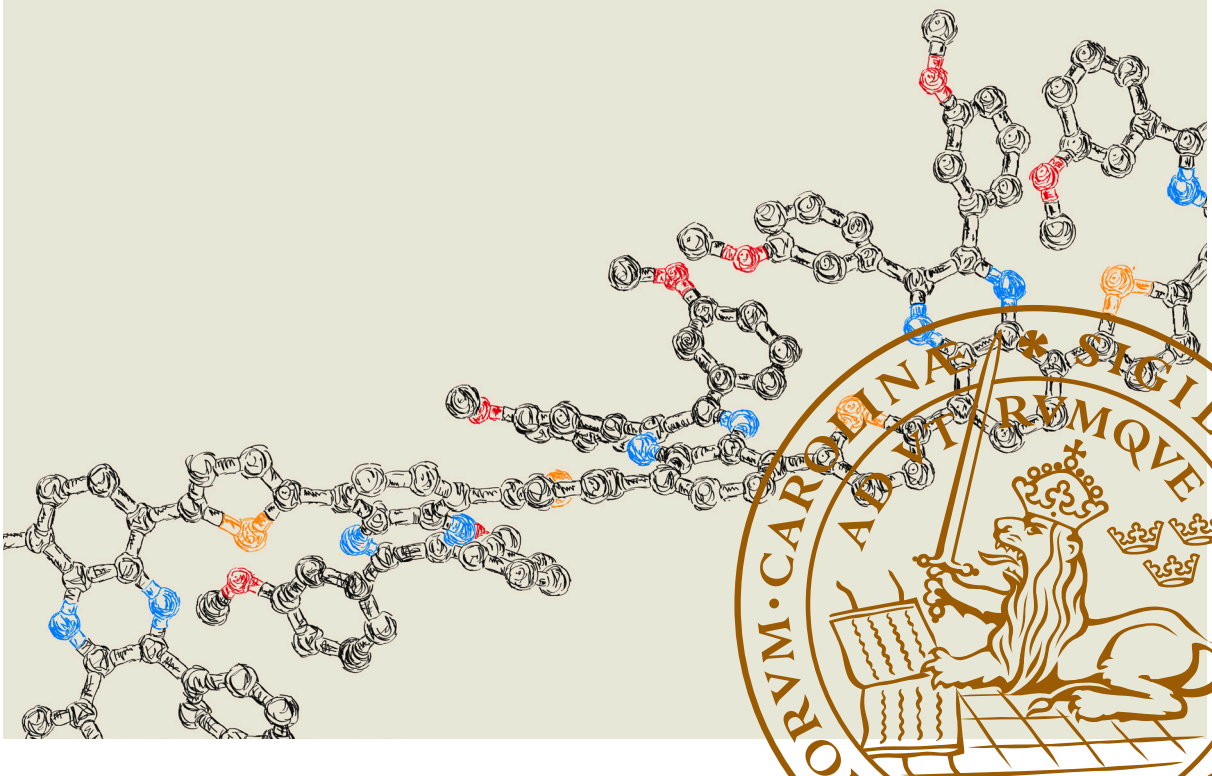

Computational Predictions of Conjugated Polymer Properties for Photovoltaic Applications

Svante Hedström

LUND
UNIVERSITY

DOCTORAL THESIS
by due permission of the Faculty of Science, Lund University, Sweden.
To be defended at 13:15, 2015-09-11,
in Hall B, Chemistry Center, Getingevägen 60, Lund.

Faculty opponent

Leif A. Eriksson, University of Gothenburg

Grading committee

Mathieu Linares, Linköping University; Ellen Moons, Karlstad University;
Michael Odelius, Stockholm University

Front cover: Artistic representation of two strands of the TQ1 polymer with truncated alkyl side-chains and with hydrogen atoms not shown.

Back cover: Artistic representation of the $PC_{61}BM$ molecule with hydrogen atoms not shown.

Doctoral thesis: "Computational Predictions of Conjugated Polymer Properties for Photovoltaic Applications"

Division of Theoretical Chemistry
Lund University
P. O. Box 124
S-221 00 Lund
Sweden
svante.hedstrom@teokem.lu.se

Department of Chemistry, Faculty of Science
Lund University
ISBN: 978-91-7422-405-4

Printed in Sweden by Media-Tryck, Lund University
Lund 2015

Organization:	Document name: Doctoral dissertation
LUND UNIVERSITY P. O. Box 124 S-221 00 Lund Sweden	Date of issue: 2015-06-10
Author: Svante Hedström	Sponsoring organization

Title: Computational Predictions of Conjugated Polymer Properties for Photovoltaic Applications

Abstract:

Organic solar cells employing fullerenes blended with conjugated polymers as the main light-absorbing material have achieved power conversion efficiencies exceeding 10%. They hold promise as an alternative energy source with many advantages in terms of long-term sustainability and reduced greenhouse gas emissions. Detailed information on the electronic and geometric structure of the molecules involved is generally not accessible through experimental means, as the typically amorphous polymer films are not readily studied with *e.g.* X-ray crystallography. Computational chemistry, and in particular quantum chemistry as used for the research presented in this thesis, can however provide molecular level insight into the properties of these conjugated polymers. (Time-dependent) density functional theory calculations are here employed on various polymers, mainly of donor–acceptor (D–A) and D–A_1–D–A_2 types. Systematic studies demonstrate how the energy levels and optical properties relate to each other, as well as to the chemical composition of the polymers. In particular focus are the traits that are important for efficient solar cells: strong absorption, suitably narrow band gap, appropriate LUMO energy *vs*. the fullerene LUMO, and extended conjugation promoting high charge carrier mobilities. Several polymers with high-performance solar cells are studied, including TQ1 where a computationally revealed unique helical geometry is used to partially rationalize its 7.08% efficiency, and the D–A_1–D–A_2 polymer P3TQTIF whose two distinct acceptor units allow two strong low-energy electronic transitions, greatly enhancing its spectral coverage. Size-converged optical properties are obtained through a scheme based on extrapolations from oligomer calculations, and a detailed comparison to experiments has facilitated the development of an empirical correction for absorption energies and strengths. These corrections are subsequently used for *a priori* predictions of polymer absorption spectra with good agreement to experiments. Finally, a strategy is presented that includes the effect of temperature, in form of thermally populated conformations with reduced conjugation and weaker and blue-shifted absorption, yielding trends in excellent agreement with experimental optical properties. Calculations are in summary able to provide deeper insights into the fundamental properties of conjugated polymers, constituting a valuable tool for the ongoing development of materials for application in high-performance organic solar cells.

Keywords:
Conjugated polymers, density functional theory, organic photovoltaics, light-harvesting capabilities, quantum chemistry, absorption spectra, electronic structure, computational predictions

Classification system and/or index terms (if any)

Supplementary bibliographical information		Language: English
ISSN and key title		ISBN: 978-91-7422-405-4
Recipient's notes	Number of pages: 216	Price
	Security classification	

List of Publications

This compilation thesis is based on the following research articles, which are found in the end of the thesis. They are referred to by their roman numerals I–VII.

I. **Light-Harvesting Capabilities of Donor–Acceptor Polymers**
S. Hedström, P. Henriksson, E. Wang, M. R. Andersson, P. Persson,
Phys. Chem. Chem. Phys. **2014**, *16*, 24853–24865.

II. **Defining Donor and Acceptor Strength in Conjugated Copolymers**
S. Hedström, E. Wang, P. Persson,
Mol. Phys. **2015**, *Submitted*.

III. **Quantum Chemical Calculations of Side-Group Stacking and Electronic Properties in Thiophene–Quinoxaline Polymers**
S. Hedström, P. Persson,
J. Phys. Chem. C **2012**, *116*, 26700–26706.

IV. **Conformation Sensitive Charge Transport in Conjugated Polymers**
L. M. Andersson, S. Hedström, P. Persson,
Appl. Phys. Lett. **2013**, *103*, 213303.

V. **Temperature-Dependent Optical Properties of Flexible Donor–Acceptor Polymers**
S. Hedström, P. Henriksson, E. Wang, M. R. Andersson, P. Persson,
J. Phys. Chem. C **2015**, *119,* 6453–6463.

VI. **Rational Design of D–A_1–D–A_2 Polymers with Superior Spectral Coverage**
S. Hedström, Q. Tao, E. Wang, P. Persson,
Phys. Chem. Chem. Phys. **2015**, *Submitted.*

VII. **D–A_1–D–A_2 Copolymers with Extended Donor Segments for Efficient Polymer Solar Cells**
Q. Tao, Y. Xia, X. Xiaofeng, S. Hedström, O. Bäcke, D. I. James, P. Persson, E. Olsson, O. Inganäs, L. Hou, W. Zhu, E. Wang,
Macromolecules **2015**, *48*, 1009–1016.

List of article contributions

I. I designed the study together with M. R. A., P. P., and P.H. I performed all calculations. I had the main responsibility of data analysis and writing of the manuscript.

II. I designed and performed the study. I had the main responsibility of data analysis and writing of the manuscript.

III. I designed the study together with P. P. I performed all calculations. I had the main responsibility of data analysis and writing of the manuscript.

IV. I performed all calculations. I had the main responsibility of analyzing the computational results, and writing the computational parts of the manuscript. I had only minor involvement in the experimental parts of the manuscript.

V. I designed the study together with P. P. I performed all calculations. I had the main responsibility of data analysis and writing of the manuscript.

VI. I designed the study together with P. P. I performed all calculations. I had the main responsibility of data analysis and writing of the manuscript.

VII. I performed all calculations. I had the main responsibility of analyzing the computational results, and writing the computational parts of the manuscript. I had only minor involvement in the other parts of the manuscript.

Publications not included in thesis

A. Ultrafast Excited State Dynamics of $Cr(CO)_4$(bpy) Revealing Triplet Energy Relaxation between 3MLCT States
F. Ma, M. Jarenmark, S. Hedström, P. Persson, E. Nordlander, A. Yartsev, *Manuscript.*

B. Ultrafast Excited State Dynamics and Coherent Control of Metal-Metal Bond Cleavage of [CpM(CO)3]2 (M = W, Mo) in Solution
F. Ma, M. Jarenmark, S. Hedström, P. Persson, E. Nordlander, A. Yartsev, *Manuscript.*

Populärvetenskaplig sammanfattning

Mänskligheten energibehov är enormt, och kommer att fortsätta öka. Fossila bränslen har använts för att tillgodose dessa behov under de senaste århundradena, men krav på långsiktig hållbarhet och drastiskt minskad klimatpåverkan har gjort att även andra energikällor behövs. Flera tusen gånger mer solenergi träffar hela tiden jorden än den energi vi använder och därför är solceller lovande för att till stor del bidra till vår framtida elektricitetsförsörjning. Den solcellsteknologi som idag dominerar marknaden är så kallade p–n-övergångar av oorganiskt kisel som omvandlar ljus till elektricitet. Tillverkningen av dessa är dock svår och dyr. Solceller som istället tillverkas av organiska, kolbaserade material uppfanns för över femtio år sedan, och har tack vare intensiv forskning visat snabbt ökande verkningsgrader de senaste tjugo åren. De har många fördelar jämfört med oorganiska celler, bl.a. är de billigare och enklare att tillverka, de är tunna och böjbara, och kan tillverkas av återvunnet material. Deras verkningsgrad, uppåt 10%, är än så länge bara ungefär hälften så hög som i kiselceller, men deras ljusabsorptionsegenskaper kan å andra sidan justeras genom att man använder olika organiska molekyler, till skillnad från kiselcellers statiska absorptionsprofil.

De forskningsresultat som presenteras i denna avhandling handlar om dessa ljusabsorberande molekyler som är det material som omvandlar solens ljusenergi till elektrisk energi. Dessa molekyler är speciella plaster, polymerer – väldigt stora molekyler som består av ungefär fem till hundra identiska mindre repeterande enheter som alla är sammanlänkade längs en kedja. Dessa polymerer är större än de flesta syntetiska molekyler men är ändå mikroskopiska; flera biljoner av dem får plats i en liten solcell i labbskala, dvs 1 cm^2 i yta och bara 100 nm tjock. Trots att en solcell innehåller så många molekyler kan många av dess egenskaper härledas från studier av enskilda polymermolekyler och det är utgångspunkten för forskningen i denna avhandling. De mest relevanta egenskaperna är de som relaterar till ljusabsorption samt laddningsgenerering och -transport. Polymererna som studerats är konjugerade, en inneboende molekylär egenskap som främjar stark ljusabsorption och god ledningsförmåga, något som är helt avgörande för solcellers effektivitet. Hundratals nya konjugerade polymerer tas fram varje år tack vare intensiv forskning. Alla ger dock inte förbättrade solceller.

Till skillnad från den traditionella föreställningen av kemi som en genomgående praktisk disciplin, är utgångspunkten för forskningen i denna avhandling ren teoretisk beräkningskemi. Det innebär att avancerad datormjukvara används för att förutspå molekylers egenskaper, utan att någonsin komma i fysisk

kontakt med dem. Det kan låta som magi, men tänk på att vi utan att göra experimentet t.ex. kan beräkna hur lång tid det tar för en boll som släpps att nå marken om vi vet höjden, bollens vikt, och gravitationskraften. På samma sätt vet vi vilka krafter som påverkar atomerna i en molekyl, och vi kan därför noggrant förutsäga många av dess egenskaper. Ljusabsorptionen, vilken är central i detta arbete, påverkar också molekylerna och dess effekt kan också beräknas. Dock är de krafter som verkar på denna mikroskopiska nivå av kvantmekanisk natur, vilket resulterar i matematiska ekvationer som blir enormt mycket mer komplicerade än i exemplet med den fallande bollen. Därför utförs beräkningarna med kvantkemisk mjukvara i en superdator. Ett antal olika superdatorer på LUNARC i Lund och NSC i Linköping har använts i detta doktorandprojekt.

Eftersom krafterna och de därav följande ekvationerna är så komplicerade krävs många approximationer och förenklingar, vilket leder till osäkerheter i hur noggranna beräkningsmetoderna och resultaten blir. Detta är en evig fråga för teoretiska forskare, som måste jämföra sina resultat med experiment i den mån det är möjligt, för att säkerställa att beräkningarna väl representerar verkligheten. Ju större molekyl, desto mer krävande blir beräkningarna. Därför är de stora polymermolekylerna som studeras här utom räckhåll för de mest exakta beräkningsmetoderna, med dagens datorkapacitet. Icke desto mindre visar de resultat som presenteras i denna avhandling att metoder baserade på så kallad täthetsfunktionalteori närmar sig förmågan att kvantitativt förutsäga några av de viktigaste egenskaperna hos konjugerade polymerer för solcellsapplikationer, t.ex. absorptionsspektra och energinivåer. Sådana förutsägelser är mycket värdefulla eftersom de kan medföra en minskning av arbetet med att designa, syntetisera och karaktärisera nya polymer med nya egenskaper. Kvantkemiska beräkningar är också värdefulla för att tolka och förstå experimentella observationer. Experiment behandlar som regel många molekyler i taget, och kan därför inte användas för att studera enskilda molekyler på detaljnivå, t.ex. deras geometri eller enskilda elektroners rörelser.

Ett stort antal polymerer har studerats i detta doktorandprojekt, ofta i samarbete med experimentella grupper på Chalmers och Linköpings Universitet. Ett sådant samarbetesprojekt har resulterat i polymeren P3TQTIF av så kallad D–A_1–D–A_2-typ som uppvisat solceller av 7.0% verkningsgrad. Ett antal andra D–A_1–D–A_2-polymerer har från beräkningar förutspåtts ge ännu bättre absorptions-egenskaper, vilket är mycket lovande. Ett av de viktigaste resultaten är utvecklandet av en beräkningsbaserad strategi för att beskriva hur olika temperaturer påverkar polymerernas elektroniska och optiska egenskaper. Tack vare den snabba utvecklingen av datorhårdvara och beräkningsmetoder kommer teoretiska beräkningar sannolikt att spela en allt större roll i utvecklandet av nya polymera material för solceller och inom andra områden. Om verkningsgraden för polymera solceller fortsätter att öka som den gjort de senaste årtiondena kommer vi sannolikt se mer av dem på marknaden, t.ex. för användning i kläder, på fönster, *etc*. där tunnhet, böjbarhet eller justerbar absorption är viktiga egenskaper.

Popular Science Summary in English

The energy demands of human society are huge and will keep increasing for the foreseeable future. Fossil fuels have largely been able to meet those demands for the last centuries, but issues of sustainability and global warming have brought about a need for alternative energy sources. The emission of the sun supplies earth with an energy that is many thousand times larger than our consumption. It is therefore very promising as a major contributor to our electricity production, through the use of solar cells, also known as photovoltaics. The currently dominating solar cell technology is based on inorganic silicon, which converts light into electricity in a so called p–n junction. The fabrication of silicon p–n junction solar cells is however complex and expensive. Another type of solar cells is made from organic, carbon-based materials and were invented over fifty years ago. Thanks to intense research, they have demonstrated sharply increasing efficiencies over the last two decades. They have many advantages over inorganic cells, such as being cheaper and easier to manufacture, very thin and mechanically flexible, and producible from renewable materials. Although their power conversion efficiency as of yet is roughly half of the silicon cells, their light-absorption properties are tunable, depending on what organic molecules are used, unlike the static absorption profile of silicon.

The research presented in this thesis concerns the properties of these light-absorbing molecules, in which the energy of the absorbed light is converted to electric power. The molecules of interest are special plastics or polymers: very large molecules made up of many identical repeating units connected along a chain. Although larger than most other synthetic molecules, they are still microscopic, and many trillions of them make up a solar cell of typical lab-scale size: 1 cm^2 in area and 100 nm thick. Despite consisting of so many polymer molecules, many of the solar cell properties can be deduced from studies of only single polymers, which is the main approach of the research herein. The most relevant properties are those that concern the absorption of light and the generation and transport of electric charge. The polymers of interest are conjugated, an intrinsic molecular property that promotes strong light-absorption and good conductivity, crucial for solar cell performance. Hundreds of new conjugated polymers are currently developed each year thanks to intense research efforts, each with different properties and varying efficiency in the solar cells where they are used.

Unlike the traditional view that chemistry is a very practical, hands-on discipline, the research in this thesis is purely computational. That means that

advanced computer software is used to predict the properties of a molecule without ever coming in physical contact with it. This may sound a bit like magic, but consider that we in principle can calculate the time it takes for a ball to fall to the ground if we know the height, the ball's weight, and the size of the gravitational force. In the same way, we know the forces that act on the atoms in a molecule, and can thus predict many of its properties. The effect of light absorption is also in principle known, and can be treated in a similar, yet somewhat different way. However, these forces that act on this microscopic level are quantum mechanical in nature, so the resulting equations are immensely more complex than the example of the falling ball, and that is why they are done with quantum chemistry software in a supercomputer rather than by hand.

Since the forces and resulting equations are so complicated, many approximations and simplifications are required, introducing uncertainties regarding the accuracy of the computational methods. This is an eternal issue for theoretical scientists, who have to rely on comparisons to experiments to validate that the calculations are reasonable representations of reality. The smaller the molecule, the less computationally demanding are the calculations. So for the large polymers studied herein, the most accurate quantum chemical methods are out of reach with today's computers. Nevertheless, the results presented in this thesis show that methods based on density functional theory are approaching the capability of quantitatively predicting some of the most important properties of conjugated polymers for photovoltaic applications, including absorption spectra and energy levels. This is very valuable, as it can significantly decrease the workload associated with the design, synthesis, and characterization of new polymers with improved properties. Quantum chemical calculations are also useful for the further interpretation and understanding of experimental observations, since experimental methods generally are restricted to the study of many molecules at a time, lacking the ability to study the details of a single molecule, for example with regards to its geometry or the movements of single electrons.

A large number of polymers have been investigated during the PhD project presented in this thesis, often in collaboration with experimental groups at Chalmers and Linköping Universities. One very successful collaborative project resulted in the P3TQTIF polymer of so called D–A_1–D–A_2 type, showing 7.0% efficiency in solar cells. Several other D–A_1–D–A_2 polymers are computationally predicted to possess even better light-harvesting traits. One of the most important achievements is the development of a computational strategy to describe how different temperatures affect the optical and electronic properties of the polymers. With the ongoing development of computer hardware and computational methods, theoretical calculations are likely to play an increasing part in the development of new polymeric materials for use in solar cells and elsewhere. If the increase in efficiency of organic solar cells keep increasing as it has in the last decades, we are likely to see more of them sold commercially, for example for use on clothes, in windows, *etc*. where mechanical flexibility and absorption-tunability is vital.

Abbreviations, in order of appearance

OPV	Organic photovoltaics
QC	Quantum chemistry
MM	Molecular mechanics
QM	Quantum mechanics
DFT	Density functional theory
PSC	Polymer solar cell
CT	Charge-transfer
EA	Electron affinity
IP	Ionization potential
HOMO	Highest occupied molecular orbital
LUMO	Lowest unoccupied molecular orbital
PCE	Power conversion efficiency
FF	Fill factor
IQE	Internal quantum efficiency
EQE	External quantum efficiency
D–A	Donor–acceptor
MO	Molecular orbital
AO	Atomic orbital
LCAO	Linear combination of atomic orbitals
STO	Slater-type orbital
GTO	Gaussian-type orbital
CGTO	Contracted Gaussian-type orbital
HF	Hartree–Fock
SCF	Self-consistent field
MP2	Møller–Plesset second order perturbation theory
CI	Configuration interaction
CC	Coupled cluster
CASSCF	Complete active space self-consistent field
XC	Exchange–correlation
GGA	Generalized gradient approximations
LC	Long-range corrected
TD-DFT	Time-dependent density functional theory
RMS	Root mean square
FWHM	Full width at half maximum
PES	Potential energy surface

Chemical compounds, in order of appearance

P3HT	Poly(3-hexylthiophene)
$PC_{61}BM$	Phenyl-C_{61}-butyric acid methyl ester
PPV	Poly(phenylene vinylene)
T	Thiophene
BTz	Benzotriazole
PT	Polythiophene
BDT	Benzodithiophene
OBDT	Dialkoxy-benzodithiophene
Fu	Furan
Se	Selenophene
Ii	Isoindigo
BTI	Bisthienoazepinedione
TPD	Thienopyrrolodione
BT	Benzothiadiazole
T34T	Thieno[3,4-b]thiophene
CDT	Cyclopentadithiophene
DTPy	Dithienopyrrole
Q	Quinoxaline
ODCB	*ortho*-dichlorobenzene
3T	Terthiophene
PzQ	Pyrazinoquinoxaline
BBT	Benzobisthiadiazole

Contents

1. Introduction 1
   - 1.1 Scope and Outline 1
   - 1.2 Organic Photovoltaics 3
     - 1.2.1 Background and History 3
     - 1.2.2 Working Mechanism 4
     - 1.2.3 Efficiency 7

2. Theory 9
   - 2.1 Quantum Mechanics 9
     - 2.1.1 Wave Functions, Operators, and Observables 10
     - 2.1.2 The Schrödinger Equation 10
   - 2.2 Quantum Chemistry 10
     - 2.2.1 The Born–Oppenheimer Approximation 11
     - 2.2.2 Linear Combination of Atomic Orbitals 11
     - 2.2.3 Basis Sets 12
     - 2.2.4 Slater Determinants 13
     - 2.2.5 The Variational Principle and Hartree-Fock Method 14
     - 2.2.6 Other Wave Function Methods 15
     - 2.2.7 Density Functional Theory 16
     - 2.2.8 Exchange–Correlation Functionals 17
     - 2.2.9 Geometry Optimizations 19
     - 2.2.10 Time-Dependent Density Functional Theory 19
   - 2.3 Excited States and Optical Properties 20

3. Donor–Acceptor Polymers 25
   - 3.1 The Donor–Acceptor Motif 25
   - 3.2 Material Modeling in Calculations 27
   - 3.3 Structural Properties 29
   - 3.4 Energy Levels 30
   - 3.5 Optical Properties 32
     - 3.5.1 Absorption Energy 32
     - 3.5.2 Absorption Strength 35
     - 3.5.3 Light-Harvesting Capability 37
   - 3.6 Donor and Acceptor Strength 38

4. The TQ1 Polymer 43
4.1 Structural Properties 43
4.2 Optical Properties 46
4.3 Electronic Properties 47
5. Temperature-Dependent Properties 50
5.1 Planarity and Conjugation 50
5.2 Temperature-Dependent Optical Spectra 51
5.3 Boltzmann-Distribution of Conformations 52
6. $D–A_1–D–A_2$ Polymers 58
6.1 Dual Peak Absorption 58
6.2 Optical Properties 60
6.2.1 Predicted Absorption Spectra 60
6.2.2 Absorption Peak Energy 64
6.2.3 Relative Peak Intensity 64
6.3 Light-Harvesting Capability 65
7. Conclusions 68
8. Outlook 70
9. Acknowledgements 72
10. References 74

1. Introduction

1.1 Scope and Outline

The research presented in this doctoral thesis concerns polymers for use in organic photovoltaics (OPV), investigated by computational chemistry. The main aim has been to rationalize and predict those properties of the conjugated polymers that are most relevant to OPV applications. The focus of the research is consequently on the polymers' structural, electronic, and optical properties on the molecular level, with the intention of using computational studies for an improved insight into the relationship between these properties, and to the applications of the polymers. Calculated results in form of orbital energies, ultraviolet–visible absorption spectra, redox potentials, *etc*. have been compared to experimental data provided by collaborating research groups, having permitted development of computational schemes capable of giving good predictions of optical properties.

The computational methods used must be able to describe the sought properties well. However, the size of the molecular system that can be investigated is limited by the chosen method, where typically a trade-off exists between computational expediency and rigor. This is visualized in Figure 1.1 where different classes of computational methods are shown to be applicable to chemical systems of entirely different size scales as a result of the computational cost scaling. Regarding OPVs, on one end of the scale are calculations of the entire active layer or even the whole solar cell, feasible with formalistic methods. On the other end of the scale fall accurate *ab initio* quantum chemistry (QC) methods which due to their computational cost generally are restricted to single molecule calculations. Molecular mechanics (MM) based methods, including *e.g.* molecular dynamics with parametrized force fields, are capable of treating large model systems of hundreds of molecules, depending on the specific approach with regards to *e.g.* coarse-graining. The combination of quantum mechanical (QM) and MM methods, termed QM/MM, has also gained significant popularity in recent years.[1] The various methods are also suited for describing processes on distinct time-scales, where the fast electron dynamics require explicit QM treatment while the much slower nuclear motions can be described with MM methods. More on how different aspects of OPVs are treated with different methods can be found in Chapter 3.2.

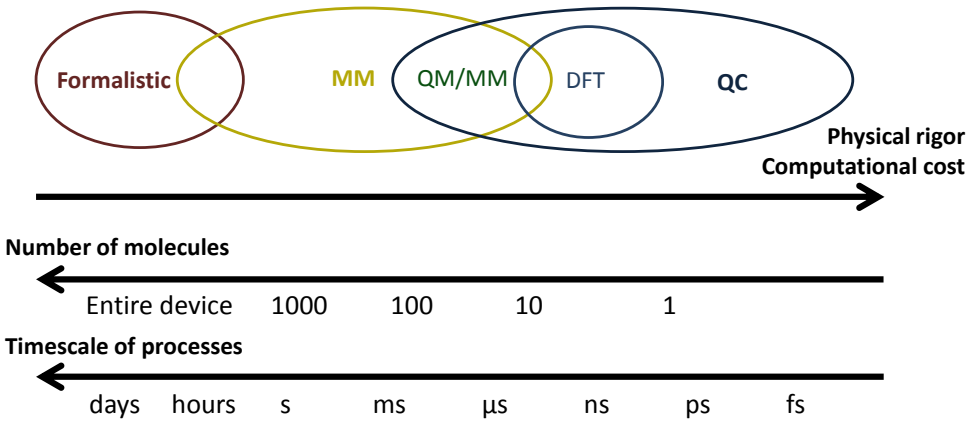

Figure 1.1. Schematic picture of the various classes of computational methods, showing the correlation between their rigor and cost, limiting the system sizes in terms of number of molecules to which they are applicable.

The research presented in this thesis mainly uses Density Functional Theory (DFT) QC methods, constituting a good compromise between accuracy and computational cost for the calculation of the aforementioned structural, electronic, and optical properties of molecules such as conjugated polymers. Nonetheless, the application of DFT is still limited to investigation of molecular systems of up to around 1000–2000 electrons, depending on the exact formulation of the DFT method, the property under investigation, and the capabilities of the hardware. The calculations presented herein consequently treat only up to a couple of molecules at a time.

This is a compilation thesis, whose foundation is the seven scientific articles included in the end. The articles are either published in, or submitted to, peer-reviewed scientific journals, and they are herein referred to as Papers I–VII. The chapters of the thesis are numbered 1–6 and are intended as a coherent summary of the work presented in the articles, with respect to results, discussions, and general conclusions. This first chapter gives the reader an introduction to the thesis, and to the application of the research: organic photovoltaics. The second chapter provides a brief overview of quantum chemistry with focus on the methods used throughout the articles. Chapters 3–6 summarize the findings of the articles, where Chapter 3 mostly corresponds to results from Papers I and II, Chapter 4 to Papers III and IV, Chapter 5 to Paper V, and Chapter 6 to Papers VI and VII. The reader of this thesis is assumed to have some chemistry or physics background, and ideally also be somewhat familiar with computational chemistry.

1.2 Organic Photovoltaics

1.2.1 Background and History

In 2012, the human energy consumption was 376 EJ or 3.76×10^{20} J.[2] While limiting the consumption is desirable, parallel efforts in increasing the sustainable production of electricity must be made. Ideally, the energy production source should also be clean, inexhaustible, and contribute as little as possible to the greenhouse effect. Each year, the total solar energy that strikes the earth surface is 14500 times our total consumption: a staggering 5459315 EJ/year.[3] Consequently, humanity could harness sunlight to completely meet the energy demands of society, given sufficiently cheap and efficient solar cells. The efficiency of solar cells is simply the amount of energy produced as electricity by the cell, divided by the incoming energy in form of solar radiation, as discussed further in Chapter 1.2.3.

The solar cell technology is almost 140 years old, and the first cell consisted simply of a layer of selenium between two electrodes.[4] Greatly improved efficiency was realized with the introduction of the semiconductor p–n junction (for positive–negative), where the active layer consists of two materials or phases being respectively electron-rich and electron-poor. Already in 1954, following the marketing of a silicon-based solar cell of 6% efficiency, the great potential of the "limitless energy of the sun" was identified by policymakers and news media.[5] Still to this day, a majority of solar cells are based on p–n junctions of crystalline silicon. They have a relatively high manufacturing cost, due to the required extensive purification of the silicon and the p- and n-doping of the material, achieved by the introduction of respectively electron-rich and electron-poor atoms as impurities. Silicon solar cells have reached 25% efficiency in the lab scale.[6] Higher efficiencies can be obtained with multi-junction solar cells, relying on the combination of several active layers of different materials with distinct spectral responses, increasing the percentage of sunlight that is effectively captured and exploited. These cells typically consist of various III-V materials, *i.e.* elements from group III and V in the periodic table, *e.g.* gallium arsenide, and the highest reported efficiency is 46%,[7] using solar concentrators. This very expensive type of solar cell is often used when high performance and low weight is much more important than low price, such as for spacecrafts and satellites.

Several alternatives to the expensive inorganic solar cells have been invented in the last decades, and are being pursued scientifically and to a lesser extent commercially. One of the first of these emerging photovoltaic technologies was the dye-sensitized solar cell,[8] where fused semiconductor nanoparticles, typically of titanium dioxide, are covered with light-absorbing dye molecules which are typically organometallic compounds. Upon light-absorption the dye transfers electrons into the semiconductor, eventually generating exploitable electric

current. Other emerging photovoltaic technologies are often variations of the dye-sensitized solar cell, *e.g.* using different light-harvesting materials such as quantum dots[9] or perovskites, the latter having shown rapidly improving efficiencies from 3.8%[10] to up to 20%[11] in only six years.

The photovoltaic technology of interest for the research in this thesis involves the employment of organic materials in the solar cell active layer, a technology known as organic photovoltaics. Solar cells of this type have many advantages compared to other technologies, such as consisting of solution-processable materials, being inexpensive, mechanically flexible, and easy to manufacture, *e.g.* through roll-to-roll printing.[12] Furthermore, they can be made from renewable materials, and their light-absorption properties can easily be tuned by using different absorbing molecules. OPVs were invented over 50 years ago,[13] and as with the inorganic solar cells, the first OPV device consisted of a single layer of active material with a very low resulting efficiency. The first two-layer OPV used thin films of smaller organic molecules in the active layer, and achieved an efficiency 0.95%.[14] A significant improvement was realized in 1995 with the bulk heterojunction layout,[15] using a conjugated polymer and a fullerene molecule as the respective p- and n-type materials, see Chapter 1.2.2 and Figure 1.2. This polymer solar cell (PSC) is to this day the dominant type of OPV and from this point on in the thesis the terms PSC and OPV are used interchangeably. Other types of OPV include those with small molecules instead of polymers, those using a second polymer of n-type instead of a fullerene, and ternary blend OPVs with more than two phases in the active layer. Multijunction OPVs are also feasible, although considerably more complicated to fabricate than single junction devices.

1.2.2 Working Mechanism

The typical PSC has two phases consisting of respectively a conjugated polymer such as poly(3-hexylthiophene) (P3HT) and a fullerene derivative such as phenyl-C_{61}-butyric acid methyl ester ($PC_{61}BM$), both depicted in Figure 1.2a and b. The conjugation arises from alternating single and double bonds along the polymer backbone, providing favorable electronic and light-harvesting properties,[16] as elaborated upon throughout Chapter 3.

The light-to-electricity power conversion process in OPVs is schematically depicted in Figure 1.2c, and delineated in the following paragraphs. The absorption of light occurs mainly in the polymer, since it generally has a wider spectral response and absorbs more strongly than the fullerene. The absorption of a photon results in an electronically excited state in the polymer, described in simple terms as one electron having extra energy; read more in Chapter 2.3. When excited, the negatively charged electron goes from the valence to the conduction band of the polymer molecule, leaving behind a positive charge in the valence band, typically viewed as an “electron hole” or simply “hole” quasiparticle. The

hole and excited electron are coulombically bound due to their opposing charges, and this bound state is called an exciton. Excitons are also quasiparticles, and have good mobility in conjugated molecules. The mobility is important, since the exciton transport towards the polymer–fullerene interface where the crucial charge separation occurs, competes with the process of spontaneous decay to the ground state accompanied by a loss of energy to the adjacent molecules as vibrational or rotational energy, *i.e.* heat, which constitutes a loss mechanism for the solar cell. In addition to the mobility, the exciton transport may also be limited by the morphology of the phases, in terms of the average distance between the point of excitation and the polymer–fullerene interface.

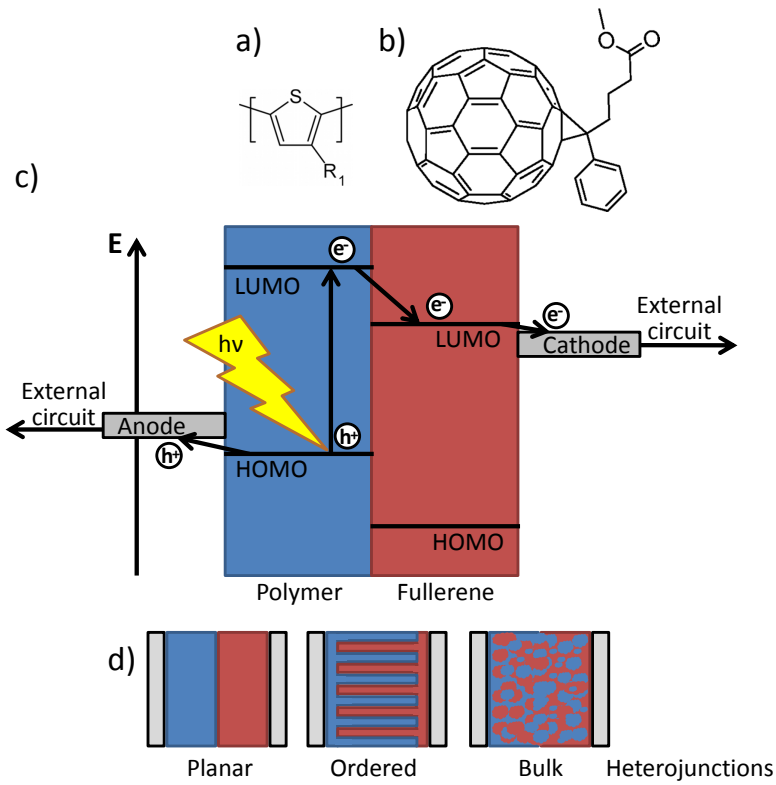

Figure 1.2. Chemical structures of the archetypal conjugated polymer P3HT (a), and the commonly used fullerene $PC_{61}BM$ (b). Working principle of a polymer solar cell (c), three different active layer heterojunction types (d).

Having reached the polymer–fullerene interface, the exciton must dissociate so that the negatively charged electron (e^-) is injected into the fullerene, leaving behind the positively charged hole (h^+) in the polymer, see Figure 1.2c. This results in what is known as a charge-transfer (CT) state. This state can be directly measured by electro- or photoluminescence,[17–19] and its characteristics in terms of

e.g. spatial extent and binding energy are very important for OPVs since it influences both the voltage and current produced by the cell. The transfer of the electron is facilitated by an intrinsically higher electron affinity (EA) of the fullerene than the polymer, imposing a strict requirement when developing new polymers: their EA must be sufficiently small for efficient electron injection into the fullerene. The ionization potential (IP), corresponding to the energy of removing an electron from a molecule, must be also greater in the fullerene than the polymer, to ensure that the hole remains in the polymer. The experimental observables IP and EA correspond respectively to the calculated electronic highest occupied molecular orbital (HOMO) and lowest unoccupied molecular orbital (LUMO), read more in Chapter 2.3.

The hole and the electron, known as charge carriers, are still strongly coulombically bound due to their opposing charges and spatial closeness, despite now residing on different molecules. They must become spatially separated for the eventual extraction of current from the device, and if they do not separate in time, the charge carriers are lost in what is called geminate recombination, *i.e.* when charge carriers originating from the same exciton recombine. The relatively strong currents produced by good PSCs reveal that the separation process can occur with efficiencies up to near 100%,[20] despite the strong electrostatic attraction. This has led to some controversy as to the exact nature of the charge separation process away from the interfaces.[21,22] One of the proposed mechanisms involves "hot" CT states,[23,24] *i.e.* that the exciton bears some extra energy, electronic or vibrational, beyond just being in the first electronically excited state, providing enough energy to escape the coulombic potential well. The study of this process is beyond the scope of this thesis.

After the electron and hole have separated, away from the polymer–fullerene interface, they travel through their respective phase towards their respective electrode. Should charge carriers of opposing charges encounter each other, they run the risk of recombining non-geminately, *i.e.* with a charge carrier generated by a different exciton. High hole-mobility of the polymer is therefore a crucial property. Another possible loss mechanism during the charge transport appears if the charge carrier was generated in a trapping region, *i.e.* an island of a phase that is unconnected to its respective electrode, which highlights the importance of the formation of a bicontinuous network of the two phases for efficient charge extraction.[15] As a consequence of these two loss processes, charge extraction is favored by thin active layers; typical thicknesses are around 100 nm.[25–28] The electrodes must have work functions that make the process of accepting the respective charge carriers energetically favorable, and the difference in work function between the two electrodes also determines the output voltage from the cell. The structures of the two phases, *i.e.* the morphology of the active layer, as well as details on the electrodes, fall outside the scope of the research presented herein.

1.2.3 Efficiency

The perhaps most important quality of any solar cell is its power conversion efficiency (PCE), defined as the percentage of the power of the incoming light P_{in} that is converted to useable electric power P_{out}, see Equation 1.1. The input power is determined by the solar light power per area E_{solar} and the area of the cell A_{cell}. The power output is given by the electric current multiplied by the voltage, corresponding to the number of charges produced per unit time multiplied by the potential energy of each charge. The maximum current is obtained during short circuit conditions, *i.e.* zero voltage, thus called the short circuit current J_{SC}. The maximum voltage appears at open circuit conditions, *i.e.* when the current approaches zero. It is known as the open circuit voltage V_{OC}. This results in a P_{out} that is described by Equation 1.1, where the actual current and voltage during operating conditions is represented by the ideal J_{SC} and V_{OC} downscaled by a so called fill factor (FF), representing non-idealities including resistive losses during operating conditions. FFs of up to 80% are reported for PSCs.[29]

$$PCE = \frac{P_{out}}{P_{in}} = \frac{J_{SC} \times V_{OC} \times FF}{E_{solar} \times A_{cell}} \quad (1.1)$$

The V_{OC} corresponds to the potential energy of the charges, and its upper limit is determined by the energy offset between the fullerene LUMO and polymer HOMO. This leads to a strong linear correlation between the OPV V_{OC} and measured polymer HOMO energy, for devices with the same fullerene molecule.[30–32] In consequence, there have been some efforts to enhance the V_{OC}s by developing polymers with a deeper HOMO,[33–35] and V_{OC}s over 1.1 V have been reported in polymer–fullerene bulk heterojunction OPVs.[36–38]

The J_{SC}, a measure of the amount of generated charges per unit time, is limited by the capability of the active layer to absorb photons, as well as to a number of loss mechanisms outlined in Chapter 1.2.2, such as trapping regions of a particular phase, exciton relaxation, and geminate and non-geminate recombination. These losses are collectively quantified by the internal quantum efficiency (IQE), defined as the number of extracted charges per number of *absorbed* photons. IQEs very close to 100% have been reported in OPVs,[20,33,39] connoting minimal electronic losses. Taking into account that only some of the incoming photons are absorbed, the external quantum efficiency (EQE) is an important parameter, defined as the number of extracted charges per number of *incoming* photons. The EQE is thus a measure of the light-to-current conversion capability of the solar cell, and it is typically reported as a function of the wavelength λ of the incoming light, which in turn is proportional to the speed c and reciprocal energy E of the photons:

$$\lambda = \frac{hc}{E} \quad (1.2)$$

As per Equation 1.3, the total J_{SC} from a device is given by the EQE multiplied with the solar emission photon flux $\Phi_{e\lambda}$, integrated over all wavelengths and multiplied with the electronic charge of each charge carrier, *i.e.* the elementary charge q_e.

$$J_{SC} = q_e \int_0^\infty \Phi_{e\lambda}^{sol} EQE_\lambda \, d\lambda \tag{1.3}$$

The fact that EQE is integrated over all λ highlights the importance of good spectral coverage of the polymer, meaning effective absorption over a wide wavelength region which also should match the solar emission, which is strongest between 450–1100 nm. The generally limiting factor for the spectral coverage is the optical band gap, corresponding to the smallest photon energy that the polymer can absorb, which is closely correlated with the electronic energy gap between HOMO and LUMO, as further described in Chapter 3.5.1. A small band gap and good spectral coverage can be achieved with a deep polymer LUMO or high polymer HOMO. However, as briefly mentioned in Chapter 1.2.2, the polymer LUMO must be above the fullerene LUMO for efficient electron injection into the fullerene. Furthermore, since a deep HOMO is correlated with a high V_{OC}, there is a trade-off between strong J_{SC} (high HOMO energy) and good V_{OC} (low HOMO energy). This trade-off generally makes the exact HOMO energy non-critical to the performance, although J_{SC} has been shown to correlate more strongly than V_{OC} with the final efficiency of OPV devices.[40] The current state of the art single junction PSCs show J_{SC}s over 19 mA cm^{-2}, resulting in PCEs over 10% using so called donor–acceptor (D–A) polymers,[41–43] described in detail throughout Chapter 3.

The efficiency development in OPVs is largely driven by the design of new polymers. The number of reported conjugated polymers is vast and ever-increasing, but the design process often involves a large degree of trial-and-error, *e.g.* by including structural elements that in other copolymer combinations have provided favorable traits. Computational chemistry is capable of providing a better understanding of the interactions and processes on the molecular level, both within and between molecules, which can be exploited for a more advised design process for new polymer systems. Furthermore, quantum chemistry methods offer the possibility for enhanced streamlining of the experimental development efforts through their capability to predict optical and electronic properties of the polymers, before synthesis. Good accuracy of computational predictions is already attainable as shown in the research presented in this thesis, and it will improve even further with the constant development of faster and more powerful computers. In Chapters 3–6 are presented results from calculations of the fundamental properties of conjugated polymers that are most relevant for efficient OPVs in terms of charge carrier mobility, energy level alignment, and light-harvesting capability.

2. Theory

This chapter is intended to give the reader sufficient qualitative understanding of the theory and methods to appreciate and follow the computational results in later chapters. It is in no way exhaustive; mainly qualitative arguments are presented, with mathematical formulae only present when these promote the qualitative understanding.

2.1 Quantum Mechanics

The name quantum mechanics (QM) originates in nature's tendency for quantization; light and matter consist of discrete units rather than a continuum, adopting discrete energy levels. Max Planck suggested in the beginning of the last century that the energy of light emitted by a black body was quantized in elements whose energies were determined by the frequency of the light ν multiplied by a constant h:

$$E = h\nu = \frac{hc}{\lambda} \tag{2.1}$$

Although Planck considered the quantization as a mathematical trick, we now know that light itself can be seen as quantized physical particles: photons. In 1905 Albert Einstein used the photon concept to explain how electrons are ejected from a material when light shines upon it, known as the photoelectric effect. This very early demonstration of the quantum nature of light is related to a phenomenon of great relevance for this thesis: the photovoltaic effect, where electrons rather than being ejected, are excited to higher energy states within the material. The exploitation of this electronic excitation energy is the basis of solar cells. Another early quantum concept of relevance for this thesis is that the electrons orbit around the atomic nuclei in quantized states, so called orbitals, each with a specific associated energy, postulated by Niels Bohr in 1914.

The following decades saw great advances in the formulation, interpretation, and unification of QM theory, including work of Planck, Einstein, Bohr, Heisenberg, Schrödinger, and many others. Being a completely fundamental theory, QM relies on a number of postulates. These are unprovable, basic

assumptions that to this day have been supported by countless experiments and calculations, thus being apparently valid and certainly highly useful.

2.1.1 Wave Functions, Operators, and Observables

One postulate of QM states that any system of particles can be completely described by a wave function Ψ. This function of time and of the positions of each particle is generally complex. Its absolute value squared, $|\Psi|^2$, corresponds at each point in time to the probability distribution function for the particles to be found at these positions. Another postulate states that any observable is associated with an operator. Together, these two postulates imply that by acting with the appropriate operator on a system's wave function, any property of the system can be obtained, including energies, momenta, positions, *etc*. Mathematically defining the wave function and the operators is often difficult for more complex systems, and solving the resulting equations exactly is impossible for all but the simplest cases.

2.1.2 The Schrödinger Equation

Newton's second law of classical mechanics, F=ma, describes how a classical system evolves in time with some initial conditions. Analogously, the corresponding evolution of a QM system is described by the time-dependent Schrödinger equation:

$$ih\frac{\partial}{\partial t}\Psi = \hat{H}\Psi \qquad (2.2)$$

Here i and h are constants, and Ĥ is the so called Hamiltonian operator which is associated with the total energy of the system whose wave function is denoted Ψ. This thesis mainly treats time-independent properties and systems, which accordingly are described by the time-independent Schrödinger equation:

$$E\Psi = \hat{H}\Psi \qquad (2.3)$$

This equation yields the total energy E of the system state, but finding the exact formulations of Ĥ and Ψ can be difficult, and solving the equation exactly is impossible for most practically relevant chemical systems.

2.2 Quantum Chemistry

Quantum chemistry (QC) is the science of applying QM equations to chemical systems in order to extract information about them. The systems can be atoms,

solids, or as in the case of this thesis: molecules, here mainly in form of polymers. Due to the aforementioned complexity of the QM equations, various approximations and simplifications of the equations are required for all but the simplest chemical systems. The interested reader is encouraged to read references 44 and 1, from which most of this chapter is adapted, or other QC textbooks.

2.2.1 The Born–Oppenheimer Approximation

The formulation of the energy operator, the Hamiltonian $\hat{H}$, varies, but in general it contains at least five contributions:

1) the attractive potential energy between the negatively charged electrons and the positive nuclei,
2) the repulsive potential energy between nuclei,
3) the repulsive potential energy between electrons,
4) the kinetic energy of the electrons, and
5) the kinetic energy of the nuclei.

In reality, solving Equation 2.3 must be done under simultaneous consideration of all these factors, an extremely difficult task for most chemical systems. The commonly used Born-Oppenheimer approximation however, separates the nuclear and electronic contributions, allowing them to be solved consecutively.[45] This essentially means that the nuclei are treated classically, which is generally an acceptable approximation since the nuclei are so heavy that their movement is negligible on the time-scale of the electron movements. The Born–Oppenheimer approximation, which also involves neglecting the 5th term above: the nuclear kinetic energy, greatly reduces the complexity and increases the feasibility of QC calculations.

2.2.2 Linear Combination of Atomic Orbitals

The predominant way to approximate the total many-electron wave function Ψ, required to solve the Schrödinger Equation 2.3, is by combining a number of atom-centered so called basis functions φ into molecular orbitals ψ:

$$\psi = \sum_{i=1}^{N} c_i \varphi_i \qquad (2.4)$$

This construction of N molecular orbitals from a linear combination of N atomic orbitals (MO-LCAO) is the typical way of obtaining quantitative many-electron wave functions, where various QC methods are used to determine the optimal coefficients c_i, as elaborated in subsequent subchapters. MO-LCAO it is also used frequently for qualitative arguments to rationalize properties of molecules, such as

the nature of bond formation, reactivities, orbital hybridizations, *etc*. Such discussions, including molecular orbital (MO) diagrams such as the one in Figure 3.1a and 6.2, are today found in practically all chemistry text books, *e.g.* references 46 and 47. This highlights how QC can promote a general understanding of chemistry outside the purely computational domain.

2.2.3 Basis Sets

The set of atomic orbitals (AO) φ used in QC to construct the molecular orbitals ψ and the many-electron wave function Ψ is known as a basis set. In general, larger basis sets give more flexibility to Ψ, leading to increased computational cost but also increased accuracy up to the point of convergence for very large basis sets. The AOs, one-electron basis functions φ, are typically described by comparatively simple mathematical equations called Slater-type orbitals (STO):[48]

$$\varphi_{nlm}^{STO} = Nr^{n-1}e^{-\zeta r}Y_l^m \qquad (2.5)$$

n, l, and m are the electron quantum numbers representing electronic shell, subshell, and specific orbital respectively, N is a normalization constant, ζ is a constant for each nucleus relating to its charge, r is the electron's distance from the nucleus, and Y_l^m are the so called spherical harmonics functions.[49] Using the STOs directly is possible, but a speed-up of QC calculations is facilitated by instead using Gaussian-type orbitals (GTO):

$$\varphi_{opq}^{GTO} = Nr^{n-1}e^{-\zeta r^2}Y_l^m \qquad (2.6)$$

These are more efficient by virtue of the much faster evaluation of integrals of the type $\int e^{-x^2} \times \int e^{-x^2}$ dx than $\int e^{-x} \times e^{-x}$ dx. In order to mimic the STOs better, typically a linear combination of a number of GTOs are used, known as contracted GTOs (CGTO). The STO-3G basis set uses three GTOs to mimic the STO for each electron. Using only one CGTO for each electron in the system is the smallest number possible, and is known as a minimal basis set. More than one CGTO per electron is often used for the valence electrons, being the most chemically relevant. Such basis sets are known as split valence basis sets, usually termed double-zeta in the case of two CGTOs per valence electron, triple-zeta for three CGTOs, *etc*. Furthermore, polarization functions can be added, which are represented by GTOs of higher subshell quantum number l than the electron, *e.g.* adding a d-type (l=3) CGTO to a p-shell (l=2) electron. To obtain a better description of anions and other systems with electron distributions that extend further from the nuclei, diffuse functions can be added which have a slower decay with increasing electron–nucleus distance. When computational cost is a concern, basis sets can employ effective core potentials, meaning that the core (non-valence) electrons are treated as an effective charge distribution rather than with

explicit basis functions. This is particularly valuable for heavy atoms with many core electrons.

In the research presented in this thesis, Pople-type basis sets are used throughout, which are labelled X-YZWG, where X is the number of GTOs linearly combined in each CGTO for the core electrons, Y is the number of GTOs per CGTO for the first basis function of the valence orbitals, and Z for the second valence basis function. In the case of triple-zeta basis sets, W represents the third valence basis function. If not otherwise noted, the basis set used for calculations presented herein is 6-31G(d,p), signifying that core electrons have 6 GTOs per CGTO, and the valence electrons are represented by 2 CGTOs constructed from respectively 3 and 1 GTOs. It also includes d- and p-type polarization functions.

2.2.4 Slater Determinants

The MOs (one-electron wave functions) ψ are made up of a linear combination of AOs φ as described in Chapter 2.2.3. The ψ are then multiplied with a spin function α or β representing the up- or down-spin of the electron, forming the one-electron spin orbitals χ. Setting up the total wave function Ψ for an N-electron system generally involves the formulation of a Slater determinant from the χ:

$$\Psi_{SD}(x_1, x_2, \dots, x_{N-1}, x_N) = \frac{1}{\sqrt{N!}} \begin{vmatrix} \chi_1(x_1) & \chi_2(x_1) & \cdots & \chi_{N-1}(x_1) & \chi_N(x_1) \\ \chi_1(x_2) & \chi_2(x_2) & \cdots & \chi_{N-1}(x_2) & \chi_N(x_2) \\ \vdots & \vdots & \ddots & \vdots & \vdots \\ \chi_1(x_{N-1}) & \chi_2(x_{N-1}) & \cdots & \chi_{N-1}(x_{N-1}) & \chi_N(x_{N-1}) \\ \chi_1(x_N) & \chi_2(x_N) & \cdots & \chi_{N-1}(x_N) & \chi_N(x_N) \end{vmatrix} \quad (2.7)$$

Here the coordinates x_i include the spatial positions and spins of each electron. The dependence on spatial coordinates of electrons leads to the dependence of Ψ to the spatial coordinates of also the nuclei. The nuclear coordinates are consequently required as input in any QC calculation, either taken from experiments or as a qualified guess from the user.

The Slater determinant approach of constructing the total many-electron wave function satisfies the requirement of anti-symmetry that goes for electrons and other fermions. It also obeys the Pauli Exclusion Principle stating that no two electrons can occupy the same quantum state simultaneously, meaning that at most one α and one β electron can occupy a single spatial MO. Apart from the orbitals occupied with electrons, also unoccupied or virtual orbitals are generated, since the number of atomic orbitals used is more than the number of electrons, as per Chapter 2.2.3, and the theory of MO-LCAO states that a number N of atomic orbitals will form the N molecular orbitals.

2.2.5 The Variational Principle and Hartree-Fock Method

The total wave function in form of the Slater determinant can take many forms, depending on the coefficients in the LCAO described in Chapter 2.2.2 and 2.2.3. To identify the coefficients that provide the most realistic total wave function one exploits the variational principle, which states that the calculated ground state energy E of a system described by an approximate wave function is always larger than the true ground state energy E_0 associated with the true wave function. Finding the most realistic approximation of the wave function Ψ is thus done by systematically and iteratively varying the basis function contributions of the molecular orbitals until the energy as given by the Schrödinger Equation 2.3 is minimized.

In the Hamiltonian operator, whose components are described qualitatively in Chapter 2.2.1, the electron–electron interaction term is generally the most challenging to evaluate, as it cannot directly operate on the one-electron wave functions. In the Hartree-Fock (HF) method,[50] each electron is approximated to experience only a mean field of the other electrons, reducing this term to a sum of one-electron operators which can be applied to the individual molecular orbitals or one-electron wave functions. Consequently, for a closed shell system, *i.e.* all orbitals populated by two electrons, the total electronic Hamiltonian consists of three one-electron terms, known as the Fock operator $\hat{F}$, summed over all N electrons with index i:

$$\hat{H}_{HF} = \sum_i \hat{F}(i) = \sum_i \left(-\frac{1}{2}\nabla_{r_i}^2 - \sum_\alpha \frac{Z_\alpha}{r_{i-\alpha}} + \sum_{j=1}^{N/2} \left(2\hat{J}_j - \hat{K}_j\right) \right) \qquad (2.8)$$

Equation 2.8 uses atomic units in which many constants are set to the numeric value of 1. The three terms correspond respectively to the kinetic energy of the electrons, the attractive potential energy between the i:th electron and each nuclei with nuclear charge Z_α, and the electron–electron interaction. To Equation 2.8 is also added the trivial nuclear–nuclear repulsions. The electron–electron terms are typically the most time-demanding to calculate as they involve double integrals over two electron positions, so called two-electron integrals. $\hat{J}$ represents the normal coulombic repulsion between electron i and j, and it is multiplied by 2 since the sum goes over half the amount of electrons. $\hat{K}$ is known as the exchange operator and it represents the energy associated with exchanging two electrons. It arises as a consequence of the anti-symmetry of the total wave function and the indistinguishability of electrons, and is a purely quantum mechanical effect that has no analogy in classical mechanics. The Fock operator of each electron acts on that electron's spatial MO, yielding the energy of that MO in an eigenvalue equation:

$$\hat{F}(i)\psi_i(x) = \varepsilon_i \psi_i(x) \qquad (2.9)$$

The formulation of $\hat{F}$ for each electron depends on the ψ of the other electrons, and Equation 2.9 is thus non-linear and is solved iteratively. Based on some starting guess of the one-electron wave functions ψ, typically based on LCAO, one formulates $\hat{F}$ and applies it to the guessed ψ, which results in an energy E and an updated ψ. The updated ψ is subsequently used to formulate an updated $\hat{F}$, and the process is then repeated several times for all electrons until the change in ε and/or ψ with each iteration is smaller than some previously defined threshold, *i.e.* having reached self-consistency. The HF method is thus known as a self-consistent field (SCF) method. The computational cost scales to the number of electrons as N^4, although mathematical tricks such as neglecting very small integrals can reduce it to N^3 without noticeable loss of accuracy, and even lower scaling is possible through more severe approximations.

As briefly mentioned in Chapter 1.2.2, the energy of the HOMO is related to the negative of the IP of that molecule, and in the context of restricted (no special description of singly occupied orbitals) HF theory, they are exactly equal. This is known as Koopmans' theorem, and in practice it is often quite inaccurate, since it disregards that the MOs change when the molecule loses or gains an electron. Although not present in its original formulation, Koopmans' theorem is sometimes also extended to include a similar relationship between the EA and the LUMO energy. This comparison is often even more precarious than the IP–HOMO, since the unoccupied orbitals have less well-founded physical meaning and are more sensitive to the choice of basis set.

2.2.6 Other Wave Function Methods

Several approximations are present in the HF method, but the one causing the largest loss of accuracy is arguably the mean field approximation: that the electron–electron interactions are not calculated rigorously. Many wave-function methods use HF as a starting point but then aim to include descriptions of this interaction, known as electron correlation. Of these so called post-HF methods, the perhaps simplest useful one is Møller-Plesset second order perturbation theory[51] (MP2) method, which has been very popular for QC calculations since the 1970s as it is reasonably efficient, scaling as N^5. As the name indicates, it is a perturbation theory method,[52] where the HF result is the 0^{th} order solution. MP methods of higher order perturbation also exist, such as MP4 and MP5. The MP methods provide more accurate energies compared to HF, but no new orbitals are produced.

Another post-HF method is configuration interaction (CI) whose starting point is the HF-computed Slater determinant. A linear combination is then formed from this HF-determinant and a number of similar determinants with some electrons excited to unoccupied orbitals. The energy is minimized by varying the coefficients in the linear combination. The very high computational cost of CI

limits its applications to small chemical systems. Coupled cluster (CC) is a typically very accurate method that also relies on a linear combination formed from the HF Slater determinant and some excited determinants, and it scales as N^6 or higher depending on if excitations of higher order than double are included.[44] As for most methods, various further approximations have been developed that reduce the scaling at the expense of the rigor.

The HF Slater determinant is not a suitable reference wave function for some chemical systems, such as those with near-degenerate ground states or under bond-breaking conditions. One may then use the complete active space (CAS)-SCF method,[53] a so called multi-reference method which like CI and CC uses several determinants. But it allows variation of the basis function coefficients within each determinant in addition to the variation of coefficients in the linear combination of Slater determinants. Usually in CASSCF, only excitations between some predetermined set of occupied and virtual orbitals are allowed in the Slater determinants. Depending on the number of these orbitals, *i.e.* the size of the active space, this method can be accurate and affordable for systems with multi-reference character.

2.2.7 Density Functional Theory

The QC methods introduced so far all use wave functions with molecular orbitals produced as linear combinations of atomic orbitals. The wave functions have known mathematical form, and when operated on by the Hamiltonians, very complicated mathematical expressions, mostly integrals, are obtained, which are typically solved numerically. Density Functional Theory (DFT), rather than the explicit wave functions, uses the electron density ρ as the main carrier of information, but its equations are in many aspects similar to those of HF.

The foundation of DFT is the Hohenberg–Kohn theorems.[54] They state that the ground state properties of a chemical system can be uniquely obtained from ρ, and that there exists a functional F[ρ] that produces the ground state energy E which is minimized for the true ground state ρ, *i.e.* it is variational. The electron density ρ(r) is a function of the three Cartesian spatial coordinates r, meaning that F[ρ] is a function of a function, knowns as a functional, explaining the name Density Functional Theory. These theorems are proven, but the problem is the exact formulation of F[ρ] which although many approximations exist, is ultimately unknown.

The Kohn–Sham framework developed in the 1960s is based on the Hohenberg–Kohn theorems and is still used today. It is an SCF methodology that as a starting point uses a non-physical system of electrons that do not interact with each other. The Kohn–Sham electronic energy is expressed as:

$$E(\rho) = T_e(\rho) + V_{ne}(\rho) + V_{ee}(\rho) + \Delta T(\rho) + \Delta V_{ee}(\rho) \qquad (2.10)$$

T_e is the kinetic energy of the non-interacting electrons, V_{ne} is the nuclear–electron potential energy, V_{ee} is the classical coulomb electron–electron repulsion. The last two terms in Equation 2.10 represent effective corrections to the kinetic energy of the electrons, and the potential energy between them, accounting for explicit electron–electron interactions. The three first terms in Equation 2.10 are very similar to the HF case in Chapter 2.2.5, although the expressions for V_{ne} and V_{ee} in DFT are rewritten as effective potentials over the electron density. Overall, this permits the formulation of single-particle eigenvalue equations analogous to the Fock-equations:

$$\left\{-\frac{1}{2}\nabla^2 + v_{eff}\right\}\psi_i(x) = \varepsilon_i\psi_i(x) \tag{2.11}$$

The one-electron energy operator is here seen to consist of the HF-formulation of the electron kinetic energy, and the remaining energy contributions formulated as an effective potential v_{eff} felt by the electron. The single-electron orbitals ψ_i are known as Kohn–Sham orbitals, with corresponding eigenvalue energies of ε_i. As in HF, these equations are solved iteratively over all electrons. The Kohn–Sham density $\rho_{KS}(r)$ is obtained from the molecular orbitals of the Slater determinant:

$$\rho_{KS}(r) = \sum_i \int |\psi_i(x)|^2 \tag{2.12}$$

DFT results tend to be less sensitive to basis set size than post-HF methods, mainly since only the occupied orbitals contribute to the ground state electronic structure of DFT.[55]

The perhaps most important difference between HF and DFT is that while the electron exchange term $\hat{K}$ appears in HF due to the antisymmetric Slater determinant wave function, in DFT it does not appear explicitly, and one instead aims to include its description in the two corrective terms appearing last in Equation 2.10. The energy resulting from these two terms is known as the exchange–correlation (XC) energy E_{XC}, with a corresponding potential V_{XC}. As the name indicates, V_{XC} typically also attempts to include descriptions of the electron–electron correlation which is absent in HF.

2.2.8 Exchange–Correlation Functionals

The main issue with the implementation of DFT is the formulation of the XC potentials V_{XC}, which are critical to the accuracy of DFT. There should in principle exist an exact formulation of V_{XC}, but it is unknown so various approximate formulations are used instead. This has the important side-effect that DFT becomes a non-variational method, *i.e.* a lower energy is not necessarily associated with a more correct ground state Ψ (or ρ). Typically V_{XC} consists of a number of terms for the exchange and correlation respectively, and in many QC

software programs the many existing exchange and correlation terms can be used in any combination. The contributions of the various terms are in many functionals determined by comparison to results either from experiments or from more accurate post-HF calculations. The resulting multitude of V_{XC} formulations are often grouped according to their complexity, labelled as rungs on "Jacob's ladder", a concept introduced by John Perdew in 2000.[56]

The first rung on Jacob's ladder corresponds to the local density approximation which exploits the fact that $V_{XC}(\rho)$ is accurately known for a uniform electron gas, *i.e.* an infinite number of electrons in a space of implicit positive charge (in order to retain charge neutrality). One then uses this known $V_{XC}(\rho)$ for the studied chemical system, resulting in $E_{XC}(\rho)$ equal to that of a uniform electron gas of the same ρ. The second rung involves additional terms that depend on the gradient (first spatial derivative) of ρ, apart from ρ itself. These are called generalized gradient approximation (GGA) functionals and generally provide greatly improved accuracy, but with little added computational cost. The third rung functionals are known as meta-GGA and include also terms that depend on the Laplacian (second derivative) of ρ.

An important problem with DFT is the so called self-interaction error which arises since in the Kohn–Sham formalism each electron interacts with the total electron density, and thus also to some extent with itself. In HF this self-interaction is explicitly cancelled by the exchange term $\hat{K}$. The electron self-interaction error can cause many problems including overestimated charge delocalization in DFT calculations. This is of particular importance for the research presented herein, as it can result in overestimated degrees of conjugation in corresponding systems, affecting both structural (*e.g.* with respect to planarity) and electronic properties (smaller band gaps, bad description of charge separated states). To remedy this, it has become common to include XC terms that include some HF exchange, *i.e.* $\hat{K}$ from Equation 2.8, acting explicitly on the molecular orbitals. These are known as hybrid functionals and represent the fourth rung on Jacob's ladder. Hybrid functionals are generally much more accurate for calculations of molecular band gap energies, partly due to cancellations of error between DFT which tends to underestimate them and HF which typically overestimates them. However, the inclusion of this non-local exchange also increases the formal computational cost scaling from N^3 to N^4, although various strategies exist that reduce the scaling.[57]

The fifth and final rung of the original formulation of Jacob's ladder uses all Kohn–Sham molecular orbitals for the evaluation of exchange and correlation, thus becoming very computationally demanding and basis set sensitive. Such functionals are so far not practically used.[58] Other additional refinements to the Kohn–Sham formalism have been developed however. So called long-range corrected (LC) functionals uses a distance-dependent amount of HF exchange,[59] which eliminates much of the problems associated with the self-interaction error. However, the suitable distance-dependence of the exchange is different for

different chemical systems and sizes.[60] The inclusion of explicit dispersion interactions have also been realized,[61] highly useful for systems where such weak interactions are important.

Several XC functionals have been evaluated for the calculations presented herein, including PBE[62] from the second rung of Jacob's ladder, B3LYP[63] from the fourth rung, M06-2X[64] which as a hybrid meta-GGA functional combines features from the third and fourth rung, and the LC functional CAM-B3LYP.[65] The functional eventually used for the majority of the calculations in this thesis is the PBE0 functional.[66] Being a hybrid functional, it includes 25% HF exchange, the remaining 75% being of local, ρ-dependent character. This functional includes comparatively few terms and is not parametrized for any certain chemistry. It is consequently expected to give consistent results over different system sizes and chemistries.[67] However, our results indicate that PBE0 tends to overestimate the conjugation, as is the case for most non-LC functionals.[68–70] Another functional used for some calculations is ωB97XD[71] which includes both some HF exchange, LC, and an empirical dispersion term. As noted in the previous paragraph, the appropriate amount of LC is system-dependent, and ωB97XD like most other LC functionals in their standard implementation uses LCs that are parametrized for smaller molecules, leading to overestimated band gaps for longer polymers.[72]

2.2.9 Geometry Optimizations

Apart from providing the minimum-energy and thus most realistic electronic structure, the Kohn–Sham formalism can be exploited for obtaining the minimum-energy geometric structure (geometry optimization), used extensively in the research of this thesis. The gradient (spatial derivative) of the potential energy of each atom is proportional to the force acting on that atom. After analytical or numerical calculation of these gradients from the potentials, the atoms are moved along the vectors of these forces according to some algorithm. At the updated geometry, the SCF electronic structure calculation as per previous paragraphs is repeated, generating new gradients. This is repeated iteratively until the forces and/or spatial displacements are smaller than a predetermined threshold. Geometries optimizations can be done with HF and in principle with any QC method, although the gradients may be difficult to derive. DFT-predicted geometries are generally good,[57,73–75] considering that post-HF methods tend to significantly outperform DFT for other properties such as energies.

2.2.10 Time-Dependent Density Functional Theory

As with most QC methods in their standard formulation, DFT treats the ground state of the chemical system. However, the excited state properties can be

evaluated with time-dependent DFT (TD-DFT), whose fundaments were developed by Runge and Gross in 1984.[76] In this formalism, a time-dependent perturbation is applied, which when in form of an electric field can provide the electronic transition energies, transition dipole moments, and other excited state properties, described further in Chapter 2.3. Since it would require a lengthy introduction to perturbation theory, it is beyond the scope of this thesis to go into detail about the theory and equations behind TD-DFT. The reader is instead encouraged to read references 1, 57, or 77. Although relying on more complex equations, TD-DFT is currently implemented in a variety of QC software.

The self-interaction error in DFT as discussed in the previous subchapter, is a problem also in TD-DFT, in particular for the description of excitations with CT character.[78–80] Since excitations of this type are generally important for conjugated polymers, TD-DFT results must be analyzed with care. Despite this, TD-DFT has become very popular for the study of excited states of a vast array of molecular systems during the last decades,[77,81,82] including conjugated systems such as the polymers being the subject of this thesis.[83–87] TD-DFT is used extensively for the excited state and optical properties of the conjugated polymers herein, presented in Chapters 3–6.

2.3 Excited States and Optical Properties

The fundament of solar cells is the absorption of light, where the energy of the absorbed photon is converted to electrical energy. The interaction between light and matter has long been an interest of science, even before the introduction of QM. With the development of QM theory and the concept of wave–particle duality of light (and matter) however, has come a significantly improved molecular level understanding of how the electronic structure of matter interplays with light.

As discussed in Chapter 2.2, the N electrons in a closed shell (even number of electrons) chemical system such as a molecule, will in the ground state occupy N/2 orbitals since two electrons of respectively spin up and down can occupy the same spatial orbital. As a result of using initially more than N/2 AOs, some unoccupied MOs are also computed. Unoccupied MOs are highly valuable tools for understanding and explaining various electronic processes, but it is important to note that they have no real physical meaning, which is why they are often referred to as virtual orbitals.[88] The absorption of light occurs as a result of interaction between matter and the electric field component of the incoming electromagnetic radiation, *i.e.* the light. In the typical case, the system is in the ground electronic state when a photon is absorbed, whose energy is used to promote the system to an electronically excited state. Due to the physical laws of energy conservation, the difference in energy between the ground and excited states must match the energy of the absorbed photon E_{abs}. For electronic

transitions, this energy generally corresponds to somewhere in the ultraviolet–visible–near infrared range, ~100–2000 nm (~12–0.5 eV).

As a simplification, the excitation can be viewed as the promotion of an electron from an occupied orbital to an unoccupied, where the energy difference of these orbitals corresponds to the excitation energy. The first (lowest-energy) excited state generally corresponds to a HOMO→LUMO transition, depicted in Figure 2.1. The second and third excited states also shown in Figure 2.1 correspond in this example to HOMO→LUMO+1 and HOMO−1→LUMO. Successive excited states correspond to promotions from deeper occupied MOs to higher unoccupied MOs. If the total number of spin up electrons is the same as spin down, the excited state is a so called singlet state. If conversely there are two more spin-up electrons than down, it is a triplet state. Excitations directly from the singlet ground state S_0 to a triplet excited state T_n generally do not occur, especially not in organic polymers without heavy atoms that facilitate spin–orbit coupling.[89,90] However, since a triplet state has lower energy than its corresponding singlet state, a so called intersystem crossing may occur, *i.e.* spin-flip relaxation from *e.g.* S_1 to T_1, albeit with low probability. As a general rule, higher excited states S_n quickly relax to the first excited state S_1 at a time-scale of picoseconds.[89]

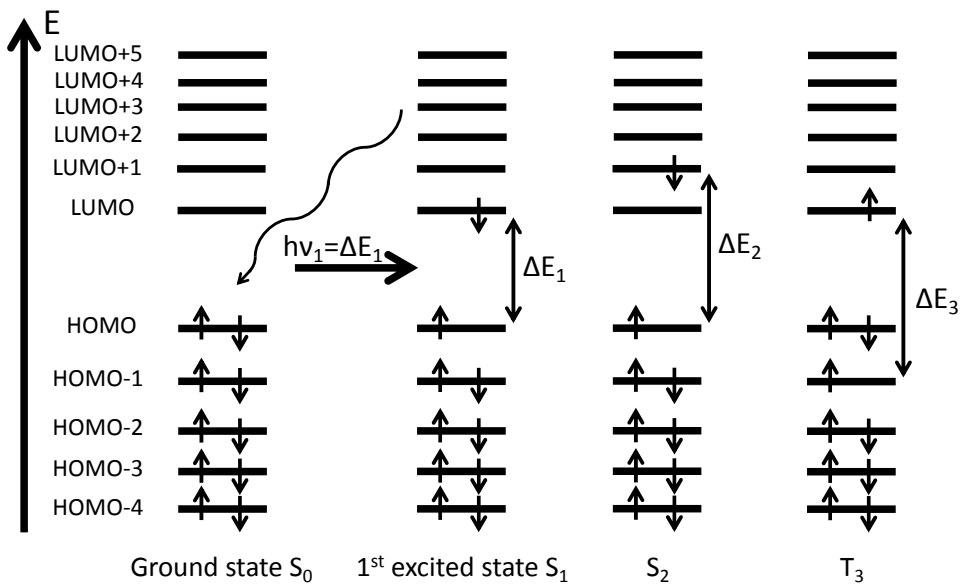

Figure 2.1. Schematic picture of the MO energy levels in a 10-electron molecule, where 5 orbitals are occupied in the ground state. The absorption of a photon with appropriate energy ΔE results in an electronically excited state where as a simplification, an electron is promoted from an occupied orbital to an unoccupied. Singlet states S have an equal number of spin-up and spin-down electrons. Triplet states T have two more spin up electrons than down (or vice versa).

Although the representation in Figure 2.1 is an often useful way of considering excited states, it is only approximate for a number of reasons:

- The target orbital is virtual before the excitation, and can upon becoming populated alter its character and energy significantly.
- Also all occupied orbitals are altered in the excitation process, including the now singly occupied origin MO, affecting their energy and other properties. This is true even if α and β (spin up and down) orbitals are considered separately, *i.e.* the unrestricted case.
- A single excitation can correspond to a mix of several orbital contributions. If there is more than one dominating contribution, the simplified picture in Figure 2.1 breaks down, losing its value even for qualitative discussions.
- The excitation may involve also vibrationally excited states, either in the ground (origin) electronic state *e.g.* at elevated temperatures, or more commonly in the excited (target) state. The combination of electronic and vibrational excitations are called vibronic transitions and the consecutive transitions to the 0^{th}, 1^{st}, 2^{nd}, *etc.* vibrational states in the electronically excited state are known as a vibronic progression. Frequently, vibronic transitions to excited vibrational states are more probable than to the 0^{th} vibrational state, affecting the absorption spectrum.

As a consequence of these effects, a more accurate view of the excitation and excited state is possible only from explicit excited state calculations rather than being inferred from the MOs, for example by analyzing the transition electron density difference through TD-DFT calculations.

While QC calculations typically treat one molecule with a specific geometry, in experiments one measures the absorption of an ensemble of molecules with a distribution of conformations at finite temperature. Since the absorption energy depends on the geometry, this leads to so called inhomogeneous broadening in experiments, resulting in experimental absorption peaks of certain spectral width, whereas single-molecule calculations yield single absorption energies. Also homogeneous broadening occurs as a result of experimental conditions, such as finite pressure and temperature. Spectral broadening can cause issues in the interpretation of absorption spectra, *e.g.* if two distinct electronic transitions are so close in energy that their corresponding absorption peaks overlap significantly, producing only one apparent peak in the spectrum. More about how the broadening affects polymer absorption spectra can be found in Chapter 3.5.

Measurements of optical properties can give indications of the MO energies. Electrochemistry experiments can provide a more direct measure of the orbital energies, in form of the oxidation and reduction potential. These correspond to the IP and EA, the energies associated with respectively the removal or addition of an electron to the system. These experiments are done at a rather long time scale, providing enough time not only to the orbitals to relax and rearrange as a reaction to the altered electronic conditions, but also to the nuclear coordinates.

Unrestricted QC calculations are capable of describing singly occupied orbitals and charged systems, and when coupled to geometry optimizations, they can be used to explicitly calculate the red-ox potentials. However, as a simplified first approximation, the experimental IP can be compared to the negative of the calculated HOMO energy and the EA to the LUMO. Known as Koopmans' theorem, this is discussed in Chapter 2.2.5 in the domain of the HF method, but is applicable also to *e.g.* DFT.[91,92] In summary, the HOMO–LUMO energy gap, the first excited state energy, and the difference between the first reduction and oxidation potentials, are all interrelated quantities but slightly different due to different conditions for the involved orbitals.[69]

The different possible electronic transitions in molecules occur with different probabilities, *i.e.* it is not certain that a photon will be absorbed when striking a molecule even if it is of suitable energy. In the so called dipole approximation, what determines the probability of absorption P_{abs} is the transition dipole moment between ground and excited state:[93]

$$P_{abs} \propto \langle \psi_{GS} | \hat{\mu} | \psi_{ex} \rangle^2 \qquad (2.13)$$

This QM expression contains the dipole operator $\hat{\mu}$ and the wave functions of the originally populated (ground) state ψ_{GS} and target (excited) state ψ_{ex}. Excitations with non-vanishing transition dipole moments are known as allowed transitions, whereas those of negligible probability are called forbidden transitions, although they can still occur due to other mechanisms than dipole transitions. An example of a forbidden transition is a spin-flipping intersystem crossing, see above. Several other directly related measures of the absorption intensity or strength are commonly used, including the oscillator strength f, and absorption cross section σ. These molecular quantities also directly relate to the experimental absorption coefficients ε. The dimensionless absorbance A of a sample of absorbing material is defined as the negative of the decadic logarithm of the percentage of the incoming light that is transmitted, *i.e.* the transmittance T:

$$A = -\log_{10} T = -\log_{10} \frac{\Phi_e^t}{\Phi_e^i} \qquad (2.14)$$

According to Lambert–Beer's law, the absorbance is proportional to the path length l through the sample, and the absorption coefficient ε and concentration c of the absorbing material:[47]

$$A = \varepsilon c l \qquad (2.15)$$

If c is the molar concentration, ε is the molar absorption coefficient. For polymers which have highly non-uniform molecular weights, a better comparison between the absorption capabilities of different polymers can be made using the mass absorption coefficient in units of L g^{-1} cm^{-1}, for which c is the mass concentration in units of g L^{-1}. For solar cell applications, higher absorption coefficients are

naturally favorable, increasing the amount of absorbed and thus useable photons, as discussed for polymers in Chapter 3.5.2.

If sufficiently accurate predictions of both absorption strengths and energies of all electronic transitions can be obtained from calculations, the absorption spectra of the whole visible region can be simulated. This would be an important achievement, and has been a stated goal for this thesis work, since efficient light-harvesting is the arguably most critical parameter for high-performance solar cells.

3. Donor–Acceptor Polymers

3.1 The Donor–Acceptor Motif

The first class of successful light-harvesting polymers for solar cell applications was electron-rich homopolymers, meaning that they only have one repeating structural unit. Prominent examples are poly(phenylene vinylene) (PPV)[94] and poly(3-hexylthiophene) (P3HT).[95] While typically exhibiting very strong absorption, they fail to capture a large part of the solar emission due to only absorbing at wavelengths below ~600 nm. Alternating electron rich (donor) and electron poor (acceptor) units along the backbone in a copolymer can provide a narrower band-gap, as shown with the first donor–acceptor (D–A) copolymers developed in 1992.[96] These polymers, polysquaraines and polycroconaines, showed maximum absorption wavelengths λ_{max} of up to 900 nm. An enormous amount of D–A polymers have since then been developed,[97–103] and used for many applications including OPVs, the main focus of this thesis.

The D–A concept is exemplified with the homodimerization of thiophene and the co-oligomerization of thiophene (T) and benzotriazole (BTz) in Figure 3.1a, demonstrating the deeper LUMO but practically unchanged HOMO energy upon introduction of the BTz acceptor unit. The lone BTz unit has slightly higher HOMO energy than the small T unit, which is simply a consequence of that larger conjugated systems have higher associated HOMO and lower LUMO energies. For longer oligomers or polymers, this effect of unit size vanishes and T proves to be more electron-rich. The calculated absorption spectra of the corresponding polymers polythiophene (PT) and PTBTz are shown in Figure 3.1b, demonstrating the lower absorption energy $E_{abs}=hc/\lambda_{abs}$ of the D–A copolymer PTBTz. The improved spectral coverage of D–A polymers generally compensates for the small loss in maximum absorption intensity compared to homopolymers, giving a significantly greater number of absorbed photons. While OPV efficiencies with homopolymers have recently reached 6.5%,[104] the D–A polymer motif is currently capable of efficiencies exceeding 10% in standard, single-junction OPV devices.[41,105]

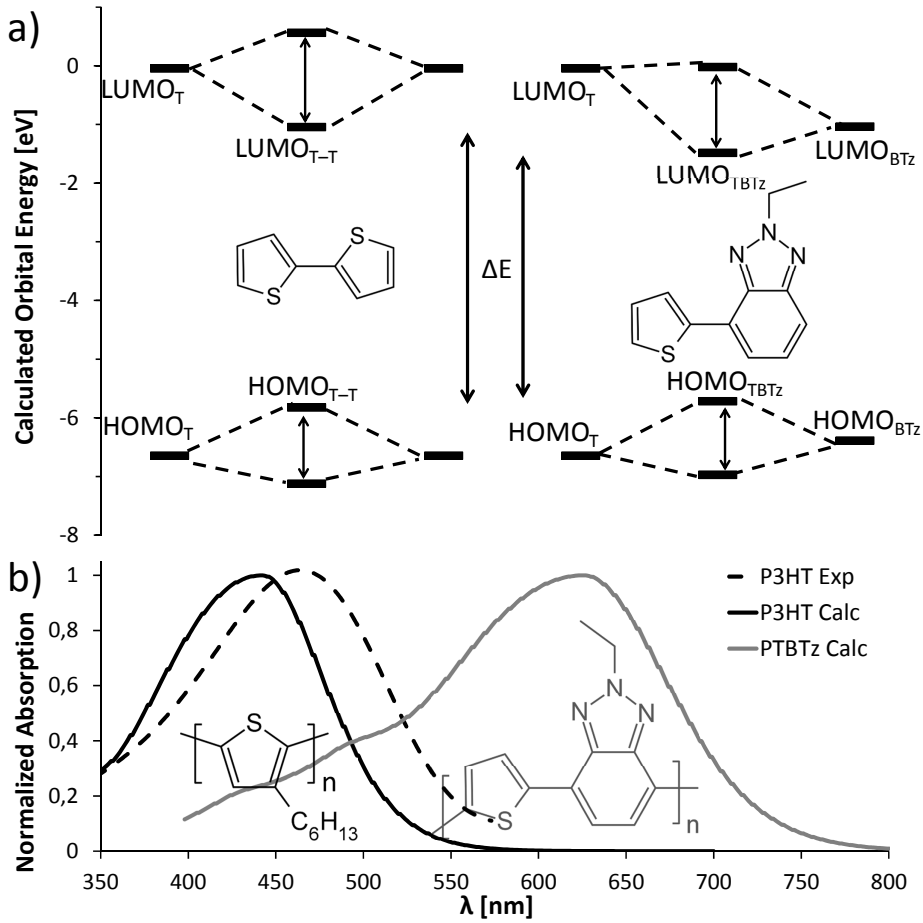

Figure 3.1. Molecular orbital diagram of the DFT-calculated frontier orbital energies of T, bithiophene (T–T), benzotriazole (BTz), and thiophene–benzotriazole (TBTz), demonstrating the narrowing of the HOMO–LUMO gap upon addition of units (a). The lower E_{LUMO} of BTz affords a smaller HOMO–LUMO gap in TBTz than in T–T, inducing a red-shift of the PTBTz polymer absorption spectra compared to P3HT (b). Experimental P3HT absorption spectrum provided by Patrik Henriksson, Chalmers University.

A very large number of donor and acceptor units have been developed since the introduction of D–A polymers. The archetypical donor unit is thiophene, its alkylated homopolymer P3HT being commonly used in OPVs before the upsurge of D–A polymers.[104,106–108] The electron donating properties of thiophene come partly from the electron-rich, formally divalent, sulfur atom. Other donor units are often variations of thiophene, for example as co-fused with additional aryl rings as in benzodithiophene (BDT), whose structure is displayed in Figure 3.2a albeit with appended alkoxy-groups (OBDT). Five different donor segments are employed in nine D–A polymers in Paper I, and they all contain some T or BDT units. In

addition to thiophene itself, seven fused thiophene derivatives are investigated as donors in Paper II, as well as furan (Fu) and selenophene (Se), analogous to thiophene but with the sulfur atom replaced by the other chalcogens oxygen and selenium. In Figure 3.2a the structures of the ten donor units studied in Paper II are depicted, representative of donors commonly applied in D–A polymers. Acceptor units typically contain electronegative nitrogen atoms, as do all of the five acceptors studied in Paper I, and the six acceptors in Paper II whose structures are shown in Figure 3.2b. While typically only one acceptor aryl unit is used per copolymer repeating unit, several adjacent donor units are often employed, such as for EWC3[109] with two thiophenes and one carbazole per repeating unit, see Figure 3.3.

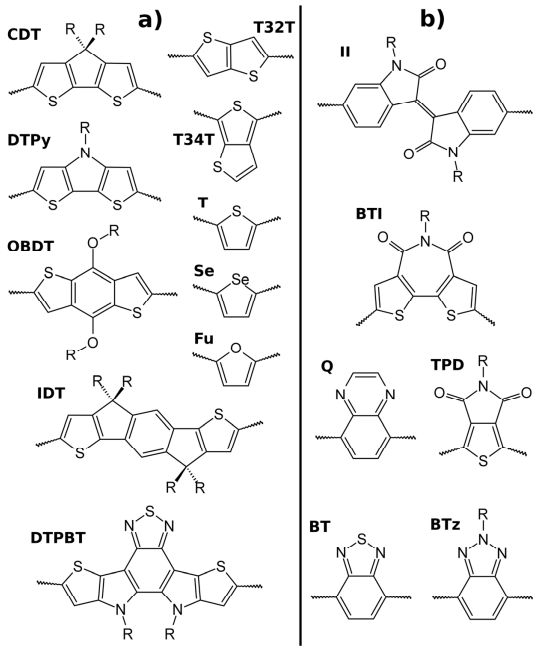

Figure 3.2. Structures of the 10 donor (a) and 6 acceptor units (b) investigated in Paper II, representative of the variety of commonly occurring units in D–A polymers. For full names of units, see Paper II.

3.2 Material Modeling in Calculations

The active layer in OPVs consists of a thin, solid film with polymer and fullerene molecules. The morphology of these films is crucial for OPV efficiency,[110] but can be difficult to assess on the molecular level with experiments due to their highly disordered nature. Semiempirical and classical mechanics computational methods

have been used to study the intermolecular interactions that govern the supramolecular structure in the respective polymer[111,112] and fullerene[113] phases, as well as the interfaces between them.[23,114–116] Detailed information of the electronic and optical properties however, require more refined quantum chemical (QC) methods, capable of describing the molecular level electronic structure and excited states. The computational time consumption for these methods typically scale unfavorably with the size of the chemical system, thus becoming restricted to studies of a few or even single molecules. Among these QC methods, rapid developments in hardware have made accurate wave function-based approaches feasible for many small to medium sized molecules with up to ~300 electrons, discussed cursorily in Chapter 2.2.6. DFT methods emerge as a suitable compromise between efficiency and accuracy for larger chemical systems such as oligomers with 200–2000 electrons, depending on the power of the hardware. Small model systems of interfaces, consisting of a short oligomer and a single fullerene molecule have recently come within reach of full DFT treatments.[117–121]

Although DFT compares favorably to other quantum chemical methods in terms of computational expedience, its normally cubical scaling to the number of electrons still necessitates approximations in the modeling of polymers. For instance, explicit treatment of the entire polymer strand is generally unfeasible since the experimental molecular masses of conjugated polymers often exceed ~ 100000 g/mol; a 330000 g/mol molecular weight average was for example reported for the TQ1 polymer.[122] Instead, computational studies are commonly based on oligomers. Calculated properties of oligomers of between three and ten repeating units are sometimes compared directly to experimental polymers.[72,123,124] Another more robust approach is to calculate the properties of a range of oligomer sizes, whose resulting properties often exhibit systematic size-dependent trends, permitting extrapolation to the polymer limit.[125–128] The extrapolated values can then be compared directly to experimental properties. Articles I, II, III, V, and VI, being those involving quantification of calculated polymer properties, all use an oligomer-based extrapolation approach for orbital energies, absorption energies, and absorption strengths, see Chapters 3.4 and 3.5.

Another approximation of the models, common in the literature and also used in the research presented here, is the truncation of saturated alkyl side-chains which are present in experiments for solubility and processability reasons whereas not significantly affecting electronic properties. A third approximation regards the solvent, typically modelled as a polarizable continuum in computational studies throughout the literature,[129–131] neglecting explicit polymer–solvent interactions. Continuum-solvent single molecule calculations can be directly compared to experimental polymer properties in solution, as done systematically in Paper I and intermittently in Papers III, V, and VI, as long as the solutions are dilute enough to not induce significant polymer–polymer aggregation. However, it is the film state of the polymer that makes up one of the two phases in the OPV active layer, generally dominating its absorption profile. Depending on the intermolecular

interactions and structure, the polymer film state optical properties sometimes deviate from the corresponding dilute solution, complicating comparisons to calculations.

As explained in Chapter 2.2.8, several DFT functionals have been evaluated for the underlying work of this thesis. In combination with some basis set tests, PBE0/6-31G(d,p) has emerged as a level of theory which gives consistent and affordable results for a wide range of chemistries and oligomer sizes. Unless otherwise noted, this level of theory is used for the results presented in Chapters 3–6. The SCF convergence threshold is electron density-based: the default "tight" setting in the G09 software.[132] The thresholds for geometry optimizations are also the default values, corresponding to a maximum force on an atom of 0.00045, a root mean square (RMS) force of 0.0003, a maximum atom displacement of 0.0018 and RMS displacement of 0.0012, all given in atomic units: Hartree/Bohr and Bohr respectively.

3.3 Structural Properties

The chemical nature of the polymer structure determines the observed properties. Improved understanding of this structure–property relationship is a fundamental goal of the research of this thesis, and of materials science in general. Properties related to polymer solubility and processability are factors requiring major consideration in synthesis and OPV device fabrication, affecting the free energy of solvation, aggregation, and the resulting morphology of the polymer films. Such properties do not directly enter in standard single molecule QC calculations however, permitting *e.g.* the omission of alkyl side-chains as mentioned in the previous section.

It is the conjugated backbones that give the polymers their signature electronic and optical properties, with strong absorption in the visible region and high charge mobilities, crucial traits for OPV applications. The chemical compositions of the donor and acceptor units are critical factors, but also conformational properties are important. Planarity for example, positively affects the conjugation, which in turn tends to enhance charge transport and optical properties in terms of red-shifted and stronger absorption.[16,133] This effect of planarity on the charge transport is one of the main points of Paper IV, outlined Chapter 4.3. The conformation dependent optical properties are studied extensively in Paper V, and is summarized in Chapter 5.

The donor and acceptor units are individually rigid, but are connected by flexible single bonds. Standard quantum chemical calculations are typically based on fully optimized structures, *i.e.* the minimum energy conformations. Though complete coplanarity between units is energetically favorable from a conjugation perspective, colliding hydrogen atoms on adjacent units and other steric hindrance

effects, induce slightly out-of-plane structures. The degree of planarity is thus determined by the chemistry of the donor and acceptor units, near the connecting single bonds along the backbone. The planarity of D–A polymers is studied in Papers I and II, and is there quantified by average out-of-plane torsion angles over the single bonds between units. The donors and acceptor units in these two papers connect with either five- or six-membered rings, and the five-membered rings give consistently flatter optimum geometries, by virtue of lesser steric hindrance. This can be seen in Figure 3.3 where four example D–A dimers have their optimized dihedral angles shown.

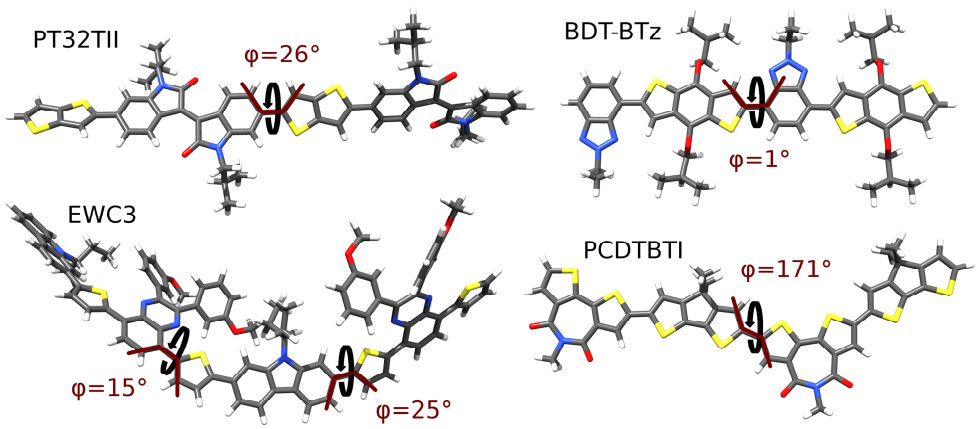

Figure 3.3. Optimized dimers of the polymers BDT-BTz and EWC3 from Paper I, and PT32TII and PCDTBTI from Paper II, showing the dihedral angles between units. The six-membered isoindigo and carbazole rings in PT32TII and EWC3 cause steric hindrance and more out-of-plane angles.

The permitted rotation around the single bonds between units also confers cis–trans (syn–anti) conformational isomerism to the polymer, with energy minima for dihedral angles both ~180° and ~0°. The cis–trans isomerism of the TQ1 polymer[134] is studied in Paper III, where we show that the more planar trans isomer confers a smaller optical band gap. The structural and optical properties of TQ1 are described in more detail in Chapter 4.

3.4 Energy Levels

The D–A polymer motif was developed for their narrower band gap as compared to homopolymers. This is achieved by the alternating electron rich donor and electron poor acceptor units along the backbone, respectively responsible for raising the HOMO and lowering the LUMO energy of the copolymer. The energy

gap between these frontier orbitals is closely related to the absorption energy, since the energy conservation laws requires that the increase in electric energy upon light absorption matches the energy of the photon. This is elaborated in more detail in Chapter 2.3.

The LUMOs of D–A polymers usually correspond mostly to the acceptor LUMO, and are mostly localized on the acceptor unit.[72,97,135] This partial localization is seen in Figure 3.4 where HOMO and LUMO of four polymers from Paper I are depicted, although the effect is less pronounced for shorter donor segments, *e.g.* in TBDT-Q. The optimum LUMO energy is closely determined by the LUMO of the electron-accepting molecule (typically a fullerene), as the energy difference between them constitutes a driving force for exciton separation at the polymer–fullerene interface. To facilitate efficient exciton splitting the copolymer LUMO energy should consequently be 0–0.3 eV higher than the fullerene LUMO.[32] For even higher LUMO energy offsets, the excess energy is lost without contributing to better exciton splitting. The fact that the copolymer LUMO is largely determined by the acceptor thus makes the choice of acceptor unit critical. Only a handful of different acceptors have been able to achieve D–A polymer solar cell power conversion efficiencies (PCEs) exceeding ~8%, among those being isoindigo (Ii),[136] bisthienoazepinedione (BTI),[29] thienopyrrolodione (TPD),[137] benzothiadiazole (BT),[41,138] and naphtobisthiadiazole.[41,139] Fine-tuning of the LUMO energy is possible by appending the acceptors with electron-donating or -withdrawing substituents, commonly fluorine atoms. Thienothiophene (T34T), though normally electron-rich, has after fluorination been used as an acceptor, yielding a PCE over 9% in OPV devices.[140,141]

For a given LUMO energy, a higher copolymer HOMO provides a narrower optical band gap, beneficial for efficient light-harvesting and strong photocurrents in OPV devices. A deep copolymer HOMO conversely, increases the voltage of the device,[31,32] as explained in Chapter 1.2.3. This voltage–current tradeoff makes the optimal HOMO energy less well defined, requiring a balancing depending on other parameters. Though the donor unit is employed for raising the energy of the copolymer HOMO, this orbital is typically delocalized over the entire backbones of polymers,[72,97] see Figure 3.4. This gives the copolymer HOMO character of both the acceptor and donor HOMOs, influencing its energy. As described in Paper II, high-HOMO acceptors such as Ii and BTz consequently yield higher HOMO energies in their copolymers than low-HOMO acceptors like BT and TPD.

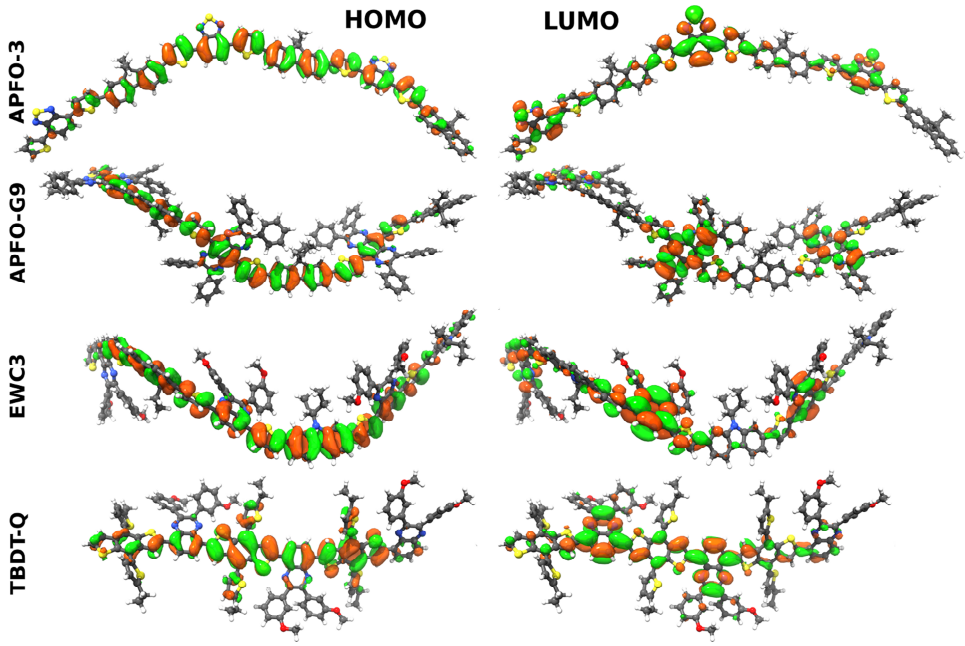

Figure 3.4. Calculated HOMO and LUMO of trimer models of four D–A polymers studied in Paper I.

The energies of the frontier orbitals HOMO and LUMO have been shown to evolve approximately linearly as a function of the reciprocal number of repeating units (1/n). For longer oligomers however, the energies converge faster than the linear functions, and various non-linear equations have been shown to give better fits to the size evolution from monomer (1/n=1) to polymer (1/n=0).[142,143,126,144] In paper I, the HOMO and LUMO of the 9 studied polymers are estimated using a fitting and extrapolation procedure based on Hückel MO theory,[144] and the significance and physics behind it is there discussed in further detail.

3.5 Optical Properties

3.5.1 Absorption Energy

As described in the previous section, the HOMO–LUMO energy gap of the polymer is closely related to the absorption energy. The term optical band gap is often used for the onset absorption energy rather than the peak absorption energy. Since standard QC calculations yield only precise absorption energies rather than

peaks of a certain width, the discussions herein will focus on the energy of maximum absorption E_{abs}.

The solar emission of photons has considerable intensity in a wide spectral region that begins at around 300 nm (3.0 eV), increases sharply and peaks around 700 nm (1.8 eV) and then decays slowly up to 2000 nm (0.6 eV). The band gap of the polymer constitutes the minimum energy the photons must have to be absorbed, resulting in zero absorption of sub-band gap photons. On the other hand, as mentioned in Chapter 2.3, higher excited states S_n quickly decay to the first excited state S_1 through internal conversion. This means that only the S_1 energy, corresponding to the band gap energy, can be exploited, and the excess energy of higher energy photons is not exploitable in OPVs. Based on these limitations, Shockley and Queisser used a detailed balance calculation to determine the maximum achievable efficiency of a p–n junction solar cell as a function of the band gap of the absorber.[145] According to such calculations, a maximum PCE of 33.7% is achievable with a band gap of 1.34 eV. The very tunable properties of D–A polymers as a function of the choice of structural units, is thus very advantageous, compared to silicon which has a suboptimal band gap of 1.1 eV which is not readily tuned. D–A polymers with E_{abs} lower than 1 eV are reported.[96,146–148] However, such low-energy absorption, apart from being lower than the Shockley–Queisser optimum, is typically accompanied by a very deep copolymer LUMO, impeding exciton separation at the fullerene interface. For OPVs specifically, if using a PCBM fullerene as the electron-accepting material, an absorption onset of 1.5 eV ~ 825 nm has been suggested as ideal,[32] although it depends on other factors such as absorption intensity and IQE.

The first (lowest energy) electronically excited state of conjugated polymers corresponds to a strongly allowed $\pi \rightarrow \pi^*$ transition,[149,150] mainly corresponding to the promotion of an electron from HOMO to LUMO. This first transition is the cause of the relatively intense first peak typically seen in the absorption spectra of D–A polymers, and since LUMO is often denser on the acceptor, it involves a partial intramolecular charge transfer (CT) from donor to acceptor unit. Subsequent absorption peaks frequently occur at 300–450 nm, whose corresponding electronic transitions typically exhibit less CT character, being more localized either within the donor segment,[151–153] or less commonly within the acceptor unit.[154,155] Generally, conjugated molecules experience a decrease in band gap with growing system size, associated with increased delocalization of the π-orbitals. This is consistent with the respective increase in HOMO and decrease in LUMO energies for increasing number of repeating units in D–A polymers as discussed in the previous section. In Figure 3.5a, the size dependence of $E_{abs}=hc/\lambda_{abs}$ is demonstrated with the calculated absorption spectra of the four BDT-BTz oligomers with 1, 2, 3, and 5 repeating units.

The evolution of the frontier orbital energies as a function of 1/n, as discussed in Chapter 3.5.1, and approximated from Hückel MO theory in Paper I, can be exploited to model the corresponding E_{abs} size evolution:

$$E_{abs}(n) \approx E_{LUMO}(n) - E_{HOMO}(n)$$
$$= \alpha_{LUMO} - \alpha_{HOMO} + 2(\beta_{LUMO} + \beta_{HOMO})cos\frac{\pi}{n+1} \qquad (3.1)$$

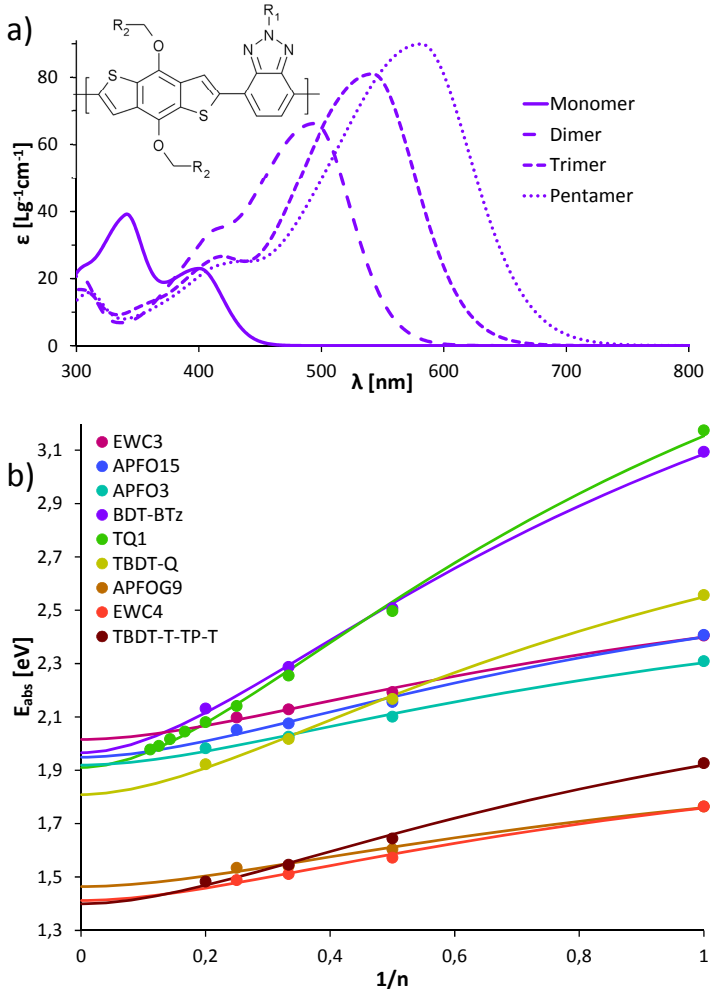

Figure 3.5. The calculated absorption spectra of BDT-BTz oligomers of 1, 2, 3, and 5 repeating units, obtained by adding an inhomogenous Gaussian broadening to calculated electronic transitions (a). Calculated first peak absorption energy E_{abs} *vs.* reciprocal oligomer size of the 9 polymers in Paper I (b). Lines are fitted to the data points according to Hückel MO theory as in Equation 3.1.

In Paper I, E_{abs} is calculated with TD-DFT on various oligomer sizes of 9 polymers, which are then fitted to Equation 3.1 using $\Delta\alpha$ and $\Sigma\beta$ as fitting parameters. The fits are very good for all polymers, and the results are presented as a function of 1/n in Figure 3.5b. The function appears linear for smaller

oligomer sizes, but saturates more quickly when approaching the polymer limit. The short repeating units of TQ1 and BDT-BTz lead to a stronger dependence of E_{abs} on n, since more repeating units are needed for the same conjugation length, compared to *e.g.* the APFO-G9 polymer[156] with a much larger repeating unit.

As mentioned in Chapter 3.3, the minimum energy conformation of polymers is typically studied in standard QC calculations. However, this would represent reality only at absolute zero temperature. At any finite temperature, a polymer ensemble in solution will exhibit a distribution of conformations, which on average is less planar than the optimized structures.[157,158] This makes calculations overestimate the planarity and conjugation,[159] leading to frequently underestimated E_{abs} in calculations.[126,128] The stochastic distribution of conformations induces an experimental "effective conjugation length", meaning the expected extension of the conjugation, as a function of the coplanarity between units. The effective conjugation length in solution at room temperature is commonly between 2–10 repeating units, depending on the length of the unit.[160–162] The effective conjugation length can be estimated as the oligomer size whose calculated absorption matches the experimental polymer absorption. The temperature-induced conformation distribution is typically inhomogeneous, *i.e.* a larger part of the polymer ensemble is on the planar side of the range of conformations since this is energetically favored, while fewer molecules adopt more twisted, higher-energy conformations. Since more planar conformations have lower associated E_{abs}, the absorption peaks of conjugated polymers typically exhibit inhomogeneous broadening, decaying more steeply towards lower energies than higher, seen *e.g.* for P3HT in Figure 3.1 and for TQ1 in Figure 4.3.

In Paper I the underestimation of E_{abs} in calculations based on optimized geometries is found to be highly systematic for the 9 studied polymers, amounting to 0.35±0.04 eV (excluding the TQ1 polymer). The TQ1 polymer shows a smaller E_{abs} underestimation by virtue of its special structural properties as presented in Chapter 4. The systematic trend is explained by the analogous nature of the backbone structures in the different polymers, with similar degrees of twisting in experiments. We introduce a simple empirical correction in Paper I by adding 0.32 eV (including TQ1 in the test set) to the calculated, extrapolated E_{abs}, which then show good agreement with the experimental results. This correction is also used in Paper VI, providing an independent validation of its applicability. Part of the ~0.32 eV underestimation can be compensated for, by including explicit temperature-dependent conformational effects, see Chapter 5, whereas the remainder is mainly attributed to limitations in the DFT functional.

3.5.2 Absorption Strength

Efficient harvesting of the solar light requires suitable absorption energy, but also high absorption strength, meaning high probability that a photon will be absorbed

when hitting the material. The molecular property that determines the absorption strength is the oscillator strength f which can be calculated with TD-DFT or other computational methods. This translates approximately to the macroscopic observable molar absorption coefficient ε according to[163]:

$$f = \frac{4ln(10)m_e c\varepsilon_0}{N_A q_e^2} \times \int \varepsilon(\nu) d\nu \qquad (3.2)$$

Here, m_e and q_e are the electron mass and charge, ε_0 is the vacuum permittivity, N_A is the Avogadro number, and ν is the light frequency. This equation is used for the absorption coefficients in Figure 3.5a above. Increasing the amount of absorbed light can be accomplished by simply making a thicker film, but in addition to increasing the material cost, this would hamper the charge extraction, so a strong absorption per unit volume, *i.e.* strong specific absorption, is the most relevant property for OPVs. Since most D–A polymers have highly similar densities around 1 kg/dm^3, this corresponds to strong absorption per unit weight, or specific absorption strength. Dividing both sides of Equation 3.2 with the molecular mass provides a relation between the specific oscillator strength F_M and the experimental mass absorption coefficients, permitting direct comparisons between experiment and calculation. Importantly, the alkyl side-chains mentioned in Chapter 3.3 do not contribute to the absorption, and are thus "dead weight". So while they are necessary for solubility, making them larger will diminish the F_M.

The calculated F_M increases linearly as a function of reciprocal number of repeating units in oligomers,[164] permitting extrapolation to $1/n \rightarrow 0$, analogously to the E_{abs} extrapolation. After extrapolation, the calculated F_M of the 9 polymers in Paper I exhibit a systematic overestimation of absorption strengths by a factor 1.65. As with absorption energies, this is rationalized from the zero-temperature calculations yielding over-idealized geometries with too strong conjugation, positively affecting the absorption strength. In further analogy to the E_{abs}, we introduce in Paper I a simple empirical correction by simply dividing calculated, extrapolated F_M values by 1.65, which then show dramatically improved agreement with experiments.

Translating experimental absorption peaks to F_M values is simply a matter of integrating the absorption coefficients numerically, *e.g.* by means of the trapezoidal rule as done in Paper I, and multiplying with the constants of Equation 3.2. Simulating absorption spectra from calculated oscillator strengths however, require some assumption of the shape of the peak. Commonly, calculated transitions are broadened with an applied Gaussian function, but its width must either be known from experiments or arbitrarily guessed, diminishing the predictive power of calculated spectra. Furthermore, the experimental peaks are generally inhomogeneously broadened due to unresolved vibronic progression and uneven distribution of conformations, as discussed in Chapter 3.5.1 and 2.3. The calculated spectra herein are, unless otherwise noted, simulated using two half Gaussians with a full-width-at-half-maximum (FWHM) of 5333.3 cm^{-1} of the high

energy half, and a 2666.7 cm^{-1} of the low energy half Gaussian, resulting in a total FWHM of 4000 cm^{-1} ≈ 0.5 eV and an inhomogeneity factor of 2.

3.5.3 Light-Harvesting Capability

As outlined in Chapter 1.2.3, the efficiency of OPVs is determined by the short circuit current J_{SC}, the open circuit voltage V_{OC} and the fill factor (FF). Of these, the J_{SC} has been found to be the best predictor to the final efficiency of the solar cell,[40] and it is largely determined by the light-harvesting capability of the polymer. The combined consideration of absorption energy and specific absorption strength gives an indication of the total light-harvesting capability of polymers, where a small but balanced E_{abs} and a large F_M is desired. In Figure 3.6 the F_M of the 9 polymers from Paper I are plotted against E_{abs}, both as experimental and as calculated and empirically corrected. In addition to showing the good accuracy of the corrected calculations (except for TQ1), Figure 3.6 demonstrates that none of the investigated polymers show simultaneous small band gap and strong absorption.

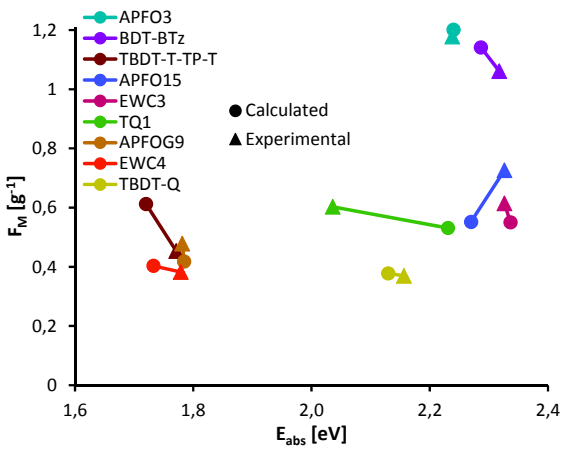

Figure 3.6. Specific absorption strengh F_M *vs.* absorption energy E_{abs} for the 9 polymers in Paper I, experimental and as calculated including an empirical correction.

The APFO-3 polymer is the strongest absorber in Paper I, showing a very high solution ε_{max} of 80 L g^{-1} cm^{-1}, having resulted in PCEs of 4.2% in OPV devices,[165,166] impressive at the time. APFO-G9 has a more ideal band gap, but its modest PCE of 2.3% is limited by its weak absorption and also by an unfavorably deep polymer LUMO energy,[156] hampering electron injection into the fullerene. TQ1 has been applied in OPVs with over 7% efficiency, attributed to ordering and morphological effects rather than superior light-harvesting;[134,167] read more in Chapter 4. Several polymers in subsequent papers display better light-harvesting

properties, as experimentally confirmed for PTI-1 in Paper V,[168] and P3TQTI-F in Paper VII, and as computationally predicted for several polymers in papers II and VI. The most efficient D–A polymers in the literature with PCEs ≥ 9.5%: PffBT4T-2OD,[41] PBDT-TS1,[140] and PTB7-DT,[42] all show strong absorption with peak E_{abs} around 1.7 eV.

The discussion so far in this chapter has revolved around the first peak optical properties, in terms of absorption energy and strength. Reliable computational predictions of these properties are certainly useful as the first peak typically is the strongest, and the excess energy of higher excited states are not exploitable due to ultrafast relaxation to the first excited state, as discussed in Chapter 3.5.1. However, calculations of the full absorption spectra are even more valuable, and to accurately predict them is a stated goal of this thesis work. As demonstrated in the following chapters, this is to some degree accomplished, using the empirical corrections as outlined above.

3.6 Donor and Acceptor Strength

The optical and other properties of the copolymers are determined by the structure, as stated in Chapter 3.3. New D–A designs largely drive the development of more efficient OPV devices, but the design process is to a large extent trial-and-error based, where experimentalists have a qualitative, intuitive feeling of the properties of the D and A units, and how they will affect the copolymer properties. QC calculations are therefore valuable for a more detailed understanding of the structure–property relationship in D–A polymers, and can guide the design process through being able to provide more quantitative traits of the units, prior to the time-consuming synthesis and characterization.

Essentially, the copolymer properties can be derived from two sources: the properties of the constituent units, and the coupling between those units. This is illustrated well in Figure 3.5, where the former source is represented by the monomer (1/n=1) point, and the coupling is reflected by the slope of the fits; a strong coupling leads to a strong size-dependence of the absorption energy, and also of other properties. The same data points are presented in Figure 3.7, but with linear fits and a different X-axis. The X-axis here is the reciprocal molecular mass of the oligomer backbones, which reduces the bias that gives smaller repeating units a steeper slope in Figure 3.5. The resulting slopes in Figure 3.7 are steeper for BDT-BTz, TQ1, TBDT-Q, and TDBT-T-TP-T, which is rationalized from that the donors in these polymers are all terminated by five-membered rings, whereas the other 5 polymers all contain fluorene or carbazole in the donors, whose six-ring termination give their copolymers larger dihedral angles and thus weaker coupling. A small out-of-plane dihedral angle is associated with good conjugation, yielding stronger electronic coupling between units, as discussed in Chapter 3.3.

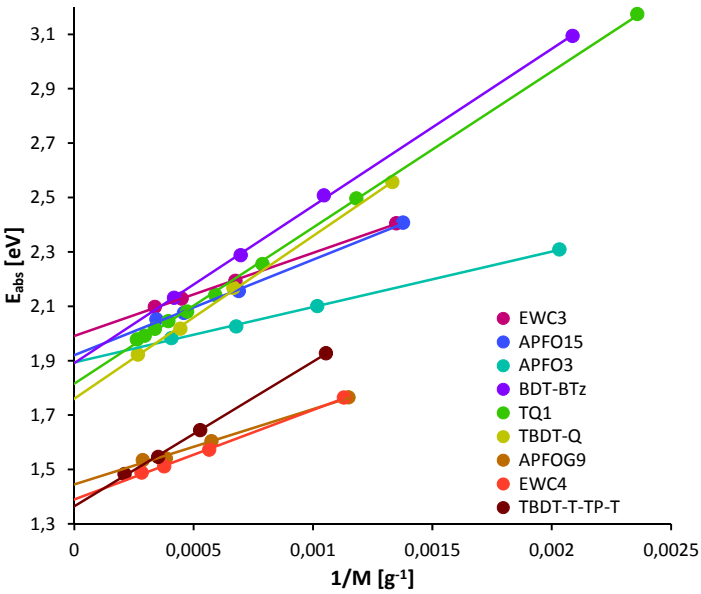

Figure 3.7. Calculated absorption energy *vs.* reciprocal molecular mass excluding side groups, for oligomers of 1–5 repeating units of the 9 polymers in Paper I.

Even though donor and acceptor units can be individually quite different, the electronic couplings between units are very similar, illustrated by the almost identical slopes within the two respective groups of copolymers of five-membered and six-membered ring donors in Figure 3.7. The similarity in coupling is exploited in Paper II, where 6 acceptors and 10 donors are studied, the donors all being five-ring terminated, see Figure 3.2.

In Paper II, we predict the optical and electronic properties of 60 D–A copolymers, both from calculations on the explicit D–A systems and from the calculated properties of the donors and acceptors individually, and use it to gain a quantitative understanding of the donor and acceptor strengths. More specifically, estimates of the HOMO and LUMO energies of the copolymers ($\langle {}^{D,A}E_{HOMO}\rangle$, $\langle {}^{D,A}E_{LUMO}\rangle$) are obtained as the weighted means of the HOMO and LUMO energies of the constituent units' homopolymers (${}^{D}E_{HOMO}$, ${}^{D}E_{LUMO}$, ${}^{A}E_{HOMO}$, and ${}^{A}E_{LUMO}$). The estimates compare favorably to the orbital energies as explicitly calculated on the copolymers (${}^{DA}E_{HOMO}$ and ${}^{DA}E_{LUMO}$), as seen in Figure 3.8a and 3.8b where they are grouped by acceptors. The HOMO estimates give an almost quantitative correlation across the 6 series, whereas the LUMOs show clear trends within the respective acceptor series but differ somewhat between acceptors. This is explained by the partial localization of LUMOs on the acceptor units for these and other D–A copolymers, while HOMOs tend to delocalize completely, see Figure 3.4.

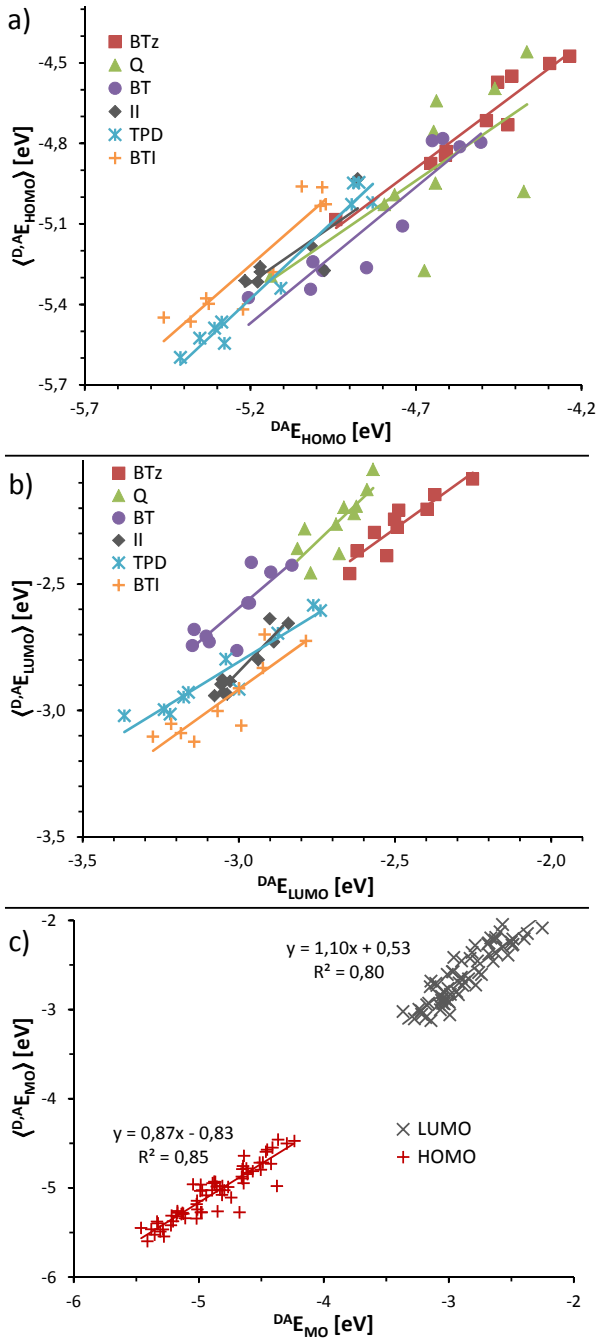

Figure 3.8. Calculated E_{HOMO} as the weighted mean of the constituent homopolymers *vs.* as directly calculated for the copolymer (a). E_{LUMO} as the weighted mean of the constituent homopolymers *vs.* as directly calculated for the copolymer (b). All frontier orbital energies, as weighted means *vs.* as calculated for the copolymers (c).

The estimation of D–A copolymer properties from calculations on only donor and acceptor homopolymers permits predictions with vastly improved scaling. With 5 donors and 5 acceptors, the orbital energies of 25 copolymer combinations can be estimated, while with 100 donors and 100 acceptors, 10000 combinations exist, constituting a quadratic scaling with number of units. Some precision is lost in the estimates, so this procedure is best suited as part of a screening process, where copolymer combinations with promising properties proceed to more refined analysis, while discarding those with *e.g.* discouragingly large band gap or unsuitable LUMO alignment *vs.* the fullerene.

The correlation between the frontier orbital energies of the donor and acceptor unit homopolymers and their copolymers also permits an assessment of the strength of the units from their homopolymer properties. In Paper II, we use the donor homopolymer ${}^{D}E_{HOMO}$ to quantify the donor strength, defined as the propensity to induce a small band gap in a D–A copolymer. Analogously, the acceptor-homopolymer ${}^{A}E_{LUMO}$ quantifies the strength of that acceptor, where a deep acceptor LUMO correlates with small copolymer band gap. Based on this measure, the donors are sorted by strength in the left hand side of Figure 3.9, where cyclopentadithiophene (CDT) and dithienopyrrole (DTPy) emerge as the strongest of the donors in Paper II, while OBDT is the weakest. Analogously for the acceptors in the right hand side of Figure 3.9, BTI and BTz are the strongest and weakest acceptors, respectively.

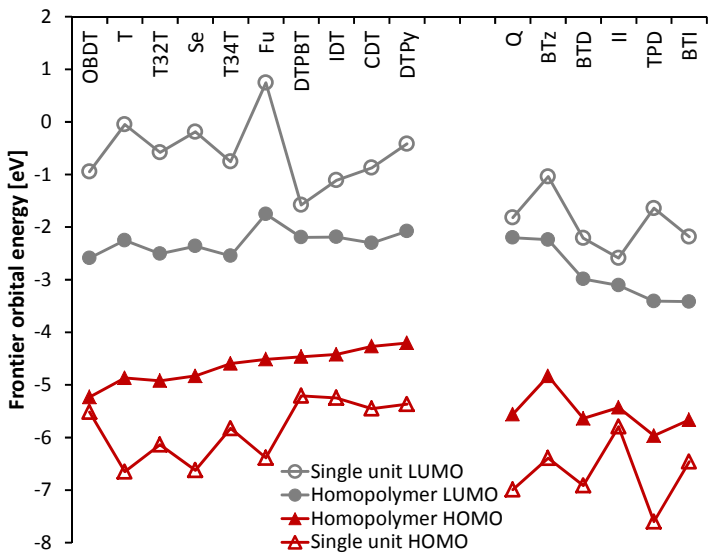

Figure 3.9. The frontier orbital energies of the single units and of the homopolymers. The latter quantifies the strength of the unit.

The above defined strength of the units relates to the E_{abs} of their D–A copolymers, but according to the results of Paper II also correlates somewhat with

the copolymer absorption intensity. The stronger donors tend to promote more intense absorption in their copolymers, whereas the inverse relation is found for the six acceptors, for which a small D–A band gap is associated with weaker absorption. This indicates that when designing D–A copolymers, strong donors are favorable both for narrowing the band gap and increasing the absorption strength, whereas the choice of optimal acceptor is less straight-forward, requiring consideration of other factors such as the polymer–fullerene weight ratio and the active layer thickness.

4. The TQ1 Polymer

The TQ1 polymer is named for its thiophene (T) donor and quinoxaline (Q) acceptor, and was first published in 2010, showing a then state of the art PCE of 6% in OPV devices.[134] By virtue of its excellent photovoltaic properties, rather simple design, and ease of manufacture, it has subsequently been comprehensively investigated;[122,169–173] as of May 2015, a search on Google Scholar on '"TQ1" conjugated polymer thiophene quinoxaline OPV' generates 84 scientific articles, books, and theses. Through the use of processing additives, an improved morphology control permitted an improved PCE of 7.08% in TQ1-based OPVs.[167] Several studies of TQ1 utilizing computational methods have also been published,[167,174–176] in addition to Papers I, III and IV herein, demonstrating the power of calculations to rationalize many experimentally observed properties in this auspicious polymer. In this chapter are presented the DFT-calculated structural, optical, and electronic properties of TQ1, contributing to the understanding of its success through insight of the molecular level traits.

4.1 Structural Properties

As discussed in detail in Chapter 3, the conjugated backbones of D–A polymers largely determine their optical and electronic traits, and usually also the structural properties, whereas the side-groups are typically present in experiments for solubility reasons. In Paper III however, we find that in the TQ1 polymer, a favorable position of the phenyl side-groups in adjacent units permit them to form an attractive stacking in the cis conformation, see Figure 4.1. The calculated TQ1 side-group phenyl–phenyl distance of 3.5 Å agrees with typical π–π interaction distances of 3.4–4.1 Å.[177,178] The stacking promotes a unique helical minimum-energy conformation, visualized for the nonamer in Figure 4.1.

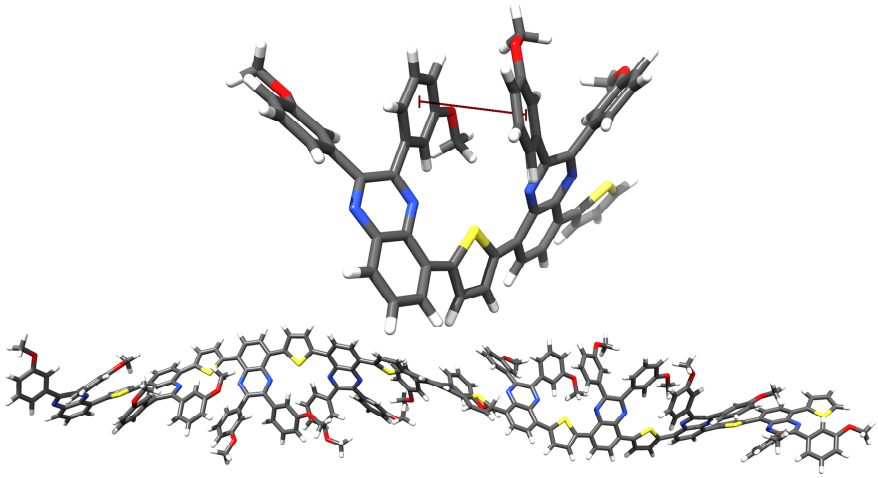

Figure 4.1. Optimized TQ1 dimer and nonamer (2 and 9 repeating units), showing the attractive stacking interaction between phenyl groups on adjacent repeating units, inducing a helical optimum geometry.

Although normally not taken under much consideration in the design of conjugated polymers, non-bonded interactions are in a few cases reported to strongly influence the backbone conformation D–A polymers.[179–181] These effects are of enormous importance in nature, being a fundament for the structure of DNA and certain proteins.[182–184] It is also of high relevance for the development of pharmaceuticals, with respect to protein–ligand interactions.[185] In larger-scale calculations, *e.g.* with (semi)-empirical force-fields, attractive dispersion terms are typically included as Lennard-Jones potentials with attractions scaling as r^{-6} to the distance between particles.[1,186] However, describing such interactions with quantum chemical methods can be challenging, as briefly discussed in Chapter 2.2.8. While attractive dispersion forces are captured by some high-level QC methods with accurate electron correlation descriptions such as coupled cluster methods, they are generally omitted in DFT.[187] To remedy this, DFT functionals have been developed that include some dispersion description, often empirically.[188–191]

In Paper III, we used the ωB97XD[71] functional with an empirical dispersion description, as well as a larger basis set, to more accurately quantify the implication of the stacking interaction on the potential energy landscape of TQ1. In Figure 4.2a, the potential energy as a function of rotation around the thiophene–quinoxaline torsion angle is plotted in the TQ1b variant without phenyl side-groups. It demonstrates the sensitivity to QC method and solvation of both the optimum dihedral angle and the rotation barrier between the cis (10–30°) and trans (140–150°) conformations. For the TQ1 dimer, when including the phenyl side-groups and their potential stacking interaction, the difference between the dispersion-including ωB97XD and the standard hybrid PBE0 functionals is

heightened, see Figure 4.2b. While the PBE0 results show almost no cis–trans preference, the ωB97XD functional assigns the cis conformation as more stable by up to 30 kJ/mol per repeating unit. The stacking cis-conformation is less planar than the trans-conformation and thus less favorable from a pure conjugation-perspective. The fact that the cis-conformation is still more stable overall, confirms that the geometric structure is determined by the attractive side-group interactions rather than the backbone for this particular polymer. However, it is important to note that these calculations are performed at 0 K with an implicit solvent and without alkyl side-chains. Effects of explicit solvent molecules and finite temperatures, as present in experiments, will complicate the situation, influencing the conformational characteristics to the point where an experimental ensemble of TQ1 polymers at the very least is expected to contain some polymers in the trans-conformation.

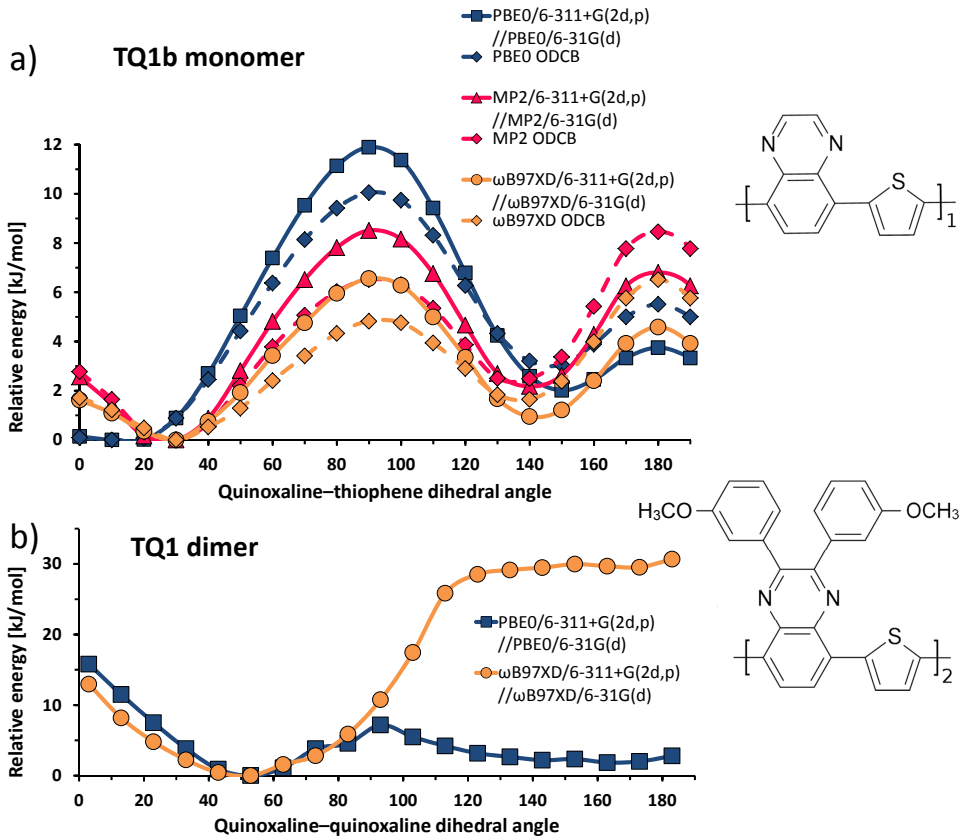

Figure 4.2. Relative system energy as a function of dihedral angle between quinoxaline and thiophene in the TQ1b monomer, calculated with two DFT functionals and the wavefunction method MP2, with and without a continuum *ortho*-dichlorobenzene (ODCB) solvent (a). System energy as a function of dihedral angle between the two quinoxaline units in the TQ1 dimer, calculated with PBE0 and ωB97XD (b).

4.2 Optical Properties

In Figure 3.6, TQ1 stands out among 9 polymers as the one where calculations do not agree with experiments. However, the comparison there is done with empirically corrected computational results, and actually TQ1 is the one polymer whose uncorrected, calculated E_{abs} shows the smallest underestimation: only 0.13 eV, compared to around 0.35 eV for the other 8 polymers. This is attributed to that the optimized, minimum-energy conformation of TQ1 is closer than other polymers to its experimental average conformation, due to the interacting side-groups partially preventing the conformational redistribution typically seen for other polymers at finite temperatures.

The calculated peak E_{abs} of TQ1 is 1.91 eV, as extrapolated from oligomer calculations as per Figure 3.5. This compares well to the experimental E_{abs} of 2.04 eV in experiments, although being slightly lower. The calculated tetramer and pentamer (4 and 5 repeating units) conversely, show slightly shorter peak wavelengths (λ_{max}) of 576 and 595 nm than the experimental 609 nm, as seen in the absorption spectra in Figure 4.3. This indicates that a size of ~5 repeating units corresponds to the experimental effective conjugation length, further corroborated by the excellent agreement in absorption coefficients, which however is partly attributed to fortuitous cancellations of error. The corresponding first electronic transition is of HOMO→LUMO character, as for most D–A polymers. This transition shows rather modest strength compared to the other polymers in Paper I, leading to a maximum absorption coefficient ε_{max} of < 40 $Lg^{-1}cm^{-1}$.

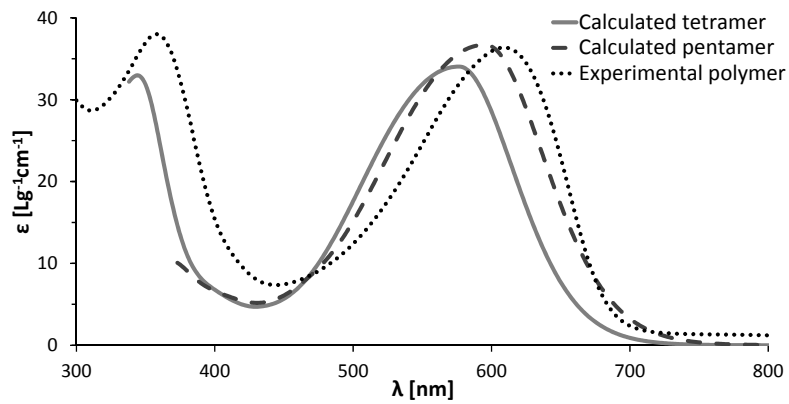

Figure 4.3. TQ1 absorption spectra, as calculated for the tetra- and pentamers, and as experimentally recorded for the polymer. Due to computational limitations, the pentamer calculation only covers the absorption > 380 nm.

The experimental emission spectrum of a neat TQ1 film, as recorded with electroluminescence measurements, peaks at 715 nm.[192] This results in a Stokes-

shift of 0.30 eV, taken as the difference in energy between the maximum absorption and maximum emission, since neither the experimental emission nor absorption spectra show resolved vibronic features. This compares reasonably with the calculated Stokes-shift of a TQ1 trimer of 0.38 eV, and an even better agreement is obtained if represented as a difference in λ_{max}: 106 nm in experiments *vs.* 111 nm in calculations. More interestingly, this 0.3 eV Stokes-shift is smaller than for many other conjugated polymers, with reported Stokes-shifts typically exceeding 0.4,[193–196] and reaching up to 0.9 eV.[197] This implies that the typical planarization of the polymer backbone in the excited state,[198–200] responsible for the red-shifting of the emission, is less pronounced for TQ1. This is coherent with the notion that the TQ1 geometry is not primarily determined by the conjugated backbone, as discussed in Chapter 4.1.

4.3 Electronic Properties

Despite the light-harvesting properties of TQ1 not being ideal, OPV efficiencies with this polymer have reached 7.08%, partly attributed to a macroscopically favorable morphology.[167] The molecular level structural ordering, as predicted in Paper III, is also beneficial for the functioning in solar cells, promoting high intramolecular mobility of excitons and charge carriers. The excellent delocalization of the frontier orbitals is visualized for the TQ1 nonamer in Figure 4.4. This is a result of that the total system energy increases sharply for more twisted geometries than the optimum. The side group attractions thus "lock" the polymer chain to a structure of extended conjugation. This demonstrates that molecular design assisted by QC calculations can promote favorable intramolecular structural ordering, while the larger-scale intermolecular ordering is generally out of reach for these methods.

Figure 4.4 also shows the electron density difference between the ground state and the first excited state, demonstrating some CT character from donor to acceptor unit. Furthermore, it also shows that electrons move from formal double bonds to formal single bonds, an effect reported also in Paper I for other polymers, explaining the previously mentioned planarization of the excited state.

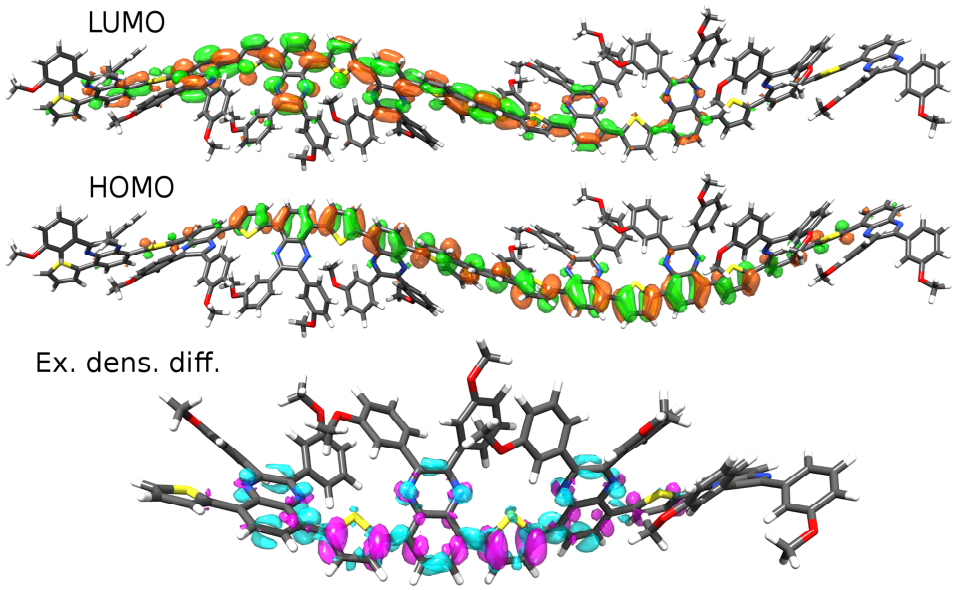

Figure 4.4. Calculated TQ1 nonamer HOMO and LUMO, demonstrating an extended delocalization of both orbitals. The first excited state electron density difference for the TQ1 tetramer, with electrons moving from purple to turquise upon excitation, indicates the CT from donor to acceptor.

As per the working mechanism of OPVs, delineated in Chapter 1.2.2, it is important that the conjugated polymer has a high hole mobility. This is warranted by the typically good delocalization of HOMO, the orbital through which hole transport mainly occurs, as displayed for TQ1 in Figure 4.4 and discussed for D–A polymers in general in Chapter 3.4. The electron mobility of the polymer has less direct impact in polymer–fullerene OPV applications, but is relevant for other applications such as organic transistors,[201] diodes,[202] or in the electron-accepting polymer in polymer–polymer OPVs.[203] The electron mobilities are often lower, rationalized from the generally more localized LUMOs through which electron transport mainly occurs, as discussed in Chapter 3.4. In TQ1 however, a very short donor unit confers spatially near-lying acceptor LUMOs, promoting a delocalization of also the copolymer LUMO, as seen in Figure 4.4. As a result of this, high TQ1 film mobilities of over 10^{-4} $cm^2V^{-1}s^{-1}$ for both holes and electrons are seen in the field effect transistor measurements carried out in Paper IV.

Another important finding in Paper IV is that while hole mobilities show an expected increase with temperature, the electron mobilities start decreasing around room temperature, far below the glass transition temperature. This is rationalized from the fact that higher temperatures entail more twisted polymer conformations, which break the LUMO delocalization. The HOMO conversely, is delocalized for any conformation; see Figure 4.5 where HOMO and LUMO for three representative conformations of the TQ1 dimer are plotted. This is anticipated to

provide reliable hole transport for the wide range of polymer conformations that are present in the disordered films in OPVs, being highly beneficial for the generation of photocurrent. In the following chapter, a more refined, quantitative analysis of the temperature dependence of structural, electronic, and optical properties is presented.

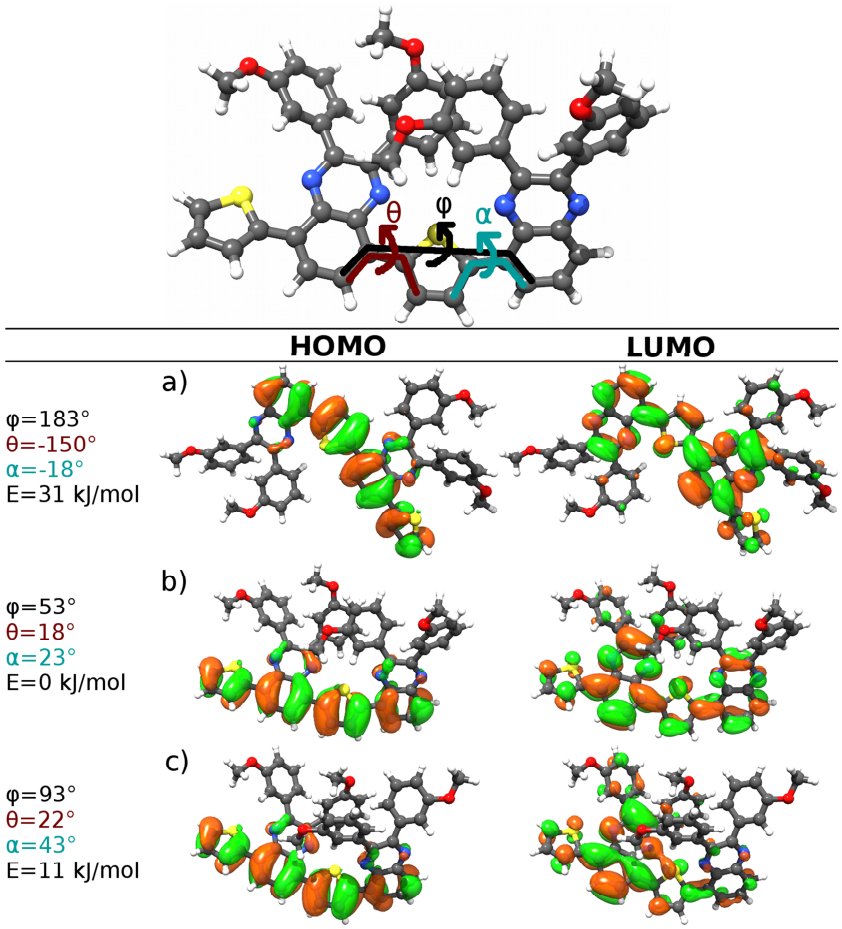

Figure 4.5. TQ1 dimer frontier orbitals for three representative geometries, showing respectively good (a), decent (b), and poor LUMO delocalization (c). HOMO is delocalized in all cases, and energies are relative to the minimum energy conformation, as calculated at the ωB97XD/6-311+G(2d,p)//6-31G(d,p) level of theory. System energies are relative to the minimum energy conformation.

5. Temperature-Dependent Properties

5.1 Planarity and Conjugation

As discussed on a qualitative level in Chapter 4.3 for the TQ1 polymer, temperature affects the planarity of the polymer backbone, critical for the degree of conjugation. Temperature is an important parameter for classical molecular dynamics and certain other calculations, but does not enter explicitly in standard QC calculations. It can however be studied implicitly, by exploring the structural energy landscape and inferring the possible effects of temperature. In lieu of an exhaustive investigation of all structural modes, the rotation around the flexible single bonds between units is studied in Paper V for a number of D–A polymers. This rotation, represented by the dihedral angle between units, is the geometric coordinate that most severely affects the crucial electronic and optical properties of conjugated systems for OPV applications. Furthermore, these rotations are more energetically accessible than other structural distortions.

The dependence on planarity of the optical properties is demonstrated in Figure 5.1, where the calculated oscillator strength f and absorption energy is plotted against the imposed dihedral angle between units for dimer models of the D–A polymers PTI-1 and APFO-3. The TD-DFT-calculated E_{abs} vary by up to 0.3 eV from a flat 180° geometry to a fully twisted 270° angle. The oscillator strength, which is directly proportional to the absorption coefficients, see Equation 3.2, demonstrates even greater sensitivity to planarity; the intensity is halved when going from planar to fully twisted angles.

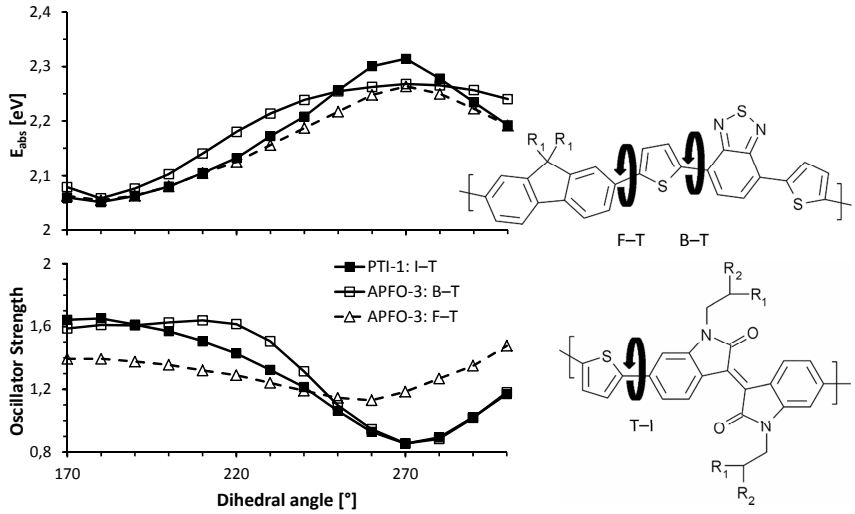

Figure 5.1. Calculated first transition absorption energy and oscillator strength *vs.* imposed T–I dihedral angle between units in a PTI-1 dimer, and for B–T and F–T angles in an APFO-3 dimer. The remaining coordinates are fully relaxed.

5.2 Temperature-Dependent Optical Spectra

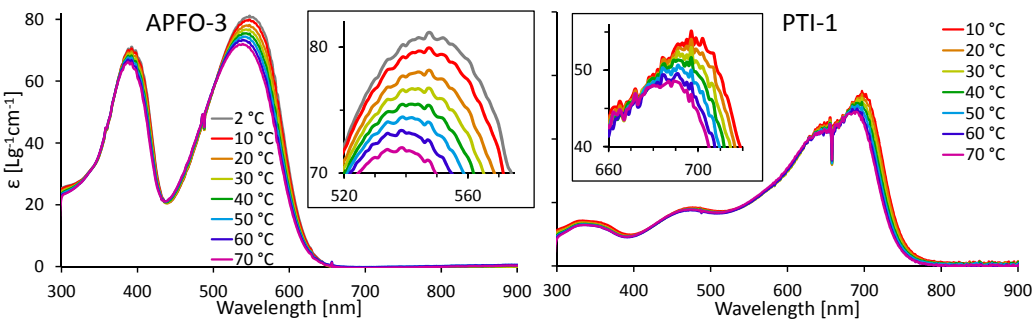

Figure 5.2. Experimental absorption spectra for two of the five investigated D–A polymers from Paper V at various temperatures. Insets depict the same spectra but zoomed in around the first respective peaks.

A polymer ensemble in solution will at a finite temperature adopt a range of conformations, whose exact distribution depends on the temperature. The various conformations, with varying degree of planarity, will also exhibit distinct spectral response. Wavelength shifts of up to 50 nm have been reported for temperature differences of up to 100°C.[134,204] Calculations however, are typically based on fully optimized structures, corresponding to a temperature of 0 K, leading to

frequently underestimated E_{abs}. The effect of temperature on optical properties is clearly visible in Figure 5.2, where experimentally recorded absorption spectra are plotted for a range of temperatures between 2 and 70 °C for two of the five investigated polymers of Paper V. In a clear and systematic trend, higher temperatures entail a blue-shifting and weakening of the first absorption peak, both being signs of diminished conjugation.

Nature strives to minimize the free energy G of a system, which consists of an enthalpy H and a temperature-dependent entropy S term:

$$G = H - TS \tag{5.1}$$

With increased temperature, the entropy gained from populating more different conformational states becomes more significant than the decrease in enthalpy from optimizing the geometry of the polymers. Since the minimum energy conformation is typically near-planar, the additional conformations permitted at higher temperatures will on average be more twisted, causing a decrease of the total average planarity of the polymer ensemble with increasing temperatures. Essentially the chain of dependences goes as follows: the temperature influences the conformations, which influences the electronic coupling and conjugation, in turn affecting the electronic properties, which determine the optical traits.

The distribution of conformations at any finite temperature is also part of the reason for the typically inhomogeneously broadened shape of D–A polymer absorption peaks, as discussed in Chapter 3.5.1. The most frequently occurring conformations are near planar, consequentially exhibiting stronger and more red-shifted absorption than more twisted conformations which are more uncommon and absorb more weakly at shorter wavelengths. Beyond the optical properties as studied here, the conformation distribution has further implications for processes in OPVs, in terms of *e.g.* CT state energies, charge carrier mobilities (typically increasing with temperature), electron-transfer, *etc*. Understanding and quantifying these effects is important for the development of OPV applications, since most reported OPV efficiencies are limited to room temperature, whereas their operating conditions can surpass 60 °C.[205]

5.3 Boltzmann-Distribution of Conformations

The significant temperature dependence of the optical properties highlights the precariousness of the common practice of comparing experimental properties to those calculated at 0 K, *i.e.* with fully optimized structures only, as briefly discussed in Chapter 3.5. By conversely accounting for these effects in the computational approach, much more accurate calculated predictions of properties are possible. Furthermore, it facilitates a decomposition of the discrepancies in

conditions between experiments and calculations, permitting more thorough assessment of *e.g.* the DFT functional and solvent model.

In Paper V, a strategy to implicitly include these thermal effects and quantify their influence on the optical properties is presented. The torsional modes around the single bonds between units are of low energy compared to other conformational modes, with shallow wells around the slightly out-of-plane energy minima. As a model system for the rotations between two conjugated rings, the biphenyl molecule has a reported optimized dihedral angle of 41–49° with various wave function methods including coupled cluster,[206] while a slightly more planar optimum is calculated with the BP86 DFT functional.[207] The energy associated with complete planarization is 11.2 kJ/mol with at the CCSD(T)/cc-pVDZ level of theory and 6.7 kJ/mol with BP86/TZ2P, while the energies for fully twisted 90° angles are 6.3 and 10.3 kJ/mol with the two methods.[206,207] The almost inverted numbers for the two methods demonstrates the common tendency for DFT to overestimate conjugation and thus planarization, as mentioned in Chapter 2.2.8.

Rather shallow, wide potential energy wells for the rotation between units is seen in the potential energy surfaces (PES) over the dihedral angle coordinate for APFO-3 and PTI-1, plotted in Figure 5.3. Compared to biphenyl, the optimum angles here are closer to the planar 0 or 180° due to less steric repulsion between hydrogen atoms on neighboring units as a result of the thiophene units. Due to their chemical similarity, the F–T and T–I bonds exhibit practically identical PESs.

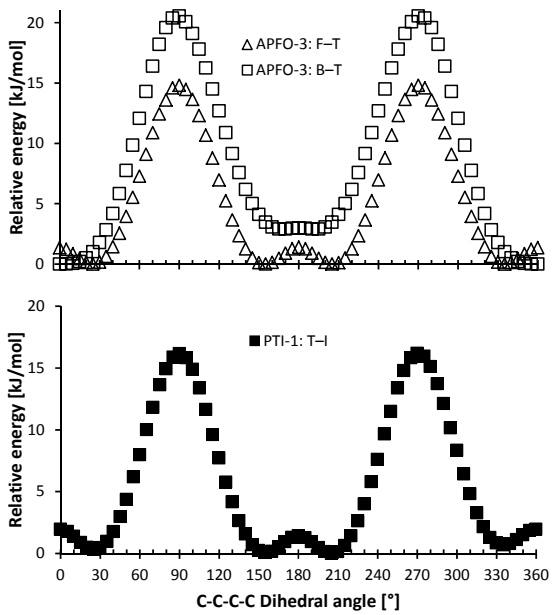

Figure 5.3. Potential energy surfaces over the dihedral angles between units in APFO-3 and PTI-1 monomers, with energies relative to the minimum within the series. Calculated with the PBE0 DFT functional.

According to Boltzmann statistics, the probability for a polymer to adopt a certain geometry depends on the free energy of that conformation relative to the minimum energy conformation, and also on the temperature:

$$P = e^{-\Delta G/RT} \tag{5.2}$$

As a result, in a hypothetical system of two allowed conformations at 25 °C, a conformation 4 kJ/mol higher than the lowest energy conformation has a 20% probability to be populated. This example shows that a wide region of dihedral angles in PTI-1 and APFO-3 can significantly contribute to the conformations of a room-temperature polymer ensemble.

Under the assumption that the torsion between units is the only relevant geometric coordinate and that the monomer PES is representative also for longer oligomers, the relative energies presented in Figure 5.3 can be applied in Equation 5.2 to predict the probability of a certain dihedral angle in the polymers. The QC calculations give only the enthalpy part of the free energy, and we here neglect the explicit entropy since it is expected to be practically equivalent for the different conformations of the single molecules. This provides a probability distribution of dihedral angles, which in Paper V is used to construct ensembles of oligomers, with dihedrals chosen stochastically but according to the Boltzmann probability. For the two polymers APFO-3 and PTI-1, for each oligomer size of 1–5 repeating units, and for two temperatures of 293 and 343 K, 10 sample systems were created with imposed dihedral angles, as chosen stochastically according to their probability distribution. After relaxing the remaining geometric coordinates, the in total 200 systems (2 polymers × 2 temperatures × 5 oligomer sizes × 10 samples) proceeded to a TD-DFT calculation of their optical properties. As expected, the samples with larger dihedral angles exhibit lower f and larger E_{abs}, and when convoluted, the spectra of the oligomer ensembles are weakened and blueshifted compared to the corresponding optimized, 0 K oligomers, as exemplified with the PTI-1 pentamer in Figure 5.4a. Extrapolation procedures, as described in Chapter 3.5.1 and 3.5.2 for the absorption energy and strength respectively, were carried out for the optical properties, and the 343 K PTI-1 oligomer ensemble ε_{max} extrapolation is as an example compared to the optimized oligomers in Figure 5.4b.

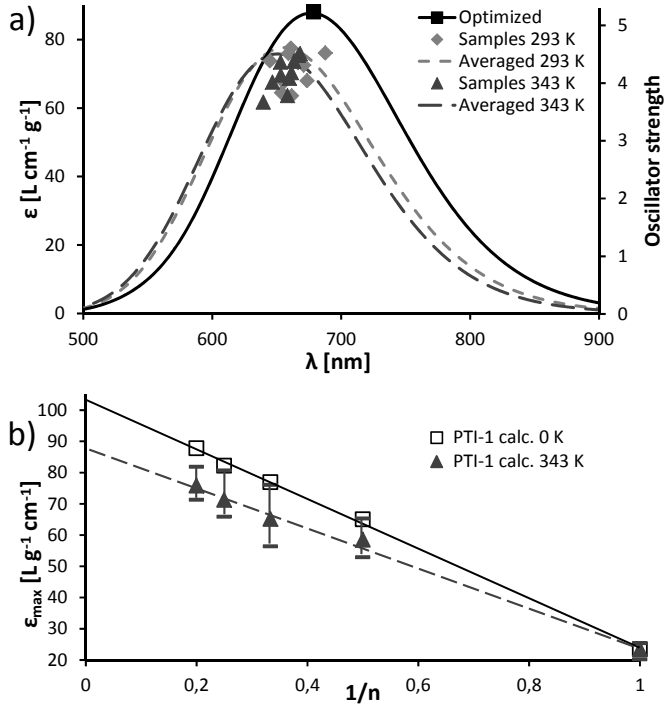

Figure 5.4. First excitation oscillator strength and wavelength of the PTI-1 pentamer at 0 K, and the 10 samples of PTI-1 pentamers at 293 and 343 K, as well as their corresponding absorption spectra, modeled by applying a homogeneous Gaussian broadening to each transition and averaging (a). Average, smallest, and largest calculated first peak maximum absorption coefficient for PTI-1 oligomer samples at 343 K, compared to optimized oligomers, corresponding to 0 K (b).

Extrapolation procedures such as exemplified in Figure 5.4b, was in Paper V carried out for E_{abs} and ε_{max} for APFO-3 and PTI-1 oligomers at 0, 293, and 343 K. The results were then compared to the corresponding experimental optical properties, as extracted from the spectra in Figure 5.2, and are plotted against temperature in Figure 5.5. Both polymers show good trend-wise agreement between calculations and experiments with respect to the temperature-dependence of both λ_{abs} and ε_{max}. The calculations still underestimate ε_{max}, although the underestimation is almost halved compared to the case of standard, 0 K calculations for both polymers. The calculated PTI-1 λ_{abs} is shorter than the first experimental peak, which is highly unusual for D–A polymers. However, the PTI-1 experimental absorption spectrum in Figure 5.2 shows a pronounced shoulder at around 650 nm, and since aggregation has been reported as an issue in isoindigo polymers,[208–211] we assign this shoulder as the single strand absorption, and the peak at ~700 nm as corresponding to an aggregated specie. Consequently, the calculated λ_{abs} should be compared to this shoulder, resulting in a picture more

consistent with other polymers. The temperature-including computational scheme introduced in Paper V reduces the underestimation of calculated E_{abs} at 293/343 K from 0.16 to 0.12/0.10 eV for PTI-1 and from 0.29 eV to 0.25/0.22 eV for APFO-3.

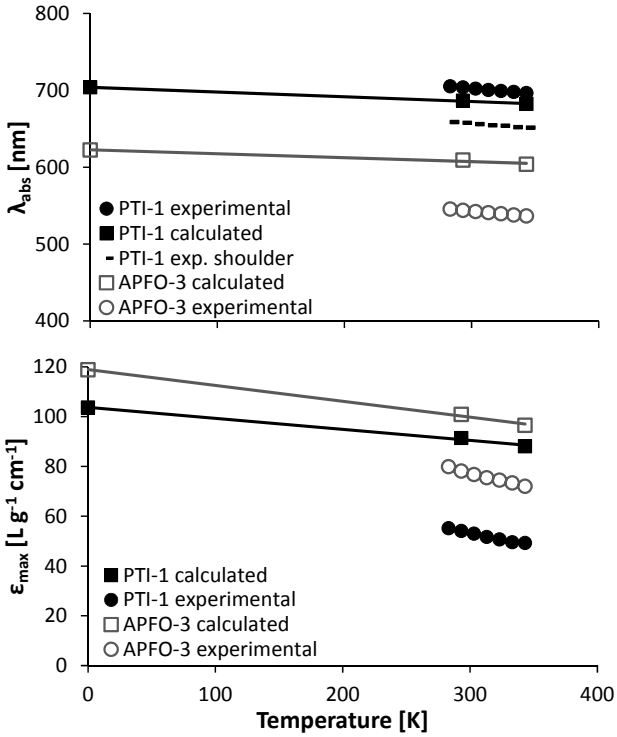

Figure 5.5. Temperature-dependent first peak absorption wavelengths and coefficients, as extrapolated from oligomer calculations including best linear fits, and as extracted from experimental absorption spectra.

The experimental temperature-dependences of the optical properties are reproduced trend-wise from the computational strategy in Paper V, permitting some conclusions to be drawn. In agreement with the results in Figure 5.1, the absorption strength is more sensitive to temperature and twisting than the absorption energy. By increasing the temperature 100 K, the absorption peak would shift ~15 nm, corresponding to less than 5% of the total absorption energy, whereas the absorption coefficients would decrease by ~12 $Lg^{-1}cm^{-1}$, corresponding to a ~15% drop.

The active inclusion of thermal effects allows their quantification, in turn permitting a decomposition of the sources of error between calculations and experiments. While this strategy improves the calculated predictions, there is a significant remaining discrepancy to experiments, which we primarily ascribe to

limitations in the standard hybrid DFT functional used: PBE0. Functionals with corrections for long-range electronic effects (LC functionals) could reduce the errors further, as they are known to reduce underestimations of E_{abs}. Lack of explicit description of the solvent molecules is another discrepancy which may be responsible for a smaller part of the error between the calculations and experiments. In Chapter 3.5 an empirical correction to calculated optical properties are used, which aims to correct for several of these shortcomings of standard QC. Applying the strategy to include temperature effects as per above, but with: a) larger sampling, b) LC functionals with less self-interaction error,[72,212] c) larger basis sets, especially for the PES calculations, and d) good implicit solvent models, is probable to yield greatly improved results compared to standard calculations based on fully optimized structures. This would substantially reduce the need for empirical corrections, as it has the potential to provide accurate yet feasible predictions of the light-harvesting capability of practically any D–A polymer candidate.

6. D–A_1–D–A_2 Polymers

6.1 Dual Peak Absorption

The success of D–A polymers during the last decade is mainly attributed to their smaller band gap and better light-harvesting compared to homopolymers, as discussed in Chapter 3.1. However, their absorption profile, typically dominated by a single peak centered somewhere between 500 and 1000 nm, still overlaps rather poorly with the wide solar emission spectrum. This is visualized in Figure 6.1 with two polymers from Paper II respectively representing narrow and wider band gap polymers. EWC3 fails to efficiently capture photons above ~600 nm, whereas APFO-G9 exhibits a wide region of negligible absorption between ~400–600 nm. Higher-energy peaks present in the spectra of both EWC3 and APFO-G9, as well as many other D–A polymers, generally have a maximum at around 300–400 nm where the solar emission is weak, thus not contributing significantly to the photocurrent.

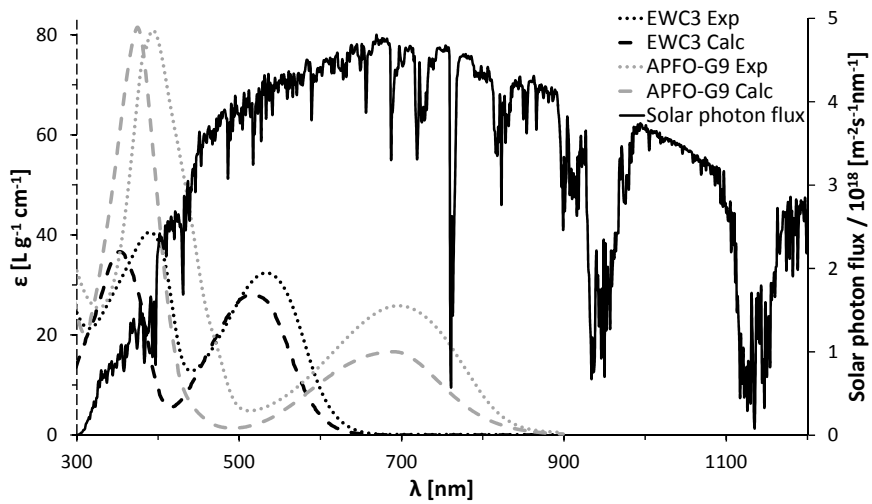

Figure 6.1. The solar emission spectrum, compared to the calculated and experimental absorption spectra of APFO-G9 and EWC3 from Paper II, representative of small and wider band-gap polymers respectively, demonstrating the typically lacking spectral coverage of D–A polymers. Solar flux spectrum taken from the National Renewable Energy Laboratory at rredc.nrel.gov/solar/spectra/am1.5

One possible approach to exploit a larger part of the solar emission, is to manufacture multijunction cells with two (tandem) or three subcells, having in the OPV case shown PCEs exceeding 11%.[213–215] These come however with a considerably increased complexity and cost of manufacture, reducing their feasibility for real-world applications. Another strategy to increase the spectral coverage of the active layer is to include more than one polymer, either in a binary (two-phase) polymer–polymer solar cell,[216,217] or a ternary (three-phase) solar cell with two polymers and a fullerene.[218,219] These two approaches have so far not been able to compete with the efficiency of standard polymer–fullerene cells due to increased difficulty in controlling the morphology and charge transport properties.

Various design motifs with more than one donor and one acceptor alternating along the backbone have been proposed, whose resulting electronic and optical properties have been exploited in attempts to maintain the favorable morphological and manufacturing properties of single junction polymer–fullerene OPVs, while absorbing over a wider spectral region.[220] The recently introduced $D–A_1–D–A_2$ design motif for conjugated polymers has shown promising characteristics in this respect, as a result of employing two acceptors with complementary optical properties.

In Paper VII, six $D–A_1–D–A_2$ polymers are experimentally investigated, with the best PCE of 7.0% reported for P3TQTI-F, a record for this type of polymer at the time of publication. The good efficiency and great J_{SC} of 15.5 mA cm^{-2} are attributed to an enhanced spectral coverage which originates in the capability of $D–A_1–D–A_2$ polymers to exhibit allowed electronic transitions from a delocalized HOMO to both LUMO and LUMO+1, residing respectively on the stronger and weaker acceptor. The two transitions are schematically visualized in Figure 6.2, along with the resulting, archetypal $D–A_1–D–A_2$ absorption spectrum with two peaks in the region of strong solar emission, *i.e.* $\lambda > 450$ nm.

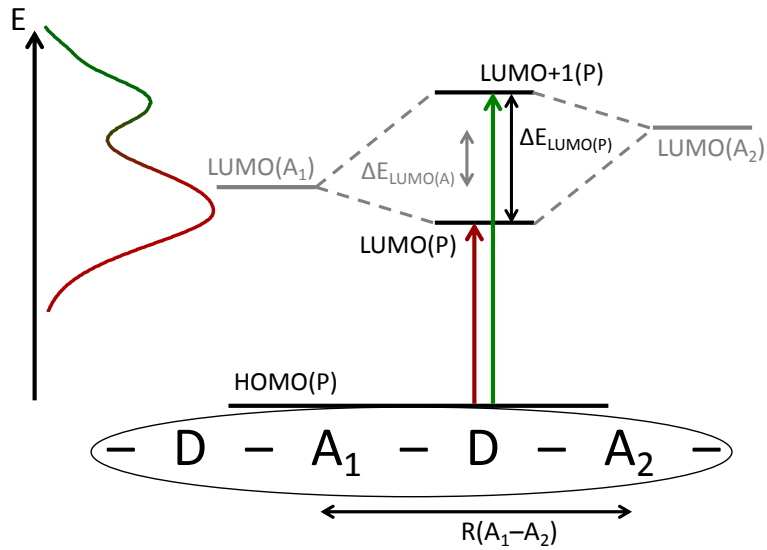

Figure 6.2. Schematic description of the energy levels and transitions in D–A_1–D–A_2 polymers.The LUMOs of the two acceptor units with an energy difference $\Delta E_{LUMO,A}$ interact, forming the copolymer LUMO and LUMO+1, whose energy gap $\Delta E_{LUMO,P}$ is larger than $\Delta E_{LUMO,A}$ by an amount that is determined by the strength of the interaction, in turn dependent on the spatial separation R(A_1–A_2). A better spectral coverage than for D–A polymers is obtained if electronic transitions to both LUMO and LUMO+1 are allowed.

6.2 Optical Properties

6.2.1 Predicted Absorption Spectra

In Paper VI, five D–A_1–D–A_2 polymers with known experimental absorption profiles were subject to calculations: P3TQTI-F and PTQTI[221] from Paper VII, and the previously unpublished PTIIBTzF, all three developed at Polymer Technology at Chalmers University, as well as PBTDPP and PBBTDPP from the literature.[146] Their calculated spectra were obtained using the empirical correction described in Chapters 3.5.1 and 3.5.2. It is based on the first peak absorption energies E_{abs} and mass absorption coefficients ε of oligomers, linearly extrapolated to 1/n→0:

$$\varepsilon_{corr}\left(E_{abs,corr}\right) = \frac{\varepsilon_{extrapol}\left(E_{abs,extrapol} + 0.32\ eV\right)}{1.6} \qquad (6.1)$$

The D–A_1–D–A_2 oligomer size whose uncorrected E_{abs} best matches $E_{abs,corr}$ had its calculated spectrum parallel-shifted so that its first peak E_{abs} matches $E_{abs,corr}$. The spectrum was then up-scaled or down-scaled so that first peak ε coincides with

ε_{corr}. In this manner, corrected, calculated spectra of the entire visible region can be produced in principle for any polymer. This is an important step towards accurate computational prediction of full absorption spectra, moving beyond simpler considerations of just the first absorption peak, while simultaneously not relying on direct comparisons between calculated oligomers and experimental polymers and hoping for cancellations of error.

Predicted spectra were obtained as per the above for the five polymers, and three of them are compared to their experimental spectra in Figure 6.3. The very good agreement in absorption energies, relative peak heights, and overall spectral shapes serves as independent validation of the empirical correction, and is very encouraging for the continued application of this strategy for predictions of absorption spectra.

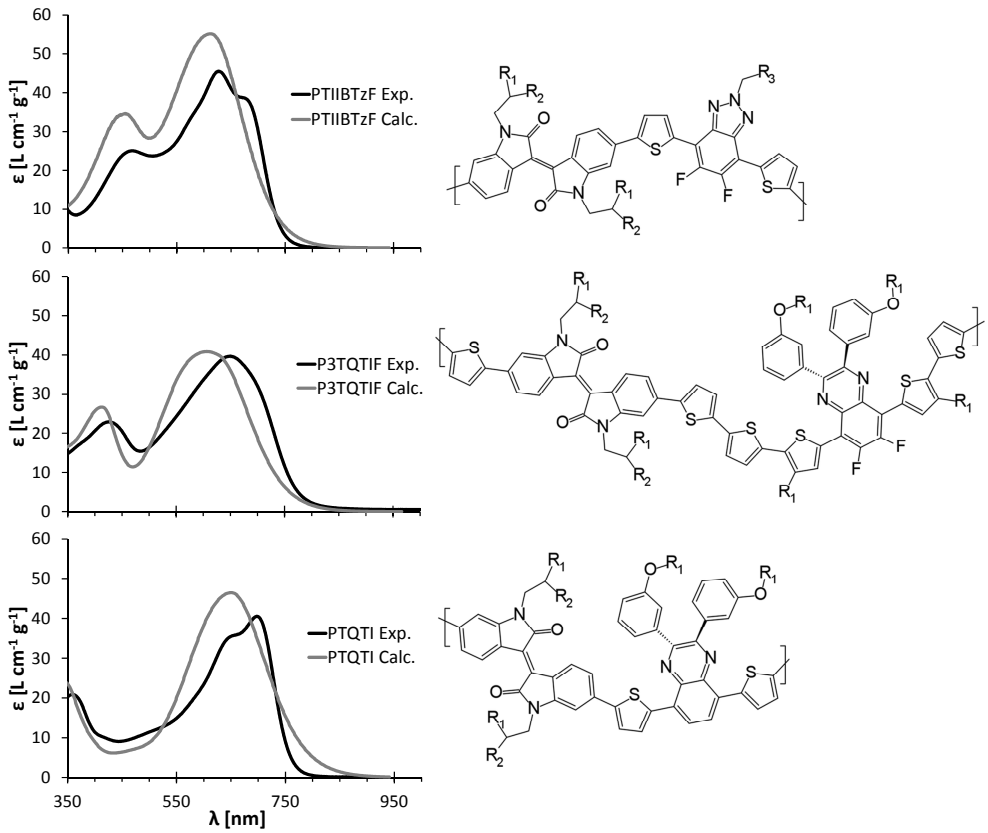

Figure 6.3. Chemical structures of three of the five D–A_1–D–A_2 polymers from Paper VI whose experimental absorption spectra are known, together with their calculated and experimental spectra. The sidegroups are R_1=1'octyl, R_2=1'-hexyl, and R_3=5'-undecyl.

The absorption spectra of both PBBTDPP (not shown here, see Paper VI) and PTIIBTzF, and to some extent PBTDPP (not shown here), exhibit clear dual-peak

character. The two peaks are revealed by calculations to correspond to transitions of dominantly HOMO→LUMO and HOMO→LUMO+1 character respectively, where LUMO mainly resides on the stronger acceptor and LUMO+1 on the weaker acceptor, in agreement with the D–A_1–D–A_2 concept described in Figure 6.2. All polymers except PTIIBTz exhibit weak peaks at around 350–400 nm, which correspond to transitions mainly within the donor segment, similar to the D–A polymer case as discussed in Chapter 3.5.1. Apart from this peak at wavelengths where the solar emission is weak, P3TQTIF has only one apparent absorption peak at lower energy. However, calculations reveal that two low-energy transitions are present in P3TQTIF too, but their energies are so similar that they are completely unresolved in the spectrum. Nevertheless, the existence of two transitions broadens the absorption and leads to better spectral coverage despite being unresolved. The orbitals involving the relevant transitions in P3TQTIF are presented in Figure 6.4. The Ii-centered LUMO and the quinoxaline-centered LUMO+1 are the target orbitals for the two strong but unresolved transitions at around 600 nm. LUMO+2, partly localized on the donor segment, is the main contributor to the weaker transition at around 400 nm. The delocalized HOMO is the origin orbital for all these three transitions in P3TQTIF. PTQTI is the only polymer exhibiting only one strong low-energy transition and consequently one absorption peak, the reasons for which can be found below.

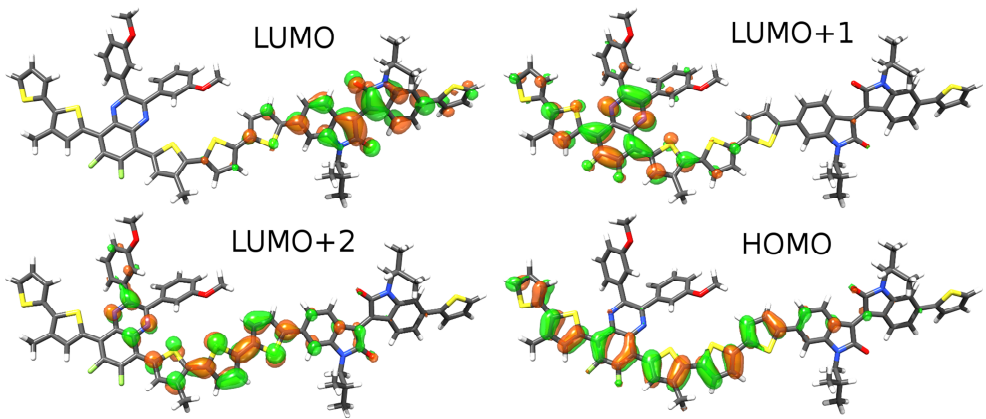

Figure 6.4. The monomer frontier orbitals for P3TQTIF, the main contributors to the strongest transitions and absorption peaks.

Encouraged by the good agreement to experiments, we applied the computational strategy for prediction of spectra on 10 new D–A_1–D–A_2 polymer candidates, for a more systematic investigation of the factors that determine the potential for double-peak absorption. The 10 polymers use 5 different two-acceptor combinations, with donors consisting of either a single thiophene unit or terthiophene, and their structures are visualized in Figure 6.5. The very weak BTz acceptor was chosen as the weaker acceptor in 8 of the copolymers to facilitate

good spectral separation of the transitions to LUMO and LUMO+1. Of the 10 D–A_1–D–A_2 polymers, 7 exhibit two clear low-energy peaks or a peak with a shoulder, all corresponding to HOMO→LUMO and HOMO→LUMO+1 transitions, with LUMO on the stronger acceptor and LUMO+1 on the weaker.

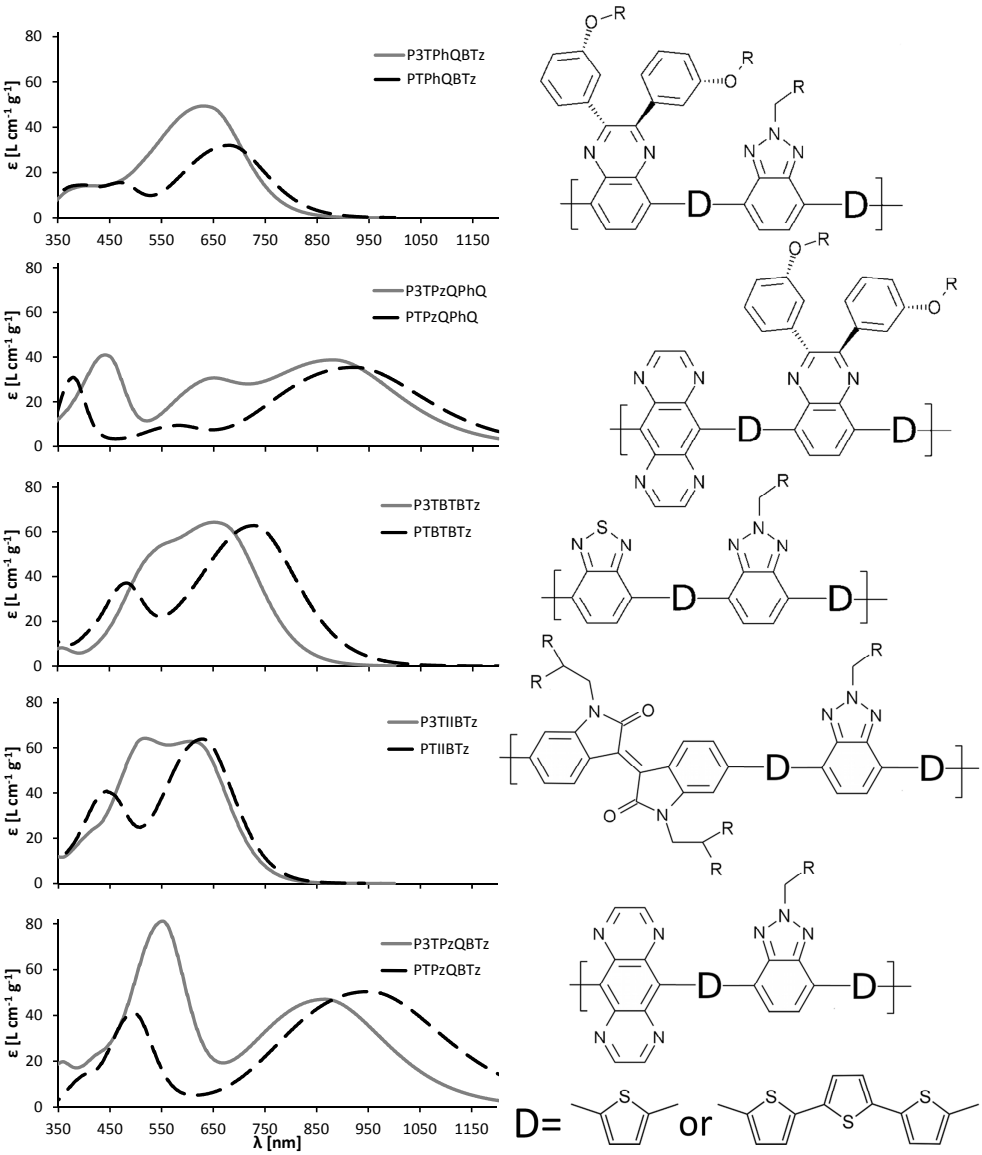

Figure 6.5. Chemical structures of the 10 D–A_1–D–A_2 polymer candidates from Paper VI, together with their calculated and empirically corrected absorption spectra. The donors (D) are either a single thiophene (T) or terthiophene (3T). The alkyl chains R are replaced by methyl groups in calculations.

6.2.2 Absorption Peak Energy

Just as for D–A polymers, the 10 D–A_1–D–A_2 polymers in Figure 6.5 show first absorption peak energies closely related to their HOMO–LUMO gap, where LUMO is mainly determined by the LUMO of the stronger acceptor. Thus, the four copolymers with the very strong pyrazinoquinoxaline (PzQ) acceptor all show first peak absorptions at λ≈900 nm, while the II and BT acceptors provide their copolymers with first peak wavelengths around 650–700 nm. For the D–A_1–D–A_2 polymers with a strong second absorption peak/shoulder, the energies of those peaks are related to the energy gap between HOMO and LUMO+1, where copolymer LUMO+1 corresponds to the weaker acceptor LUMO, as outlined in Figure 6.2. BTz accordingly induces secondary peaks at ~500 nm in the 6 bottom polymers in Figure 6.5.

According to a MO theory argument, the two orbitals $\varphi_{LUMO,A1}$ and $\varphi_{LUMO,A2}$ interact and mix in the copolymer, with a mixing coefficient λ that depends on their spatial and energetic separation:[222]

$$\lambda_{LUMO-LUMO} \cong \frac{k\langle\varphi_{LUMO,A_1}|\varphi_{LUMO,A_2}\rangle}{E_{LUMO,A_2} - E_{LUMO,A_1}} \propto \frac{e^{-\beta R(A_1-A_2)}}{\Delta E_{LUMO,A}} \qquad (6.2)$$

This means that the copolymer LUMO and LUMO+1 are pushed apart in energy, by an amount that increases with decreasing separation in space and energy of the non-interacting acceptor LUMOs. The resulting two absorption peaks are thus considerably further apart in the spectra of the polymers with a short T donor in Figure 6.5, than for those with greater LUMO–LUMO distance as induced by the longer 3T donor, clearly seen for all except the top two polymers in Figure 6.5. The length of the donor segment is thus, in conjunction with the acceptor units' LUMO energies, parameters that can be chosen to tune the energies of the two absorption peaks.

6.2.3 Relative Peak Intensity

The relative strengths of the two low-energy absorption peaks from the dual absorption can be rationalized from viewing the D–A_1 and D–A_2 parts as an interacting excitonic J-dimer, where the dimeric optical properties depend on the electronic coupling between the two parts. Without going into details (the interested reader is encouraged to read reference 223 or other photophysics text books), strong excited state interaction between the a=D–A_1 and b=D–A_2 parts results in that the total wave functions Ψ and transition dipole moments M of the first S_1 and second excited state S_2 become linear combinations of the non-interacting wave functions ψ and transition dipole moments μ:[223]

$$\Psi(S_1) = \frac{1}{\sqrt{2}}(\psi_a^*\psi_b + \psi_a\psi_b^*) \quad M(S_1) = \frac{1}{\sqrt{2}}(\mu_a + \mu_b)$$
$$\Psi(S_2) = \frac{1}{\sqrt{2}}(\psi_a^*\psi_b - \psi_a\psi_b^*) \quad M(S_2) = \frac{1}{\sqrt{2}}(\mu_a - \mu_b) \qquad (6.3)$$

This leads to a strengthening of the S_1 transition dipole moment at the expense of S_2, since the transition dipole moment vectors are almost parallel along the backbone of the polymers. This explains why the S_2 transition is of negligible intensity for PTQTI in Figure 6.3 and P3TPhQBTz, PTPhQBTz, and PTPzQPhQ in the top of Figure 6.5: strong excited state interaction between D–A_1 and D–A_2 as a result of small energetic and spatial separation between the two acceptor LUMOs. As an overall consequence of this, the polymers with the short T donor show consistently weaker second peaks than the 3T donor cases in Figure 6.5.

For conversely weak interactions between the D–A_1 and D–A_2 excitonic parts, they absorb more independently of each other. This leads to a D–A_1–D–A_2 spectrum resembling a combination of the two corresponding D–A polymer spectra, as is the case for P3TPzQBTz and to some extent P3TIIBTz and P3TBTBTz, as seen in Figure 6.5. This proves beneficial for the overall spectral coverage.

6.3 Light-Harvesting Capability

In Chapter 3.5.3 we defined the light-harvesting capability of D–A polymers as the ability to absorb strongly at a suitably low wavelength. However, this measure only considers the first absorption peak, and an improved quantification is desirable for D–A_1–D–A_2 polymers whose advantage is the potential for an additional low-energy absorption peak. In Paper VI we introduce a more refined analysis for the quantification of the light-harvesting capabilities of the 15 D–A_1–D–A_2 polymers. The calculated polymer absorption coefficients ε(poly) are used together with the calculated coefficients of the $PC_{71}BM$ fullerene ε(PC71BM), to provide an estimate of how many photons the OPV active layer will absorb per unit time. This corresponds to the EQE, under the assumption that all absorbed photons produce one electric charge each without losses, *i.e.* IQE=100%. The EQE integrated with the solar photon flux $\Phi_{e\lambda}$ and multiplied with the elementary charge q_e gives the short circuit current:

$$J_{SC}^{theo} = q_e \int_0^{\infty} \Phi_{e\lambda}^{sol} EQE \, d\lambda \approx q_e \int_0^{\infty} \Phi_{e\lambda}^{sol} (1 - 10^{-A}) \, d\lambda$$
$$\approx q_e \sum_{\lambda=350}^{2000} \Phi_{e\lambda}^{sol} \left(1 - 10^{-\frac{2d\rho\left(1.5\varepsilon(poly)+\varepsilon(PC71BM)\right)}{2}}\right) \quad (6.4)$$

Apart from that the IQE=100%, the application of Equation 6.4 relies on several more assumptions: the active layer film thickness d=100 nm, the density of the film ρ=1 g cm^{-3}, a 1:1 polymer:$PC_{71}BM$ mass ratio, full reflectivity of the bottom electrode yielding two optical passes through the active layer. The factor 1.5 in Equation 6.4 arises from the fact that the transition dipole moments are assumed to be perfectly parallel to the backbones of the polymers, which during spin-coating become parallel to the surface of the film, increasing the polymer absorption by a factor 1.5 compared to a 3D-isotropic solution.[224,225]

Thorough investigations of the relation between the absorption and current generation in OPV films have been made, taking into account the effects of internal reflection, interference, and diffuse scattering.[226,227] Though disregarding many of these processes, the rough estimates of J_{SC} presented in Paper VI are useful for comparisons of the light-harvesting capabilities between polymers. The theoretical J_{SC} of all 15 polymers are listed in Table 6.1, showing that the longer donor segments in the 3T variants gives larger currents by virtue of stronger second peaks, except for PnTBTBTz where the redshifted first peak with the single T donor results in better light-harvesting. The very large J_{SC} estimated for the D–A_1–D–A_2 copolymers with PzQ and benzobisthiadiazole (BBT) are misleading, as the LUMO energies of these are expected to be lower than that of PCBM, hampering electron injection and lowering the IQE drastically. P3TQTIF shows a slightly lower theoretical estimate than the experimentally determined J_{SC} of 15.5 mA cm^{-2}, assigned mainly to the underestimation of absorption wavelengths seen in Figure 6.3. The theoretical J_{SC} in Table 6.1, in particular of PBTDPP and PnTBTBTz, compare favorably to the state of the art D–A polymer OPV devices with J_{SC}s of up to 19 mA cm^{-2}.[41] However, such direct comparisons to experiments are precarious, owing to the many approximations in the theoretical model which is better suited for qualitative comparisons between calculated polymers.

Table 6. 1. Theoretical estimates of J_{SC} of the 15 D–A_1–D–A_2 polymers in Paper VI.

Polymer	$J_{SC,theo}$ [mA/cm^2]		
	(n=1)	(n=2)	(n=3)
PTQTI	15.4		
P3TQTIF			14.6
PTIIBTzF	17.2		
PBTDPP		28.0	
PBBTDPP		35.8	
PnTPhQBTz	14.8		16.9
PnTPzQPhQ	21.2		27.3
PnTBTBTz	24.2		21.2
PnTIIBTz	18.2		18.3
PnTPzQBTz	27.9		30.4

P3TQTIF can be used in solar cells of 7.0% efficiency, as demonstrated in Paper VII, but still shows inferior light-harvesting capability compared to most D–A_1–D–A_2 polymers in Paper VI. This is very encouraging for the continued development of new, more efficient D–A_1–D–A_2 systems, where the choice of acceptors and donor segments can be guided by computational results. Of particular value is that the absorption spectra as fully predicted from calculations are in such good agreement with the experiments over the entire visible region, as demonstrated for five D–A_1–D–A_2 polymers in Paper VI. This highlights the emerging opportunities for quantitative predictions of the light-harvesting capabilities of practically any conjugated polymer through first principles quantum chemical calculations.

7. Conclusions

Theoretical research should aid the progress of the corresponding fields of knowledge. There are two dominant ways in which computational chemistry can accomplish this. The first derives from the ability to rationalize experimentally observed trends and properties, *i.e.* its explicative power. This has been of enormous importance during the last century, much thanks to the development of quantum mechanics which has been used to elucidate the electronic structure, first of atoms, and later molecules of increasing sizes. The second reason for the usefulness of computational chemistry is its capacity to predict many properties before the experiments are performed, *i.e.* its predictive power. Quantum chemical calculations can predict *e.g.* geometric and optical properties, as they derive from the electronic structure of the molecules. Using sufficiently capable methods is a prerequisite for accurate predictions, but the most comprehensive quantum chemistry methods generally come with a prohibitively high computational cost for studies of macromolecules such as polymers. Approaches based on DFT calculations are however feasible for predictions of respectable quality.

In this thesis, results are presented that highlight both the explicative and predictive power of quantum chemistry. Several results of explicative value are found in Chapters 3–6. In Chapter 3, systematic calculations of 60 D–A polymers are used to explain how different electronic and optical properties correlate to each other, and to the chemical composition with respect to the D and A units. For example, estimates of the HOMO and LUMO energies of D–A copolymers are obtained as weighted means of the HOMO and LUMO of the corresponding D and A homopolymers. In Chapter 4, experimentally recorded hole and electron mobilities of the TQ1 polymer are related to the delocalization of the corresponding orbitals HOMO and LUMO, and an unusual temperature dependence profile of the electron mobility is rationalized from the calculated LUMO showing a diminished delocalization for more twisted geometries. Related to this are the observed trends in Chapter 5: a number of D–A polymers exhibit an absorption that is weakened and blue-shifted with increasing temperature. This too is explained by a thermal population of more twisted conformations with weakened conjugation. In Chapter 6, the tendency for some D–A_1–D–A_2 polymers to exhibit two strong absorption peaks at long wavelengths is rationalized from a MO theory argument involving the interactions between the A_1 and A_2 LUMOs, promoting strong electronic transitions to both of these LUMOs in the copolymer, on the condition that these LUMOs are sufficiently separated in space and energy.

With regards to predictive power, some steps have been made in this thesis work. Experimental data for the geometry is generally not available for the typically amorphous D–A polymers, but quantum chemical calculations can predict the geometry of the polymer chains. The geometry has further implications for the electronic properties, for example as shown for the TQ1 polymer in Chapter 4, where the minimum energy conformation exhibits a unique helical geometry with extended conjugation, promoted by stacking interactions between phenyl side groups on neighboring units. Polymers are generally too large to be modeled in their entirety in quantum chemistry calculations, and many of their properties can therefore be challenging to predict. However, in Chapter 3 a strategy based on extrapolations of calculated oligomer properties is presented, where systematic comparisons to experiments for nine polymers have permitted the development of an empirical correction for the absorption energy and specific absorption strength. This empirical correction yields calculated optical properties in very good agreement with experiments among the nine D–A polymers, but also for polymers outside the test set, *e.g.* five D–A_1–D–A_2 polymers in Paper VI, whose more advanced design concept make quantitative calculations even more important. Predictions of optical properties can be difficult due to differences in conditions compared to experiments *e.g.* with respect to temperature. In Chapter 5, results are presented that are based on a methodology taking into account the effect of temperature on the low-energy structural modes that most affect the optical properties: the dihedral angles between units. Calculated temperature-dependences obtained this way for the APFO-3 and PTI-1 polymers reproduce the experimental trends well, and can if applied to other polymers be used for predictions of their temperature-sensitive optical properties.

Properties that have been difficult to calculate *a priori* due to the large size of polymer molecules are now becoming accessible through developments in computational methodologies and hardware. One such property is absorption spectra, whose accurate prediction requires computationally demanding quantum chemistry methods. It is here shown that an oligomer extrapolation approach based on TD-DFT calculations, combined with an empirical correction for the absorption energy and strength, has the capacity to quantitatively predict absorption spectra over the entire visible region. The good agreement is shown for three D–A_1–D–A_2 polymers in Figure 6.3, where the PTIIBTzF polymer was synthesized after its computationally predicted absorption profile had been found promising. Regarding this new polymer class, calculations formed part of the design process of the first generation of D–A_1–D–A_2 polymers presented in Paper VII, resulting in an impressive efficiency of 7.0%. In Paper VI, several candidates are presented that possess even greater predicted light-harvesting capabilities, demonstrating the superior spectral coverage facilitated by this design motif. In conclusion, quantum chemical calculations have the potential to contribute significantly to the field of conjugated polymer research, through providing better understanding and predictions of structural, electronic, and optical properties.

8. Outlook

Taking the work presented herein as a point of origin, there are several possible routes for continued research efforts. The effect of temperature on the absorption profile for example, has only been semi-rigorously investigated in Paper V, and only for two polymers. More thorough consideration of *e.g.* sampling size, basis sets, solvents, *etc.* would enhance the robustness of the methodology. Its application to other interesting polymers could provide additional valuable insights. For example to PDTTTPD, a polymer showing an almost 200 nm blue-shift when the temperature is increased from 19°C to 120°C;[228] or to TQ1, where the effects of the unique structural properties could be better understood by probing the temperature-dependence of its electronic structure; or to PffBT4T-2OD in which strong aggregation causes a significant red-shift of the experimental solution absorption for lower temperatures, complicating the interpretation of its spectra but being partly responsible for the 10.8% efficiency of its solar cells.[41]

Most of the calculations in this thesis are performed with the hybrid PBE0 XC functional. It gives more consistent results than many other functionals, but tends to significantly overestimate the conjugation, impacting not only electronic, but also structural and optical properties of polymers. Functionals less beset by self-interaction errors have recently been developed, that employ a system-dependent degree of LC.[60,229] These non-empirically tuned range-separated functionals have been used in calculations of conjugated polymers with highly encouraging results,[72,230,231] and should be considered for any quantum chemical study of these types of systems. The more accurate predictions of *e.g.* optical properties with these methods could be used for a re-assessment of the empirical correction described in Chapter 3.5, decreasing the magnitude of the correction and improving the reliability of spectral predictions.

The computational toolbox for conjugated polymers now includes *a priori* predictions of absorption spectra, temperature-dependent optical properties, theoretical estimates of short circuit currents, and comparative energy level assessments. With these, a highly systematic investigation of a large set of polymer candidates is possible, *e.g.* through building upon the library of 60 D–A polymers introduced in Paper II. This is anticipated to be of value in the quest for improved efficiency in OPVs, which to a large extent is determined by the molecular level properties. Polymers of the D–A_1–D–A_2 motif have shown particularly promising light-harvesting properties, and as demonstrated throughout

Chapter 6, calculations have the potential to contribute to a rational design of new candidates within this advanced class of polymers.

Finally, calculations of supramolecular systems of interest for OPVs, including several fullerene molecules and polymer chains, are becoming accessible through the development of faster computers. Such studies are already being performed with QM/MM methods, but more quantitative results could be obtained with comprehensive quantum chemical investigations.

9. Acknowledgements

Alice, my wife-to-be in a week's time after the submission of this thesis. Your support during the last months' thesis writing has been enormously important. This work would perhaps have been possible without you, but what value would it have in a colorless world? I love you, and am looking forward to whatever life will bring us.

Lotta and Björn, I take strength in knowing that you are proud of me. I am proud of you too, and I actually think sometimes that I have been unfairly lucky to have you as parents. In my most humble moments, I think I have inherited the best of your respective traits.

Petter. What a journey. Four and a half years of your enthusiastic supervision and enjoyable collaboration. No fights or major disagreements (yet), which is rather amazing. Or maybe more fights would have gotten us that elusive acceptance from JACS? It has been an honor being the first PhD student to whom you were the official main supervisor, and I already envy your future students.

To all former and current group members, thank you for great discussions at group meetings, for moral and scientific support, and for all the fun we have had outside working hours. Marta, you were the best office mate I could have wished for. I am really impressed with your thesis actually, especially given the circumstances, and I have been reading it a lot as inspiration for my own writing. Lisa, you were the main source of energy for the group, and after two years the group did not feel the same without you. Thanks for all the glögg, baked goods, jello shots, *etc.* Hannes, I really blame you for choosing a fancy job at Volvo instead of pursuing an academic career, with all the glory and fame it brings! Your Matlab skills were invaluable. Korina, you at least made the right choice to go on to do a PhD. I am sure you are doing great in Copenhagen although you of course secretly miss Sweden. Fredric, it is hard to fill Marta's office-mate shoes, but you are getting there. Sam, your stay here was short but very sweet. Really hope that we will meet again, perhaps in the US somewhere?

Paulius, it is hard to top your acknowledgement to me, but at least I can say that it has been a true pleasure having you around at work throughout our entire PhDs and at "my place" for three years almost to the day. I have been very lucky to have a friend with whom I have so much in common. Looking forward to many more nights of LANs and other parties. Evelina, thanks for all the interesting discussions. You are a good scientist, and you have the power to shape your own career on your own terms from now on.

Thousand thanks to Teokem Thursday Troops. Principally PhDs plus Post-docs. Some stayed short sessions, some several semesters. Great gaming generally going. Periodically patronizing pubs plus parties. No-one named, no-one neglected!

The Teokem seniors also deserve thanks for nice discussions *e.g.* during fika breaks. Special thanks to Per-Åke for fact-checking the theory in Chapter 2.

Thanks to the people at Chemical Physics. Arkady, although too far away for everyday supervision, you have been there when I have needed you and your support has been appreciated. Now we just need to get those metal complex papers submitted!. Thanks to Villy for helping to fund the project. Thanks to Ivan for nice polymer discussions and the best course throughout my PhD, I really should have taken it sooner.

Thanks to the people at Polymer Technology at Chalmers University. Ergang, without your enthusiastic collaboration my PhD would not have been what it is. Unlike many experimentalists, you actually seem to trust our calculations. Mats and Patrik, collaborations as fruitful as ours are not easily found I believe.

Mattias, thank you for a very efficient collaboration. Thanks also to the rest of the Swedish OPV community for rewarding yet friendly meetings.

10. References

(1) Cramer, C. J. *Essentials of Computational Chemistry: Theories and Models*; Wiley: New York, 2013.

(2) *Key World Energy Statistics*; Energy Data Summary; International Energy Agency: Paris, 2014.

(3) Ginley, D.; Green, M. A.; Collins, R. Solar Energy Conversion Toward 1 Terawatt. *MRS Bull.* **2008**, *33* (04), 355–364.

(4) Adams, W. G.; Day, R. E. The Action of Light on Selenium. *Philos. Trans. R. Soc. Lond.* **1877**, *167*, 313–349.

(5) Cleveland, C. J. *Concise Encyclopedia of the History of Energy*; Elsevier Science, 2009.

(6) *Panasonic HIT® Solar Cell Achieves World's Highest Energy Conversion Efficiency of 25.6% at Research Level*; Panasonic Corporation: Osaka, 2014.

(7) *New World Record for Solar Cell Efficiency at 46% French-German Cooperation Confirms Competitive Advantage of European Photovoltaic Industry*; Soitec, CEA-Leti, Fraunhofer ISE: Bernin and Freiburg, 2014.

(8) O'Regan, B.; Grätzel, M. A Low-Cost, High-Efficiency Solar Cell Based on Dye-Sensitized Colloidal TiO2 Films. *Nature* **1991**, *353* (6346), 737–740.

(9) Kamat, P. V. Quantum Dot Solar Cells. The Next Big Thing in Photovoltaics. *J. Phys. Chem. Lett.* **2013**, *4* (6), 908–918.

(10) Kojima, A.; Teshima, K.; Shirai, Y.; Miyasaka, T. Organometal Halide Perovskites as Visible-Light Sensitizers for Photovoltaic Cells. *J. Am. Chem. Soc.* **2009**, *131* (17), 6050–6051.

(11) Jeon, N. J.; Noh, J. H.; Yang, W. S.; Kim, Y. C.; Ryu, S.; Seo, J.; Seok, S. I. Compositional Engineering of Perovskite Materials for High-Performance Solar Cells. *Nature* **2015**, *517* (7535), 476–480.

(12) Søndergaard, R.; Hösel, M.; Angmo, D.; Larsen-Olsen, T. T.; Krebs, F. C. Roll-to-Roll Fabrication of Polymer Solar Cells. *Mater. Today* **2012**, *15* (1–2), 36–49.

(13) Melvin, C.; Richard, K. D. Photoelectric Cell Using Organic Materials. US3057947 A, October 9, 1962.

(14) Tang, C. W. Two-layer Organic Photovoltaic Cell. *Appl. Phys. Lett.* **1986**, *48* (2), 183–185.

(15) Yu, G.; Gao, J.; Hummelen, J. C.; Wudl, F.; Heeger, A. J. Polymer Photovoltaic Cells: Enhanced Efficiencies via a Network of Internal Donor-Acceptor Heterojunctions. *Science* **1995**, *270* (5243), 1789–1791.

(16) Salaneck, W. R.; Stafström, S.; Brédas, J. L. *Conjugated Polymer Surfaces and Interfaces: Electronic and Chemical Structure of Interfaces for Polymer Light Emitting Devices*; Cambridge University Press: Cambridge, 2003.

(17) Kraabel, B.; McBranch, D. W.; Lee, C.; Sariciftci, N. S.; Heeger, A. J. Subpicosecond Photo-Induced Electron Transfer from Conjugated Polymers to C60. In *Fullerenes and Photonics*; 1994; Vol. 2284, pp 194–207.

(18) Veldman, D.; Meskers, S. C. J.; Janssen, R. A. J. The Energy of Charge-Transfer States in Electron Donor–Acceptor Blends: Insight into the Energy Losses in Organic Solar Cells. *Adv. Funct. Mater.* **2009**, *19* (12), 1939–1948.

(19) Deibel, C.; Strobel, T.; Dyakonov, V. Role of the Charge Transfer State in Organic Donor–Acceptor Solar Cells. *Adv. Mater.* **2010**, *22* (37), 4097–4111.

(20) Park, S. H.; Roy, A.; Beaupre, S.; Cho, S.; Coates, N.; Moon, J. S.; Moses, D.; Leclerc, M.; Lee, K.; Heeger, A. J. Bulk Heterojunction Solar Cells with Internal Quantum Efficiency Approaching 100%. *Nat Photon* **2009**, *3* (5), 297–302.

(21) Bakulin, A. A.; Rao, A.; Pavelyev, V. G.; van Loosdrecht, P. H. M.; Pshenichnikov, M. S.; Niedzialek, D.; Cornil, J.; Beljonne, D.; Friend, R. H. The Role of Driving Energy and Delocalized States for Charge Separation in Organic Semiconductors. *Science* **2012**, *335* (6074), 1340–1344.

(22) Vandewal, K.; Albrecht, S.; Hoke, E. T.; Graham, K. R.; Widmer, J.; Douglas, J. D.; Schubert, M.; Mateker, W. R.; Bloking, J. T.; Burkhard, G. F.; et al. Efficient Charge Generation by Relaxed Charge-Transfer States at Organic Interfaces. *Nat Mater* **2014**, *13* (1), 63–68.

(23) Jailaubekov, A. E.; Willard, A. P.; Tritsch, J. R.; Chan, W.-L.; Sai, N.; Gearba, R.; Kaake, L. G.; Williams, K. J.; Leung, K.; Rossky, P. J.; et al. Hot Charge-Transfer Excitons Set the Time Limit for Charge Separation at Donor/acceptor Interfaces in Organic Photovoltaics. *Nat Mater* **2013**, *12* (1), 66–73.

(24) Lee, J.; Vandewal, K.; Yost, S. R.; Bahlke, M. E.; Goris, L.; Baldo, M. A.; Manca, J. V.; Voorhis, T. V. Charge Transfer State Versus Hot Exciton Dissociation in Polymer−Fullerene Blended Solar Cells. *J. Am. Chem. Soc.* **2010**, *132* (34), 11878–11880.

(25) Günes, S.; Neugebauer, H.; Sariciftci, N. S. Conjugated Polymer-Based Organic Solar Cells. *Chem. Rev.* **2007**, *107* (4), 1324–1338.

(26) Yip, H.-L.; Jen, A. K.-Y. Recent Advances in Solution-Processed Interfacial Materials for Efficient and Stable Polymer Solar Cells. *Energy Environ. Sci.* **2012**, *5* (3), 5994–6011.

(27) Zhou, H.; Yang, L.; You, W. Rational Design of High Performance Conjugated Polymers for Organic Solar Cells. *Macromolecules* **2012**, *45* (2), 607–632.

(28) Deledalle, F.; Shakya Tuladhar, P.; Nelson, J.; Durrant, J. R.; Kirchartz, T. Understanding the Apparent Charge Density Dependence of Mobility and Lifetime in Organic Bulk Heterojunction Solar Cells. *J. Phys. Chem. C* **2014**, *118* (17), 8837–8842.

(29) Guo, X.; Zhou, N.; Lou, S. J.; Smith, J.; Tice, D. B.; Hennek, J. W.; Ortiz, R. P.; Navarrete, J. T. L.; Li, S.; Strzalka, J.; et al. Polymer Solar Cells with Enhanced Fill Factors. *Nat. Photonics* **2013**, *7* (10), 825–833.

(30) Brabec, C. J.; Cravino, A.; Meissner, D.; Sariciftci, N. S.; Fromherz, T.; Rispens, M. T.; Sanchez, L.; Hummelen, J. C. Origin of the Open Circuit Voltage of Plastic Solar Cells. *Adv. Funct. Mater.* **2001**, *11* (5), 374–380.

(31) Gadisa, A.; Svensson, M.; Andersson, M. R.; Inganäs, O. Correlation between Oxidation Potential and Open-Circuit Voltage of Composite Solar Cells Based on Blends of Polythiophenes/ Fullerene Derivative. *Appl. Phys. Lett.* **2004**, *84* (9), 1609–1611.

(32) Scharber, M. C.; Mühlbacher, D.; Koppe, M.; Denk, P.; Waldauf, C.; Heeger, A. J.; Brabec, C. J. Design Rules for Donors in Bulk-Heterojunction Solar Cells—Towards 10 % Energy-Conversion Efficiency. *Adv. Mater.* **2006**, *18* (6), 789–794.

(33) Chen, H.-Y.; Hou, J.; Zhang, S.; Liang, Y.; Yang, G.; Yang, Y.; Yu, L.; Wu, Y.; Li, G. Polymer Solar Cells with Enhanced Open-Circuit Voltage and Efficiency. *Nat. Photonics* **2009**, *3* (11), 649–653.

(34) Zhou, H.; Yang, L.; Stoneking, S.; You, W. A Weak Donor−Strong Acceptor Strategy to Design Ideal Polymers for Organic Solar Cells. *ACS Appl. Mater. Interfaces* **2010**, *2* (5), 1377–1383.

(35) Huo, L.; Hou, J.; Zhang, S.; Chen, H.-Y.; Yang, Y. A Polybenzo[1,2-b:4,5-B′]dithiophene Derivative with Deep HOMO Level and Its Application in High-Performance Polymer Solar Cells. *Angew. Chem. Int. Ed.* **2010**, *49* (8), 1500–1503.

(36) Bijleveld, J. C.; Verstrijden, R. A. M.; Wienk, M. M.; Janssen, R. A. J. Maximizing the Open-Circuit Voltage of Polymer: Fullerene Solar Cells. *Appl. Phys. Lett.* **2010**, *97* (7), 073304.

(37) He, X.; Gao, F.; Tu, G.; Hasko, D.; Hüttner, S.; Steiner, U.; Greenham, N. C.; Friend, R. H.; Huck, W. T. S. Formation of Nanopatterned Polymer Blends in Photovoltaic Devices. *Nano Lett.* **2010**, *10* (4), 1302–1307.

(38) Warnan, J.; Cabanetos, C.; Bude, R.; El Labban, A.; Li, L.; Beaujuge, P. M. Electron-Deficient N-Alkyloyl Derivatives of Thieno[3,4-C]pyrrole-4,6-Dione Yield Efficient Polymer Solar Cells with Open-Circuit Voltages > 1 V. *Chem. Mater.* **2014**, *26* (9), 2829–2835.

(39) Zhang, Q.; Kan, B.; Liu, F.; Long, G.; Wan, X.; Chen, X.; Zuo, Y.; Ni, W.; Zhang, H.; Li, M.; et al. Small-Molecule Solar Cells with Efficiency over 9%. *Nat Photon* **2015**, *9* (1), 35–41.

(40) Jackson, N. E.; Savoie, B. M.; Marks, T. J.; Chen, L. X.; Ratner, M. A. The Next Breakthrough for Organic Photovoltaics? *J. Phys. Chem. Lett.* **2015**, *6* (1), 77–84.

(41) Liu, Y.; Zhao, J.; Li, Z.; Mu, C.; Ma, W.; Hu, H.; Jiang, K.; Lin, H.; Ade, H.; Yan, H. Aggregation and Morphology Control Enables Multiple Cases of High-Efficiency Polymer Solar Cells. *Nat. Commun.* **2014**, *5* (5293).

(42) Liu, C.; Yi, C.; Wang, K.; Yang, Y.; Bhatta, R. S.; Tsige, M.; Xiao, S.; Gong, X. Single-Junction Polymer Solar Cells with Over 10% Efficiency by a Novel Two-Dimensional Donor–Acceptor Conjugated Copolymer. *ACS Appl. Mater. Interfaces* **2015**, *7* (8), 4928–4935.

(43) Chen, J.-D.; Cui, C.; Li, Y.-Q.; Zhou, L.; Ou, Q.-D.; Li, C.; Li, Y.; Tang, J.-X. Single-Junction Polymer Solar Cells Exceeding 10% Power Conversion Efficiency. *Adv. Mater.* **2015**, *27* (6), 1035–1041.

(44) Szabo, A.; Ostlund, N. S. *Modern Quantum Chemistry: Introduction to Advanced Electronic Structure Theory*; Dover Publications: New York, 2012.

(45) Born, M.; Oppenheimer, R. Zur Quantentheorie Der Molekeln. *Ann. Phys.* **1927**, *389* (20), 457–484.

(46) Jones, L.; Atkins, P. W. *Chemistry: Molecules, Matter, and Change*; W.H. Freeman: New York, 2000.

(47) Oxtoby, D.; Gillis, H.; Butler, L. *Principles of Modern Chemistry*; Cengage Learning: Boston, 2015.

(48) Slater, J. C. Atomic Shielding Constants. *Phys. Rev.* **1930**, *36* (1), 57.

(49) Müller, C. *Spherical Harmonics*; Springer: Berlin, 1966.

(50) Hartree, D. R. The Wave Mechanics of an Atom with a Non-Coulomb Central Field. Part I. Theory and Methods. *Math. Proc. Camb. Philos. Soc.* **1928**, *24* (01), 89–110.

(51) Møller, C.; Plesset, M. S. Note on an Approximation Treatment for Many-Electron Systems. *Phys. Rev.* **1934**, *46* (7), 618–622.

(52) Kato, T. *Perturbation Theory for Linear Operators*; Classics in Mathematics; Springer: Berlin, Heidelberg, 2012.

(53) Roos, B. O.; Taylor, P. R.; Siegbahn, P. E. M. A Complete Active Space SCF Method (CASSCF) Using a Density Matrix Formulated Super-CI Approach. *Chem. Phys.* **1980**, *48* (2), 157–173.

(54) Hohenberg, P.; Kohn, W. Inhomogeneous Electron Gas. *Phys. Rev.* **1964**, *136* (3B), B864–B871.

(55) Jensen, F. *Introduction to Computational Chemistry*; Wiley: New York, 2013.

(56) Perdew, J. P.; Schmidt, K. Jacob's Ladder of Density Functional Approximations for the Exchange-Correlation Energy. *AIP Conf. Proc.* **2001**, *577* (1), 1–20.

(57) Neese, F. Prediction of Molecular Properties and Molecular Spectroscopy with Density Functional Theory: From Fundamental Theory to Exchange-Coupling. *Theory Comput. Contemp. Coord. Chem.* **2009**, *253* (5–6), 526–563.

(58) Perdew, J. P.; Ruzsinszky, A.; Tao, J.; Staroverov, V. N.; Scuseria, G. E.; Csonka, G. I. Prescription for the Design and Selection of Density Functional Approximations: More Constraint Satisfaction with Fewer Fits. *J. Chem. Phys.* **2005**, *123* (6), 062201.

(59) Tsuneda, T.; Hirao, K. Long-Range Correction for Density Functional Theory. *Wiley Interdiscip. Rev. Comput. Mol. Sci.* **2014**, *4* (4), 375–390.

(60) Baer, R.; Livshits, E.; Salzner, U. Tuned Range-Separated Hybrids in Density Functional Theory. *Annu. Rev. Phys. Chem.* **2010**, *61* (1), 85–109.

(61) Grimme, S. Density Functional Theory with London Dispersion Corrections. *Wiley Interdiscip. Rev. Comput. Mol. Sci.* **2011**, *1* (2), 211–228.

(62) Perdew, J. P.; Burke, K.; Ernzerhof, M. Generalized Gradient Approximation Made Simple. *Phys. Rev. Lett.* **1996**, *77* (18), 3865–3868.

(63) Becke, A. D. Density-Functional Thermochemistry. III. The Role of Exact Exchange. *J. Chem. Phys.* **1993**, *98* (7), 5648–5652.

(64) Zhao, Y.; Truhlar, D. The M06 Suite of Density Functionals for Main Group Thermochemistry, Thermochemical Kinetics, Noncovalent Interactions, Excited States, and Transition Elements: Two New Functionals and Systematic Testing of Four M06-Class Functionals and 12 Other Functionals. *Theor. Chem. Acc. Theory Comput. Model. Theor. Chim. Acta* **2008**, *120* (1), 215–241.

(65) Yanai, T.; Tew, D. P.; Handy, N. C. A New Hybrid Exchange–correlation Functional Using the Coulomb-Attenuating Method (CAM-B3LYP). *Chem. Phys. Lett.* **2004**, *393* (1-3), 51–57.

(66) Adamo, C.; Barone, V. Toward Reliable Density Functional Methods without Adjustable Parameters: The PBE0 Model. *J. Chem. Phys.* **1999**, *110* (13), 6158–6170.

(67) Grimme, S. Accurate Calculation of the Heats of Formation for Large Main Group Compounds with Spin-Component Scaled MP2 Methods. *J. Phys. Chem. A* **2005**, *109* (13), 3067–3077.

(68) Körzdörfer, T.; Brédas, J.-L. Organic Electronic Materials: Recent Advances in the DFT Description of the Ground and Excited States Using Tuned Range-Separated Hybrid Functionals. *Acc. Chem. Res.* **2014**, *47*, 3284–3291.

(69) Savoie, B. M.; Jackson, N. E.; Marks, T. J.; Ratner, M. A. Reassessing the Use of One-Electron Energetics in the Design and Characterization of Organic Photovoltaics. *Phys. Chem. Chem. Phys.* **2013**, *15* (13), 4538–4547.

(70) Wykes, M.; Milián-Medina, B.; Gierschner, J. Computational Engineering of Low Bandgap Copolymers. *Front. Chem.* **2013**, *1* (35), 35.

(71) Chai, J.-D.; Head-Gordon, M. Long-Range Corrected Hybrid Density Functionals with Damped Atom-Atom Dispersion Corrections. *Phys. Chem. Chem. Phys.* **2008**, *10* (44).

(72) Pandey, L.; Doiron, C.; Sears, J. S.; Bredas, J.-L. Lowest Excited States and Optical Absorption Spectra of Donor-Acceptor Copolymers for Organic Photovoltaics: A New Picture Emerging from Tuned Long-Range Corrected Density Functionals. *Phys. Chem. Chem. Phys.* **2012**, *14* (41), 14243–14248.

(73) Eriksson, L. A.; Pettersson, L. G. M.; Siegbahn, P. E. M.; Wahlgren, U. On the Accuracy of Gradient Corrected Density Functional Methods for Transition Metal Complexes. *J. Chem. Phys.* **1995**, *102* (2), 872–878.

(74) Bühl, M.; Kabrede, H. Geometries of Transition-Metal Complexes from Density-Functional Theory. *J. Chem. Theory Comput.* **2006**, *2* (5), 1282–1290.

(75) Neese, F.; Schwabe, T.; Grimme, S. Analytic Derivatives for Perturbatively Corrected "double Hybrid" Density Functionals: Theory, Implementation, and Applications. *J. Chem. Phys.* **2007**, *126* (12), 124115.

(76) Runge, E.; Gross, E. K. U. Density-Functional Theory for Time-Dependent Systems. *Phys. Rev. Lett.* **1984**, *52* (12), 997–1000.

(77) Ullrich, C. *Time-Dependent Density-Functional Theory: Concepts and Applications*; Oxford Graduate Texts; OUP Oxford, 2012.

(78) Dreuw, A.; Weisman, J. L.; Head-Gordon, M. Long-Range Charge-Transfer Excited States in Time-Dependent Density Functional Theory Require Non-Local Exchange. *J. Chem. Phys.* **2003**, *119* (6), 2943–2946.

(79) Magyar, R. J.; Tretiak, S. Dependence of Spurious Charge-Transfer Excited States on Orbital Exchange in TDDFT: Large Molecules and Clusters. *J. Chem. Theory Comput.* **2007**, *3* (3), 976–987.

(80) Manzhos, S.; Segawa, H.; Yamashita, K. Computational Dye Design by Changing the Conjugation Order: Failure of LR-TDDFT to Predict Relative Excitation Energies in Organic Dyes Differing by the Position of the Methine Unit. *Chem. Phys. Lett.* **2012**, *527* (0), 51–56.

(81) Laurent, A. D.; Jacquemin, D. TD-DFT Benchmarks: A Review. *Int. J. Quantum Chem.* **2013**, *113* (17), 2019–2039.

(82) Jacquemin, D.; Mennucci, B.; Adamo, C. Excited-State Calculations with TD-DFT: From Benchmarks to Simulations in Complex Environments. *Phys. Chem. Chem. Phys.* **2011**, *13* (38), 16987–16998.

(83) Guillaumont, D.; Nakamura, S. Calculation of the Absorption Wavelength of Dyes Using Time-Dependent Density-Functional Theory (TD-DFT). *Dyes Pigments* **2000**, *46* (2), 85–92.

(84) Meguellati, K.; Ladame, S.; Spichty, M. A Conceptually Improved TD-DFT Approach for Predicting the Maximum Absorption Wavelength of Cyanine Dyes. *Dyes Pigments* **2011**, *90* (2), 114–118.

(85) Jacquemin, D.; Perpète, E. A.; Scuseria, G. E.; Ciofini, I.; Adamo, C. TD-DFT Performance for the Visible Absorption Spectra of Organic Dyes: Conventional versus Long-Range Hybrids. *J. Chem. Theory Comput.* **2008**, *4* (1), 123–135.

(86) Ma, J.; Li, S.; Jiang, Y. A Time-Dependent DFT Study on Band Gaps and Effective Conjugation Lengths of Polyacetylene, Polyphenylene, Polypentafulvene, Polycyclopentadiene, Polypyrrole, Polyfuran, Polysilole, Polyphosphole, and Polythiophene. *Macromolecules* **2002**, *35* (3), 1109–1115.

(87) Tao, J.; Tretiak, S.; Zhu, J.-X. Prediction of Excitation Energies for Conjugated Polymers Using Time-Dependent Density Functional Theory. *Phys. Rev. B* **2009**, *80* (23), 235110.

(88) Nalewajski, R. F. *Perspectives in Electronic Structure Theory*; Springer: Berlin, Heidelberg, 2012.

(89) Valeur, B.; Berberan-Santos, M. N. *Molecular Fluorescence: Principles and Applications*; Wiley: New York, 2013.

(90) Johansson, E. M. J.; Odelius, M.; Plogmaker, S.; Gorgoi, M.; Svensson, S.; Siegbahn, H.; Rensmo, H. Spin−Orbit Coupling and Metal−Ligand Interactions in Fe(II), Ru(II), and Os(II) Complexes. *J. Phys. Chem. C* **2010**, *114* (22), 10314–10322.

(91) Gritsenko, O. V.; Baerends, E. J. The Analog of Koopmans' Theorem in Spin-Density Functional Theory. *J. Chem. Phys.* **2002**, *117* (20), 9154–9159.

(92) Tsuneda, T.; Song, J.-W.; Suzuki, S.; Hirao, K. On Koopmans' Theorem in Density Functional Theory. *J. Chem. Phys.* **2010**, *133* (17), 174101.

(93) Sathyanarayana, D. N. *Electronic Absorption Spectroscopy and Related Techniques*; Universities Press: Hyderabad, 2001.

(94) Sariciftci, N. S.; Smilowitz, L.; Heeger, A. J.; Wudl, F. Photoinduced Electron Transfer from a Conducting Polymer to Buckminsterfullerene. *Science* **1992**, *258* (5087), 1474–1476.

(95) Hotta, S.; Rughooputh, S. D. D. V.; Heeger, A. J.; Wudl, F. Spectroscopic Studies of Soluble poly(3-Alkylthienylenes). *Macromolecules* **1987**, *20* (1), 212–215.

(96) Havinga, E. E.; Hoeve, W.; Wynberg, H. A New Class of Small Band Gap Organic Polymer Conductors. *Polym. Bull.* **1992**, *29* (1-2), 119–126.

(97) Van Mullekom, H. A. M.; Vekemans, J. A. J. M.; Havinga, E. E.; Meijer, E. W. Developments in the Chemistry and Band Gap Engineering of Donor-Acceptor Substituted Conjugated Polymers. *Mater. Sci. Eng. R Rep.* **2001**, *32* (1), 1–40.

(98) Ajayaghosh, A. Donor-Acceptor Type Low Band Gap Polymers: Polysquaraines and Related Systems. *Chem. Soc. Rev.* **2003**, *32* (4), 181–191.

(99) Kroon, R.; Lenes, M.; Hummelen, J. C.; Blom, P. W. M.; de Boer, B. Small Bandgap Polymers for Organic Solar Cells (Polymer Material Development in the Last 5 Years). *Polym. Rev.* **2008**, *48* (3), 531–582.

(100) Chen, J.; Cao, Y. Development of Novel Conjugated Donor Polymers for High-Efficiency Bulk-Heterojunction Photovoltaic Devices. *Acc. Chem. Res.* **2009**, *42* (11), 1709–1718.

(101) Li, Y. Molecular Design of Photovoltaic Materials for Polymer Solar Cells: Toward Suitable Electronic Energy Levels and Broad Absorption. *Acc. Chem. Res.* **2012**, *45* (5), 723–733.

(102) Zhang, Z.-G.; Wang, J. Structures and Properties of Conjugated Donor-Acceptor Copolymers for Solar Cell Applications. *J. Mater. Chem.* **2012**, *22* (10), 4178–4187.

(103) Kularatne, R. S.; Magurudeniya, H. D.; Sista, P.; Biewer, M. C.; Stefan, M. C. Donor–acceptor Semiconducting Polymers for Organic Solar Cells. *J. Polym. Sci. Part Polym. Chem.* **2013**, *51* (4), 743–768.

(104) Zhao, G.; He, Y.; Li, Y. 6.5% Efficiency of Polymer Solar Cells Based on poly(3-Hexylthiophene) and Indene-C60 Bisadduct by Device Optimization. *Adv. Mater.* **2010**, *22* (39), 4355–4358.

(105) Green, M. A.; Emery, K.; Hishikawa, Y.; Warta, W.; Dunlop, E. D. Solar Cell Efficiency Tables (Version 45). *Prog. Photovolt. Res. Appl.* **2015**, *23* (1), 1–9.

(106) Dang, M. T.; Hirsch, L.; Wantz, G. P3HT:PCBM, Best Seller in Polymer Photovoltaic Research. *Adv. Mater.* **2011**, *23* (31), 3597–3602.

(107) Vanlaeke, P.; Swinnen, A.; Haeldermans, I.; Vanhoyland, G.; Aernouts, T.; Cheyns, D.; Deibel, C.; D'Haen, J.; Heremans, P.; Poortmans, J.; et al. P3HT/PCBM Bulk Heterojunction Solar Cells: Relation between Morphology and Electro-Optical Characteristics. *Sol. Energy Mater. Sol. Cells* **2006**, *90* (14), 2150–2158.

(108) Hwang, I.-W.; Moses, D.; Heeger, A. J. Photoinduced Carrier Generation in P3HT/PCBM Bulk Heterojunction Materials. *J. Phys. Chem. C* **2008**, *112* (11), 4350–4354.

(109) Wang, E.; Hou, L.; Wang, Z.; Ma, Z.; Hellström, S.; Zhuang, W.; Zhang, F.; Inganäs, O.; Andersson, M. R. Side-Chain Architectures of 2,7-Carbazole and Quinoxaline-Based Polymers for Efficient Polymer Solar Cells. *Macromolecules* **2011**, *44* (7), 2067–2073.

(110) Hörmann, U.; Lorch, C.; Hinderhofer, A.; Gerlach, A.; Gruber, M.; Kraus, J.; Sykora, B.; Grob, S.; Linderl, T.; Wilke, A.; et al. Voc from a Morphology Point of View: The Influence of Molecular Orientation on the Open Circuit Voltage of

Organic Planar Heterojunction Solar Cells. *J. Phys. Chem. C* **2014**, *118* (46), 26462–26470.

(111) De Leener, C.; Hennebicq, E.; Sancho-Garcia, J.-C.; Beljonne, D. Modeling the Dynamics of Chromophores in Conjugated Polymers: The Case of Poly(2-Methoxy-5-(2′-Ethylhexyl)oxy 1,4-Phenylene Vinylene) (MEH-PPV). *J. Phys. Chem. B* **2009**, *113* (5), 1311–1322.

(112) Alexiadis, O.; Mavrantzas, V. G. All-Atom Molecular Dynamics Simulation of Temperature Effects on the Structural, Thermodynamic, and Packing Properties of the Pure Amorphous and Pure Crystalline Phases of Regioregular P3HT. *Macromolecules* **2013**, *46* (6), 2450–2467.

(113) Frigerio, F.; Casalegno, M.; Carbonera, C.; Nicolini, T.; Meille, S. V.; Raos, G. Molecular Dynamics Simulations of the Solvent- and Thermal History-Dependent Structure of the PCBM Fullerene Derivative. *J. Mater. Chem.* **2012**, *22* (12), 5434–5443.

(114) Linares, M.; Beljonne, D.; Cornil, J.; Lancaster, K.; Brédas, J.-L.; Verlaak, S.; Mityashin, A.; Heremans, P.; Fuchs, A.; Lennartz, C.; et al. On the Interface Dipole at the Pentacene−Fullerene Heterojunction: A Theoretical Study. *J. Phys. Chem. C* **2010**, *114* (7), 3215–3224.

(115) Yost, S. R.; Wang, L.-P.; Van Voorhis, T. Molecular Insight Into the Energy Levels at the Organic Donor/Acceptor Interface: A Quantum Mechanics/Molecular Mechanics Study. *J. Phys. Chem. C* **2011**, *115* (29), 14431–14436.

(116) Fu, Y.-T.; Risko, C.; Brédas, J.-L. Intermixing at the Pentacene-Fullerene Bilayer Interface: A Molecular Dynamics Study. *Adv. Mater.* **2013**, *25* (6), 878–882.

(117) Liu, T.; Troisi, A. Absolute Rate of Charge Separation and Recombination in a Molecular Model of the P3HT/PCBM Interface. *J. Phys. Chem. C* **2011**, *115* (5), 2406–2415.

(118) Marchiori, C. F. N.; Koehler, M. Dipole Assisted Exciton Dissociation at Conjugated Polymer/fullerene Photovoltaic Interfaces: A Molecular Study Using Density Functional Theory Calculations. *Synth. Met.* **2010**, *160* (7-8), 643–650.

(119) Tamura, H.; Burghardt, I.; Tsukada, M. Exciton Dissociation at Thiophene/Fullerene Interfaces: The Electronic Structures and Quantum Dynamics. *J Phys Chem C* **2011**, *115* (20), 10205–10210.

(120) Kanai, Y.; Grossman, J. C. Insights on Interfacial Charge Transfer Across P3HT/Fullerene Photovoltaic Heterojunction from Ab Initio Calculations. *Nano Lett.* **2007**, *7* (7), 1967–1972.

(121) Sen, K.; Crespo-Otero, R.; Weingart, O.; Thiel, W.; Barbatti, M. Interfacial States in Donor–Acceptor Organic Heterojunctions: Computational Insights into Thiophene-Oligomer/Fullerene Junctions. *J. Chem. Theory Comput.* **2013**, *9* (1), 533–542.

(122) Hou, L.; Wang, E.; Bergqvist, J.; Andersson, B. V.; Wang, Z.; Müller, C.; Campoy-Quiles, M.; Andersson, M. R.; Zhang, F.; Inganäs, O. Lateral Phase Separation Gradients in Spin-Coated Thin Films of High-Performance Polymer:Fullerene Photovoltaic Blends. *Adv. Funct. Mater.* **2011**, *21* (16), 3169–3175.

(123) McCormick, T. M.; Bridges, C. R.; Carrera, E. I.; DiCarmine, P. M.; Gibson, G. L.; Hollinger, J.; Kozycz, L. M.; Seferos, D. S. Conjugated Polymers: Evaluating DFT

Methods for More Accurate Orbital Energy Modeling. *Macromolecules* **2013**, *46* (10), 3879–3886.

(124) Salvatori, P.; Mosconi, E.; Wang, E.; Andersson, M.; Muccini, M.; De Angelis, F. Computational Modeling of Isoindigo-Based Polymers Used in Organic Solar Cells. *J. Phys. Chem. C* **2013**, *117* (35), 17940–17954.

(125) Ford, W. K.; Duke, C. B.; Salaneck, W. R. Electronic Structure of Polypyrrole and Oligomers of Pyrrole. *J. Chem. Phys.* **1982**, *77* (10), 5030–5039.

(126) Gierschner, J.; Cornil, J.; Egelhaaf, H.-J. Optical Bandgaps of Π-Conjugated Organic Materials at the Polymer Limit: Experiment and Theory. *Adv. Mater.* **2007**, *19* (2), 173–191.

(127) Zade, S. S.; Zamoshchik, N.; Bendikov, M. From Short Conjugated Oligomers to Conjugated Polymers. Lessons from Studies on Long Conjugated Oligomers. *Acc. Chem. Res.* **2010**, *44* (1), 14–24.

(128) Risko, C.; McGehee, M. D.; Brédas, J.-L. A Quantum-Chemical Perspective into Low Optical-Gap Polymers for Highly-Efficient Organic Solar Cells. *Chem. Sci.* **2011**, *2* (7), 1200–1218.

(129) Fischer, F. S. U.; Tremel, K.; Saur, A.-K.; Link, S.; Kayunkid, N.; Brinkmann, M.; Herrero-Carvajal, D.; Navarrete, J. T. L.; Delgado, M. C. R.; Ludwigs, S. Influence of Processing Solvents on Optical Properties and Morphology of a Semicrystalline Low Bandgap Polymer in the Neutral and Charged States. *Macromolecules* **2013**, *46* (12), 4924–4931.

(130) Reish, M. E.; Nam, S.; Lee, W.; Woo, H. Y.; Gordon, K. C. A Spectroscopic and DFT Study of the Electronic Properties of Carbazole-Based D–A Type Copolymers. *J. Phys. Chem. C* **2012**, *116* (40), 21255–21266.

(131) Azazi, A.; Mabrouk, A.; Chemek, M.; Kreher, D.; Alimi, K. DFT Modeling of Conjugated Copolymers Photophysical Properties: Towards Organic Solar Cell Application. *Synth. Met.* **2014**, *198* (0), 314–322.

(132) Frisch, M.; Trucks, G.; Schlegel, H.; Scuseria, G.; Robb, M.; Cheeseman, J.; Scalmani, G.; Barone, V.; Mennucci, B.; Petersson, G.; et al. Gaussian 09, Revision A.02, 2009.

(133) Coropceanu, V.; Cornil, J.; da Silva Filho, D. A.; Olivier, Y.; Silbey, R.; Brédas, J.-L. Charge Transport in Organic Semiconductors. *Chem. Rev.* **2007**, *107* (4), 926–952.

(134) Wang, E.; Hou, L.; Wang, Z.; Hellström, S.; Zhang, F.; Inganäs, O.; Andersson, M. R. An Easily Synthesized Blue Polymer for High-Performance Polymer Solar Cells. *Adv. Mater.* **2010**, *22* (46), 5240–5244.

(135) Jespersen, K. G.; Beenken, W. J. D.; Zaushitsyn, Y.; Yartsev, A.; Andersson, M.; Pullerits, T.; Sundström, V. The Electronic States of Polyfluorene Copolymers with Alternating Donor-Acceptor Units. *J. Chem. Phys.* **2004**, *121* (24), 12613–12617.

(136) Deng, Y.; Liu, J.; Wang, J.; Liu, L.; Li, W.; Tian, H.; Zhang, X.; Xie, Z.; Geng, Y.; Wang, F. Dithienocarbazole and Isoindigo Based Amorphous Low Bandgap Conjugated Polymers for Efficient Polymer Solar Cells. *Adv. Mater.* **2014**, *26* (3), 471–476.

(137) Cabanetos, C.; El Labban, A.; Bartelt, J. A.; Douglas, J. D.; Mateker, W. R.; Fréchet, J. M. J.; McGehee, M. D.; Beaujuge, P. M. Linear Side Chains in

Benzo[1,2-b:4,5-b′]dithiophene–Thieno[3,4-C]pyrrole-4,6-Dione Polymers Direct Self-Assembly and Solar Cell Performance. *J. Am. Chem. Soc.* **2013**, *135* (12), 4656–4659.

(138) Zhang, M.; Gu, Y.; Guo, X.; Liu, F.; Zhang, S.; Huo, L.; Russell, T. P.; Hou, J. Efficient Polymer Solar Cells Based on Benzothiadiazole and Alkylphenyl Substituted Benzodithiophene with a Power Conversion Efficiency over 8%. *Adv. Mater.* **2013**, *25* (35), 4944–4949.

(139) Yang, T.; Wang, M.; Duan, C.; Hu, X.; Huang, L.; Peng, J.; Huang, F.; Gong, X. Inverted Polymer Solar Cells with 8.4% Efficiency by Conjugated Polyelectrolyte. *Energy Environ. Sci.* **2012**, *5* (8), 8208–8214.

(140) Ye, L.; Zhang, S.; Zhao, W.; Yao, H.; Hou, J. Highly Efficient 2D-Conjugated Benzodithiophene-Based Photovoltaic Polymer with Linear Alkylthio Side Chain. *Chem. Mater.* **2014**, *26* (12), 3603–3605.

(141) He, Z.; Zhong, C.; Su, S.; Xu, M.; Wu, H.; Cao, Y. Enhanced Power-Conversion Efficiency in Polymer Solar Cells Using an Inverted Device Structure. *Nat. Photonics* **2012**, *6* (9), 591–595.

(142) Kuhn, W. Über Das Absorptionsspektrum Der Polyene. *Helv. Chim. Acta* **1948**, *31* (6), 1780–1799.

(143) Hutchison, G. R.; Zhao, Y.-J.; Delley, B.; Freeman, A. J.; Ratner, M. A.; Marks, T. J. Electronic Structure of Conducting Polymers: Limitations of Oligomer Extrapolation Approximations and Effects of Heteroatoms. *Phys. Rev. B* **2003**, *68* (3), 035204.

(144) Torras, J.; Casanovas, J.; Alemán, C. Reviewing Extrapolation Procedures of the Electronic Properties on the Π-Conjugated Polymer Limit. *J. Phys. Chem. A* **2012**, *116* (28), 7571–7583.

(145) Shockley, W.; Queisser, H. J. Detailed Balance Limit of Efficiency of P-n Junction Solar Cells. *J. Appl. Phys.* **1961**, *32* (3), 510–519.

(146) Yuen, J. D.; Fan, J.; Seifter, J.; Lim, B.; Hufschmid, R.; Heeger, A. J.; Wudl, F. High Performance Weak Donor–Acceptor Polymers in Thin Film Transistors: Effect of the Acceptor on Electronic Properties, Ambipolar Conductivity, Mobility, and Thermal Stability. *J. Am. Chem. Soc.* **2011**, *133* (51), 20799–20807.

(147) Yuen, J. D.; Kumar, R.; Zakhidov, D.; Seifter, J.; Lim, B.; Heeger, A. J.; Wudl, F. Ambipolarity in Benzobisthiadiazole-Based Donor–Acceptor Conjugated Polymers. *Adv. Mater.* **2011**, *23* (33), 3780–3785.

(148) Steckler, T. T.; Zhang, X.; Hwang, J.; Honeyager, R.; Ohira, S.; Zhang, X.-H.; Grant, A.; Ellinger, S.; Odom, S. A.; Sweat, D.; et al. A Spray-Processable, Low Bandgap, and Ambipolar Donor−Acceptor Conjugated Polymer. *J. Am. Chem. Soc.* **2009**, *131* (8), 2824–2826.

(149) Moliton, A.; Hiorns, R. C. Review of Electronic and Optical Properties of Semiconducting Π-Conjugated Polymers: Applications in Optoelectronics. *Polym. Int.* **2004**, *53* (10), 1397–1412.

(150) Kertesz, M.; Choi, C. H.; Yang, S. Conjugated Polymers and Aromaticity. *Chem. Rev.* **2005**, *105* (10), 3448–3481.

(151) Beaujuge, P. M.; Amb, C. M.; Reynolds, J. R. Spectral Engineering in Π-Conjugated Polymers with Intramolecular Donor−Acceptor Interactions. *Acc. Chem. Res.* **2010**, *43* (11), 1396–1407.

(152) Banerji, N.; Gagnon, E.; Morgantini, P.-Y.; Valouch, S.; Mohebbi, A. R.; Seo, J.-H.; Leclerc, M.; Heeger, A. J. Breaking Down the Problem: Optical Transitions, Electronic Structure, and Photoconductivity in Conjugated Polymer PCDTBT and in Its Separate Building Blocks. *J. Phys. Chem. C* **2012**, *116* (21), 11456–11469.

(153) Zhang, B.; Zhang, H.; Li, X.; Li, W.; Sun, P.; Yang, W. Synthesis, Characterization, and Large Two-Photon Absorption Cross-Sections of Solid Red-Emitting 1,4-Diketo-3,6-Diphenylpyrrolo [3,4-c]pyrrole/3,6-Carbazole/ Terfluorene Copolymers. *J. Polym. Sci. Polym. Chem.* **2011**, *49* (14), 3048–3057.

(154) Li, S.-B.; Duan, Y.-A.; Geng, Y.; Li, H.-B.; Zhang, J.-Z.; Xu, H.-L.; Zhang, M.; Su, Z.-M. A Designed Bithiopheneimide-Based Conjugated Polymer for Organic Photovoltaic with Ultrafast Charge Transfer at donor/PC71BM Interface: Theoretical Study and Characterization. *Phys. Chem. Chem. Phys.* **2014**, *16*, 25799–25808.

(155) Pina, J.; Seixas de Melo, J. S.; Eckert, A.; Scherf, U. Unusual Photophysical Properties of Conjugated, Alternating Indigo-Fluorene Copolymers. *J. Mater. Chem. A* **2015**, *3* (12), 6373–6382.

(156) Zhang, F.; Bijleveld, J.; Perzon, E.; Tvingstedt, K.; Barrau, S.; Inganäs, O.; Andersson, M. R. High Photovoltage Achieved in Low Band Gap Polymer Solar Cells by Adjusting Energy Levels of a Polymer with the LUMOs of Fullerene Derivatives. *J. Mater. Chem.* **2008**, *18* (45), 5468–5474.

(157) Westenhoff, S.; Beenken, W. J. D.; Yartsev, A.; Greenham, N. C. Conformational Disorder of Conjugated Polymers. *J. Chem. Phys.* **2006**, *125* (15), 154903.

(158) Yaliraki, S. N.; Silbey, R. J. Conformational Disorder of Conjugated Polymers: Implications for Optical Properties. *J. Chem. Phys.* **1996**, *104* (4), 1245–1253.

(159) Sancho-García, J. .; Brédas, J. .; Cornil, J. Assessment of the Reliability of the Perdew–Burke–Ernzerhof Functionals in the Determination of Torsional Potentials in Π-Conjugated Molecules. *Chem. Phys. Lett.* **2003**, *377* (1–2), 63–68.

(160) Shand, M. L.; Chance, R. R.; LePostollec, M.; Schott, M. Raman Photoselection and Conjugation-Length Dispersion in Conjugated Polymer Solutions. *Phys. Rev. B* **1982**, *25* (7), 4431–4436.

(161) Rossi, G.; Chance, R. R.; Silbey, R. Conformational Disorder in Conjugated Polymers. *J. Chem. Phys.* **1989**, *90* (12), 7594–7601.

(162) Grimsdale, A. C.; Müllen, K. Oligomers and Polymers Based on Bridged Phenylenes as Electronic Materials. *Macromol. Rapid Commun.* **2007**, *28* (17), 1676–1702.

(163) Atkins, P.; Friedman, R. *Molecular Quantum Mechanics*, 4th ed.; Oxford University Press: New York, 2005.

(164) Barford, W. *Electronic and Optical Properties of Conjugated Polymers*; Oxford University Press: Oxford, 2013.

(165) Slooff, L. H.; Veenstra, S. C.; Kroon, J. M.; Moet, D. J. D.; Sweelssen, J.; Koetse, M. M. Determining the Internal Quantum Efficiency of Highly Efficient Polymer Solar Cells through Optical Modeling. *Appl. Phys. Lett.* **2007**, *90* (14), 143506.

(166) Inganäs, O.; Svensson, M.; Zhang, F.; Gadisa, A.; Persson, N. K.; Wang, X.; Andersson, M. R. Low Bandgap Alternating Polyfluorene Copolymers in Plastic Photodiodes and Solar Cells. *Appl. Phys. Mater. Sci. Process.* **2004**, *79* (1), 31–35.

(167) Kim, Y.; Yeom, H. R.; Kim, J. Y.; Yang, C. High-Efficiency Polymer Solar Cells with a Cost-Effective Quinoxaline Polymer through Nanoscale Morphology Control Induced by Practical Processing Additives. *Energy Environ. Sci.* **2013**, *6* (6), 1909–1916.

(168) Wang, E.; Ma, Z.; Zhang, Z.; Vandewal, K.; Henriksson, P.; Inganäs, O.; Zhang, F.; Andersson, M. R. An Easily Accessible Isoindigo-Based Polymer for High-Performance Polymer Solar Cells. *J. Am. Chem. Soc.* **2011**, *133* (36), 14244–14247.

(169) Carle, J. E.; Andreasen, B.; Tromholt, T.; Madsen, M. V.; Norrman, K.; Jorgensen, M.; Krebs, F. C. Comparative Studies of Photochemical Cross-Linking Methods for Stabilizing the Bulk Hetero-Junction Morphology in Polymer Solar Cells. *J. Mater. Chem.* **2012**, *22* (46), 24417–24423.

(170) Yeo, J.-S.; Yun, J.-M.; Jung, Y.-S.; Kim, D.-Y.; Noh, Y.-J.; Kim, S.-S.; Na, S.-I. Sulfonic Acid-Functionalized, Reduced Graphene Oxide as an Advanced Interfacial Material Leading to Donor Polymer-Independent High-Performance Polymer Solar Cells. *J. Mater. Chem. A* **2014**, *2* (2), 292–298.

(171) Vandewal, K.; Tvingstedt, K.; Inganäs, O. Polarization Anisotropy of Charge Transfer Absorption and Emission of Aligned Polymer:fullerene Blend Films. *Phys. Rev. B* **2012**, *86* (3), 035212.

(172) Xia, Y.; Hou, L.; Ma, K.; Wang, B.; Xiong, K.; Liu, P.; Liao, J.; Wen, S.; Wang, E. Pyramid Shape of Polymer Solar Cells: A Simple Solution to Triple Efficiency. *J. Phys. Appl. Phys.* **2013**, *46* (30), 305101.

(173) Vithanage, D. A.; Wang, E.; Wang, Z.; Ma, F.; Inganäs, O.; Andersson, M. R.; Yartsev, A.; Sundström, V.; Pascher, T. Charge Carrier Dynamics of Polymer:Fullerene Blends: From Geminate to Non-Geminate Recombination. *Adv. Energy Mater.* **2014**, *4* (8), 1301706.

(174) Zhuang, W.; Zhen, H.; Kroon, R.; Tang, Z.; Hellstrom, S.; Hou, L.; Wang, E.; Gedefaw, D.; Inganäs, O.; Zhang, F.; et al. Molecular Orbital Energy Level Modulation through Incorporation of Selenium and Fluorine into Conjugated Polymers for Organic Photovoltaic Cells. *J. Mater. Chem. A* **2013**, *1* (43), 13422–13425.

(175) Dutta, G. K.; Kim, T.; Choi, H.; Lee, J.; Kim, D. S.; Kim, J. Y.; Yang, C. Synthesis of Fluorinated Analogues of a Practical Polymer TQ for Improved Open-Circuit Voltages in Polymer Solar Cells. *Polym. Chem.* **2014**, *5* (7), 2540–2547.

(176) Jackson, N. E.; Kohlstedt, K. L.; Savoie, B. M.; Olvera de la Cruz, M.; Schatz, G. C.; Chen, L. X.; Ratner, M. A. Conformational Order in Aggregates of Conjugated Polymers. *J. Am. Chem. Soc.* **2015**.

(177) Sinnokrot, M. O.; Valeev, E. F.; Sherrill, C. D. Estimates of the Ab Initio Limit for Π−π Interactions: The Benzene Dimer. *J. Am. Chem. Soc.* **2002**, *124* (36), 10887–10893.

(178) Roesky, H. W.; Andruh, M. The Interplay of Coordinative, Hydrogen Bonding and Π-Π Stacking Interactions in Sustaining Supramolecular Solid-State Architectures.:

A Study Case of bis(4-Pyridyl)- and bis(4-Pyridyl-N-Oxide) Tectons. *Coord. Chem. Rev.* **2003**, *236* (1-2), 91–119.

(179) Jackson, N. E.; Savoie, B. M.; Kohlstedt, K. L.; Olvera de la Cruz, M.; Schatz, G. C.; Chen, L. X.; Ratner, M. A. Controlling Conformations of Conjugated Polymers and Small Molecules: The Role of Nonbonding Interactions. *J. Am. Chem. Soc.* **2013**, *135* (28), 10475–10483.

(180) Yum, S.; An, T. K.; Wang, X.; Lee, W.; Uddin, M. A.; Kim, Y. J.; Nguyen, T. L.; Xu, S.; Hwang, S.; Park, C. E.; et al. Benzotriazole-Containing Planar Conjugated Polymers with Noncovalent Conformational Locks for Thermally Stable and Efficient Polymer Field-Effect Transistors. *Chem. Mater.* **2014**, *26* (6), 2147–2154.

(181) Lee, W.; Kim, G.-H.; Ko, S.-J.; Yum, S.; Hwang, S.; Cho, S.; Shin, Y.-H.; Kim, J. Y.; Woo, H. Y. Semicrystalline D–A Copolymers with Different Chain Curvature for Applications in Polymer Optoelectronic Devices. *Macromolecules* **2014**, *47* (5), 1604–1612.

(182) Meyer, E. A.; Castellano, R. K.; Diederich, F. Interactions with Aromatic Rings in Chemical and Biological Recognition. *Angew. Chem. Int. Ed.* **2003**, *42* (11), 1210–1250.

(183) Tavernelli, I.; Di Iorio, E. E. The Interplay between Protein Dynamics and Frustration of Non-Bonded Interactions as Revealed by Molecular Dynamics Simulations. *Chem. Phys. Lett.* **2001**, *345* (3–4), 287–294.

(184) Bahar, I.; Jernigan, R. L. Inter-Residue Potentials in Globular Proteins and the Dominance of Highly Specific Hydrophilic Interactions at Close separation1. *J. Mol. Biol.* **1997**, *266* (1), 195–214.

(185) Böhm, H. J.; Schneider, G.; Mannhold, R.; Kubinyi, H.; Folkers, G. *Protein-Ligand Interactions: From Molecular Recognition to Drug Design*; Methods and Principles in Medicinal Chemistry; Wiley: New York, 2006.

(186) Nilsson, J. A.; Eriksson, L. A.; Laaksonen, A. Molecular Dynamics Simulations of Plastoquinone in Solution. *Mol. Phys.* **2001**, *99* (3), 247–253.

(187) Johnson, E. R.; Mackie, I. D.; DiLabio, G. A. Dispersion Interactions in Density-Functional Theory. *J. Phys. Org. Chem.* **2009**, *22* (12), 1127–1135.

(188) Grimme, S. Semiempirical GGA-Type Density Functional Constructed with a Long-Range Dispersion Correction. *J. Comput. Chem.* **2006**, *27* (15), 1787–1799.

(189) Peverati, R.; Baldridge, K. K. Implementation and Performance of DFT-D with Respect to Basis Set and Functional for Study of Dispersion Interactions in Nanoscale Aromatic Hydrocarbons. *J. Chem. Theory Comput.* **2008**, *4* (12), 2030–2048.

(190) Von Lilienfeld, O. A.; Tavernelli, I.; Rothlisberger, U.; Sebastiani, D. Optimization of Effective Atom Centered Potentials for London Dispersion Forces in Density Functional Theory. *Phys. Rev. Lett.* **2004**, *93* (15), 153004.

(191) Kong, J.; Gan, Z.; Proynov, E.; Freindorf, M.; Furlani, T. R. Efficient Computation of the Dispersion Interaction with Density-Functional Theory. *Phys. Rev. A* **2009**, *79* (4), 042510.

(192) Tang, Z.; Andersson, L. M.; George, Z.; Vandewal, K.; Tvingstedt, K.; Henriksson, P.; Kroon, R.; Andersson, M. R.; Inganäs, O. Interlayer for Modified Cathode in

Highly Efficient Inverted ITO-Free Organic Solar Cells. *Adv. Mater.* **2012**, *24* (4), 554–558.

(193) Liu, K.; Li, Y.; Yang, M. Novel 1,4-Diketo-3,6-Diphenyl pyrrolo[3,4-C]pyrrole (DPP)-Based Copolymers with Large Stokes Shift. *J. Appl. Polym. Sci.* **2009**, *111* (4), 1976–1984.

(194) Deibel, C.; Mack, D.; Gorenflot, J.; Schöll, A.; Krause, S.; Reinert, F.; Rauh, D.; Dyakonov, V. Energetics of Excited States in the Conjugated Polymer poly(3-Hexylthiophene). *Phys. Rev. B* **2010**, *81* (8), 085202.

(195) Tieke, B.; Rabindranath, A. R.; Zhang, K.; Zhu, Y. Conjugated Polymers Containing Diketopyrrolopyrrole Units in the Main Chain. *Beilstein J. Org. Chem.* **2010**, *6*, 830–845.

(196) Colladet, K.; Fourier, S.; Cleij, T. J.; Lutsen, L.; Gelan, J.; Vanderzande, D.; Huong Nguyen, L.; Neugebauer, H.; Sariciftci, S.; Aguirre, A.; et al. Low Band Gap Donor−Acceptor Conjugated Polymers toward Organic Solar Cells Applications. *Macromolecules* **2007**, *40* (1), 65–72.

(197) Dutta, T.; Woody, K. B.; Parkin, S. R.; Watson, M. D.; Gierschner, J. Conjugated Polymers with Large Effective Stokes Shift: Benzobisdioxole-Based Poly(phenylene Ethynylene)s. *J. Am. Chem. Soc.* **2009**, *131* (47), 17321–17327.

(198) Banerji, N. Sub-Picosecond Delocalization in the Excited State of Conjugated Homopolymers and Donor-Acceptor Copolymers. *J. Mater. Chem. C* **2013**, *1* (18), 3052–3066.

(199) Hwang, I.; Scholes, G. D. Electronic Energy Transfer and Quantum-Coherence in Π-Conjugated Polymers. *Chem. Mater.* **2011**, *23* (3), 610–620.

(200) Westenhoff, S.; Beenken, W. J. D.; Friend, R. H.; Greenham, N. C.; Yartsev, A.; Sundström, V. Anomalous Energy Transfer Dynamics due to Torsional Relaxation in a Conjugated Polymer. *Phys. Rev. Lett.* **2006**, *97* (16), 166804.

(201) Yan, H.; Chen, Z.; Zheng, Y.; Newman, C.; Quinn, J. R.; Dotz, F.; Kastler, M.; Facchetti, A. A High-Mobility Electron-Transporting Polymer for Printed Transistors. *Nature* **2009**, *457* (7230), 679–686.

(202) McNeill, C. R.; Abrusci, A.; Zaumseil, J.; Wilson, R.; McKiernan, M. J.; Burroughes, J. H.; Halls, J. J. M.; Greenham, N. C.; Friend, R. H. Dual Electron Donor/electron Acceptor Character of a Conjugated Polymer in Efficient Photovoltaic Diodes. *Appl. Phys. Lett.* **2007**, *90* (19), 193506.

(203) Babel, A.; Zhu, Y.; Cheng, K.-F.; Chen, W.-C.; Jenekhe, S. A. High Electron Mobility and Ambipolar Charge Transport in Binary Blends of Donor and Acceptor Conjugated Polymers. *Adv. Funct. Mater.* **2007**, *17* (14), 2542–2549.

(204) Yang, C.; Orfino, F. P.; Holdcroft, S. A Phenomenological Model for Predicting Thermochromism of Regioregular and Nonregioregular Poly(3-Alkylthiophenes). *Macromolecules* **1996**, *29* (20), 6510–6517.

(205) Katz, E. A.; Faiman, D.; Tuladhar, S. M.; Kroon, J. M.; Wienk, M. M.; Fromherz, T.; Padinger, F.; Brabec, C. J.; Sariciftci, N. S. Temperature Dependence for the Photovoltaic Device Parameters of Polymer-Fullerene Solar Cells under Operating Conditions. *J. Appl. Phys.* **2001**, *90* (10), 5343–5350.

(206) Sancho-García, J. C.; Cornil, J. Anchoring the Torsional Potential of Biphenyl at the Ab Initio Level: The Role of Basis Set versus Correlation Effects. *J. Chem. Theory Comput.* **2005**, *1* (4), 581–589.

(207) Poater, J.; Solà, M.; Bickelhaupt, F. M. Hydrogen–Hydrogen Bonding in Planar Biphenyl, Predicted by Atoms-In-Molecules Theory, Does Not Exist. *Chem. – Eur. J.* **2006**, *12* (10), 2889–2895.

(208) Wang, E.; Mammo, W.; Andersson, M. R. 25th Anniversary Article: Isoindigo-Based Polymers and Small Molecules for Bulk Heterojunction Solar Cells and Field Effect Transistors. *Adv. Mater.* **2014**, *26* (12), 1801–1826.

(209) Lei, T.; Cao, Y.; Zhou, X.; Peng, Y.; Bian, J.; Pei, J. Systematic Investigation of Isoindigo-Based Polymeric Field-Effect Transistors: Design Strategy and Impact of Polymer Symmetry and Backbone Curvature. *Chem. Mater.* **2012**, *24* (10), 1762–1770.

(210) Xu, X.; Cai, P.; Lu, Y.; Choon, N. S.; Chen, J.; Hu, X.; Ong, B. S. Synthesis and Characterization of thieno[3,2-B]thiophene-Isoindigo-Based Copolymers as Electron Donor and Hole Transport Materials for Bulk-Heterojunction Polymer Solar Cells. *J. Polym. Sci. Polym. Chem.* **2013**, *51* (2), 424–434.

(211) Zhuang, W.; Bolognesi, M.; Seri, M.; Henriksson, P.; Gedefaw, D.; Kroon, R.; Jarvid, M.; Lundin, A.; Wang, E.; Muccini, M.; et al. Influence of Incorporating Different Electron-Rich Thiophene-Based Units on the Photovoltaic Properties of Isoindigo-Based Conjugated Polymers: An Experimental and DFT Study. *Macromolecules* **2013**, *46* (21), 8488–8499.

(212) Kronik, L.; Stein, T.; Refaely-Abramson, S.; Baer, R. Excitation Gaps of Finite-Sized Systems from Optimally Tuned Range-Separated Hybrid Functionals. *J. Chem. Theory Comput.* **2012**, *8* (5), 1515–1531.

(213) Zhou, H.; Zhang, Y.; Mai, C.-K.; Collins, S. D.; Bazan, G. C.; Nguyen, T.-Q.; Heeger, A. J. Polymer Homo-Tandem Solar Cells with Best Efficiency of 11.3%. *Adv. Mater.* **2015**, *27* (10), 1767–1773.

(214) Yusoff, A. R. bin M.; Kim, D.; Kim, H. P.; Shneider, F. K.; da Silva, W. J.; Jang, J. A High Efficiency Solution Processed Polymer Inverted Triple-Junction Solar Cell Exhibiting a Power Conversion Efficiency of 11.83%. *Energy Environ. Sci.* **2015**, *8* (1), 303–316.

(215) Chen, C.-C.; Chang, W.-H.; Yoshimura, K.; Ohya, K.; You, J.; Gao, J.; Hong, Z.; Yang, Y. An Efficient Triple-Junction Polymer Solar Cell Having a Power Conversion Efficiency Exceeding 11%. *Adv. Mater.* **2014**, *26* (32), 5670–5677.

(216) Facchetti, A. Polymer Donor–polymer Acceptor (all-Polymer) Solar Cells. *Mater. Today* **2013**, *16* (4), 123–132.

(217) Lin, Y.; Zhan, X. Non-Fullerene Acceptors for Organic Photovoltaics: An Emerging Horizon. *Mater. Horiz.* **2014**, *1* (5), 470–488.

(218) Ameri, T.; Khoram, P.; Min, J.; Brabec, C. J. Organic Ternary Solar Cells: A Review. *Adv. Mater.* **2013**, *25* (31), 4245–4266.

(219) Yang, Y. M.; Chen, W.; Dou, L.; Chang, W.-H.; Duan, H.-S.; Bob, B.; Li, G.; Yang, Y. High-Performance Multiple-Donor Bulk Heterojunction Solar Cells. *Nat Photon* **2015**, *9* (3), 190–198.

(220) Kang, T. E.; Kim, K.-H.; Kim, B. J. Design of Terpolymers as Electron Donors for Highly Efficient Polymer Solar Cells. *J. Mater. Chem. A* **2014**, *2* (37), 15252–15267.

(221) Sun, W.; Ma, Z.; Dang, D.; Zhu, W.; Andersson, M. R.; Zhang, F.; Wang, E. An Alternating D-A1-D-A2 Copolymer Containing Two Electron-Deficient Moieties for Efficient Polymer Solar Cells. *J. Mater. Chem. A* **2013**, *1* (37), 11141–11144.

(222) Rauk, A. *Orbital Interaction Theory of Organic Chemistry*; Wiley: New York, 2004.

(223) Lanzani, G. *The Photophysics behind Photovoltaics and Photonics*; Wiley: New York, 2012.

(224) Campoy-Quiles, M.; Etchegoin, P. G.; Bradley, D. D. C. On the Optical Anisotropy of Conjugated Polymer Thin Films. *Phys. Rev. B* **2005**, *72* (4), 045209.

(225) Marshall, G. M.; Lopinski, G. P.; Bensebaa, F.; Dubowski, J. J. Surface Dipole Layer Potential Induced IR Absorption Enhancement in N-Alkanethiol SAMs on GaAs(001). *Langmuir* **2009**, *25* (23), 13561–13568.

(226) Pettersson, L. A.; Roman, L. S.; Inganäs, O. Modeling Photocurrent Action Spectra of Photovoltaic Devices Based on Organic Thin Films. *J. Appl. Phys.* **1999**, *86* (1), 487–496.

(227) Burkhard, G. F.; Hoke, E. T.; McGehee, M. D. Accounting for Interference, Scattering, and Electrode Absorption to Make Accurate Internal Quantum Efficiency Measurements in Organic and Other Thin Solar Cells. *Adv. Mater.* **2010**, *22* (30), 3293–3297.

(228) Li, Z.; Malenfant, P.; Tao, Y.; Ding, J. Thermochromic and Photovoltaic Properties of an Alternating Copolymer of Dithieno[3,2-b:2′,3′-D]thiophene and Thieno[3,4-C]pyrrole-4,6-Dione. *Macromol. Chem. Phys.* **2013**, *214* (4), 447–452.

(229) Stein, T.; Eisenberg, H.; Kronik, L.; Baer, R. Fundamental Gaps in Finite Systems from Eigenvalues of a Generalized Kohn-Sham Method. *Phys. Rev. Lett.* **2010**, *105* (26), 266802.

(230) Körzdörfer, T.; Sears, J. S.; Sutton, C.; Brédas, J.-L. Long-Range Corrected Hybrid Functionals for Π-Conjugated Systems: Dependence of the Range-Separation Parameter on Conjugation Length. *J. Chem. Phys.* **2011**, *135* (20), 204107.

(231) Minami, T.; Nakano, M.; Castet, F. Nonempirically Tuned Long-Range Corrected Density Functional Theory Study on Local and Charge-Transfer Excitation Energies in a Pentacene/C60 Model Complex. *J. Phys. Chem. Lett.* **2011**, *2* (14), 1725–1730.

Paper I

PCCP

PAPER

View Article Online
View Journal | View Issue

Cite this: *Phys. Chem. Chem. Phys.*, 2014, **16**, 24853

Light-harvesting capabilities of low band gap donor–acceptor polymers†

Svante Hedström,[a] Patrik Henriksson,[b] Ergang Wang,[b] Mats R. Andersson[bc] and Petter Persson*[a]

Received 18th July 2014,
Accepted 6th October 2014

DOI: 10.1039/c4cp03191a

www.rsc.org/pccp

A series of nine donor–acceptor polymers, including three new and six polymers from previous work, have been investigated experimentally and theoretically. The investigation focuses on narrow band gaps and strong absorptions of the polymers, where experimentally determined first peak absorption energies range from 1.8 to 2.3 eV, and peak absorption coefficients vary between 19–67 L g^{-1} cm^{-1}. An overall assessment of each polymer's light-harvesting capability is made, and related to the chemical structure. Oligomer calculations using density functional theory are extrapolated to obtain size-converged polymer properties, and found to reproduce the experimental absorption trends well. Accurate theoretical predictions of absorption energies to within 0.06 eV of experiments, and absorption strength to within 12%, are obtained through the introduction of an empirical correction scheme. The computational and experimental results provide insight for the design of polymers with efficient absorption, concerning the intrinsic properties of the constituent units and the use of bulky side-groups.

Introduction

Organic photovoltaics (OPVs) are promising as energy producing devices.[1–3] They typically consist of a conjugated polymer capable of absorbing visible light, mixed with a Buckminster-fullerene derivative. Since the polymer is the main light-absorbing component, the choice of polymer dictates the optical response of the cell. Poly(3-hexyl-thiophene-2,5-diyl) (P3HT) has been very commonly used since the late 20th century,[4] but its limited spectral coverage has prompted extensive research to find donor–acceptor (D–A) copolymers with better light-harvesting capabilities.[5–8] These D–A polymers consist of alternating electron-donating and -accepting moieties along the conjugated backbone, and by varying these building blocks, the absorption profile of the polymer can be tuned. Several experimental[5,9–11] and computational[12–16] studies have been published recently on D–A polymers yielding high-efficiency solar cells. The most important optical properties of D–A polymers are the absorption strength and optical band gap. Strong absorption and narrow optical band gaps of <2 eV both contribute to the number of photons absorbed and thus the external quantum efficiency (EQE),[2] and current (J) generated by the OPV device.

Optical and electronic properties of polymers typically depend on the conformation which is sensitive to the environment, as well as being hard to determine experimentally. In this study, polymers have been studied experimentally in solution, providing a good opportunity for deeper understanding of the intrinsic properties of individual polymer chains, and for detailed comparison with molecular quantum chemical calculations. Computational analysis provides a deeper understanding of the structure–property relationship in polymers, which can guide the development strategies for new polymer motifs. Quantitative calculations of optical properties furthermore have the potential to reduce the time-consuming effort of synthesizing a large number of D–A polymers, and subsequently making films and analyzing them experimentally. This aids the development of more efficient OPVs,[5,17–19] even though complete accuracy of the computational methods remain a challenge. Single-molecule calculations constitute a stepping stone towards more elaborate calculations of polymer films and blends where intermolecular interactions play a more significant role.

Six previously reported D–A polymers with various donor and acceptor components and diverse optical traits are here investigated: APFO-3,[20] APFO-15,[21] APFO-G9,[22] EWC3,[23] and TQ1,[24] developed at Polymer Technology at Chalmers University, and BDT-BTz.[25] Three new polymers were synthesized for the first

[a] *Division of Theoretical Chemistry, Lund University, P.O. Box 124, S-221 00 Lund, Sweden. E-mail: petter.persson@teokem.lu.se; Fax: +46-462228648; Tel: +46-462223311*

[b] *Department of Chemical and Biological Engineering/Polymer Technology, Chalmers University of Technology, S-412 96 Gothenburg, Sweden*

[c] *Ian Wark Research Institute, University of South Australia, Mawson Lakes, South Australia 5095, Australia*

† Electronic supplementary information (ESI) available: Images of optimized monomers; square wave voltammetry measurement plots; tabulated polymer E_{abs} and F_M; details on size dependence of absorption strengths; synthesis procedure for the polymers TBDT-Q, TBDT-T-TP-T, BDT-BTz, and EWC4; calculated excitation data. See DOI: 10.1039/c4cp03191a

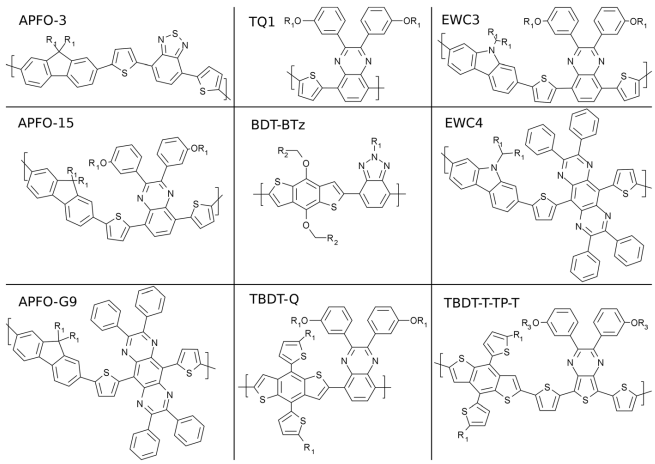

Chart 1 Chemical structures of the nine investigated polymers. R_1 = 1′-octyl, R_2 = 3′-heptyl, R_3 = 1′-hexyl.

time to further explore chemical components conferring narrow band gaps and/or strong absorption: TBDT-Q named for its thienylbenzodithiophene (TBDT) donor and quinoxaline (Q) acceptor, TBDT-T-TP-T with a thiophene–thienylbenzodithiophene–thiophene donor and thienopyrazine (TP) acceptor, and EWC4 with a thiophene–carbazole–thiophene donor and pyrazinoquinoxaline (PzQ) acceptor. TBDT-Q, BDT-BTz, and TQ1 consist of one donor and one acceptor ring-system per repeating unit, whereas the remaining six polymers have donors of type T–X–T where X = fluorene, carbazole, or thienyl-benzodithiophene and T = thiophene. Overall, this set of selected polymers represents the diversity in structures and properties covered by D–A polymers applied in OPVs today. Five different donor and five acceptor units are used throughout the nine polymers, and their structures are outlined in Chart 1.

This article is centered on the assessment of light-harvesting capabilities across the series of nine polymers, with particular emphasis on narrow band gaps and strong absorption. Quantitative comparison between experimental measurements and calculated results was used to develop a highly accurate computational scheme for size-converged absorption energies and strengths, providing the means to efficiently predict experimental properties. In the results sections, structural features of the nine polymers are first presented, followed by electronic properties, and a discussion regarding light-harvesting potential. The outcomes of measurements and calculations are finally discussed and compared in order to identify promising polymer design strategies.

Methods

General

Unless otherwise stated all reactions were performed under nitrogen atmosphere and all chemicals were bought from Sigma-Aldrich or Acros and used as received. Anhydrous THF was dried over and distilled from sodium benzophenone ketyl under an atmosphere of dry nitrogen.

Optical characterization

Absorption spectra were measured using a Perkin Elmer 900 UV/VIS/NIR. Samples were prepared by dissolving ~1 mg polymer in 50 mL of *ortho*-dichlorobenzene (*o*-DCB), which was chosen for its good dissolving capacity, while its absorption in the UV region does not affect the results which focus on the red-most absorption peaks of the polymers. The polymer solutions were heated up to ensure complete dissolution of the polymer into the solvent and then allowed to cool down to room temperature before the spectra were recorded. The experimental absorption coefficients ε (in L g^{-1} cm^{-1}) were calculated from Beer–Lambert's law: $A = \varepsilon cl$.

Electrochemical characterization

Square-wave voltammetric measurements were carried out using a 0.1 M solution of tetrabutylammonium hexafluorophosphate in anhydrous acetonitrile as supporting electrolyte at a scan rate of 125 mV s^{-1}. A CH-Instruments 650 D electrochemical workstation using a three electrode setup was used, consisting of a Ag/Ag^+ reference electrode and platinum wires as working- and counter electrodes. The polymer was deposited onto the working electrode from chloroform solution. The electrolyte was bubbled with nitrogen gas prior to each experiment in order to remove oxygen from the system. During the scans the nitrogen inlet was raised above the electrolyte surface to not disturb the measurement. After each experiment a calibration scan using the ferrocene/ferrocenium (Fc/Fc^+) redox reaction was performed. The highest occupied (HOMO) and lowest unoccupied molecular orbital (LUMO) energy levels were approximated from the third oxidation and reduction scan respectively, using the peak

values and setting the oxidative potential of Fc/Fc^+ *vs.* the normal hydrogen electrode (NHE) to 0.630 V[26] and the NHE *vs.* vacuum to 4.5 V.[27]

Size exclusion chromatography

Waters Alliance GPCV2000 with refractive index detector columns: Waters Styvagel HT GE × 1, Waters Styvagel HMW GE × 2. The operating temperature was 135 °C, the eluent used was 1,2,4-trichlorobenzene and the dissolution time was 2 h. The samples were filtered prior to analysis (0.45 μm) and the concentration was 0.5 mg mL^{-1}. The molecular masses were calculated using polystyrene standards for relative calibration.

Synthesis

See ESI† for the synthesis details of the polymers TBDT-Q, TBDT-T-TP-T, BDT-BTz, and EWC4.

Calculations

Density functional theory (DFT) relaxations at the PBE0[28]/6-31G(d,p) level of theory were conducted on oligomers with 1, 2, 3, and 5 repeating units, except where the pentamer size was deemed too computationally demanding, and was replaced by a tetramer. TQ1 oligomers with 1–9 repeating units underwent relaxations at the same level. Long alkyl side-chains were truncated to shorter ones, depending on branching and chemical environment. Time dependent (TD)-DFT was then applied to each system in order to calculate the lowest energy vertical excitations that constitute the first absorption peak in the respective polymers. An extended TD-DFT scheme including excitations that cover the entire visible region was applied to the oligomer lengths that give the best match to the respective experimental spectrum. $PC_{61}BM$ underwent a PBE0/6-31G(d,p) calculation. BDT-BTz, TQ1, APFO-G9, TBDT-Q, and TBDT-T-TP-T were subject to TD-DFT calculations using an *o*-DCB polarizable continuum model (PCM) solvent. All DFT calculations were carried out with the Gaussian 09 package.[29]

Results

Structural properties

The average molecular weights of the polymers were determined by size exclusion chromatography (SEC). Table 1 shows that the polymers display considerable variation in weights and polydispersity indices. Optical traits generally depend somewhat on the number of repeating units until they converge for longer polymers. It is assumed that the weights in Table 1, corresponding in all cases to at least 7 repeating units, are sufficiently large for convergence.

The polymers were modeled as oligomers for the computational investigation, due to size restrictions of the first-principle quantum chemical methods. Oligomers of 1–5 repeating units were optimized computationally in order to determine the minimum energy conformation. Like most conjugated D–A polymers,[6] the oligomers consist of stiff, planar ring-systems, connected by flexible single bonds along the backbones. Though a planar geometry is favored from an electronic conjugation perspective, the optimizations yield geometries with the ring-systems out of plane by 3–22° (see Table 1), due to steric hindrance. The non-planarity varies significantly between the polymers, with BDT-BTz and TBDT-T-TP-T having the smallest average angles corresponding to 3.5° and 4.2° out of plane respectively, which is due to the lack of H–H collisions between rings in these two polymers, (see the optimized monomers in Fig. S1, ESI†). APFO-G9, EWC4, and TQ1 have the largest calculated dihedral angles ~20° due to their bulky phenyl side-groups which for TQ1 imposes a helical minimum energy conformation.[30] Even larger dihedrals have been reported for TQ1 in the *trans*-conformation,[31] but our calculations suggest the *cis*-form as the minimum-energy geometry.

The fact that the rigid ring-systems can rotate over the single bonds between them bestows conformational isomerism. Local structural energy minima occurs when the dihedral angle between neighboring units is either slightly larger or smaller than 0° or 180° respectively, generating four local minima per single bond. In the monomers, the number of such single bonds range between one in BDT-BTz to seven in APFO-G9, EWC4, and TBDT-T-TP-T, which for the latter means that under the approximation that the dihedral angles are individually independent, up to 28 locally optimized geometries must be compared to identify the global minimum for each polymer. However, the recurrence of certain structural elements reduces the number of conformations requiring exploration.

Long alkyl side-chains are included in the synthesized polymers for increased solubility.[31] Since such effects are beyond the scope of this study, the chains are replaced by shorter alkanes in the calculations that focus on electronic properties. All polymers except APFO-3 and BDT-BTz also contain off-backbone phenyl- and thiophene moieties. The weight fractions of side-groups are reported in Table 1.

Electronic structure

Electronic structure properties of the D–A polymers are crucial for the functioning of the solar cell. In particular, HOMO and

Table 1 Structural properties. Molar mass averages, M_n and M_w, in kDa of the polymers measured by SEC. Weight fraction of the off-backbone side-groups in %. The average calculated dihedral angles between aryl rings along the backbone in optimized trimers, expressed as number of degrees out-of-plane

	BDTBTz	TBDTTTPT	APFO3	APFO15	TBDTQ	EWC3	TQ1	APFOG9	EWC4
M_n/kDa	8.1	8.5	18	15	8.7	23	56	11	12
M_w/kDa	21	74	32	36	18	62	170	26	22
Sidegroup/%	51	61	33	58	72	59	66	52	52
Out-of-plane/°	3.5	4.2	14.0	15.1	16.3	19.3	20.0	21.4	21.9

LUMO frontier orbitals typically constitute the origin and target orbital of the first electronic excitation, respectively. The polymer HOMO is furthermore responsible for hole-transport to the anode, while the electron should be injected from the polymer LUMO to the fullerene after excitation. Calculated HOMOs and LUMOs are depicted in Fig. 1. Generally, the HOMOs have good delocalization over the polymer backbones, favoring efficient hole-transport.[16] The LUMOs are more determined by the acceptor unit, so *e.g.* APFO-15, EWC-3, TBDT-Q, and TQ1 consequently exhibit very similar appearance between them since these all employ a Q acceptor. The LUMOs are also denser at the respective acceptor moieties, particularly apparent for the polymers with T–X–T donors where the acceptors are more spatially separated from each other. The frontier orbitals strongly affect the first electronic transition densities, also depicted in Fig. 1. The tendency for LUMO to be localized on the acceptor unit induces a clear D–A effect for all polymers, with electrons moving from donor to acceptor upon excitation. This can be exploited to give more narrow band gaps by choosing acceptors with deeper LUMO level, such as PzQ in APFO-G9 and EWC4.

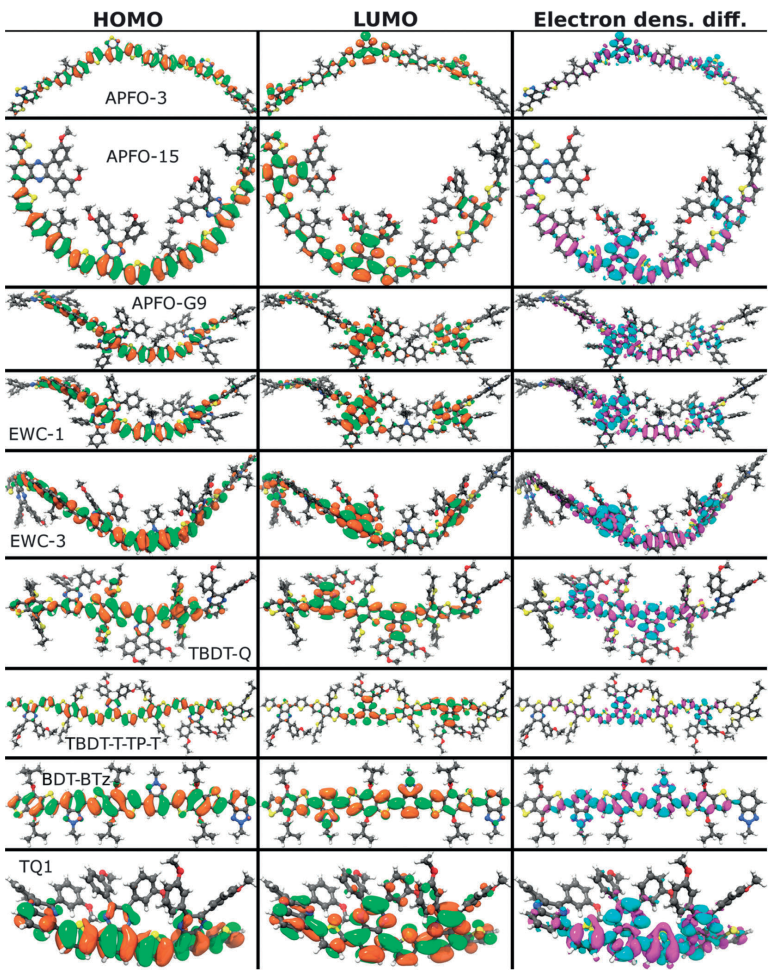

Fig. 1 Frontier orbitals (isovalue = 0.015), and excited state electron density difference (isovalue = 0.0004) of optimized trimers, with electrons being transferred from purple to turquoise upon excitation. Calculated with TD-PBE0/6-31G(d,p). Note that a short repeating unit leads to a short trimer.

Furthermore, it is evident that electronic excitation generates larger electron density in the single bonds between ring-systems, giving them an increased double-bond character in the excited state, which in turn accounts for the trend among conjugated systems that the excited state is more planar than the ground state.[32–37]

The polymer HOMO and LUMO energies are important since the difference between them is related to the optical energy of maximum absorption (E_{abs}). In addition, the LUMO(fullerene)–HOMO(polymer) energy difference determines the open circuit voltage of the cell, while the LUMO(polymer)–LUMO(fullerene) energy offset constitutes the electron injection driving force. Since our calculations are based on smaller oligomers, we employ an extrapolation technique to obtain size-converged frontier orbital energies, as follows. According to the tight binding approximation in theory of solids, a single orbital of a monomer splits into n orbitals upon oligomerization to a linear n-mer, with each orbital's energy given by the formula:[38]

$$E_k(n) = \alpha + 2\beta\cos\left(\frac{k\pi}{n+1}\right) \quad k = 1, 2, \ldots, n \qquad (1)$$

where α is the energy of the corresponding non-split orbital (that of a monomer, $n = 1$). The parameters α and β are fitted to the calculated oligomer HOMO and LUMO energies, and the resulting function is plotted *vs.* the inverse oligomer length, $1/n$, in Fig. 2.

The extrapolated frontier orbital energies in Fig. 2 show spreads of ~0.5 eV for both HOMO and LUMO, owing to the diverse chemical composition of the polymers. The suggested[4,39–41] minimum energy difference between polymer and fullerene LUMO 0.30–0.35 eV for efficient electron injection is fulfilled by all polymers herein. The HOMOs are more size-dependent than the LUMOs, which can be rationalized from the orbital pictures in the Fig. 1, where HOMOs display continuous density along the entire backbone, whereas the LUMOs are more isolated on acceptor moieties, making their energies less size-sensitive. The steeper slopes for the smaller polymers in Fig. 2 is explained by the fact that polymers with shorter repeat units require more repeating units than a polymer with a long repeat unit to achieve the same extent of orbital delocalization. The polymers with only two ring-systems per unit: TQ1, BDT-BTz, and TBDT-Q show even more size-dependent LUMO energies, which is due to stronger delocalization of their LUMOs, as seen in Fig. 1. Conversely, APFO-G9 and EWC4 exhibit negligible LUMO stabilization for increasing oligomer length, explained by the fact that their LUMOs are very isolated on their PzQ acceptors, and thus do not further delocalize upon polymerization.

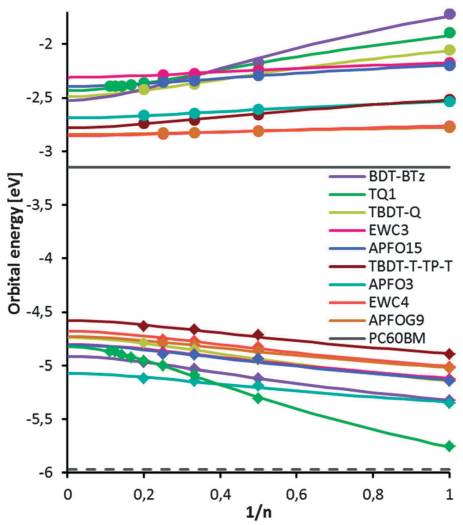

Fig. 2 Calculated HOMO (diamonds) and LUMO (circles) energies as a function of inverse oligomer size, compared to the HOMO and LUMO energies of $PC_{61}BM$, solid and dotted lines, respectively. All energies calculated with PBE0/6-31G(d,p). Lines are fitted to the points according to the tight binding approximation of eqn (1).

The polymers with the same acceptor exhibit very similar extrapolated LUMO energy in Fig. 2. APFO-G9 and EWC4 display the lowest LUMO energies, due to the strong electron-deficiency of their PzQ acceptor. The TBDT-T-TP-T LUMO energy is slightly higher, followed by APFO-3 with a benzothiadiazole (BTD) acceptor, and the benzotriazole (BTz) containing BDT-BTz. Q is the weakest of the acceptors employed, leading to the higher LUMO energies of EWC3, APFO15, TQ1, and TBDT-Q, which may limit their spectral coverage in the lower energy region. Similarly to the LUMO case, the order of the extrapolated HOMOs exhibits the same effect of dependence on acceptor unit, although less pronounced. APFO-3 displays the lowest HOMO energy which contributes to its high V_{OC} of 1.0 eV,[42] whereas TBDT-T-TP-T has the highest HOMO, ~0.5 eV higher than APFO-3. For all polymers, the largest calculated oligomer size (4–5 repeating units) has a LUMO energy converged to within 0.02 eV of the extrapolated value, whereas the greater size-dependence of the HOMOs leads to largest oligomer energies up to 0.11 eV short of the polymeric extrapolated estimate.

The HOMO and LUMO levels were also investigated experimentally by square wave voltammetry (SWV), measurement plots can be found in ESI.† The polymer oxidation potential, *i.e.* extraction of electrons, is related to the HOMO of the material. Respectively, the reduction of the material corresponds to the reception of electrons, related to the LUMO.[43–45] The ordering between polymers is retained in calculations except for TBDT-T-TP-T and EWC3. The experimental SWV peaks in Table 2 are, however, of consistently lower energy than calculated HOMO and LUMO, which is generally the case for conjugated, organic systems.[46–50] The difference is due to the fact that experimental orbital energies are not observables, but are derived from redox-potentials which can only be strictly compared to calculated redox energies. Comparing to calculated orbital energies is possible according to Koopman's theorem, though the disregard of orbital relaxation and solvent effects makes it highly approximate.[51] Furthermore, uncertainty arises in the comparison of wide experimental peaks to calculated point values. The discrepancy in HOMO energy between the two methods is similar for all

Table 2 Square wave voltammetry peak values *vs.* vacuum in eV (see Fig. S2 (ESI) for plots), and HOMO and LUMO as calculated with PBE0/6-31G(d,p). Sorted by experimental HOMO–LUMO gap

	EWC4	APFOG9	BDTQ	TQ1	EWC3	BDTTTPT	APFO3	APFO15	BDTBTz
$HOMO_{SWV}$	−5.7	−5.7	−5.8	−5.7	−5.8	−5.8	−6.0	−6.1	−5.9
$LUMO_{SWV}$	−3.9	−4.0	−3.6	−3.3	−3.3	−3.3	−3.2	−3.2	−2.9
$HOMO_{calc}$	−4.7	−4.7	−4.7	−4.8	−4.8	−4.6	−5.1	−4.8	−4.9
$LUMO_{calc}$	−2.9	−2.8	−2.5	−2.4	−2.3	−2.8	−2.7	−2.4	−2.5
H–L gap_{SWV}	1.7	1.7	2.3	2.4	2.5	2.5	2.8	2.9	3.1
H–L gap_{calc}	1.8	1.9	2.3	2.4	2.5	1.8	2.4	2.4	2.4

polymers, amounting to 0.87–1.26 eV. The overestimations of calculated LUMOs show a greater variation: 0.35–1.11 eV, owing to their virtual nature,[52] which is responsible for discrepancies in HOMO–LUMO gaps of −0.71 to +0.16 eV between the two methods.

Absorption spectra

Experimental polymer solution absorption spectra are shown in Fig. 3, providing an overview of the light-harvesting capabilities of the polymers. There are obvious differences between the measured absorption profiles of the investigated polymers, which are related to their chemical structure. Six of the polymers exhibit classical "double hump" absorption characteristics, while the three (T)BDT-containing polymers show more irregular spectra with additional peaks, making their absorption more panchromatic. Since the solar emission is weak at wavelengths shorter than ∼400 nm, it is for all nine polymers the first, red-most, absorption peak that is most relevant for photovoltaic purposes.

The peak wavelengths ($\lambda_{absmax} = hc/E_{abs}$) of these first peaks range between 533 and 700 nm. The calculated HOMO–LUMO gaps agree better to calculated E_{abs} than to experimental HOMO–LUMO gaps, since the former do not involve orbital relaxation, unlike the latter which are approximated from redox-potentials. The novel polymers TBDT-T-TP-T and EWC4 have the smallest optical band gaps, with absorption onsets at ∼900 nm, similar to APFO-G9, mainly attributed to the low LUMO afforded by their strong acceptors PzQ and TP. APFO-3, APFO-15, EWC3 and BDT-BTz all have absorption onsets at ∼620 nm, which for APFO-3 is attributed to its low HOMO energy, and for the other three mainly due to high LUMO energies. They thus fail to capture significant part of the solar emission.

The maximum absorption coefficients ε_{max}, of the polymers appear related to the acceptor unit. APFO-3 with a BTD acceptor exhibit the greatest first peak absorption coefficient, 67 L cm^{-1} g^{-1}, followed by BDT-BTz. The polymers with PzQ and TP acceptors absorb the weakest; leaving Q as an intermediate absorbing acceptor, except in TBDT-Q whose very low ε_{max} is partly explained by that it has the lowest M_w of all polymers, see Table 1.

Following a common,[15,53–56] but non-predictive practice, the experimental polymer spectra in Fig. 3 are compared to calculated spectra of oligomers whose sizes are chosen *a posteriori* to

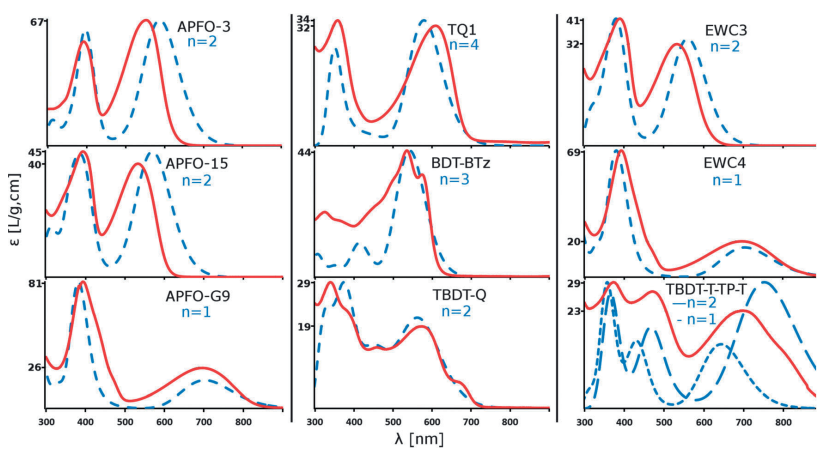

Fig. 3 Experimental (red) and calculated (blue) absorption spectra of the investigated polymers. Experimental as recorded in *o*-DCB solvent. The experimental ε-values for the absorption maxima are marked on the *y*-axis, with secondary (lower) ε-values indicating the red-most peak maxima where this is not the most intense peak for that polymer. The calculated TD-DFT spectra were obtained by a 3000 cm^{-1} Gaussian broadening, and with absorption intensities normalized to match the most intense experimental peak. Numbers of repeating units (*n*) in the oligomer calculations were chosen to match experimental spectra. The TD-DFT calculations include only states $\gtrsim$300 nm due to computational limitations.

match the experimental absorption profiles. This provides good agreement between calculated and experimental spectra regarding the general shapes as well as relative peak heights, in particular for the "double-hump" cases. For TBDT-T-TP-T, and to some extent also for APFO-3 and APFO-15, the experimental absorption is blueshifted compared to the calculated dimer but redshifted *vs.* the monomer, which demonstrates the precariousness of relating small and well defined oligomers to long and polydisperse experimental polymers. The Gaussian broadening of 3000 cm^{-1} that is arbitrarily chosen for calculated spectra, is in most cases slightly narrower than experimental peak widths, particularly for EWC4 and APFO-G9. Furthermore, this Gaussian function is symmetric, while the experimental broadening is inhomogeneous, extending further to the shorter wavelengths due to unresolved vibronic progression and uneven distributions of conformations. In the following sections we describe and apply a procedure which relies on extrapolations to size-converged properties, rather than an *ad hoc* choice of oligomer size as above. This permits accurate prediction of size-consistent absorption wavelengths and intensities which provides an in-depth understanding of the potential for efficient photon collection of these polymers based on their chemical structure and electronic properties.

Absorption energies

In recent years, low band gap polymers have been sought after, due to their ability to absorb a greater portion of the solar emission spectrum, yielding larger photo-currents.[6] However, a low absorption threshold typically leads to a lower voltage output from the cell, and finding the ideal absorption energy becomes a complex optimization problem. A rough, qualitative estimation of the first transition energy of absorption (E_{abs}) in a copolymer can be can be made from the HOMO and LUMO of the donor and acceptor units, since the frontier orbitals of the copolymer are constructed from these units. For instance, polymers with the low-LUMO acceptor PzQ exhibit low E_{abs}, both herein (APFO-G9 and EWC4) and elsewhere,[57] in contrast to *e.g.* the Q acceptor.

Any quantitative prediction of calculated E_{abs} however, requires a more elaborate quantum chemical treatment, *e.g.* with TD-DFT, which we employ to obtain calculated absorption energies (E_{abs}) and intensities for oligomers of 1–5 repeating units (excitations listed in ESI†). To obtain polymeric estimates from oligomer calculations, calculated E_{abs} are often extrapolated to the polymer limit by fitting them to a linear function *vs.* inverse number of repeating units ($1/n$),[58–61] but more physically rigorous, non-linear approaches also exist.[62–64] Since the optical band gap is strongly related to the HOMO–LUMO gap, we can rewrite eqn (1) in terms of $E_{abs}(n)$:

$$E_{abs}(n) \approx E_{LUMO} - E_{HOMO} = \alpha_{LUMO} - \alpha_{HOMO} - 2(\beta_{LUMO} + \beta_{HOMO}) \cos\frac{\pi}{n+1} \quad (2)$$

This function describes the size dependence of the HOMO–LUMO gap, and thus approximately that of E_{abs}. TD-DFT calculated

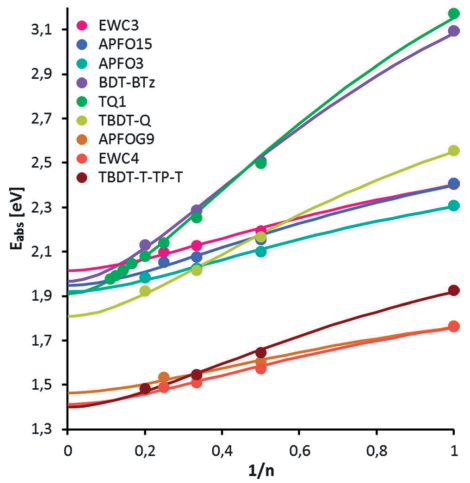

Fig. 4 Calculated first peak absorption energy (E_{abs}) as function of inverse oligomer size. Lines are fitted according to the tight binding approximation of eqn (2). Color order from violet to red according to extrapolated E_{abs}.

$E_{abs}(n)$ were fitted to the right-hand side of eqn (2) using two fitting parameters: $(\alpha_{LUMO} - \alpha_{LUMO})$ and $(\beta_{LUMO} + \beta_{HOMO})$. The fits are good in all cases, as seen in Fig. 4 where they are plotted *vs.* the inverse oligomer length, together with calculated oligomer absorption energies. TQ1, BDT-BTz, and TBDT-Q exhibit steeper slopes, as their shorter repeat unit necessitates more units for conjugation convergence, analogously to the orbital energy convergence in Fig. 2. It is noticeable that polymers having common acceptors yield comparable results, *i.e.* APFO-G9 *vs.* EWC4 and APFO-15 *vs.* EWC3.

Comparisons between experiment and calculations are complicated due to the difference in conditions, *e.g.* with respect to temperature, system size, solvents, *etc.*[62] The extrapolated, calculated E_{abs} are compared to the experimental peak E_{abs} in Fig. 5, where a systematic underestimation of the calculated values is apparent for all polymers. This is because the calculations are based on the minimum energy conformation of the oligomers, whereas under room-temperature conditions, a multitude of conformations is present. The optimized structures are usually more planar than the actual range of conformations. Planarity is associated with red-shifted absorption,[65–68] so calculated absorption energies typically represent the lower limit of experimental E_{abs}. Solvent effects and unresolved vibronic progression, present in experimental spectra but absent in calculations, further adds to the discrepancy.

Despite the diverse nature of the studied polymers and their wide range of absorption energies, the underestimation of calculated E_{abs} is practically constant over the series, within a narrow range of 0.31–0.38 eV, except for TQ1 for which it is limited to 0.13 eV since TQ1 is restricted to an experimental

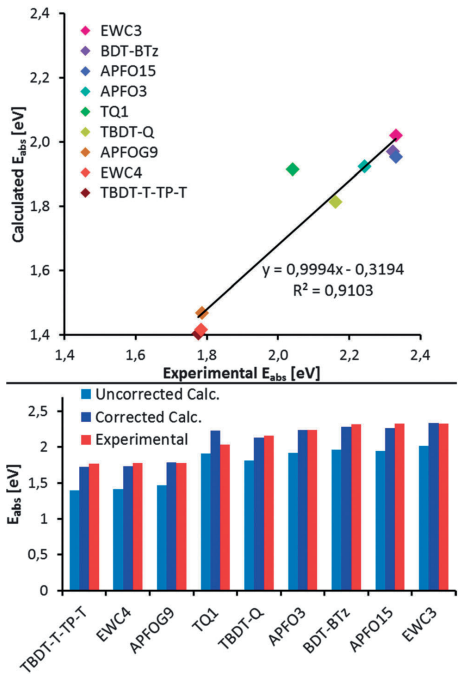

Fig. 5 Top: calculated *vs.* experimental peak E_{abs}, with best linear fit. Bottom: calculated E_{abs} with and without correction, as well as experimental. The calculated E_{abs} corresponds to the extrapolation to $1/n \rightarrow 0$ in Fig. 4. The correction corresponds to a constant +0.32 eV amendment.

geometry closer to the optimized (calculated) structure due to its phenyl side-groups.[30] The calculated E_{abs} are plotted against experimental in the top panel of Fig. 5, and the best linear fit exhibits a slope of virtually unity and an intercept of −0.32 eV. An empirical correction consisting of the addition of the 0.32 eV average underestimation to the calculated series is introduced to compensate for the highly systematic discrepancy. The uncorrected and corrected calculated E_{abs} are compared to the experimental numbers in the bottom panel of Fig. 5. With the empirical correction, calculated E_{abs} match the experiments very well, exhibiting accuracy to within 0.06 eV, or 3% error to experiment for all polymers except TQ1. This is remarkable considering the large spread of experimental absorption energies of the series, ranging from 1.77–2.33 eV. Similar kinds of empirical corrections have commonly been applied to other types of calculated results, such as vibrational spectra,[69–74] and NMR shifts,[75–79] but also to electronic and optical properties.[80–84]

Several computational shortcomings contribute to the total, uncorrected error. While implicit solvent effects have a minor influence on the E_{abs}, <0.05 eV (see Table S3, ESI†), explicit solvent and thermal/conformational effects contribute to the underestimation of calculated E_{abs}. Importantly, hybrid DFT functionals such as PBE0 used here, are known to overestimate the conjugation and planarity in conjugated polymers,[64,85–87] leading to calculations predicting unrealistically flat geometries and red-shifted electronic transitions. Part of the calculated underestimation of E_{abs} can also be explained by experimental limitations: SEC measurements are known to overestimate the molar masses of D–A polymers. This stems from the fact that SEC uses the flexible polystyrene as a reference, whereas D–A polymers are generally more rigid. Further theoretical and experimental studies may elucidate the individual contributions from the respective sources of error.

Absorption strengths

While the absorption energy should not be too small or too large, a greater absorption strength is monotonically favorable for the OPV performance, since stronger absorption leads to larger currents, up to the limit of all photons absorbed. The electronic transport properties of an OPV are favored by a thin device, so to maximize absorption per device thickness, high absorption intensity per polymer volume is desired. This is equivalent to strong absorption per weight since most polymers have a density very close to 1 kg dm^{-3}.

The first peak absorption intensities of the polymers herein were calculated for oligomers of 1–5 repeating units. The intensities as calculated with TD-DFT are expressed as oscillator strengths (f), an extensive property that increases linearly with oligomer length.[88] Calculated oscillator strengths divided by the oligomer molar mass yield a more relevant, intensive property: specific absorption strength (F_M). These are plotted *vs.* inverse number of repeating units in Fig. 6. In agreement with theory and previous reports,[62,89–93] a linear relation is evident for all polymers, allowing extrapolation to the polymer limit (see ESI† for details). Size-converged specific absorption strengths are thereby obtained, despite performing the calculations on smaller oligomers. It is noticeable that the polymers with lighter repeating unit BDT-BTz, APFO-3, and TQ1 are more size-dependent than the heavier ones, leading for APFO-3 and BDT-BTz to very strong calculated polymeric absorption, ~2 kg^{-1}. TQ1 is the only polymer whose monomer does not follow the linear trend, a consequence of its unique ability to adopt a helical geometry in oligomers larger than the monomer.[30]

The specific absorption strength, F_M, is related to the absorption coefficients of the first peak through the relation:[38]

$$F_M = \frac{4\ln(10)m_e c\varepsilon_0}{N_A e^2 M_W} \times \int \varepsilon(\nu)\mathrm{d}\nu \qquad (3)$$

where m_e and e are the electron mass and charge respectively, ε_0 is the vacuum permittivity, N_A is the Avogadro number, ν is the light frequency, M_W is the measured molecular weight average and the factor ln(10) enters since ε is the decadic (as opposed to natural), molar absorption coefficient. Accordingly, experimental F_M values are obtained by taking the integral over the first experimental absorption peak, as approximated through the trapezoidal rule to the local spectral minimum after the peak.

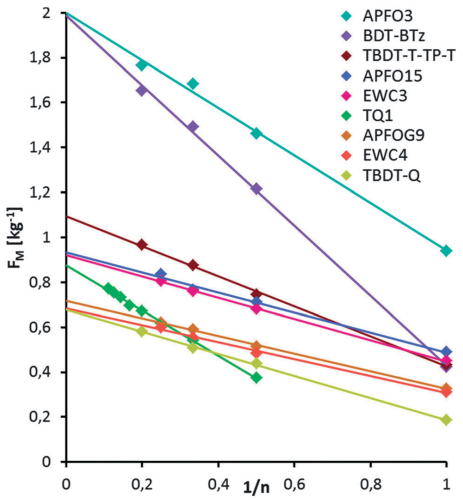

Fig. 6 Calculated specific absorption strengths, F_M, *vs.* inverse oligomer order. Lines are best linear fits, extrapolated to $1/n = 0$.

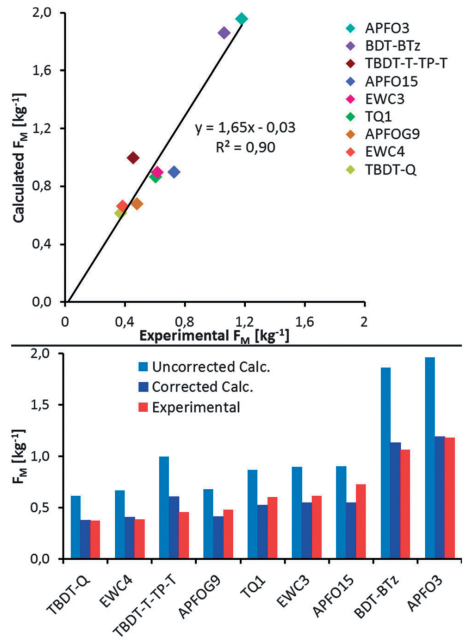

Fig. 7 Top: calculated *vs.* experimental absorption strengths, F_M, for the investigated polymers, with best linear fit. Bottom: comparison of uncorrected and corrected calculated absorption strengths to experimental absorption strengths, sorted by experimental values.

The experimental F_M show a trend-wise agreement with ε_{max} since the peak widths are similar, see Fig. 3.

In Fig. 7, the experimental F_M values are compared to the calculated ones, taken from the linear fit extrapolation in Fig. 6. Analysis and quantification of the discrepancies provides possibility to assess and compensate for the errors, analogously to the E_{abs} case in the previous section. The best linear fit of calculated *vs.* experimental absorption strengths exhibits a negligible intercept, demonstrating that the overestimation is proportional to F_M, as seen in the top panel of Fig. 7. The slope of 1.65 indicates a consistent error, meaning that dividing calculated F_M values by 1.65 constitutes an empirical correction that provides significantly more accurate theoretical estimates, as demonstrated in the bottom panel of Fig. 7. The correction improves the mean absolute error from 0.40 to 0.07 kg^{-1}.

The uncorrected errors in oscillator strength are larger here than in many studies of smaller molecules.[94–97] This can be explained in terms of the non-ideality of experimental conditions, where thermal effects and solvent interactions induce conformational twists, kinks, and coils in the polymer chains which reduce the conjugation[16] and consequently the absorption intensity. The polarizability of the solvent affects the transition dipole moment in the polymers and thus the absorption strength. The F_M of five of the polymers was calculated using TD-DFT with an *o*-DCB polarizable continuum model solvent, showing in all cases stronger absorption than vacuum calculations (see Fig. S8, ESI†). The effect of the solvent decreases with increasing oligomer size, leading to extrapolated F_M values 2–15% larger than the vacuum calculations. This is in decent agreement with other studies showing that continuum solvent models do not affect the absorption strength in polymers by more than ~10%.[98–100] Overestimated masses from SEC are also responsible for part of the discrepancy between calculation and experiment. The findings suggest that the calculations represent the upper bound of experimental absorption strengths, in the limit of extended, non-kinked, non-coiled polymer chains. The comparison of absorption strengths between polymers is relatively uncommon, in particular in computational studies where the intensities in calculations are often normalized when related to experimental spectra.[13,101–107] Normalized absorption comparisons permit assessment of relative peak height and wavelength but not the intensity which is important for the performance of OPVs. Accurate quantum chemical predictions of specific absorption strengths as demonstrated here are therefore important for modeling, aimed at rational design of new and better light-harvesting polymers.

BDT-BTz and APFO-3 are the strongest absorbers as seen in Fig. 7, attributed to their respective BTz and BTD acceptors, and their very flat minimum-energy geometries, as seen in Table 1. APFO-3 furthermore has the lowest side-group weight fraction of the studied polymers. These side-groups give a negligible contribution to the first peak absorption and are thus "dead weight" with respect to the excitations, which is further corroborated by the lack of frontier orbital density on these groups in Fig. 1. TBDT-Q, with the highest side-group weight ratio as

listed in Table 1, consequently demonstrates the weakest specific absorption. Thus, stronger absorption is obtained by developing more streamlined polymers with a low side-group-to-backbone weight ratio, although some alkyl side-chains are required for solubility. While this study is limited to repeating units with a 1-to-1 D/A ratio, Beaujuge *et al.* have previously reported the effect of the D/A ratio on the absorption strength.[108] They also propose the disregard of the side-chain mass for a more fair comparison of the intrinsic specific absorption strength between polymers with different repeating units.

The absorption intensity assessment here only treats the first absorption peak, whereas consecutive peaks also may contribute to the photoelectric conversion efficiency in working OPVs. Secondary peaks may even be more important, *e.g.* APFO-G9 and EWC4 show much more intense peaks at ~400 nm, making those polymers suitable in tandem OPVs. It may therefore be interesting to extend the investigation of optical traits to the whole visible region in future studies.

Light-harvesting capability

The output power of an OPV is a product of the current J and the voltage V. The current depends on, among other things, the absorptivity, whereas the voltage is limited by the polymer's band gap and its HOMO energy relative to the fullerene LUMO. Scharber *et al.* have developed a method to anticipate the maximum energy-conversion efficiency of a polymer/$PC_{61}BM$ solar cell as a function of the polymer LUMO and band gap.[41] According to that study, the ideal polymer band gap is around 1.5 eV, assuming an ideal polymer LUMO energy 0.3 eV higher than the fullerene LUMO. APFO-G9 has a near-ideal LUMO 0.30 eV higher than the $PC_{61}BM$ LUMO. Furthermore the E_{abs} of APFO-G9 lies very near the above mentioned optimum 1.5 eV, and would thus score very high in the model of Scharber's *et al.* However, that study does not take the absorption intensity into account explicitly, but rather approximates the EQE to 65% at all wavelengths above the band gap, and thus fails to predict the relatively bad performance of APFO-G9 due to its weak absorption.[22] Assessing also the absorption strength allows for a more complete evaluation of the light-harvesting potential of a polymer in single-junction OPVs. If one moreover permits the use of other fullerene acceptors with different LUMO energies, the polymer LUMO becomes a less crucial parameter. This leaves F_M and E_{abs} as the most important intrinsic polymer light-harvesting properties for efficient OPVs, although charge transport and other attributes still affect the device performance. Experimental and calculated F_M and E_{abs} are compared in Fig. 8 for all polymers included in the present investigation.

The large variation in chemical structure of the polymer selection manifests itself as a considerably scattered distribution in Fig. 8. This figure shows that the calculations provide a good assessment of the light-harvesting properties of the different polymers, as the discrepancy to experiments for all the individual polymers is significantly smaller than the overall spread of these traits across the polymer series. APFO-3 and BDT-BTz score best on absorption strength, attributed to the respective BTD and BTz acceptors, and for APFO-3 also to its low side-group weight ratio.

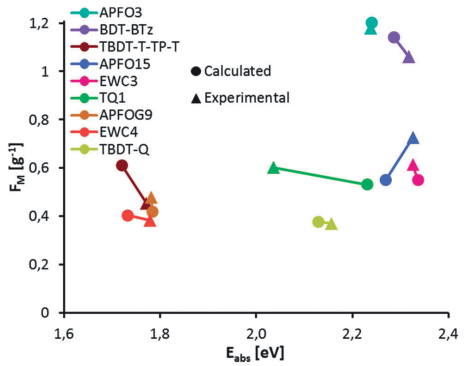

Fig. 8 Light-harvesting capability plot for the investigated polymers showing the absorption strength, F_M, *vs.* E_{abs}. The plot includes a comparison of calculated values to experimental results. The calculated F_M and E_{abs} are taken from the extrapolated, corrected values shown in Fig. 6 and 7 respectively.

However, the efficiency of these two polymers is limited by their higher absorption energy, and for BDT-BTz also by poorer LUMO alignment *vs.* PCBM.[25] Fluorination of BTz-containing polymers lowers the LUMO energy, and can give device efficiencies above 7%.[10] The low-LUMO PzQ acceptor of EWC4 confers an in this respect near-ideal, lower E_{abs} of 1.73 eV, but it is the second weakest absorber of the investigated polymers, also attributed to the PzQ acceptor. The novel polymer TBDT-T-TP-T exhibits the lowest energy of absorption, but its high side-group ratio of 61% induces a relatively low F_M of 0.60 kg^{-1}. TBDT-Q is the only new polymer with an experimental E_{abs} in the central region of Fig. 8, *i.e.* between 1.9 and 2.3 eV, but its limited F_M below 0.40 kg^{-1} weakens its suitability for application in OPVs.

In summary this study highlights the current difficulty of finding D–A polymers that simultaneously display small optical band gap and strong absorption. To achieve such traits, one firstly needs to carefully choose appropriate acceptor units (and to some extent also donors). *E.g.* the BTD acceptor grants strong and reasonably low-energy absorption, which is why device efficiencies over 8% have been achieved using a this acceptor,[109] while the weak absorption of PzQ makes it unsuitable in conventional D–A polymer OPVs. Secondly, it is advised to avoid inclusion of too large side-groups that are "dead weight" with respect to the absorption strength. Thirdly, a sufficient degree of polymerization during synthesis, *i.e.* high enough polymer molecular weight is also beneficial for stronger and lower energy absorption.

Conclusions

Light-harvesting capabilities of a series of donor–acceptor type polymers have been investigated using a combination of experiments and calculations. The focus of the investigation concerns the ability to identify polymer candidates with promising optical

characteristics at an early stage, specifically strong absorption at an adequately narrow band gap. The investigated set of polymers exhibits a significant span of experimentally determined first peak energies (E_{abs}) in solution from *ca.* 1.8 eV to *ca.* 2.3 eV, as well as having mass absorption intensities that vary by a factor of three.

Size-converged electronic and optical properties have here been obtained by means of oligomer calculations, extrapolated to the polymer limit. The calculated polymer absorption energies show a trend-wise agreement with experiments, but are systematically underestimated. The clear, consistent trend between calculated and experimental E_{abs} enables the introduction of an empirical correction, which yields quantitative prediction of peak absorption energy to within an accuracy of 0.06 eV. The experimental and calculated absorption strengths per unit weight (F_M), vary by up to a factor of three across the polymer series, which is considerably more than E_{abs}. Nevertheless, the calculated specific absorption strengths (F_M) display an error to the experimental values limited to 12%, following the introduction of an empirical correction to the calculations. The quantitatively accurate calculations of absorption energies and intensities together provide good possibilities to predict intrinsic light-harvesting capabilities of D–A polymers. This offers a deeper understanding of the physical properties that govern the electronic and optical processes in the polymers, and also makes calculations an efficient tool to assess the suitability of the polymers in an OPV context.

Of the polymers in this study, APFO-3 scores best on absorption strength, concurring with its high performance in solar cells.[20,42] This derives from its light repeating unit, with small side-group to backbone ratio, and the intrinsic properties of its BTD acceptor. Three of the investigated polymers: APFO-G9, EWC4, and TBDT-T-TP-T, show significantly lower optical band gaps of around 1.7 eV, owing mainly to the deep-LUMO acceptors PzQ and TP. The remaining six polymers all have band gaps above 2.0 eV. However, none of the here investigated polymers simultaneously display both suitably low E_{abs} and high F_M, suggesting that there is significant room for further improvements in the design of D–A polymers for efficient OPVs. One such opportunity is to focus on acceptor units with promising intrinsic electronic properties, and to pursue polymers with high backbone weight-ratio since side-groups do not contribute to light-absorption.

In a broader perspective, the ability to reliably predict light-harvesting capabilities of new polymers is an important part of the search for novel and improved solar cell materials that is largely driven by efficient screening of a wide range of materials. The here adopted predictive approach is already starting to yield promising results for the design of new polymers currently under development.

Conflicts of interest

The authors declare no competing financial interests.

Acknowledgements

The work was funded by the Swedish research council (VR), the Knut and Alice Wallenberg (KAW) Foundation, and The Swedish Energy Agency (Energimyndigheten). NSC and LUNARC are acknowledged for computer resources used. We thank Dr Christian Müller at Chalmers University of Technology for valuable discussions.

References

1 C. J. Brabec, S. Gowrisanker, J. J. M. Halls, D. Laird, S. Jia and S. P. Williams, *Adv. Mater.*, 2010, **22**, 3839–3856.
2 G. Li, R. Zhu and Y. Yang, *Nat. Photonics*, 2012, **6**, 153–161.
3 G. Yu, J. Gao, J. C. Hummelen, F. Wudl and A. J. Heeger, *Science*, 1995, **270**, 1789–1791.
4 G. Dennler, M. C. Scharber and C. J. Brabec, *Adv. Mater.*, 2009, **21**, 1323–1338.
5 H.-Y. Chen, J. Hou, S. Zhang, Y. Liang, G. Yang, Y. Yang, L. Yu, Y. Wu and G. Li, *Nat. Photonics*, 2009, **3**, 649–653.
6 J. Chen and Y. Cao, *Acc. Chem. Res.*, 2009, **42**, 1709–1718.
7 H. A. M. van Mullekom, J. A. J. M. Vekemans, E. E. Havinga and E. W. Meijer, *Mater. Sci. Eng., R*, 2001, **32**, 1–40.
8 Y. Li, *Acc. Chem. Res.*, 2012, **45**, 723–733.
9 Z. He, C. Zhong, S. Su, M. Xu, H. Wu and Y. Cao, *Nat. Photonics*, 2012, **6**, 591–595.
10 S. C. Price, A. C. Stuart, L. Yang, H. Zhou and W. You, *J. Am. Chem. Soc.*, 2011, **133**, 4625–4631.
11 Z. Ma, E. Wang, M. E. Jarvid, P. Henriksson, O. Inganas, F. Zhang and M. R. Andersson, *J. Mater. Chem.*, 2012, **22**, 2306–2314.
12 X. Song, W. Hua, Y. Ma, C. Wang and Y. Luo, *J. Phys. Chem. C*, 2012, **116**, 23938–23944.
13 J. Ku, Y. Lansac and Y. H. Jang, *J. Phys. Chem. C*, 2011, **115**, 21508–21516.
14 L. Pandey, C. Risko, J. E. Norton and J.-L. Brédas, *Macromolecules*, 2012, **45**, 6405–6414.
15 L. Zhang, K. Pei, M. Yu, Y. Huang, H. Zhao, M. Zeng, Y. Wang and J. Gao, *J. Phys. Chem. C*, 2012, **116**, 26154–26161.
16 L. M. Andersson, S. Hedström and P. Persson, *Appl. Phys. Lett.*, 2013, **103**, 213303.
17 M.-H. Chen, J. Hou, Z. Hong, G. Yang, S. Sista, L.-M. Chen and Y. Yang, *Adv. Mater.*, 2009, **21**, 4238–4242.
18 J. Hou, Z. Tan, Y. Yan, Y. He, C. Yang and Y. Li, *J. Am. Chem. Soc.*, 2006, **128**, 4911–4916.
19 C.-P. Chen, S.-H. Chan, T.-C. Chao, C. Ting and B.-T. Ko, *J. Am. Chem. Soc.*, 2008, **130**, 12828–12833.
20 O. Inganäs, M. Svensson, F. Zhang, A. Gadisa, N. K. Persson, X. Wang and M. R. Andersson, *Appl. Phys. A: Mater. Sci. Process.*, 2004, **79**, 31–35.
21 A. Gadisa, W. Mammo, L. M. Andersson, S. Admassie, F. Zhang, M. R. Andersson and O. Inganäs, *Adv. Funct. Mater.*, 2007, **17**, 3836–3842.
22 F. Zhang, J. Bijleveld, E. Perzon, K. Tvingstedt, S. Barrau, O. Inganas and M. R. Andersson, *J. Mater. Chem.*, 2008, **18**, 5468–5474.
23 E. Wang, L. Hou, Z. Wang, Z. Ma, S. Hellström, W. Zhuang, F. Zhang, O. Inganäs and M. R. Andersson, *Macromolecules*, 2011, **44**, 2067–2073.

24 E. Wang, L. Hou, Z. Wang, S. Hellström, F. Zhang, O. Inganäs and M. R. Andersson, *Adv. Mater.*, 2010, **22**, 5240–5244.
25 Z. Zhang, B. Peng, B. Liu, C. Pan, Y. Li, Y. He, K. Zhou and Y. Zou, *Polym. Chem.*, 2010, **1**, 1441–1447.
26 V. V. Pavlishchuk and A. W. Addison, *Inorg. Chim. Acta*, 2000, **298**, 97–102.
27 A. J. Bard and L. R. Faulkner, *Electrochemical Methods: Fundamentals and Applications*, Wiley, New York, 2nd edn, 2000.
28 C. Adamo and V. Barone, *J. Chem. Phys.*, 1999, **110**, 6158–6170.
29 M. Frisch, G. Trucks, H. Schlegel, G. Scuseria, M. Robb, J. Cheeseman, G. Scalmani, V. Barone, B. Mennucci, G. Petersson, H. Nakatsuji, M. Caricato, X. Li, H. Hratchian, A. Izmaylov, J. Bloino, G. Zheng, J. Sonnenberg, M. Hada, M. Ehara, K. Toyota, R. Fukuda, J. Hasegawa, M. Ishida, T. Nakajima, Y. Honda, O. Kitao, H. Nakai, T. Vreven, J. Montgomery, J. Peralta, F. Ogliaro, M. Bearpark, J. Heyd, E. Brothers, K. Kudin, V. Staroverov, R. Kobayashi, J. Normand, K. Raghavachari, A. Rendell, J. Burant, S. Iyengar, J. Tomasi, M. Cossi, N. Rega, J. Millam, M. Klene, J. Knox, J. Cross, V. Bakken, C. Adamo, J. Jaramillo, R. Gomperts, R. Stratmann, O. Yazyev, A. Austin, R. Cammi, C. Pomelli, J. Ochterski, R. Martin, K. Morokuma, V. Zakrzewski, G. Voth, P. Salvador, J. Dannenberg, S. Dapprich, A. Daniels, Ö. Farkas, J. Foresman, J. Ortiz, J. Cioslowski and D. Fox, 2009.
30 S. Hedström and P. Persson, *J. Phys. Chem. C*, 2012, **116**, 26700–26706.
31 E. Wang, J. Bergqvist, K. Vandewal, Z. Ma, L. Hou, A. Lundin, S. Himmelberger, A. Salleo, C. Müller, O. Inganäs, F. Zhang and M. R. Andersson, *Adv. Energy Mater.*, 2013, **3**, 806–814.
32 T. Nelson, S. Fernandez-Alberti, V. Chernyak, A. E. Roitberg and S. Tretiak, *J. Phys. Chem. B*, 2011, **115**, 5402–5414.
33 S. Tretiak, A. Saxena, R. L. Martin and A. R. Bishop, *Phys. Rev. Lett.*, 2002, **89**, 097402.
34 M. Belletête, P.-L. T. Boudreault, M. Leclerc and G. Durocher, *THEOCHEM*, 2010, **962**, 33–37.
35 R. Siebert, A. Winter, U. S. Schubert, B. Dietzek and J. Popp, *J. Phys. Chem. C*, 2010, **114**, 6841–6848.
36 S. Westenhoff, W. J. D. Beenken, R. H. Friend, N. C. Greenham, A. Yartsev and V. Sundström, *Phys. Rev. Lett.*, 2006, **97**, 166804.
37 G. Lanzani, M. Nisoli, V. Magni, S. De Silvestri, G. Barbarella, M. Zambianchi and R. Tubino, *Phys. Rev. B: Condens. Matter Mater. Phys.*, 1995, **51**, 13770–13773.
38 P. Atkins and R. Friedman, *Molecular Quantum Mechanics*, Oxford University Press, New York, 4th edn, 2005.
39 J.-L. Brédas, D. Beljonne, V. Coropceanu and J. Cornil, *Chem. Rev.*, 2004, **104**, 4971–5004.
40 L. J. A. Koster, V. D. Mihailetchi and P. W. M. Blom, *Appl. Phys. Lett.*, 2006, **88**, 093511.
41 M. C. Scharber, D. Mühlbacher, M. Koppe, P. Denk, C. Waldauf, A. J. Heeger and C. J. Brabec, *Adv. Mater.*, 2006, **18**, 789–794.
42 L. H. Slooff, S. C. Veenstra, J. M. Kroon, D. J. D. Moet, J. Sweelssen and M. M. Koetse, *Appl. Phys. Lett.*, 2007, **90**, 143506.
43 C. M. Cardona, W. Li, A. E. Kaifer, D. Stockdale and G. C. Bazan, *Adv. Mater.*, 2011, **23**, 2367–2371.
44 T. Johansson, W. Mammo, M. Svensson, M. R. Andersson and O. Inganas, *J. Mater. Chem.*, 2003, **13**, 1316–1323.
45 S. Admassie, O. Inganäs, W. Mammo, E. Perzon and M. R. Andersson, *Synth. Met.*, 2006, **156**, 614–623.
46 A. Facchetti, *Chem. Mater.*, 2010, **23**, 733–758.
47 A. Rajca, P. J. Boratyński, A. Olankitwanit, K. Shiraishi, M. Pink and S. Rajca, *J. Org. Chem.*, 2012, **77**, 2107–2120.
48 J. K. Sørensen, J. Fock, A. H. Pedersen, A. B. Petersen, K. Jennum, K. Bechgaard, K. Kilså, V. Geskin, J. Cornil, T. Bjørnholm and M. B. Nielsen, *J. Org. Chem.*, 2010, **76**, 245–263.
49 L. Leroyer, C. Lepetit, A. Rives, V. Maraval, N. Saffon-Merceron, D. Kandaskalov, D. Kieffer and R. Chauvin, *Chem. – Eur. J.*, 2012, **18**, 3226–3240.
50 P. Chen, R. A. Lalancette and F. Jäkle, *Angew. Chem., Int. Ed.*, 2012, **51**, 7994–7998.
51 M. A. M. Leenen, F. Cucinotta, L. Viani, A. Mavrinskiy, W. Pisula, J. Gierschner, J. Cornil, A. Prodi-Schwab, H. Thiem, K. Müllen and L. De Cola, *J. Phys. Chem. B*, 2010, **114**, 14614–14620.
52 G. Zhang and C. B. Musgrave, *J. Phys. Chem. A*, 2007, **111**, 1554–1561.
53 Y. Li, T. Pullerits, M. Zhao and M. Sun, *J. Phys. Chem. C*, 2011, **115**, 21865–21873.
54 S. Ko, E. T. Hoke, L. Pandey, S. Hong, R. Mondal, C. Risko, Y. Yi, R. Noriega, M. D. McGehee, J.-L. Brédas, A. Salleo and Z. Bao, *J. Am. Chem. Soc.*, 2012, **134**, 5222–5232.
55 C. Risko, M. D. McGehee and J.-L. Bredas, *Chem. Sci.*, 2011, **2**, 1200–1218.
56 A. Azazi, A. Mabrouk and K. Alimi, *Comput. Theor. Chem.*, 2011, **978**, 7–15.
57 Q. Peng, X. Liu, Y. Qin, J. Xu, M. Li and L. Dai, *J. Mater. Chem.*, 2011, **21**, 7714–7722.
58 W. K. Ford, C. B. Duke and W. R. Salaneck, *J. Chem. Phys.*, 1982, **77**, 5030–5039.
59 J. Cornil, I. Gueli, A. Dkhissi, J. C. Sancho-Garcia, E. Hennebicq, J. P. Calbert, V. Lemaur, D. Beljonne and J. L. Bredas, *J. Chem. Phys.*, 2003, **118**, 6615–6623.
60 T. T. Steckler, X. Zhang, J. Hwang, R. Honeyager, S. Ohira, X.-H. Zhang, A. Grant, S. Ellinger, S. A. Odom, D. Sweat, D. B. Tanner, A. G. Rinzler, S. Barlow, J.-L. Brédas, B. Kippelen, S. R. Marder and J. R. Reynolds, *J. Am. Chem. Soc.*, 2009, **131**, 2824–2826.
61 O. Kwon and M. L. McKee, *J. Phys. Chem. A*, 2000, **104**, 7106–7112.
62 J. Gierschner, J. Cornil and H.-J. Egelhaaf, *Adv. Mater.*, 2007, **19**, 173–191.
63 S. S. Zade, N. Zamoshchik and M. Bendikov, *Acc. Chem. Res.*, 2010, **44**, 14–24.
64 M. Wykes, B. Milián-Medina and J. Gierschner, *Front. Chem.*, 2013, **1**, 35.

65 J. Kim and T. M. Swager, *Nature*, 2001, **411**, 1030–1034.
66 F. C. Krebs and H. Spanggaard, *J. Org. Chem.*, 2002, **67**, 7185–7192.
67 K. Becker and J. M. Lupton, *J. Am. Chem. Soc.*, 2005, **127**, 7306–7307.
68 Y. Lee, Y. M. Nam and W. H. Jo, *J. Mater. Chem.*, 2011, **21**, 8583–8590.
69 W. F. Murphy, J. M. Fernandez-Sanchez and K. Raghavachari, *J. Phys. Chem.*, 1991, **95**, 1124–1139.
70 G. Rauhut and P. Pulay, *J. Phys. Chem.*, 1995, **99**, 3093–3100.
71 V. Chiş, *Chem. Phys.*, 2004, **300**, 1–11.
72 C. A. Jimenez-Hoyos, B. G. Janesko and G. E. Scuseria, *Phys. Chem. Chem. Phys.*, 2008, **10**, 6621–6629.
73 B. A. Hess, L. J. Schaad, P. Carsky and R. Zahradnik, *Chem. Rev.*, 1986, **86**, 709–730.
74 K. K. Irikura, R. D. Johnson and R. N. Kacker, *J. Phys. Chem. A*, 2005, **109**, 8430–8437.
75 T. Bally and P. R. Rablen, *J. Org. Chem.*, 2011, **76**, 4818–4830.
76 J. Vaara, *Phys. Chem. Chem. Phys.*, 2007, **9**, 5399–5418.
77 D. A. Forsyth and A. B. Sebag, *J. Am. Chem. Soc.*, 1997, **119**, 9483–9494.
78 P. Cimino, L. Gomez-Paloma, D. Duca, R. Riccio and G. Bifulco, *Magn. Reson. Chem.*, 2004, **42**, S26–S33.
79 A. S. Edison, J. L. Markley and F. Weinhold, *J. Phys. Chem.*, 1993, **97**, 11657–11665.
80 X. Nie, S. Zhuo, G. Maeng and K. Sohlberg, *Int. J. Photoenergy*, 2009, **2009**, 294042.
81 K. Meguellati, S. Ladame and M. Spichty, *Dyes Pigm.*, 2011, **90**, 114–118.
82 G. R. Hutchison, M. A. Ratner and T. J. Marks, *J. Phys. Chem. A*, 2002, **106**, 10596–10605.
83 L. Zhang, G. H. Peslherbe and H. M. Muchall, *Photochem. Photobiol.*, 2006, **82**, 324–331.
84 J. J. Finnerty and R. Koch, *J. Phys. Chem. A*, 2009, **114**, 474–480.
85 B. M. Savoie, N. E. Jackson, T. J. Marks and M. A. Ratner, *Phys. Chem. Chem. Phys.*, 2013, **15**, 4538–4547.
86 T. Körzdörfer and J.-L. Brédas, *Acc. Chem. Res.*, 2014, DOI: 10.1021/ar500021t.
87 Y. Zhao and D. G. Truhlar, *J. Phys. Chem. A*, 2006, **110**, 10478–10486.
88 W. Barford, *Electronic and Optical Properties of Conjugated Polymers*, Oxford University Press, Oxford, 2013.
89 E. Mena-Osteritz, F. Zhang, G. Götz, P. Reineker and P. Bäuerle, *Beilstein J. Nanotechnol.*, 2011, **2**, 720–726.
90 S. Tretiak, A. Saxena, R. L. Martin and A. R. Bishop, *J. Phys. Chem. B*, 2000, **104**, 7029–7037.
91 B. Grimm, C. Risko, J. D. Azoulay, J.-L. Bredas and G. C. Bazan, *Chem. Sci.*, 2013, **4**, 1807–1819.
92 T. Wagersreiter and S. Mukamel, *J. Chem. Phys.*, 1996, **104**, 7086–7098.
93 W. Li, T. Maddux and L. Yu, *Macromolecules*, 1996, **29**, 7329–7334.
94 D. Guillaumont and S. Nakamura, *Dyes Pigm.*, 2000, **46**, 85–92.
95 M. Miura, Y. Aoki and B. Champagne, *J. Chem. Phys.*, 2007, **127**, 084103.
96 N. N. Matsuzawa, A. Ishitani, D. A. Dixon and T. Uda, *J. Phys. Chem. A*, 2001, **105**, 4953–4962.
97 Y. Kawashita, K. Yabana, M. Noda, K. Nobusada and T. Nakatsukasa, *THEOCHEM*, 2009, **914**, 130–135.
98 P. Salvatori, E. Mosconi, E. Wang, M. Andersson, M. Muccini and F. De Angelis, *J. Phys. Chem. C*, 2013, **117**, 17940–17954.
99 A. Lee, K. H. Kim, D. Kim, S.-H. Choi, Y. Park, C.-H. Seok, J.-W. Park, K. Choi, E. S. Yoo and D. H. Jung, *Comput. Mater. Sci.*, 2010, **49**, S251–S255.
100 L. Pandey, C. Doiron, J. S. Sears and J.-L. Bredas, *Phys. Chem. Chem. Phys.*, 2012, **14**, 14243–14248.
101 C. F. N. Marchiori, N. A. D. Yamamoto, I. R. Grova, A. G. Macedo, M. Paulus, C. Sternemann, S. Huotari, L. Akcelrud, L. S. Roman and M. Koehler, *Org. Electron.*, 2012, **13**, 2716–2726.
102 C. A. Rozzi, S. Maria Falke, N. Spallanzani, A. Rubio, E. Molinari, D. Brida, M. Maiuri, G. Cerullo, H. Schramm, J. Christoffers and C. Lienau, *Nat. Commun.*, 2013, **4**, 1602.
103 E. Badaeva, M. R. Harpham, R. Guda, O. Süzer, C.-Q. Ma, P. Bäuerle, T. Goodson and S. Tretiak, *J. Phys. Chem. B*, 2010, **114**, 15808–15817.
104 F.-C. Wu, Y.-C. Huang, H.-L. Cheng, W.-Y. Chou and F.-C. Tang, *J. Phys. Chem. C*, 2011, **115**, 15057–15066.
105 R. Grisorio, G. Allegretta, G. Romanazzi, G. P. Suranna, P. Mastrorilli, M. Mazzeo, M. Cezza, S. Carallo and G. Gigli, *Macromolecules*, 2012, **45**, 6396–6404.
106 P.-T. Wu, T. Bull, F. S. Kim, C. K. Luscombe and S. A. Jenekhe, *Macromolecules*, 2009, **42**, 671–681.
107 Z. Guo, S. A. Jenekhe and O. V. Prezhdo, *Phys. Chem. Chem. Phys.*, 2011, **13**, 7630–7636.
108 P. M. Beaujuge, C. M. Amb and J. R. Reynolds, *Acc. Chem. Res.*, 2010, **43**, 1396–1407.
109 M. Zhang, Y. Gu, X. Guo, F. Liu, S. Zhang, L. Huo, T. P. Russell and J. Hou, *Adv. Mater.*, 2013, **25**, 4944–4949.

Paper II

Defining Donor and Acceptor Strength in Conjugated Copolymers

Svante Hedström[†]*, Ergang Wang,*[‡] *and Petter Persson*[†]*

[†]Division of Theoretical Chemistry, Lund University. P.O. Box 124, S-221 00 Lund, Sweden.
[‡]Department of Chemical and Biological Engineering/Polymer Technology, Chalmers University of Technology, S-412 96 Gothenburg, Sweden

svante.hedstrom@teokem.lu.se +46-462223336
ergang@chalmers.se +46-317723410
*petter.persson@teokem.lu.se +46-462223311

Acknowledgements

NSC and LUNARC are thanked for computer resources used.

Funding

This work was funded by the Swedish Research Council (VR).

Abstract

The progress in efficiency of organic photovoltaics is largely driven by the development of new donor–acceptor (D–A) copolymers. The number of possible D–A combinations escalates rapidly with the ever-increasing number of donor and acceptor units, and the design process often involves a trial-and-error approach. We here present a computationally efficient methodology for the prediction of optical and electronic properties of D–A copolymers based on DFT calculations of donor- and acceptor-only homopolymers. 10 donors and 6 acceptors are studied, as well as all of their 60 D–A copolymer combinations, showing absorption energies of 1.6–2.3 eV, and absorption strengths varying by up to a factor of 2.5. Focus lies on exhibited trends in frontier orbital energies, optical band gaps, and absorption intensities, as well as their relation to the molecular structure. Based on the results, we define donor and acceptor strength, and quantify it for all investigated units. The light-harvesting capabilities of the 60 D–A copolymers were also assessed. This gives a valuable theoretical guideline with the potential to reduce the efforts in the synthesis part of the design of new D–A copolymers.

Keywords
Donor–acceptor polymers, DFT calculations, homopolymers, frontier orbitals, light-harvesting capabilities.

Introduction

Organic photovoltaics (OPV) is a promising technology for producing clean, cheap, and sustainable electric energy.[1–4,5] Typically, the active layer of OPVs consist of a light-harvesting, conjugated polymer and a fullerene derivative. Homopolymers such as poly-3-hexylthiophene (P3HT) and poly-(phenyl vinylene) (PPV) were the dominant light-harvesting species of OPVs in the last century, P3HT more recently achieving efficiencies exceeding 6%.[6] The mismatch between the solar emission spectrum with strong emission over a wide spectral region >450 nm, and the absorption of the homopolymers with onsets at < 500 nm, has compelled the development of lower band gap polymers. The dominant strategy to reduce the band gap is to use units of alternating high HOMO and low LUMO energy, known as electronic donors and acceptors respectively.[7–9] Compared to P3HT, the first donor–acceptor (D–A) conjugated copolymer displayed a considerably lower absorption energy (E_{abs}) of 1.35 eV in chloroform solution.[10] D–A polymers typically include donor units chosen for their ability to increase the copolymer HOMO energy (E_{HOMO}), and acceptor units lowering the copolymer

LUMO energy (E_{LUMO}). The resulting narrow band gaps have facilitated D–A polymer-based OPVs with efficiencies exceeding 10%.[11,12]

The frontier orbitals HOMO and LUMO in D–A polymers typically show significant delocalization over the conjugated π-system, making their energies dependent on system size, or degree of polymerization.[2,13] The respective increase and decrease of E_{HOMO} and E_{LUMO} upon polymerization is examplified with the homodimerization of thiophene and the co-oligomerization of thiophene–benzotriazole (TBTz) in Figure 1. The orbital energies reveal a smaller HOMO–LUMO gap for TBTz than T–T due to the deeper LUMO of BTz than T, demonstrating the potential for narrower gaps with D–A copolymers compared to homopolymers.

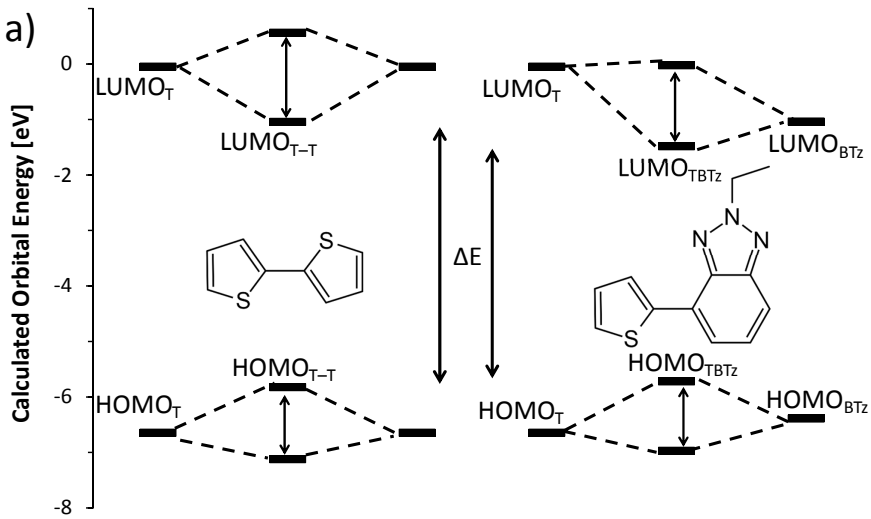

Figure 1. Molecular orbital diagram of the calculated frontier orbital energies of thiophene (T), bithiophene (T–T), benzotriazole (BTz), and thiophene–benzotriazole (TBTz), demonstrating the frontier orbital energy splitting upon addition of units, narrowing the HOMO–LUMO gap. The lower E_{LUMO} of BTz affords a smaller HOMO–LUMO gap in TBTz than in T–T.

By adding more units, the oligomer HOMO is further destabilized, and LUMO is correspondingly stabilized, until they converge at a certain HOMO–LUMO gap when the systems approach the polymer limit. The energy change of two orbitals φ_1 and φ_2 upon dimerization is dependent on the strength of the orbital-orbital interactions, described by an interaction coefficient $\lambda_{1\text{-}2}$, which in turn depends on the overlap of the interacting orbitals, as outlined in equation (1).[14] For chemically similar systems such as these conjugated aryl rings, the spatial overlaps and energy differences are of comparable magnitudes, making the $\lambda_{1\text{-}2}$ similar, and the orbital energy evolution upon oligomerization analogous for different units. A coplanar polymer geometry, *i.e.* a small dihedral angle between

the donor and acceptor, increases the orbital overlap and therefore enhances the HOMO–LUMO gap reduction upon polymerization. Steric repulsion between hydrogen atoms on neighboring units will push those units out-of-plane from each other, weakening the conjugation. This steric effect is greater for six-membered than five-membered rings.

$$\lambda_{1-2} \propto \frac{\langle \varphi_1 | \varphi_2 \rangle}{\varepsilon_1 - \varepsilon_2} \quad (1)$$

Frontier orbital energies of D–A polymers are highly important for OPV applications for two main reasons. The first is that the lowest energy electronic excitation of D–A polymers is predominantly of HOMO→LUMO character,[15–19] generally involving some charge transfer (CT) from donor to acceptor unit. The HOMO–LUMO energy gap thus relates to the optical band gap of the polymer, which determines what portion of the solar emission can be absorbed. More absorbed photons result in an increased electrical current J produced by the cell. The second reason relates to the orbital energy alignment between polymer and acceptor fullerene material. The optimal polymer E_{LUMO} is suggested to be 0.0–0.3 eV above the fullerene E_{LUMO};[20] the difference acting as a necessary driving force for exciton separation at the polymer–fullerene interface. A too large offset would however result in a loss of voltage V output.

Computational methods such as density functional theory (DFT) are commonly employed when studying conjugated polymers, as they are capable of quantifying and elucidating molecular level properties such as orbital shapes and energies or molecular geometries, which may be difficult or impossible to assess with experimental methods.[21–26] Calculated HOMO and LUMO energies are related to the ionization potential and the electron affinity respectively via Koopmans' theorem, although it is quite approximate due to neglect of orbital relaxation effects. Nevertheless, frontier orbital energies calculated with DFT have been shown to produce useful results in terms of both trends and absolute values.[27–29] Predictions of traits like absorption energies and strengths may also be made with DFT, reducing the experimental effort required to characterize the large number of emerging polymer designs.

In this article, ten donors and six acceptors are studied, selected to be representative of the wide diversity of units commonly used in D–A polymers for OPV applications. They are studied both individually and in 60 D–A copolymer combinations. The donors are 4,8-dialkoxy-benzodithiophene (OBDT), thiophene (T), thieno[3,2-b]thiophene (T32T), selenophene (Se), thieno[3,4-b]thiophene (T34T), furan (Fu), dialkyl-dithienopyrrole-benzothiadiazole (DTPBT), 4,4,9,9-tetraalkyl-indacenodithiophene (IDT), 4,4-bisalkyl-cyclopentadithiophene (CDT), and 4-alkyl-dithienopyrrole (DTPy). The acceptors are quinoxaline (Q), 2-alkyl-benzotriazole (BTz), benzothiadiazole (BT), N,N′-dialkyl-isoindigo (II), 5-alkyl-thienopyrrole-dione (TPD), and N-alkoxy-bisthienoazepine-4,6-dione (BTI). The chemical structures of all donor units are presented in Chart 1a and all acceptor

units in Chart 1b. All donors have chemically similar connecting points, being of a 5-ring thiophene type, whereas the acceptors show more varied structure around their connection points. The Q acceptor has frequently been appended with alkoxyphenyl side-groups in synthesis, which slightly tunes its electronic properties as well as enhances the solubility.[30,21] For computational efficiency we here investigate the bare quinoxaline unit. We investigate T34T as a donor unit, although when appended with electron-withdrawing substituents such as fluorine or ester groups, T34T can act as an electron acceptor.[31–33] All donors contain electron-rich sulfur, selenium, or oxygen atoms, while all acceptors contain electron-poor nitrogen atoms.

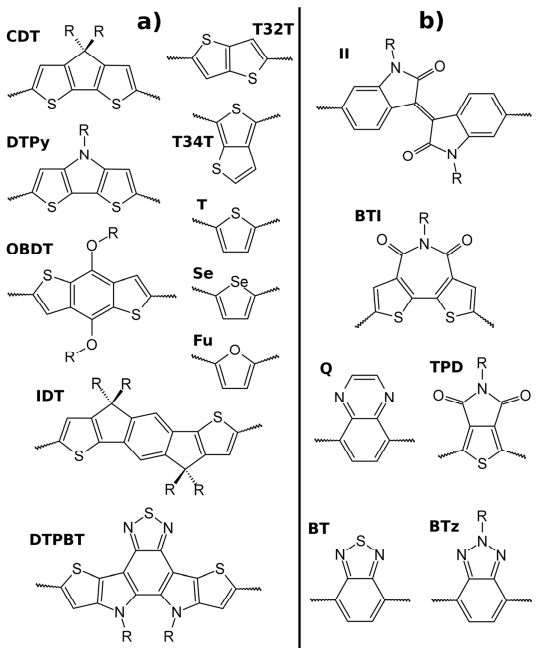

Chart 1. Chemical structures of the investigated donors (a) and acceptors (b). The solubilizing alkyl groups R, are truncated to shorter alkyl chains in the computational modelling.

Experimental experience regarding redox potentials, optical band gaps, and other properties of copolymers can give an indication of the typically loosely defined 'strength' of the donors and acceptors. However, a more quantitative and well defined measure of donor and acceptor strength is obtainable through calculations where the orbital contributions, energies, and interactions, as well as absorption characteristics, can be more exactly quantified. The objective of this investigation is to define and quantify the donor and acceptor strength of the units, through systematic analysis of trends in electronic and optical properties, crucial for OPV applications. Particular attention is given to the frontier orbital energies of

individual D and A units ($^{D1}E_{HOMO}$, $^{D1}E_{LUMO}$, $^{A1}E_{HOMO}$, and $^{A1}E_{LUMO}$), of donor and acceptor homopolymers ($^{D}E_{HOMO}$, $^{D}E_{LUMO}$, $^{A}E_{HOMO}$, and $^{A}E_{LUMO}$), and of their D–A copolymer combinations ($^{DA}E_{HOMO}$, $^{DA}E_{LUMO}$). These are compared to the calculated homo- and co-polymer absorption energies and strengths, and the results are also related to the chemical structures of the constituent units and the interactions between them. Finally, the light-harvesting capabilities of the 60 D–A copolymers are predicted.

Computational Details

All calculations were performed at the DFT PBE0[34]/6-31G(d,p) level of theory with the Gaussian 09 package.[35]. Structural optimizations were conducted on the 60 monomers and dimers from combinations of 10 donors and 6 acceptor units. The 6 acceptors were also optimized as homo-oligomers of 1–4 repeating units, while homo-oligomers of 1–3 repeating units were optimized for the 10 donor units, except the lightest T, Fu, and T32T donors for which also the tetramers were studied. Time dependent (TD)-DFT was applied to all co-oligomers and donor-only homo-oligomers, to calculate the lowest energy vertical excitations that constitute the first absorption peak in the respective polymers. Long alkyl side-chains were truncated to shorter ones, depending on branching and chemical environment, since these chains typically do not significantly affect the intrinsic electronic properties of conjugated systems.

Results and Discussion

Copolymer and homopolymer frontier orbitals

The D–A polymer frontier orbitals HOMO and LUMO are of great importance for OPV applications, since they largely determine the relevant optical and electronic properties of the polymers. The HOMO–LUMO energy gap correlates closely to the optical band gap, while their spatial overlap partly determines the first absorption peak intensity which typically corresponds to a HOMO→LUMO transition. From all combinations of the 10 donors and 6 acceptors in Chart 1, 60 D–A co-oligomers of 1 and 2 repeating units were constructed and their frontier orbital energies and shapes were calculated with DFT after structural optimization. As exemplified by PIDTBT and POBDTII in Figure 2(a), the calculated LUMOs are mainly localized on the acceptors, while calculated copolymer HOMOs are evenly delocalized over the entire backbones, a tendency commonly reported for

D–A polymers.[36,37,15,21] Since computationally demanding first-principles calculations are limited to shorter oligomers, extrapolation techniques are commonly used to approximate the polymeric orbital energies. The oligomer orbital energies are typically plotted as a function of inverse number of repeating units, 1/n,[38,15,39] and can then be approximately fitted to a linear (empirical) or other more physical, non-linear equations,[40] and extrapolated to $1/n \rightarrow 0$. The linear fitting procedure is compared to a Kuhn fit[41] for PTII in Figure 2(b), demonstrating the small difference in resulting polymer orbital energies between the two extrapolation methods.

After linear extrapolation, the 60 D–A copolymer LUMO energies ($^{DA}E_{LUMO}$) are plotted against the 6 single unit acceptor LUMO energies ($^{A1}E_{LUMO}$) in series of 10 donors in Figure 2(c), exhibiting a very weak and scattered correlation where the coefficients of determination (r^2 values) of the series vary between 0.27 and 0.84. The 60 copolymer HOMO energies ($^{DA}E_{HOMO}$) show a similarly scattered correlation to the 10 single donor unit HOMO energies ($^{D1}E_{HOMO}$) in Figure 2(d), with r^2 ranging from 0.09 to 0.66, and the $^{DA}E_{HOMO}$s are seen to depend strongly on the choice of acceptor. Thus, the simplified picture of the copolymer HOMO being solely determined by the single donor, and the LUMO by the single acceptor unit, is not a useful approximation.

The significant degree of delocalization of LUMO and particularly HOMO as seen in Figure 2(a) makes the single donor or acceptor unit incapable of faithfully representing the influence of the unit on the copolymer properties. The spatial confinement in singe units in contrast to the delocalization in polymers, affects the orbital energy according to band theory: the longer the conjugation, the lower E_{LUMO} and higher E_{HOMO}, see Figure 1 and Figure 2(b). To create a better representation of the donor and acceptor influence, we constructed donor-only and acceptor-only homo-oligomers. Their resulting calculated homo-oligomer orbitals are fully delocalized; see Figure S1 in the Supporting Information. Analogously to the D–A co-oligomer case, the homo-oligomers frontier orbital energies were plotted *vs.* the reciprocal number of repeating units (1/n) and linearly extrapolated to the polymer limit, *i.e.* $1/n \rightarrow 0$. The resulting homopolymer HOMO energies ($^{HP}E_{HOMO}$) and homopolymer LUMO energies ($^{HP}E_{LUMO}$) are plotted in Figure 2(e), where they are also compared to the single unit orbital energies ($^{1}E_{HOMO}$ and $^{1}E_{LUMO}$). The extrapolated homopolymer frontier orbitals will influence the band gap of their copolymers. The size-evolution of homo- and co-polymer orbital energies should be fairly analogous, due to the energetic similarity of the individual unit frontier orbitals (all within ~2 eV of each other as shown in Figure 2(e)), as well as by the structural similarity of these conjugated, organic aryl ring-systems. One factor that weakens this analogy is the difference in planarity between the acceptors based on six-membered rings (II, BTz, BT, and Q) and five-membered rings (BTI and TPD), due to less steric repulsion between units given by the latter.

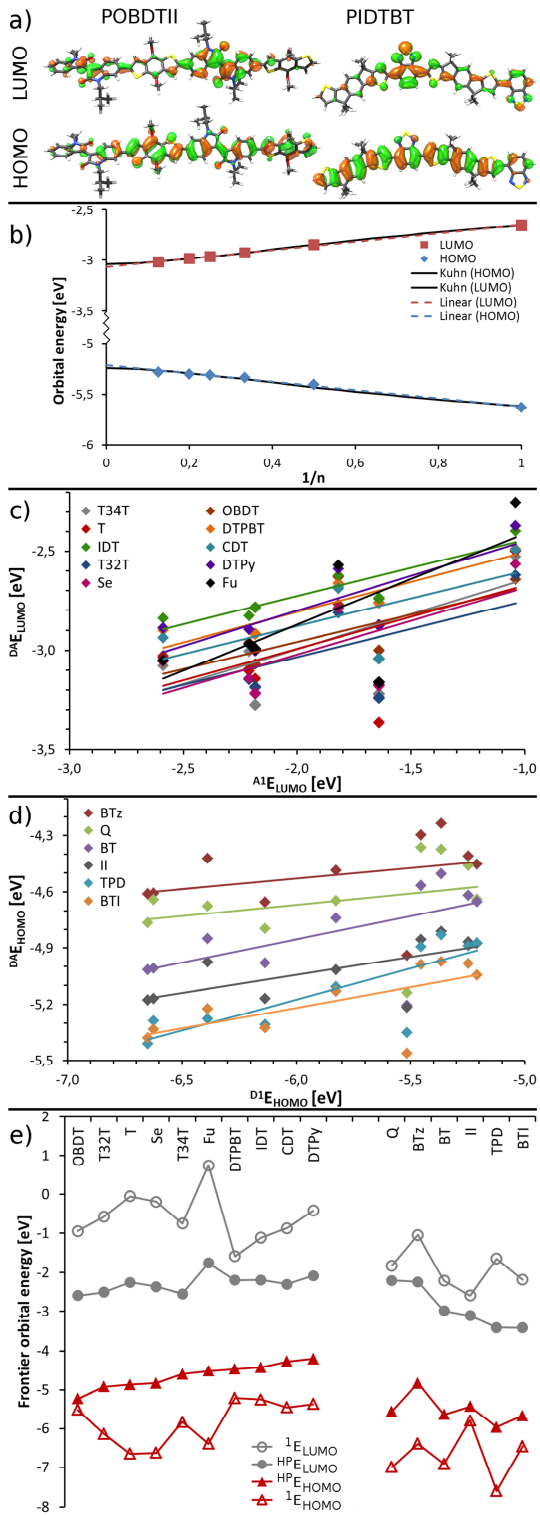
a)
POBDTII
PIDTBT
LUMO
HOMO
b)
Orbital energy [eV]
1/n
LUMO
HOMO
Kuhn (HOMO)
Kuhn (LUMO)
Linear (LUMO)
Linear (HOMO)
c)
T34T
T
IDT
T32T
Se
OBDT
DTPBT
CDT
DTPy
Fu
DAELUMO [eV]
A1ELUMO [eV]
d)
BTz
Q
BT
II
TPD
BTI
DAEHOMO [eV]
D1EHOMO [eV]
e)
Frontier orbital energy [eV]
OBDT
T32T
T
Se
T34T
Fu
DTPBT
IDT
CDT
DTPy
Q
BTz
BT
II
TPD
BTI
1ELUMO
HPELUMO
HPEHOMO
1EHOMO

Figure 2. Calculated LUMO and HOMO for PIDTBT and POBDTII dimers, isovalue=0.02 (a). Calculated frontier orbital energies of PTII *vs.* inverse number of repeating units, with linear fit in dashed and Kuhn fit in solid lines (b). Calculated $^{DA}E_{HOMO}$ *vs.* $^{D1}E_{HOMO}$ (c) and $^{DA}E_{LUMO}$ *vs.* $^{A1}E_{LUMO}$ (d). Calculated frontier orbital energies of donors (left) and acceptors (right) as single units (1) and as homopolymers (HP), with donors sorted by ascending $^{HP}E_{HOMO}$ and acceptors sorted by descending $^{HP}E_{LUMO}$ (e).

In Figure 3(a), the 1/n→0-extrapolated HOMO energies of the 10 donor-only homopolymers ($^{D}E_{HOMO}$) are compared to the corresponding $^{DA}E_{HOMO}$ in series of the 6 acceptors, showing a strong correlation with high r^2 values of 0.73–0.97, although the absolute value depends on the acceptor. Less intuitive is the exhibited correlation (r^2=0.29–0.88) between the donor homopolymer LUMO energies ($^{D}E_{LUMO}$) and the $^{DA}E_{LUMO}$ for all of the acceptors in Figure 3(b), except II and TPD for which r^2<0.1. This challenges the simplified view that the copolymer LUMO is solely determined by the acceptor unit. However, the slope of the HOMO correlation in Figure 3(a) is much steeper than the LUMO correlation in Figure 3(b), indicating that the donor unit still influences the copolymer HOMO more strongly than it does the LUMO, in agreement with the conventional picture of D–A polymers. Figure 3(b) also shows that for the high-LUMO acceptors BTz and Q, the donors have a greater influence on the copolymer LUMO, due to the enhanced interaction between donor LUMO and acceptor LUMO when they are closer in energy, in agreement with equation (1). The $^{DA}E_{HOMO}$ and $^{DA}E_{LUMO}$ are plotted against the 6 acceptor homopolymer HOMO energies ($^{A}E_{HOMO}$) and LUMO energies ($^{A}E_{LUMO}$) in series of the 10 donors, in Figures 3(c) and 3(d). Consistent with the conventional picture of D–A polymers, the $^{A}E_{LUMO}$s (Figure 3(d)) show a decent correlation, (r^2=0.57–0.96) although some codependence is found also for the $^{A}E_{HOMO}$s, albeit weaker and more scattered (r^2=0.41–0.71).

The trends exhibited among the donors in Figure 3(a) and 3(b) permits a qualitative estimation of the D–A copolymer orbital energies from the choice of donor; particularly the $^{DA}E_{HOMO}$ is strongly correlated to the $^{D}E_{HOMO}$. We thus propose the $^{D}E_{HOMO}$ as a rough but quantitative measure of donor strength, defined as the unit's potential for yielding a small band gap in a D–A copolymer. The strength of the 10 studied donors is thus represented by their sorting in Figure 2(e), from weakest (OBDT) to strongest (CDT and DTPy). Importantly, this differs greatly from the ordering of the single unit $^{D1}E_{HOMO}$, due to the orbital energies' strong dependence on unit size. The acceptors can be considered in the same way: since a deeper $^{A}E_{LUMO}$ is correlated with a deep $^{DA}E_{LUMO}$, we propose the use of $^{A}E_{LUMO}$ to quantify acceptor strength. This $^{A}E_{LUMO}$ is not as good a predictor of the D–A band gap as is the $^{D}E_{HOMO}$, due to the previously mentioned more uniform geometries of the donor homopolymers than acceptor homopolymers with respect to coplanarity. Nevertheless, the acceptors in Figure 2(e) are thus roughly sorted from the weakest (Q and BTz) to the strongest (TPD and BTI).

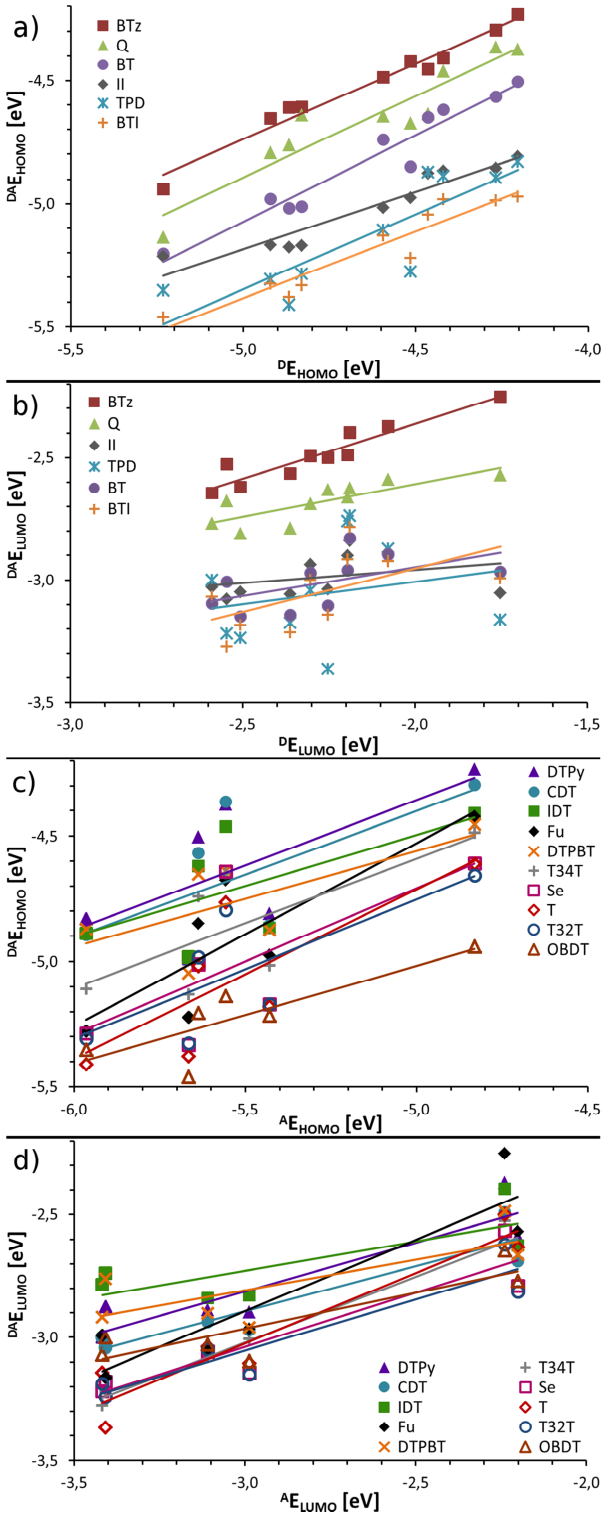
a)
BTz
Q
BT
II
TPD
BTI
$^{DA}E_{HOMO}$ [eV]
$^{D}E_{HOMO}$ [eV]
b)
BTz
Q
II
TPD
BT
BTI
$^{DA}E_{LUMO}$ [eV]
$^{D}E_{LUMO}$ [eV]
c)
DTPy
CDT
IDT
Fu
DTPBT
T34T
Se
T
T32T
OBDT
$^{DA}E_{HOMO}$ [eV]
$^{A}E_{HOMO}$ [eV]
d)
DTPy
CDT
IDT
Fu
DTPBT
T34T
Se
T
T32T
OBDT
$^{DA}E_{LUMO}$ [eV]
$^{A}E_{LUMO}$ [eV]

Figure 3. D–A copolymer orbital energies *vs.* corresponding homopolymer orbital energies. $^{DA}E_{HOMO}$ *vs.* $^{D}E_{HOMO}$ (a), $^{DA}E_{LUMO}$ *vs.* $^{D}E_{LUMO}$ (b), $^{DA}E_{HOMO}$ *vs.* $^{A}E_{HOMO}$ (c), $^{DA}E_{LUMO}$ *vs.* $^{A}E_{LUMO}$ (d).

The influence of the donor on the $^{DA}E_{HOMO}$ is smallest for the copolymers with the largest acceptor II, revealed by the gentler slope of the II-series in Figure 3(a) and (b) compared to the other acceptors. Furthermore, the influence of the acceptor unit is greatest for the smallest donor Fu, indicated by the steeper slope of the Fu-series in Figure 3(c) and 3(d). This suggests that the physical size of a unit partly determines its influence on its copolymer orbital energies. Thus, for each D–A copolymer, we constructed arithmetic means of the frontier orbital energies from the two corresponding donor and acceptor homopolymers, weighted to the unit molecular masses (^{A1}M and ^{D1}M), according to equation (2) and equation (3).

$$\langle {}^{D,A}E_{HOMO} \rangle = \frac{{}^{D}E_{HOMO} \times {}^{D1}M + {}^{A}E_{HOMO} \times {}^{A1}M}{{}^{D1}M + {}^{A1}M} \quad (2)$$

$$\langle {}^{D,A}E_{LUMO} \rangle = \frac{{}^{D}E_{LUMO} \times {}^{D1}M + {}^{A}E_{LUMO} \times {}^{A1}M}{{}^{D1}M + {}^{A1}M} \quad (3)$$

These weighted means of the frontier orbital energies ($\langle {}^{D,A}E_{HOMO} \rangle$ and $\langle {}^{D,A}E_{LUMO} \rangle$) are plotted against the $^{DA}E_{HOMO}$ and $^{DA}E_{LUMO}$ as explicitly calculated on the copolymers in Figure 4(a) and (b) respectively, in series of the 6 acceptors. The correlation is strong for the HOMOs in Figure 4(a), with r^2 values of 0.67–0.96, except for the D–A polymers with the Q acceptor in Figure 4(a) (r^2=0.48) since the minimum energy geometry of the Q-copolymers varies between a cis- (thiophene S in the same direction as quinoxaline N) and trans-conformation (thiophene H towards quinoxaline N). The clear correlation signifies that the band formation is analogous in the homopolymer and the copolymer case, due to the chemical similarity of the constituent units, as well as their comparable frontier orbital energies. The E_{LUMO} trends in Figure 4(b) are clear within each of the 6 series (r^2=0.66–0.91), but are slightly different for the different acceptors, confirming that the choice of acceptor unit still affects the copolymer LUMO more than the donor does. Furthermore, DFT is known to be less reliable for virtual, unoccupied orbitals.[27] Overall, these weighted mean $\langle {}^{D,A}E_{HOMO} \rangle$ and $\langle {}^{D,A}E_{LUMO} \rangle$ exhibit the capability to predict explicitly calculated D–A frontier orbital energies to within ~0.1 eV over a ~1.4 eV interval.

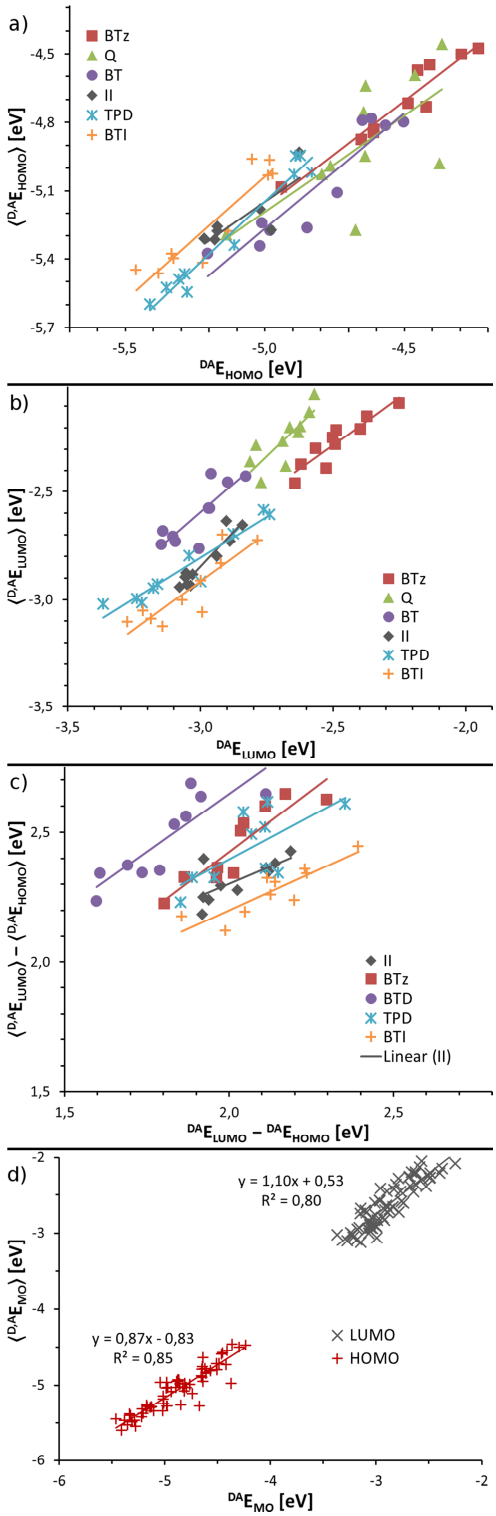
a)
BTz
Q
BT
II
TPD
BTI
-4,5
-4,8
-5,1
-5,4
-5,7
-5,5
-5,0
-4,5
⟨DAEHOMO⟩ [eV]
DAEHOMO [eV]
b)
-2,5
-3,0
-3,5
-3,5
-3,0
-2,5
-2,0
⟨DAELUMO⟩ [eV]
DAELUMO [eV]
c)
2,5
2,0
1,5
1,5
2,0
2,5
⟨DAELUMO⟩ – ⟨DAEHOMO⟩ [eV]
DAELUMO – DAEHOMO [eV]
II
BTz
BTD
TPD
BTI
Linear (II)
d)
-2
-3
-4
-5
-6
-6
-5
-4
-3
-2
⟨DAEMO⟩ [eV]
DAEMO [eV]
y = 1,10x + 0,53
R² = 0,80
y = 0,87x - 0,83
R² = 0,85
LUMO
HOMO

Figure 4. $\langle {}^{D,A}E_{HOMO} \rangle$ from equation (2) *vs.* ${}^{DA}E_{HOMO}$ as directly calculated for the copolymer (a). $\langle {}^{D,A}E_{LUMO} \rangle$ from equation (3) *vs.* ${}^{DA}E_{LUMO}$ as directly calculated for the copolymer (b). $\langle {}^{D,A}E_{HOMO} \rangle - \langle {}^{D,A}E_{LUMO} \rangle$ energy gap *vs.* ${}^{DA}E_{HOMO} - {}^{DA}E_{LUMO}$. (c). All 60 D–A copolymer frontier orbital energies, as weighted means *vs.* as directly calculated for the copolymers (d).

The linear fit slopes are similar for all six acceptors, in particular for the HOMO energies, further demonstrated in Figure 4(d) where all E_{HOMO} and E_{LUMO} energies are plotted as weighted means *vs.* as calculated for the explicit copolymers. The clearness of the overall trend justifies the assumption that it would persist for any other relatively similar acceptor unit. By combining the results in Figure 4(a) and (b), the HOMO–LUMO gap of the copolymers are obtained and plotted in Figure 4(c), as weighted means from the homopolymer orbital energies *vs.* as calculated for the copolymers. Here the correlation is weaker due to the addition of uncorrelated errors, but a general trend is retained. The Q series is not shown due to the above mentioned cis/trans variation. A systematic parametrization of equation (2) and in particular equation (3), may permit better quantitative predictions, but such a procedure is beyond the scope of this study.

The large number of existing donor and acceptor units leads to the existence of an even greater number of potential combinations thereof, *i.e.* as D–A copolymers. By using the above described weighted-mean-approach, one can estimate *e.g.* 900 copolymer frontier orbital energies from calculations on only 30 donors and 30 acceptors, increasing computational efficiency quadratically compared to the treatment of the copolymers explicitly, with a reasonably small loss of accuracy. This allows for vastly efficient screening of D–A combinations, discarding inferior copolymer candidates with *e.g.* unsuitable LUMO level alignment to the fullerene, or too large HOMO–LUMO gap for good spectral coverage, while more promising candidates can proceed to a more refined scrutiny.

Absorption Energies

While efficient predictions of orbital energies are useful, a perhaps even more vital property of D–A polymers is the optical band gap, or energy of maximum absorption (${}^{DA}E_{abs}$). Fitting and extrapolation of oligomer calculations, similar to those for orbital energies in Figure 2(b), have commonly been used both computationally and experimentally for ${}^{DA}E_{abs}$, providing the means to estimate the polymer absorption from oligomer calculations.[15,37,38,40] Calculated and extrapolated ${}^{DA}E_{abs}$ are generally underestimated compared to experiments, explained by differences in conditions; calculations are done at 0 K with at best implicit solvent models, whereas experimental polymers generally exhibit higher absorption energies due to *e.g.* thermal and explicit solvent effects that disrupt the planar structure.[18,42]

To compensate for these effects that cause a systematic underestimation of calculated $^{DA}E_{abs}$, an empirical correction scheme has previously been developed,[15] and is giving promising results in ongoing research. The details on the correction are outlined in the Supporting Information. After applying this correction to $^{DA}E_{abs}$ as calculated with TD-DFT for oligomers and extrapolated to $1/n \rightarrow 0$, they are compared to the calculated $^{DA}E_{LUMO} - {}^{DA}E_{HOMO}$ gaps in Figure 5(a), demonstrating a very a strong correlation with r^2 of 0.85–0.98 within each of the 6 acceptor-series. Furthermore, the slopes of the best linear fits in Figure 5(a) are very close to unity while the intercepts are negligible, making the calculated polymer HOMO–LUMO gaps almost quantitatively representative of the absorption energies. Thus, to approximately predict the $^{DA}E_{abs}$, it is sufficient to determine the HOMO–LUMO gap, rendering the computer-resource demanding TD-DFT calculations necessary only when further precision or the full absorption spectrum is required. Moreover, using the weighted mean scheme from the previous section, the $^{DA}E_{abs}$ of new polymers can be estimated from DFT-calculations of only homo-oligomers of the respective donors and acceptors. Since the number of copolymer combinations increases quadratically with the number of acceptor and donor units, such predictions can favorably be used for immensely efficient screening procedures.

The frontier orbital energies of the donor-only homopolymers $^{D}E_{HOMO}$ and $^{D}E_{LUMO}$ were in the previous section shown to correlate with the corresponding copolymer $^{DA}E_{HOMO}$ and $^{DA}E_{LUMO}$, in Figures 3(a) and 3(b). The absorption energies of these homopolymers ($^{D}E_{abs}$), are calculated with TD-DFT for oligomers and extrapolated to $1/n \rightarrow 0$, and subsequently compared to the corresponding $^{DA}E_{abs}$ in Figure 5(b). Some trendwise agreement is apparent with r^2=0.63–0.77, although the homopolymers have considerably blue-shifted absorption compared to the copolymers and the absolute value is quite different for the 6 distinct acceptor units. It follows that in analogy to the frontier orbital energies, also the $^{DA}E_{abs}$ can be expressed as a mean of the constituent unit's homopolymers, as per equation (4).

$$\langle {}^{D,A}E_{abs} \rangle = \frac{{}^{D}E_{abs} + {}^{A}E_{abs}}{2} \qquad (4)$$

For $\langle {}^{D,A}E_{abs} \rangle$, the straight arithmetic mean (not weighted to unit mass) provides the stronger correlation. This mean $\langle {}^{D,A}E_{abs} \rangle$ is plotted against the $^{DA}E_{abs}$ as calculated directly on the copolymer systems in Figure 5(c), and a good correlation within the respective series is obtained. However, part of the discrepancy between the different acceptor-series remains, suggesting that other factors must be taken into account for a truly predictive formulation of $\langle {}^{D,A}E_{abs} \rangle$ from the homopolymer properties. For example, the planarity of the acceptor-only homopolymers varies significantly, from 4.8° average out-of-plane dihedral angle for BTI to 50.2° for Q, whereas the donor-only homopolymers exhibit more uniform average dihedral angles; all within 12.0–18.8° except the smallest Fu donor with a 0.0° average out-of-plane torsion angle. Further refinement and parametrization of equation (4)

may provide a better quantitative estimate of the copolymer absorption energy, but lies beyond the scope of this study.

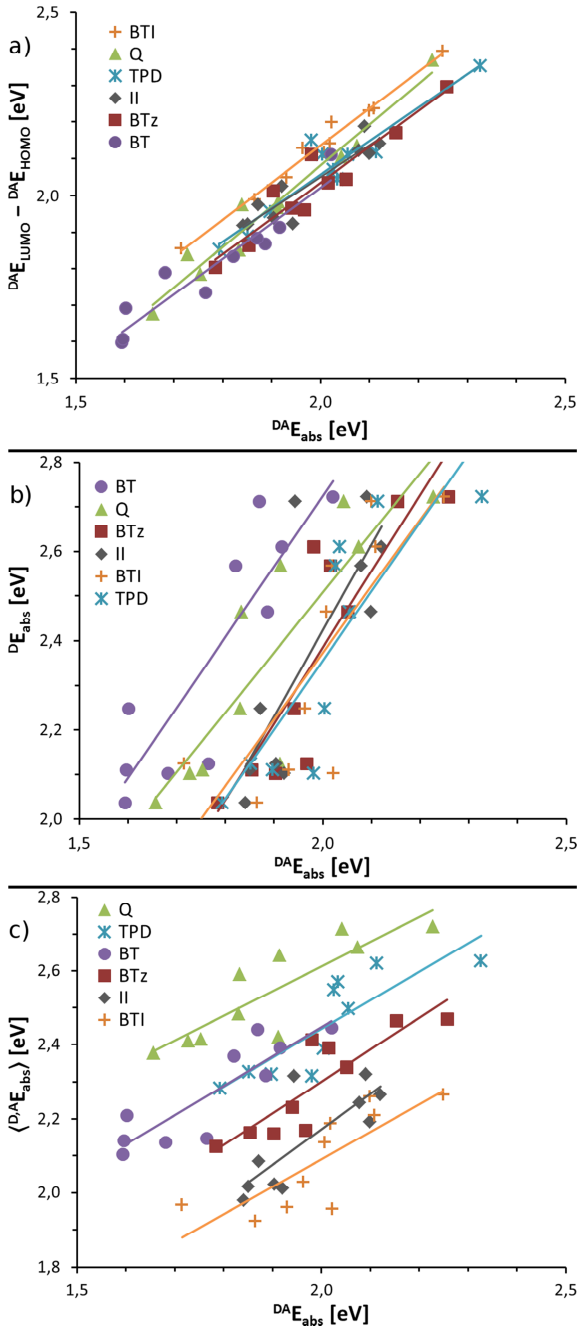

Figure 5. Calculated copolymer HOMO–LUMO gap *vs.* copolymer absorption energy from TD-DFT calculations (a). Donor-only homopolymer absorption energy *vs.* copolymer absorption energy (b). Calculated $\langle {}^{D,A}E_{abs} \rangle$ from equation (4) *vs.* ${}^{DA}E_{abs}$ calculated directly for the copolymers (c).

In Table 1, we list the calculated ${}^{DA}E_{abs}$ of all 60 copolymers, including their averages over the respective acceptor- and donor-series, as well as the ${}^{D}E_{abs}$ of the donor-only homopolymers. The ${}^{DA}E_{abs}$ averages correlate strongly with the strength of the unit, particularly for the donor case as seen in Figure 6, where also the ${}^{D}E_{abs}$ is shown to correlate to the donor strength. Overall, the three quantities in Figure 6: ${}^{D}E_{HOMO}$ (donor strength), ${}^{DA}E_{abs}$, and ${}^{D}E_{abs}$, also presented in the three rightmost columns in Table 1, all unambiguously identify OBDT as the weakest and DTPy and CDT as the strongest donors. For the acceptors, the aforementioned variation in planarity gives the flat homopolymers of BTI and TPD misleadingly deep LUMOs, whereas the very twisted Q-homopolymer affords a considerably higher ${}^{A}E_{LUMO}$ than reflected by its copolymer ${}^{DA}E_{LUMO}$.

Table 1. Absorption energy in [eV] as calculated with TD-DFT for all copolymers (${}^{DA}E_{abs}$) with averages over the series, and for the donor-only homopolymers (${}^{D}E_{abs}$). Also corresponding donor and acceptor strengths: ${}^{D}E_{HOMO}$ and ${}^{A}E_{LUMO}$, by which the rows and columns are sorted.

Acceptor Donor	**BTz**	**Q**	**BT**	**II**	**TPD**	**BTI**	**Ave.**	**${}^{D}E_{abs}$**	**${}^{D}E_{HOMO}$**
OBDT	2.26	2.23	2.02	2.09	2.33	2.25	2.20	2.72	-5.2
T	1.98	2.07	1.92	2.12	2.03	2.11	2.04	2.61	-4.9
T32T	2.02	1.91	1.82	2.08	2.03	2.02	1.98	2.57	-4.9
Se	2.05	1.83	1.89	2.10	2.06	2.01	1.99	2.46	-4.8
T34T	1.97	1.91	1.77	1.90	1.85	1.72	1.85	2.12	-4.6
Fu	2.15	2.04	1.87	1.94	2.11	2.10	2.04	2.71	-4.5
DTPBT	1.94	1.83	1.60	1.87	2.00	1.96	1.87	2.25	-4.5
IDT	1.90	1.73	1.68	1.92	1.98	2.02	1.87	2.10	-4.4
CDT	1.78	1.66	1.59	1.84	1.79	1.87	1.76	2.04	-4.3
DTPy	1.85	1.75	1.60	1.85	1.90	1.93	1.81	2.11	-4.2
Ave.	1.99	1.90	1.78	1.97	2.01	2.00	1.94	2.34	
${}^{A}E_{LUMO}$	-2.2	-2.2	-3.0	-3.1	-3.4	-3.4			

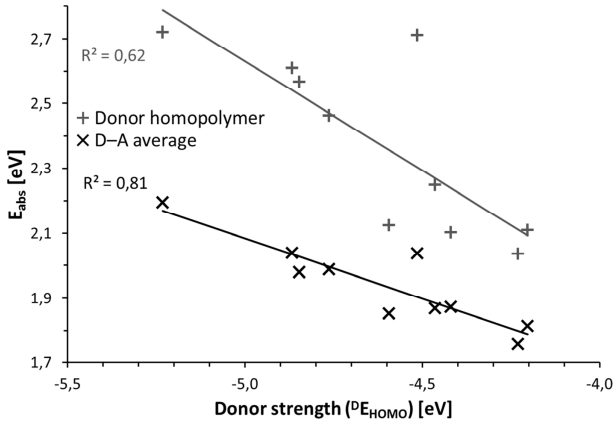

Figure 6. The absorption energies of the 10 donor homopolymers and of the 60 D–A copolymers averaged over the 6 acceptor series *vs.* the donor strengths defined as ${}^{D}E_{HOMO}$. The two dependent and the one independent variable correspond to the three rightmost columns in Table 1 respectively.

Absorption Strengths

A narrow polymer optical band gap is necessary to harvest as large portion as possible of the solar emission, reflected by an increase in the short circuit current (J_{SC}) of the device. J_{SC} is also affected by the absorption strength of the polymer, where a strong absorption per unit volume is desired since it permits thin active layers with large optical densities. The first peak calculated oscillator strength per unit mass (F_M) which is directly proportional to the integrated mass absorption coefficients, has previously been used to quantify the specific absorption strength of D–A polymers.[15] Generally, F_M values increase linearly when plotted against 1/n,[38,43,44,15] and as for the absorption energies in the previous section, the polymeric F_M are obtained by linearly extrapolating to $1/n \rightarrow 0$. In Table 2, we list all 60 calculated D–A copolymer specific absorption strengths (${}^{DA}F_M$), their averages across the respective donor- and acceptor-series, and compare it to the donor homopolymer specific absorption strength (${}^{D}F_M$) and ${}^{D}E_{HOMO}$. Since the absorption per volume is the relevant quantity for OPVs and the mass is used only to approximate the volume, the molecular mass of furan and selenophene were set to the thiophene mass, as these three units are expected to occupy the same volume. Furthermore, an arbitrary alkyl side-chain ratio of 33 wt% was assumed for the ${}^{DA}F_M$ estimations.

From Table 2, it is seen that the T34T donor gives lower ${}^{DA}F_M$ in its copolymers due to a significant steric hindrance to the acceptors caused by its vertical geometry, perpendicular to the backbone, resulting in less planar copolymer geometries. The D–A polymers with the BTz acceptor show consistently stronger specific absorption than with the other acceptors. In a rough,

qualitative trend, the donor units in Table 2 with higher $^{D}E_{HOMO}$ demonstrate stronger specific absorption in their D–A copolymers. Figure 7 shows that the $^{D}F_{M}$ correlate roughly with the corresponding $^{DA}F_{M}$, permitting a qualitative assessment of a donor unit's potential for strong absorption in D–A polymers from studying only its homopolymer. The Fu donor appears as an outlier in Figure 7, conferring considerably lower $^{DA}F_{M}$ than indicated by the homopolymer $^{D}F_{M}$. We rationalize this from its small size in combination with a relatively deep HOMO, its mediocre electron-richness thereby failing to balance the electron-poorness of the acceptors.

Table 2. Specific absorption strength in [kg^{-1}] as calculated with TD-DFT for all copolymers ($^{DA}F_{M}$) with averages, and for the donor-only homopolymers ($^{D}F_{M}$) . These are compared to, and sorted by, the donor-only homopolymer HOMO energies in [eV].

Acceptor Donor	**BTz**	**Q**	**BT**	**II**	**TPD**	**BTI**	**Mean**	**$^{D}F_{M}$**	**$^{D}E_{HOMO}$**
OBDT	1.45	0.78	0.86	0.89	1.13	1.02	1.02	1.94	-5.2
T	1.55	0.97	1.05	1.14	1.12	1.35	1.20	2.41	-4.9
T32T	1.72	1.22	1.16	1.21	1.24	1.31	1.31	2.73	-4.9
Se	1.56	0.94	1.09	1.20	1.06	1.36	1.20	2.32	-4.8
T34T	1.09	0.72	0.78	0.98	0.72	1.14	0.90	1.68	-4.6
Fu	1.39	0.85	0.85	1.14	1.12	1.29	1.11	2.75	-4.5
DTPBT	1.66	0.97	1.03	1.09	1.19	0.94	1.15	2.39	-4.5
IDT	1.44	1.15	1.03	1.14	1.01	1.20	1.16	2.50	-4.4
CDT	1.59	1.19	1.14	1.25	1.01	1.28	1.24	2.57	-4.3
DTPy	1.76	1.22	1.11	1.28	1.16	1.33	1.31	2.84	-4.2
Mean	1.52	1.00	1.01	1.13	1.08	1.22	1.16	2.41	

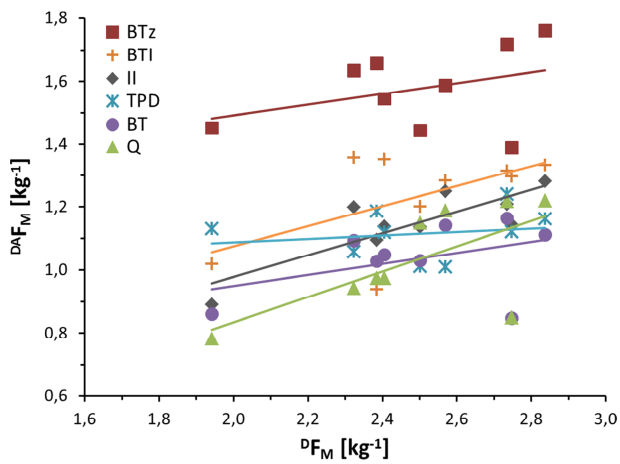

Figure 7. The calculated copolymer $^{DA}F_{M}$ *vs.* the donor-only homopolymer $^{D}F_{M}$. The T34T donor is excluded due to the significantly twisted optimized geometry of its polymers.

Light-harvesting Capability

The combined consideration of absorption energy and strength permits an assessment of the light-harvesting capability of a copolymer,[15] which determines its suitability for OPV application. While a low but balanced E_{abs} of ~1.5 eV has been proposed as the optimum for OPV efficiency,[20] a stronger absorption is monotonically favorable. In Figure 8, $^{DA}F_M$ is plotted against $^{DA}E_{abs}$ for a number of representative copolymer series in a Light-Harvesting Capability plot,[15] with the top left of the graph constituting the desired regions for efficient OPVs. Corresponding plots including all 60 copolymers can be found in the Supporting Information. In Figure 8(a), the copolymers with three of the donors are shown, representing strong, medium, and weak donor cases, respectively. As previously shown in Table 2, a positive correlation between low band gap and strong absorption is demonstrated in Figure 8(a), resulting in the identification of the strong DTPy and CDT donor units as the most promising light-harvesting components in D–A polymers, while the OBDT copolymers exhibit inferior light-harvesting capability with concomitantly weak and unfavorably blue-shifted absorption. Benzodithiophene is commonly appended with electron-rich thienyl side-groups,[31,33,45,46] yielding a stronger donor which according to our results promotes better light-harvesting than OBDT with alkoxy side-groups. The reported 'weak donor–strong acceptor' strategy for increasing the open circuit voltage (V_{OC}) while maintaining a reasonably small band gap,[47–50] is thus deemed ineffective, since a weak donor will decrease J_{SC} due to both a blue-shifting and weakening of the absorption, and J_{SC} has been shown to correlate more strongly than V_{OC} with the final efficiency of the OPV device.[51]

The copolymers of three representative acceptors have their F_M plotted against E_{abs} in Figure 8(b). Here, a weak inverse correlation between low band gap and strong absorption is revealed, making the assessment of acceptor strength more ambiguous than donor strength. The BT copolymers exhibit the smallest band gaps, the definition of a strong acceptor, but also the weakest absorption. The BTz copolymers conversely have the largest $^{DA}F_M$, but also the highest $^{DA}E_{abs}$. The choice of suitable acceptor unit for efficient solar cells is thus less straightforward, and must be made in conjunction with other fabrication parameters such as active layer film thickness and polymer–fullerene weight-ratio.

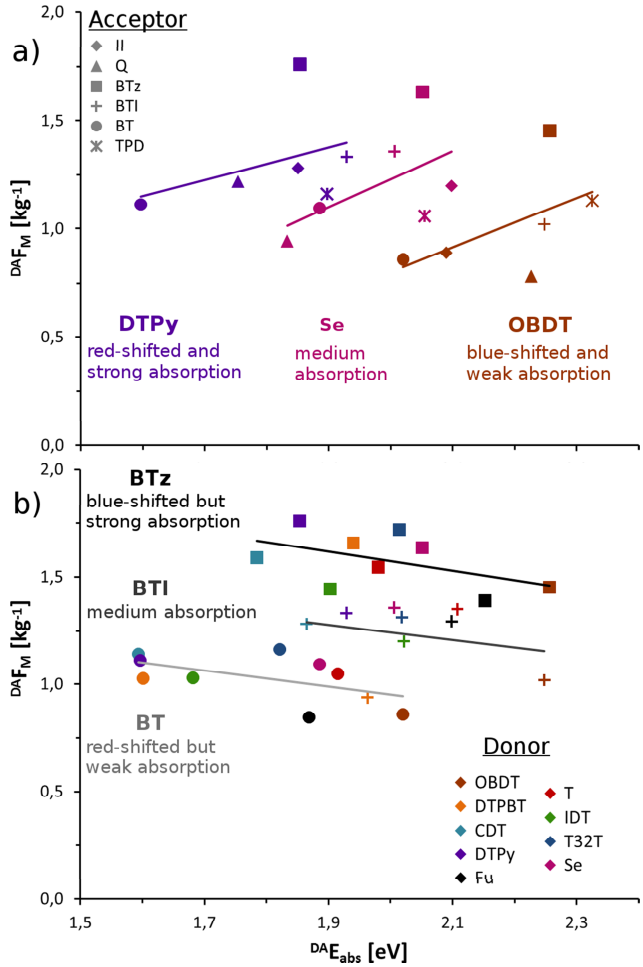

Figure 8. Light-Harvesting Capability plots. Calculated specific absorption strengths $^{DA}F_M$ *vs.* absorption energy $^{DA}E_{abs}$ for three representative donor-series of respectively strong (DTPy), medium (Se), and weak (OBDT) donors, where data point color represents donor, and marker type represents acceptor (a). Calculated $^{DA}F_M$ *vs.* $^{DA}E_{abs}$ for three representative acceptor-series of respectively strong (BT), medium (BTI), and weak (BTz) acceptors (b). Results for all 6 acceptors and all 10 donors are found in the Supporting Information.

As demonstrated in Figure 8(a) and (b), the calculated specific absorption strengths $^{DA}F_M$ varies more across the acceptors than the studied donors, despite the larger number of different donors studied. $^{DA}E_{abs}$ on the other hand, appears more strongly dependent on the donor unit. These trends can be exploited when designing new D–A polymers, permitting a fine-tuning of the absorption strength or energy as a function of the chosen acceptor or donor, respectively. While a previous computational study of 9 D–A copolymers failed to identify any polymer with concomitant strong and low-energy absorption,[15] here several polymers

demonstrate promising optical properties in this respect. Based on the calculated absorption energies and strengths, the D–A combination of a CDT or DTPy donor with a BT, Q, or BTz acceptor, is predicted to possess the most favorable light-harvesting capabilities for efficient OPVs, in terms of suitably low band gap and strong absorption.

Conclusions

A multitude of different donor and acceptor units have been used successfully in D–A polymer combinations for OPV applications. They are often described by their donor or acceptor 'strengths' relative to other units, where the strength qualitatively connotes the ability to induce a narrow band gap. These strengths can be difficult to assess since the size-differences of the units affect the evolution of electronic properties upon going from isolated units to polymers. We here use first principles DFT and TD-DFT methods to assess the donor and acceptor strengths through systematic investigation of electronic and optical properties of D–A systems.

Results presented here show that electronic traits of 60 D–A polymers are well represented by the properties of homopolymers of the corresponding 10 donor and 6 acceptor units. The exhibited strong correlations between the homopolymers and copolymers are facilitated by analogous electronic coupling between units, due to their relatively similar chemistry and energy levels (all HOMOs and LUMOs within ~2 eV across the 10 donors and 6 acceptors). The frontier orbital energies of the donor and acceptor homopolymers combined into weighted means, which reproduce the frontier orbital energies of the corresponding D–A copolymers with good accuracy. This allows for an efficient estimation of the ${}^{DA}E_{HOMO}$ and ${}^{DA}E_{LUMO}$ of a set of copolymers whose number increases quadratically with the number of donor and acceptor units. Importantly, this also permits an explicit quantification of the donor and acceptor strengths using calculated homopolymer ${}^{D}E_{HOMO}$ and ${}^{A}E_{LUMO}$ respectively. OBDT and DTPy are consequently determined to be the respective weakest and strongest donor, while BTz and BT emerge as the weakest and strongest acceptor.

The donor and acceptor strengths of the units are furthermore shown to correlate with their corresponding D–A polymer optical properties, where intense specific absorption together with a suitably small band gap reflects the general light-harvesting capability of the polymers. Strong donors and acceptors both correlate with small absorption energies, coherent with the intuitive view of unit strength. Less commonly assessed, we also show that the specific absorption intensities of donor homopolymers are correlated with those of the corresponding D–A copolymers, permitting a semi-quantitative estimation of the D–A polymer absorption intensity from its donor properties. In addition, intense D–A copolymer

absorption appears correlated with strong donors (giving small $^{DA}E_{abs}$), facilitating a concomitant red-shift and increase in absorption by employing strong donor units. The inverse trend is revealed for acceptors, implying a trade-off between narrow band gap and high absorption coefficients when choosing acceptor unit. We consequently identify the combination of a CDT or DTPy donor with a BT, Q, or BTz acceptor as the D–A copolymers with the most promising light-harvesting capability.

In a larger perspective, our results show that systematic investigation of D–A polymers units can reveal useful trends, exploitable in the design of new light-harvesters for OPV applications, where the performance is largely determined by the molecular level properties of the conjugated polymers, governing the light-harvesting capability as well as charge separation and transport properties of the device. Computational methods are still far from predicting the exact experimental properties of conjugated polymers, due to differences in conditions and shortcomings of the methods. But with sufficiently accurate and computationally inexpensive calculations, the screening process for new D–A copolymer designs can be greatly aided by calculations, having the potential to readily eliminate polymer candidates with inferior properties, and to propose more promising ones for refined scrutiny.

Associated Content

Supporting information

Calculated homopolymer orbitals, details on oscillator strengths and absorption coefficients, details on empirical corrections of E_{abs} and F_M, light-harvesting properties for all 60 D–A copolymers. This material is available online.

References

(1) Darling, S. B.; You, F. *RSC Adv.* **2013**, *3* (39), 17633.

(2) Li, G.; Zhu, R.; Yang, Y. *Nat. Photonics* **2012**, *6* (3), 153.

(3) Po, R.; Bernardi, A.; Calabrese, A.; Carbonera, C.; Corso, G.; Pellegrino, A. *Energy Environ. Sci.* **2014**, *7* (3), 925.

(4) Janssen, R. A. J.; Nelson, J. *Adv. Mater.* **2013**, *25* (13), 1847.

(5) Kippelen, B.; Bredas, J.-L. *Energy Environ. Sci.* **2009**, *2* (3), 251.

(6) Zhao, G.; He, Y.; Li, Y. *Adv. Mater.* **2010**, *22* (39), 4355.

(7) Li, Y. *Acc. Chem. Res.* **2012**, *45* (5), 723.

(8) Zhu, Z.; Waller, D.; Gaudiana, R.; Morana, M.; Mühlbacher, D.; Scharber, M.; Brabec, C. *Macromolecules* **2007**, *40* (6), 1981.

(9) Beaujuge, P. M.; Amb, C. M.; Reynolds, J. R. *Acc. Chem. Res.* **2010**, *43* (11), 1396.

(10) Havinga, E. E.; Hoeve, W.; Wynberg, H. *Polym. Bull.* **1992**, *29* (1-2), 119.

(11) Liu, Y.; Zhao, J.; Li, Z.; Mu, C.; Ma, W.; Hu, H.; Jiang, K.; Lin, H.; Ade, H.; Yan, H. *Nat. Commun.* **2014**, *5*.

(12) Chen, J.-D.; Cui, C.; Li, Y.-Q.; Zhou, L.; Ou, Q.-D.; Li, C.; Li, Y.; Tang, J.-X. *Adv. Mater.* **2015**, *27* (6), 1035.

(13) Nelson, J. *Mater. Today* **2011**, *14* (10), 462.

(14) Rauk, A. *Orbital Interaction Theory of Organic Chemistry*; Wiley: New York, 2004.

(15) Hedström, S.; Henriksson, P.; Wang, E.; Andersson, M. R.; Persson, P. *Phys. Chem. Chem. Phys.* **2014**, *16* (45), 24853.

(16) Mondal, R.; Ko, S.; Norton, J. E.; Miyaki, N.; Becerril, H. A.; Verploegen, E.; Toney, M. F.; Bredas, J.-L.; McGehee, M. D.; Bao, Z. *J. Mater. Chem.* **2009**, *19* (39), 7195.

(17) Gibson, G. L.; McCormick, T. M.; Seferos, D. S. *J. Am. Chem. Soc.* **2011**, *134* (1), 539.

(18) Hedström, S.; Henriksson, P.; Wang, E.; Andersson, M. R.; Persson, P. *J. Phys. Chem. C* **2015**, *119*, 6453.

(19) Risko, C.; McGehee, M. D.; Bredas, J.-L. *Chem. Sci.* **2011**, *2* (7), 1200.

(20) Scharber, M. C.; Mühlbacher, D.; Koppe, M.; Denk, P.; Waldauf, C.; Heeger, A. J.; Brabec, C. J. *Adv. Mater.* **2006**, *18* (6), 789.

(21) Hedström, S.; Persson, P. *J. Phys. Chem. C* **2012**, *116* (51), 26700.

(22) Pandey, L.; Risko, C.; Norton, J. E.; Brédas, J.-L. *Macromolecules* **2012**, *45* (16), 6405.

(23) Salvatori, P.; Mosconi, E.; Wang, E.; Andersson, M.; Muccini, M.; De Angelis, F. *J. Phys. Chem. C* **2013**, *117* (35), 17940.

(24) Wang, E.; Bergqvist, J.; Vandewal, K.; Ma, Z.; Hou, L.; Lundin, A.; Himmelberger, S.; Salleo, A.; Müller, C.; Inganäs, O.; Zhang, F.; Andersson, M. R. *Adv. Energy Mater.* **2013**, *3* (6), 806.

(25) Ma, H.; Qin, T.; Troisi, A. *J. Chem. Theory Comput.* **2014**, *10* (3), 1272.

(26) Wykes, M.; Milián-Medina, B.; Gierschner, J. *Front. Chem.* **2013**, *1* (35), 35.

(27) Zhang, G.; Musgrave, C. B. *J. Phys. Chem. A* **2007**, *111* (8), 1554.

(28) Hamel, S.; Duffy, P.; Casida, M. E.; Salahub, D. R. *J. Electron Spectrosc. Relat. Phenom.* **2002**, *123* (2–3), 345.

(29) McCormick, T. M.; Bridges, C. R.; Carrera, E. I.; DiCarmine, P. M.; Gibson, G. L.; Hollinger, J.; Kozycz, L. M.; Seferos, D. S. *Macromolecules* **2013**, *46* (10), 3879.

(30) Wang, E.; Hou, L.; Wang, Z.; Hellström, S.; Zhang, F.; Inganäs, O.; Andersson, M. R. *Adv. Mater.* **2010**, *22* (46), 5240.

(31) Ye, L.; Zhang, S.; Zhao, W.; Yao, H.; Hou, J. *Chem. Mater.* **2014**, *26* (12), 3603.

(32) He, Z.; Zhong, C.; Su, S.; Xu, M.; Wu, H.; Cao, Y. *Nat. Photonics* **2012**, *6* (9), 591.

(33) Fu, G.; Yang, S.; Shi, J.; Zhang, Z.; Liu, B.; Zhao, X.; Li, G.; Li, X. *Prog. Photovolt. Res. Appl.* **2014**.

(34) Adamo, C.; Barone, V. *J. Chem. Phys.* **1999**, *110* (13), 6158.

(35) Frisch, M.; Trucks, G.; Schlegel, H.; Scuseria, G.; Robb, M.; Cheeseman, J.; Scalmani, G.; Barone, V.; Mennucci, B.; Petersson, G.; Nakatsuji, H.; Caricato, M.; Li, X.; Hratchian, H.; Izmaylov, A.; Bloino, J.; Zheng, G.; Sonnenberg, J.; Hada, M.; Ehara, M.; Toyota, K.; Fukuda, R.; Hasegawa, J.; Ishida, M.; Nakajima, T.; Honda, Y.; Kitao, O.; Nakai, H.; Vreven, T.; Montgomery, J.; Peralta, J.; Ogliaro, F.; Bearpark, M.; Heyd, J.; Brothers, E.; Kudin, K.; Staroverov, V.; Kobayashi, R.; Normand, J.; Raghavachari, K.; Rendell, A.; Burant, J.; Iyengar, S.; Tomasi, J.; Cossi, M.; Rega, N.; Millam, J.; Klene, M.; Knox, J.; Cross, J.; Bakken, V.; Adamo, C.; Jaramillo, J.; Gomperts, R.; Stratmann, R.; Yazyev, O.; Austin, A.; Cammi, R.; Pomelli, C.; Ochterski, J.; Martin, R.; Morokuma, K.; Zakrzewski, V.; Voth, G.; Salvador, P.; Dannenberg, J.; Dapprich, S.; Daniels, A.; Farkas; Foresman, J.; Ortiz, J.; Cioslowski, J.; Fox, D. Gaussian 09, Revision A.02, 2009.

(36) Van Mullekom, H. A. M.; Vekemans, J. A. J. M.; Havinga, E. E.; Meijer, E. W. *Mater. Sci. Eng. R Rep.* **2001**, *32* (1), 1.

(37) Pandey, L.; Doiron, C.; Sears, J. S.; Bredas, J.-L. *Phys. Chem. Chem. Phys.* **2012**, *14* (41), 14243.

(38) Gierschner, J.; Cornil, J.; Egelhaaf, H.-J. *Adv. Mater.* **2007**, *19* (2), 173.

(39) Zade, S. S.; Zamoshchik, N.; Bendikov, M. *Acc. Chem. Res.* **2010**, *44* (1), 14.

(40) Torras, J.; Casanovas, J.; Alemán, C. *J. Phys. Chem. A* **2012**, *116* (28), 7571.

(41) Kuhn, W. *Helv. Chim. Acta* **1948**, *31* (6), 1780.

(42) Andersson, L. M.; Hedström, S.; Persson, P. *Appl. Phys. Lett.* **2013**, *103* (21), 213303.

(43) Grimm, B.; Risko, C.; Azoulay, J. D.; Bredas, J.-L.; Bazan, G. C. *Chem. Sci.* **2013**, *4* (4), 1807.

(44) Tretiak, S.; Saxena, A.; Martin, R. L.; Bishop, A. R. *J. Phys. Chem. B* **2000**, *104* (30), 7029.

(45) Yang, T.; Wang, M.; Duan, C.; Hu, X.; Huang, L.; Peng, J.; Huang, F.; Gong, X. *Energy Environ. Sci.* **2012**, *5* (8), 8208.

(46) Wang, N.; Chen, Z.; Wei, W.; Jiang, Z. *J. Am. Chem. Soc.* **2013**, *135* (45), 17060.

(47) Zhou, H.; Yang, L.; Stoneking, S.; You, W. *ACS Appl. Mater. Interfaces* **2010**, *2* (5), 1377.

(48) Zhou, H.; Yang, L.; Stuart, A. C.; Price, S. C.; Liu, S.; You, W. *Angew. Chem.* **2011**, *123* (13), 3051.

(49) Zhou, H.; Yang, L.; Price, S. C.; Knight, K. J.; You, W. *Angew. Chem. Int. Ed.* **2010**, *49* (43), 7992.

(50) Qin, C.; Fu, Y.; Chui, C.-H.; Kan, C.-W.; Xie, Z.; Wang, L.; Wong, W.-Y. *Macromol. Rapid Commun.* **2011**, *32* (18), 1472.

(51) Jackson, N. E.; Savoie, B. M.; Marks, T. J.; Chen, L. X.; Ratner, M. A. *J. Phys. Chem. Lett.* **2015**, *6* (1), 77.

Paper III

THE JOURNAL OF PHYSICAL CHEMISTRY C

Article

pubs.acs.org/JPCC

Quantum Chemical Calculations of Side-Group Stacking and Electronic Properties in Thiophene−Quinoxaline Polymers

Svante Hedström and Petter Persson*

Division of Theoretical Chemistry, Lund University, P.O. Box 124, S-221 00 Lund, Sweden

● *Supporting Information*

ABSTRACT: Organic bulk heterojunction (BHJ) solar cells offer a viable source of solar energy. Structural organization is crucial in BHJ cells but hard to achieve and assess due to limitations in experimental methodology. Quantum chemical methods have here been used to gain further insight into the geometric and optical properties of a promising light-harvesting polymer, poly[2,3-bis(3-octyloxyphenyl)-quinoxaline-5,8-diyl-*alt*-thiophene-2,5-diyl] (TQ1). Calculations show that favorable positions of the two alkoxyphenyl side groups on each TQ1 monomer allow nonbonded side-group stacking interactions with the neighboring units in both directions. This yields a unique, helical geometry with enhanced intramolecular ordering that promotes extensive electronic conjugation. Adequate description of this effect requires computational methods that include dispersion corrections. A strategy based on such side-group interactions is proposed for designing new polymers.

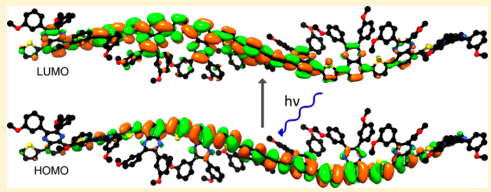

■ INTRODUCTION

Organic electronics is important for a range of modern applications that includes displays, printed plastic circuits, and photovoltaic devices.[1,2] In particular, organic solar cells have potential for easy roll-to-roll fabrication, offering an interesting alternative to traditional silicon-based p/n-junction photovoltaic devices which require high-purity silicon and cannot compete against fossil and nuclear energy sources in cost per electric power.[3] Organic solar cells consist of a photoactive mix of electron-donating and -accepting species, typically a polymer and some fullerene derivative, the latter often being phenyl-C61-butyric acid methyl ester[4] ($PC_{60}BM$).[5] Efficient BHJ solar cells have most commonly been based on poly[phenylene vinylenes], or poly[alkyl-thiophenes], such as poly[3-hexyl-thiophene] (P3HT).[6] The latter has been combined with indene-C_{60} bisadduct to manufacture cells showing an overall efficiency of 6.5%[7] owing partly to the high hole mobility of P3HT, reported to ∼0.05 $cm^2/V{\cdot}s$.[8,9] Recently, donor−acceptor (D−A) copolymers have received increasing attention because of their potential to give larger photocurrent and the possibility to fine tune the absorption by chemically altering the building blocks of the polymer. A novel D−A-type polymer, TQ1 (for thiophene−quinoxaline), synthesized by Wang et al. has shown good spectral properties and been successfully applied in solar cells with high performance.[10] This polymer exhibits absorption on higher wavelengths than many of its predecessors, such as P3HT.[11]

One major challenge for making efficient molecular devices is to control the electronic properties in polymer materials that allow significant structural flexibility at the molecular level. In P3HT solar cells, intermolecular ordering is of great importance[12] since a regioregular polymer phase facilitates hole transport through it.[13] High ordering in the polymer bulk will also lead to a HOMO that is energetically higher lying in the center of the polymer region than at the disordered polymer−fullerene interface.[14] This facilitates the crucial charge transfer where the holes travel away from the interface, toward the anode. However, in many functional polymers there can be significant disorder in terms of both intramolecular structure (disorder of the monomer units along a single polymer strand) and intermolecular structure (lack of systematic packing of the polymer strands). Typically, the backbone of a polymer is selected to provide the fundamental electronic properties, while side groups can be used to control intermolecular interactions, e.g., solubility. Refined mechanisms to induce intrachain ordering exist, e.g., hydrogen bonding between base pairs in DNA, but such approaches are rarely used in the synthesis of photoactive polymers. With disorder follows difficulties to control the electronic features fully, with potential problems, e.g., formation of localized trap states, or inadequate delocalization and conduction capabilities of holes. An additional complication is that the lack of long-range order makes it difficult to characterize the structure experimentally; there are generally no available crystal structures for disordered materials. Structural and other properties of polymers have however been successfully investigated in computational studies.[15−17]

To accurately describe nonbonded attractions, dispersion effects must be taken into account, which most DFT methods cannot do.[18−21] However, certain modern functionals that by

Received: August 13, 2012
Revised: November 13, 2012
Published: November 17, 2012

various means include descriptions of London forces have been applied in recent computational studies of systems where such effects are relevant, both with intermolecular[22,23] and intramolecular[24,25] dispersion interactions. These functionals have been shown to reproduce experimental and higher level theory results of nonbonded interactions well.[26−30] In some studies of polymers, dispersion-including functionals have been employed to describe polymer−polymer interchain and polymer−fullerene interactions.[31−33]

Here we present computational results for TQ1, with particular focus on a unique stacking effect predicted by calculations on TQ1 oligomers. To further clarify the role of the side groups, TQ1 is also compared with a second polymer poly[quinoxaline-5,8-diyl-*alt*-thiophene-2,5-diyl], here called TQ1b, that has the same backbone as TQ1 but lacks the alkoxyphenyl side groups. Moreover, variants of TQ1 with different side chains on the phenyl rings were studied (see Figure S1, Supporting Information). Monomer structures of the investigated polymers are shown in Chart 1. Electronic and optical properties of TQ1 oligomers are also investigated.

Chart 1. Chemical Structures of Alkoxy-Truncated TQ1 and TQ1b

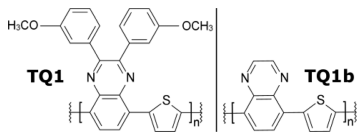

METHODS

All calculations were conducted with the Gaussian 09 package.[34] In most calculations, the $C_8H_{17}O$ side chains were truncated to methoxy groups. TQ1 dimer optimizations and corresponding counterpoise (cp) calculations on the stacking alkoxy-phenyl rings were carried out with PBE0[35] and two DFT functionals that include dispersion: M062X[36] and ωB97XD[37] using 6-31G(d,p) basis set, followed by single-point 6-311+G(2d,p) calculations. Wave function-based second-order Møller−Plesset perturbation theory[38] (MP2) was applied for optimized scans over dihedral angles for TQ1b monomer as a complement to the corresponding density functionals ωB97XD and PBE0, all using the 6-311+G(2d,p)//6-31G(d,p) basis set and an implicit integral equation formalism polarizable continuum model[39] *o*-dichlorobenzene solvent. Similarly, for TQ1b and TQ1 dimers, scans were conducted at same levels of theory excluding MP2, starting from the optimized PBE0 angle. TQ1 and TQ1b *cis* and *trans* were optimized up to the nonamer at the PBE0/6-31G(d,p) level, followed by single-point calculations for TQ1 with ωB97XD/6-31G(d,p) up to the hexamer. Excitations were obtained using time-dependent (TD)-DFT calculations at the PBE0/6-31G(d,p) level of theory. The influence of side chains was investigated by optimizing TQ1 dimers with methoxy groups in the para position, octylxoxy side chains, and no side chains, respectively, using PBE0/6-31G(d,p) and ωB97XD/6-31G(d,p), the former method subsequently applied for TDDFT calculations. $PC_{60}BM$ was studied at the PBE0/6-311+G(2d,p)//PBE0/6-31G(d,p) level of theory. Results are presented below first for structural and second for electronic properties.

RESULTS

Like many polymers, TQ1 and TQ1b contain backbones of stiff planar ring units that can rotate quite easily relative to each other around the carbon−carbon bonds that connect them. Two dihedral angles, φ_1 and φ_2, characterize the ring−ring twists, as illustrated for the TQ1 dimer in Figure 1. The

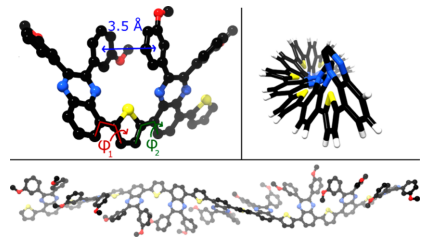

Figure 1. Side-group stacking and helical propagation of TQ1. (Top left) Relaxed *cis*-dimer with side-group phenyl ring distance and dihedral angles φ_1 and φ_2. (Top right) Relaxed *cis*-hexamer with side groups hidden. (Bottom) Relaxed *cis*-nonamer (H atoms not shown).

individual T−Q dihedral angles have two distinct local minima: one with a small dihedral angle (as shown in Figure 1) and one with a dihedral angle close to 180° (not shown). This is typical for many polymer systems where planar structures are favored due to increased electronic conjugation, but there is H−H steric repulsion that pushes neighboring rings somewhat out of plane. In the minimum energy conformation of the TQ1 monomer $\varphi_1 = \varphi_2 = 18.6°$, increasing to an average of 21.4° in the relaxed di- and longer oligomers. The corresponding angle for TQ1b is around 14° for all sizes. Quinoxaline−thiophene dihedral angles have previously been estimated in DFT studies to be between 3.2°[40] and 26.1°[41] depending on neighboring substituents. Dutta et al. reported a single-molecule bisphenylquinoxaline−thiophene dihedral angle of 12.1° calculated at the B3LYP/6-31G(d) level.[42] This can be compared to crystallographically obtained torsion angles between a thiophene and a phenyl ring that range from 7.2°[43] to 26.8°[44] depending on the chemical environment and packing, whereas DFT-calculated angles in the gas phase for such a system vary between 14.0°[45] and 21.8°.[46]

Considering the structural ordering in oligomers, quinoxaline groups from neighboring monomers can point in approximately the same direction, as shown for the TQ1 dimer in Figure 1, if both involved dihedral angles (φ_1 and φ_2) are small (*cis* conformation) or both dihedral angles are large, ∼180° (*cis2*, see Figure S2, Supporting Information). Alternatively, neighboring quinoxaline groups point roughly in opposite directions (*trans*, see Figure S2, Supporting Information) if one of the two dihedral angles is small and the other is large. The relative stabilities of the *cis*, *cis2*, and *trans* conformations have been calculated for the TQ1 (Table 1) and TQ1b (Table 2) dimers.

The results for the TQ1b dimer indicate that there are small energy differences of up to a few kJ/mol between the three investigated conformations. This suggests that a variety of arrangements between neighboring units in polymers would be represented under normal conditions, resulting in significant structural disorder along a polymer chain of TQ1b. The reasons

dx.doi.org/10.1021/jp308063u | J. Phys. Chem. C 2012, 116, 26700−26706

Table 1. Calculated Stabilities of Three Dimer Conformers of TQ1 (in kJ/mol) Relative to the *cis*-Conformer with Positive Numbers Signifying Less Stable Structures

method	*cis*	*cis2*	*trans*	*trans*-cp[a]
PBE0/6-31G(d,p)	0.00	7.32	2.52	−5.51
PBE0/6-311+G(2d,p)//PBE0/6-31G(d,p)	0.00	7.83	1.80	−1.07
ωB97XD/6-31G(d,p)//PBE0/6-31G(d,p)	0.00	25.38	25.97	18.85
ωB97XD/6-31G(d,p)	0.00	23.89	31.27	19.78
ωB97XD/6-311+G(2d,p)//ωB97XD/6-31G(d,p)	0.00	26.30	29.56	25.93
M062X/6-311+G(2d,p)//M062X/6-31G(d,p)	0.00	23.36	24.91	20.62

[a]Counterpoise corrected.

Table 2. Calculated Stabilities of Three Dimer Conformers of TQ1b (in kJ/mol) Relative to the Most Stable Conformer

method	*cis*	*cis2*	*trans*
PBE0/6-31G(d,p)	0.00	6.03	0.19
PBE0/6-311+G(2d,p)//PBE0/6-31G(d,p)	0.00	6.28	0.26
ωB97XD/6-31G(d,p)	0.00	3.08	0.22
ωB97XD/6-311+G(2d,p)//ωB97XD/6-31G(d,p)	0.00	2.88	0.30

for the relative instability of *cis2* TQ1b fall outside the scope of this article but are intended for investigation in a later paper.

In contrast, the results given in Table 1 for TQ1 show a significant preference for the *cis* conformation over the other two conformations. The increased stability of the *cis* conformation is apparent already with the hybrid DFT functional PBE0, although basis set superposition error (BSSE) effects complicate a quantification of the stacking effect.[47] The cp corrections lower the *cis* over *trans* preference to the point of making *trans* slightly more stable with the PBE0 functional.

Using the dispersion-corrected functionals ωB97XD and M062X, the *cis* form is calculated to be stabilized compared to the *trans* form by ca. 20−25 kJ/mol for the dimer. Overall, results in Tables 1 and 2 show little basis set dependence.

Because the only difference between TQ1 and TQ1b are the side groups, stabilization of the TQ1 *cis*-conformer must be related to these. We ascribe this effect to an attraction of the alkoxyphenyl side groups on neighboring units. The attractive nature of the side-group interaction is surprising because any such attractions would be expected to be weaker than the steric repulsions between neighboring side groups. However, the TQ1 dimer structure in Figure 1 visualizes an unusually favorable structural stacking arrangement formed between the alkoxyphenyl side groups of neighboring monomer units in the TQ1 polymer that allows attractive interactions without seriously distorting the ideal backbone arrangement. The neighboring phenyl rings are almost parallel, and their distance of 3.5 Å corresponds well with reported π−π interaction distances of 3.4−4.1 Å[48−50] depending on the amount of parallel displacement.[51] Even though the concept of π−π stacking is most important for conjugated systems of 10 atoms or more,[52] other van der Waals interactions contribute to the attraction between this kind of planar hydrocarbon system.[53] These conclusions are supported by the increased *cis* stabilization given by the DFT functionals that include dispersion description.

To further investigate the interaction between neighboring units, scans over the dihedral angle quinoxaline−thiophene for TQ1b monomer and over quinoxaline−quinoxaline in TQ1 and TQ1b dimers were conducted. These scans are shown in Figure 2, demonstrating a very deep energy well for TQ1

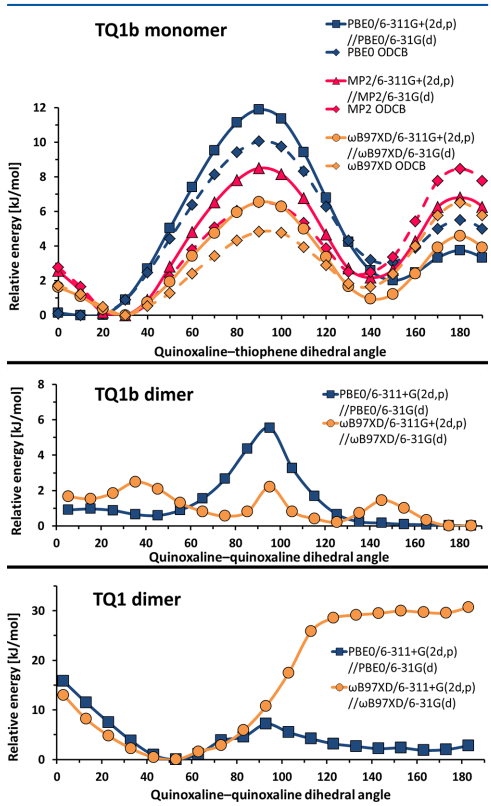

Figure 2. Potential energy scan over the dihedral angle between thiophene−quinoxaline in TQ1b monomer (top), quinoxaline−quinoxaline in TQ1b dimer (middle), and quinoxaline−quinoxaline in TQ1 dimer (bottom). All energies relative to the minimum within the series. ODCB refers to calculations at the same level of theory as above with an implicit *o*-dichlorobenzene solvent, which is the solvent used for TQ1 in ref 10.

around the *cis*-optimized geometry, which indicates that a TQ1 polymer strand is unlikely to break the conjugation by adopting a quinoxaline−quinoxaline angle larger than 53°. Traditionally, DFT has been known to overestimate π conjugation,[54] leading to a too small optimal torsion angle between rings in conjugated systems and too large rotational barriers.[55,56] In the topmost graph of Figure 2, however, the relative PBE0 energy at the MP2 minimum geometry is only about 1.0 kJ/mol and vice versa for the MP2 energy at the PBE0 optimum geometry. The modern, long-range-corrected ωB97XD functional yields the same optimum dihedral angle as MP2 and an even lower rotational barrier.

dx.doi.org/10.1021/jp308063u | *J. Phys. Chem. C* 2012, 116, 26700−26706

Alkoxy side chain variations were finally investigated for the dimer. Counterpoise-corrected ωB97XD/6-31G(d,p) calculations indicate that the presence of alkoxy groups increases the *cis* vs *trans* stability somewhat for both *m*-methoxy (19.78 kJ/mol) and *p*-methoxy positions (15.85 kJ/mol) compared to the nonsubstituted phenyl side groups (7.94 kJ/mol). Alkoxy substituents are electron donating, and the para position should thus be more energetically favorable than the meta position. However, TQ1 is synthesized as meta substituted,[10] and the difference in electronic structure between TQ1-meta, TQ1-para, and nonsubstituted phenyl group TQ1 results in slightly different optical spectra (see Figure S3, Supporting Information). The side-group interaction is calculated to be strengthened further with the full *m*-octyloxy side chains (35.8 kJ/mol), supporting the presence of a favorable side-group interaction. However, full characterization of the *m*-octyloxy systems requires consideration of further effects, including intermolecular interactions (e.g., polymer−polymer, polymer−PCBM, or polymer−solvent) as well as interactions between the side chains from different parts of the polymer chain, beyond the scope of the present investigation.

The side-group stacking evident in the dimer arises from a surprising structural match of neighboring units due to the particular chemical structure of TQ1. The two alkoxyphenyl groups on each monomer unit are furthermore placed in such a special arrangement that they are able to form favorable stacking in both directions. This creates a striking helical arrangement of the entire polymer in which the side groups turn around a gradually twisted backbone axis. This is demonstrated for an optimized TQ1 nonamer in Figure 1. Furthermore, Figure 3 shows that the stacking in the *cis* form

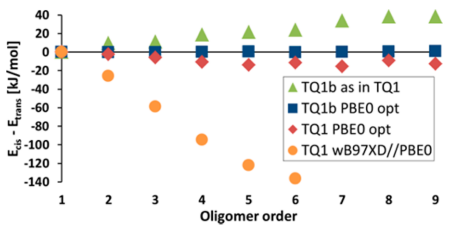

Figure 3. Energy difference between all-*cis* and all-*trans* conformations of TQ1 and TQ1b. "TQ1b as in TQ1" refers to a single-point calculation of TQ1b with the backbone geometry of PBE0-optimized TQ1. All results obtained using the 6-31G(d,p) basis set.

provides increased relative stabilization for longer oligomers, indicating that the stacking is not hampered by the additional constraints from simultaneous interactions of several units. By making further stability comparisons of the *cis* to *trans* form, one can better understand the long-range structural organization. Relative energies of the *cis* and *trans* oligomers for TQ1 and TQ1b containing up to nine units, are plotted in Figure 3.

For TQ1b, there is essentially no energy difference between the optimized *cis* and *trans* forms (blue squares in Figure 3), consistent with the dimer results in Table 2. For TQ1, the *cis* form is calculated to be favored energetically over the *trans* form for all oligomer lengths, more so with the ωB97XD functional (yellow circles in Figure 3) than with PBE0 (red diamonds). The ωB97XD series shows that stabilization of *cis* survives even for longer chains and progresses almost linearly.

When taking the fully optimized TQ1, stripping it of the side groups, and then computing the energies of this TQ1b structure without further optimization (green triangles in Figure 3), the *trans* form is preferred. This means that though the *cis* form is most favorable for TQ1 as a whole, it involves a suboptimal backbone geometry. The total *cis*−*trans* difference consists of backbone effects and side-group interactions. Thus, the side-group interaction, $E_{interact}$, can be quantified by taking the total *cis*−*trans* difference and subtracting the backbone effect

$$E_{interact} = \Delta E_{TQ1} - \Delta E_{TQ1\text{-backbone}} \quad (1)$$

where ΔE_{TQ1} and $\Delta E_{TQ1\text{-backbone}}$ are the *cis*−*trans* energy differences for the full oligomer and for TQ1b in the TQ1 geometry, respectively. For the dimer, which has one side-group stacking, cp-corrected $E_{interact}$ amounts to −11.6 kJ/mol with PBE0/6-311+G(2d,p)//PBE0/6-31G(d,p) and −29.1 kJ/mol with ωB97XD/6-311+G(2d,p)//ωB97XD/6-31G(d,p), which is a strong nonbonded attraction.

A helical polymer has been reported by Knaapila et al.[57] However, TQ1 is, to the best of our knowledge, unique in that it is the side groups rather than the backbone that determine the helix-like overall structure.

Calculated frontier orbitals, shown for the nonamer in Figure 4, retain good delocalization over the entire oligomers,

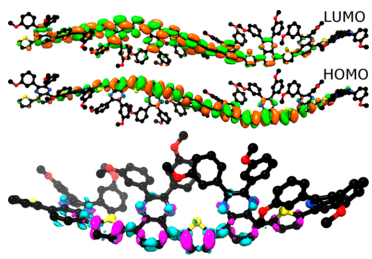

Figure 4. (Top) Frontier orbitals of TQ1 *cis*-nonamer. (Bottom) Tetramer electron density difference (isovalue 0.001) between the first excited state and the ground state with electrons being transferred from purple to turquoise upon excitation. All calculated with PBE0/6-31G(d,p).

indicating that the long-range conjugation remains intact, despite the moderate nonplanarity of the oligomer. For TQ1, an unusually high degree of intramolecular order and conjugation length facilitates efficient hole transport within the chains, without the need to impose interchain packing and ordering as discussed above for P3HT. The internal quantum efficiency in PCSs is limited by the charge carrier mobility, depending on device thickness, morphology, and temperature.[58] Since breaking the side-group stacking at any point would be energetically unfavorable, the calculations indicate that TQ1 chains are straighter and more kink free than other polymers, leading to a greater effective transport distance within a single molecule. Figure 4 indicates the D−A character of TQ1; the HOMO has slightly more density at the thiophene, whereas the LUMO is denser at the quinoxaline moiety. The calculated first excitation electron density difference also points toward thiophene donating electrons to quinoxaline when TQ1 undergoes excitation.

dx.doi.org/10.1021/jp308063u | J. Phys. Chem. C 2012, 116, 26700−26706

In a polymer solar cell, the LUMO energy of the polymer must be higher than that of the acceptor material, the difference acting as a driving force for electron injection into the latter. For TQ1 and $PC_{60}BM$, the calculated difference between their LUMO energies amounts to 0.87 eV at the *cis*-pentamer PBE0/6-311+G(2d,p)//PBE0/6-31G(d,p) level, enough for efficient injection according to the suggested 0.30−0.35 eV as the minimum required energy difference.[59−61] In Figure 5, the evolution of TQ1 LUMO as a function of inverse system size, evaluated with PBE0/6-31G(d,p), is practically linear, and when extrapolated to the polymer limit an injection driving force of 0.68 eV is obtained. TQ1 HOMO has a more pronounced system size dependency, to the point where the calculated energy of the monomer HOMO is barely higher than that of $PC_{60}BM$, whereas for the larger oligomers the HOMO lays well over 1 eV higher than $PC_{60}BM$.

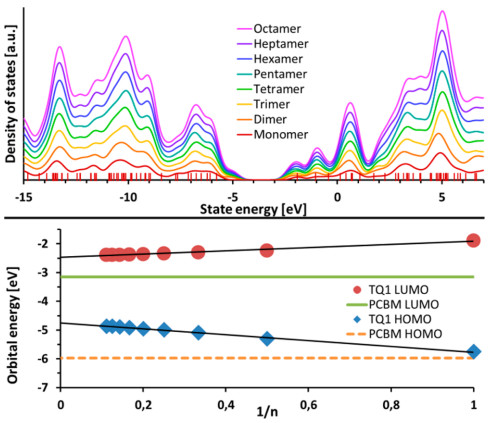

Figure 5. (Top) PDoS for the eight smallest *cis*-oligomers of TQ1. Also, individual states for the monomer. (Bottom) Frontier orbitals of TQ1 as a function of inverse oligomer order with best linear fit in black lines. Also, HOMO and LUMO energies of $PC_{60}BM$. All calculated with PBE0/6-31G(d,p).

The HOMO−LUMO gap of the polymer is related to the absorption threshold. Recently, much effort has been made to find polymers which absorb at higher wavelengths to make use of a larger portion of the solar emission.[62−65] This has favored polymers with small a HOMO−LUMO gap, but a larger gap allows for higher voltage of the solar cell, so finding an optimal gap size is essential. Calculated TQ1 *cis*-nonamer orbitals in vacuo HOMO = −4.87 eV and LUMO = −2.39 eV results in a direct band gap of 2.48 eV, coinciding with the experimental gap obtained with square wave voltametry.[10] For the same system, TD-DFT gives a first excitation energy of 1.98 eV. A projected density of states plot (PDoS) for TQ1 is shown in Figure 5, created by adding a Gaussian-shape broadening of 0.2 eV to the individual states. The PDoS demonstrates the band gap and the resulting conduction and valence bands, analogous to those present in inorganic semiconductors. The general shape of the PDoS does not change noticeably with increasing oligomer order, indicating that the states maintain their energies when additional units of TQ1 are added.

Absorption spectra for visible light were constructed for *cis*-oligomers with 1−5 units by applying a Gaussian broadening of 3000 cm^{-1} full-width at medium height to the calculated vertical excitations (listed in Table S1, Supporting Information). Normalized to a maximum intensity of unity, a comparison to experimental absorption is presented in Figure 6. Note that the second peak at ∼300 nm is most intense for the three smallest oligomers, being surpassed by the first peak lying at ∼600 nm for the tetra- and pentamers. These latter oligomer sizes show optical responses that agree well with the experimental spectrum. For all system sizes, the intense first absorption peak corresponds to the first calculated excitation, i.e., HOMO to LUMO. The convergence of this first excitation energy for *trans* and *cis* forms, respectively, together with an extrapolation to the bulk limit is also shown in Figure 6.

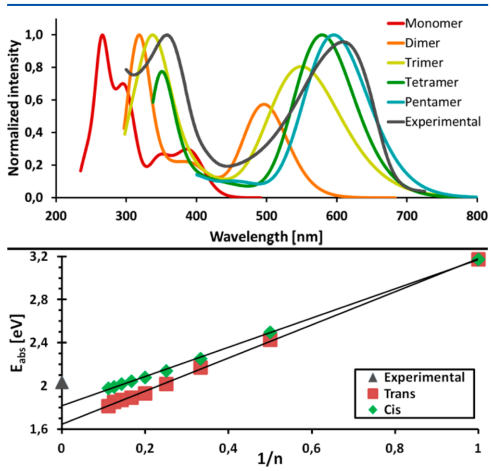

Figure 6. (Top) TQ1 absorption spectra normalized to a maximum intensity of 1 arbitrary unit; experimental[10] and as calculated for *cis*-oligomers. Due to computational limitations, only excitations down to 356 nm could be reached for the pentamer, missing the ∼300 nm peak. (Bottom) First excitation energy as a function of inverse oligomer order for TQ1 with best linear fits. Also, polymer experimental first absorption peak.

The calculated excitation wavelengths overshoot the experimental value at the tetramer level for the *trans* form but not until the heptamer for the *cis* form. The latter's increased excitation energy stems from its larger dihedral angles. The *cis* form's better agreement with experimental optical results further strengthens the notion that it is experimentally favored over the *trans* form. Note that the extrapolation to the polymer limit in Figure 6 would be valid only if the conjugation length equaled the polymer length, whereas in reality it is limited to some finite value due to abrupt kinks at certain points along the chain[66,67] or continuous thermal conformational disorder.[68,69] Reported polymer effective conjugation lengths vary from as little as a single unit for some polymers,[70] around five units for others, and [71] up to 8[72] and 10 units for P3HT.[73] The calculated absorption wavelength of TQ1 matches experimental polymeric results best around the tetra- to hexamer level. However, optical and electronic results are often not fully converged at this size, despite having been previously used for quantitative calculations.[15]

dx.doi.org/10.1021/jp308063u | J. Phys. Chem. C 2012, 116, 26700−26706

In Figure S3, Supporting Information, absorption spectra of dimers are plotted for systems with *p*-methoxy and *m*-methoxy side chains and without side chains. The two main absorption peaks are similar for all cases, although the presence of alkoxy chains gives rise to a shoulder at around 400 nm. The influence of the alkoxy side chain length was tested by optimizing TQ1 with *m*-octyloxy side chains, with following TDDFT calculations yielding an absorption spectrum highly similar to the *m*-methoxy case (see Figure S3, Supporting Information).

■ CONCLUSIONS

Calculations show a surprising ability of the TQ1 strands to achieve improved helix-like intrachain organization due to side-group attractions, promoting long-range conjugation. This contributes to providing a computational rationalization of the experimentally demonstrated efficient performance of this particular polymer,[10] e.g., in terms of high hole mobility. In addition, it is concluded that standard hybrid DFT functionals such as PBE0 or B3LYP are not adequate for calculations on this type of systems. These methods do not describe the intramolecular dispersion present in TQ1, and this could lead to results being even qualitatively flawed by not correctly assigning the minimum energy geometry. This has deeper impact on subsequent absorption calculations, which are geometry sensitive, as seen for TQ1 in Figure 6.

Our calculations on thiophene−quinoxaline oligomer variants show that the side groups have a significant effect on both structural and optical properties due to intramolecular interactions. In a broader perspective, side-group interactions provide a new strategy to achieve enhanced intrachain structural organization and concomitant control of electronic properties in a wider range of polymers for molecular electronics applications. Such stacking effects are hard to predict from schematic structural drawings alone and may not be readily characterized experimentally in disordered materials. This makes computational modeling a particularly valuable tool to pursue this strategy further.

■ ASSOCIATED CONTENT

● Supporting Information

Structures of *cis2* and *trans*; calculated *cis* excitation data. Absorption spectra for TQ1 dimer variants. Three-dimensional rotatable figure of TQ1 *cis*-nonamer in xyz format. This material is available free of charge via the Internet at http://pubs.acs.org.

■ AUTHOR INFORMATION

Corresponding Author

*Phone: +46-462223311. Fax: +46-462228648. E-mail: petter.persson@teokem.lu.se.

Notes

The authors declare no competing financial interest.

■ ACKNOWLEDGMENTS

We thank Arkady Yartsev, Mats Andersson, Olle Inganäs, and Villy Sundström for valuable comments. Patrik Henriksson is thanked for experimental absorption data. This work was funded by the Swedish research council (V.R.). NSC and LUNARC are acknowledged for computer resources used.

■ REFERENCES

(1) Facchetti, A. *Chem. Mater.* **2010**, *23*, 733−758.
(2) O'Neill, M.; Kelly, S. M. *Adv. Mater.* **2011**, *23*, 566−584.
(3) *Annual Energy Outlook*; U.S. Energy Information Administration: Washington, DC, 2011.
(4) Hummelen, J. C.; Knight, B. W.; LePeq, F.; Wudl, F.; Yao, J.; Wilkins, C. L. *J. Org. Chem.* **1995**, *60*, 532−538.
(5) Günes, S.; Neugebauer, H.; Sariciftci, N. S. *Chem. Rev.* **2007**, *107*, 1324−1338.
(6) Dennler, G.; Scharber, M. C.; Brabec, C. J. *Adv. Mater.* **2009**, *21*, 1323−1338.
(7) Zhao, G.; He, Y.; Li, Y. *Adv. Mater.* **2010**, *22*, 4355−4358.
(8) Sirringhaus, H.; Tessler, N.; Friend, R. H. *Science* **1998**, *280*, 1741−1744.
(9) Bao, Z.; Dodabalapur, A.; Lovinger, A. *Appl. Phys. Lett.* **1996**, *69*, 4108−4110.
(10) Wang, E.; Hou, L.; Wang, Z.; Hellström, S.; Zhang, F.; Inganäs, O.; Andersson, M. R. *Adv. Mater.* **2010**, *22*, 5240−5244.
(11) Hoppe, H.; Sariciftci, S. *JMR* **2004**, *19*, 1924−1945.
(12) Brinkmann, M.; Rannou, P. *Macromolecules* **2011**, *42*, 1125−1130.
(13) Kim, Y.; Cook, S.; Tuladhar, S. M.; Choulis, S. A.; Nelson, J.; Durrant, J. R.; Bradley, D. D. C.; Giles, M.; McCulloch, I.; Ha, C.-S.; Ree, M. *Nat. Mater.* **2006**, *5*, 197−203.
(14) Tu, G.; Bilge, A.; Adamczyk, S.; Forster, M.; Heiderhoff, R.; Balk, L. J.; Mühlbacher, D.; Morana, M.; Koppe, M.; Scharber, M. C.; Choulis, S. A.; Brabec, C. J.; Scherf, U. *Macromol. Rapid Commun.* **2007**, *28*, 1781−1785.
(15) Risko, C.; McGehee, M. D.; Bredas, J.-L. *Chem. Sci* **2011**, *2*, 1200−1218.
(16) Sun, L.; Bai, F.-Q.; Zhao, Z.-X.; Zhang, H.-X. *Sol. Energy Mater. Sol. Cells* **2011**, *95*, 1800−1810.
(17) Lenz, A.; Kariis, H.; Pohl, A.; Persson, P.; Ojamäe, L. *Chem. Phys.* **2011**, *384*, 44−51.
(18) Kristyán, S.; Pulay, P. *Chem. Phys. Lett.* **1994**, *229*, 175−180.
(19) Johnson, E. R.; Mackie, I. D.; DiLabio, G. A. *J. Phys. Org. Chem.* **2009**, *22*, 1127−1135.
(20) Tuma, C.; Daniel Boese, A.; C. Handy, N. *Phys. Chem. Chem. Phys.* **1999**, *1*, 3939−3947.
(21) Tsuzuki, S.; Uchimaru, T.; Tanabe, K. *Chem. Phys. Lett.* **1998**, *287*, 202−208.
(22) Marom, N.; Tkatchenko, A.; Rossi, M.; Gobre, V. V.; Hod, O.; Scheffler, M.; Kronik, L. *J. Chem. Theory Comput.* **2011**, *7*, 3944−3951.
(23) Schreiner, P. R.; Chernish, L. V.; Gunchenko, P. A.; Tikhonchuk, E. Y.; Hausmann, H.; Serafin, M.; Schlecht, S.; Dahl, J. E. P.; Carlson, R. M. K.; Fokin, A. A. *Nature* **2011**, *477*, 308−311.
(24) Ehrlich, S.; Moellmann, J.; Grimme, S. *Acc. Chem. Res.* **2012**10.1021/ar3000844.
(25) Mourik, T. v. *J. Chem. Theory Comput.* **2008**, *4*, 1610−1619.
(26) Miao, J.; Hua, S.; Li, S. *Chem. Phys. Lett.* **2012**, *541*, 7−11.
(27) Wallnoefer, H. G.; Fox, T.; Liedl, K. R.; Tautermann, C. S. *Phys. Chem. Chem. Phys.* **2010**, *12*, 14941−14949.
(28) Zhao, Y.; Truhlar, D. G. *J. Chem. Theory Comput.* **2011**, *7*, 669−676.
(29) Schenker, S.; Schneider, C.; Tsogoeva, S. B.; Clark, T. *J. Chem. Theory Comput.* **2011**, *7*, 3586−3595.
(30) Riley, K. E.; Pitoňák, M.; Jurečka, P.; Hobza, P. *Chem. Rev.* **2010**, *110*, 5023−5063.
(31) Mondal, R.; Becerril, H. A.; Verploegen, E.; Kim, D.; Norton, J. E.; Ko, S.; Miyaki, N.; Lee, S.; Toney, M. F.; Bredas, J.-L.; McGehee, M. D.; Bao, Z. *J. Mater. Chem.* **2010**, *20*, 5823−5834.
(32) Campbell, K.; Gurun, B.; Sumpter, B. G.; Thio, Y. S.; Bucknall, D. G. *J. Phys. Chem. B* **2011**, *115*, 8989−8995.
(33) Tamura, H.; Burghardt, I.; Tsukada, M. *J. Phys. Chem. C* **2011**, *115*, 10205−10210.
(34) Frisch, M.; Trucks, G.; Schlegel, H.; Scuseria, G.; Robb, M.; Cheeseman, J.; Scalmani, G.; Barone, V.; Mennucci, B.; Petersson, G.; Nakatsuji, H.; Caricato, M.; Li, X.; Hratchian, H.; Izmaylov, A.; Bloino, J.; Zheng, G.; Sonnenberg, J.; Hada, M.; Ehara, M.; Toyota, K.; Fukuda, R.; Hasegawa, J.; Ishida, M.; Nakajima, T.; Honda, Y.; Kitao, O.; Nakai, H.; Vreven, T.; Montgomery, J.; Peralta, J.; Ogliaro, F.;

Bearpark, M.; Heyd, J.; Brothers, E.; Kudin, K.; Staroverov, V.; Kobayashi, R.; Normand, J.; Raghavachari, K.; Rendell, A.; Burant, J.; Iyengar, S.; Tomasi, J.; Cossi, M.; Rega, N.; Millam, J.; Klene, M.; Knox, J.; Cross, J.; Bakken, V.; Adamo, C.; Jaramillo, J.; Gomperts, R.; Stratmann, R.; Yazyev, O.; Austin, A.; Cammi, R.; Pomelli, C.; Ochterski, J.; Martin, R.; Morokuma, K.; Zakrzewski, V.; Voth, G.; Salvador, P.; Dannenberg, J.; Dapprich, S.; Daniels, A.; Farkas; Foresman, J.; Ortiz, J.; Cioslowski, J.; Fox, D. *Gaussian 09*, Revision A.02; Gaussian, Inc.,: Wallingford, CT, 2009.

(35) Adamo, C.; Barone, V. *J. Chem. Phys.* **1999**, *110*, 6158−6170.

(36) Zhao, Y.; Truhlar, D. *Theor. Chem. Acc.* **2008**, *120*, 215−241.

(37) Chai, J.-D.; Head-Gordon, M. *Phys. Chem. Chem. Phys.* **2008**, 10.

(38) Møller, C.; Plesset, M. S. *Phys. Rev.* **1934**, *46*, 618−622.

(39) Cances, E.; Mennucci, B.; Tomasi, J. *J. Chem. Phys.* **1997**, *107*, 3032−3041.

(40) Wang, Y.; Peng, Q.; Hou, Q.; Zhao, K.; Liang, Y.; Li, B. *Theor. Chem. Acc.* **2011**, *129*, 257−270.

(41) Sun, L.; Bai, F.-Q.; Zhao, Z.-X.; Yang, B.-Z.; Zhang, H.-X. *J. Polym. Sci., B: Polym. Phys.* **2010**, *48*, 2099−2107.

(42) Dutta, G. K.; Patil, S. *Org. Electron.* **2012**, *13*, 1266−1276.

(43) Tavazzi, S.; Miozzo, L.; Silvestri, L.; Mora, S.; Spearman, P.; Moret, M.; Rizzato, S.; Braga, D.; Diagne Diaw, A. K.; Gningue-Sall, D.; Aaron, J.-J.; Yassar, A. *Cryst. Growth Des.* **2010**, *10*, 2342−2349.

(44) Pu, S.-Z.; Liu, G.; Chen, B.; Wang, R.-J. *Acta Crystallogr., Sect. C* **2005**, *61*, o599−o601.

(45) Li, R.; Lv, X.; Shi, D.; Zhou, D.; Cheng, Y.; Zhang, G.; Wang, P. *J. Phys. Chem. C* **2009**, *113*, 7469−7479.

(46) Zgou, H.; Hamidi, M.; Bouachrine, M. *J. Mol. Struct.-THEOCHEM* **2007**, *814*, 25−32.

(47) Kestner, N. R.; Combariza, J. E. In *Reviews in Computational Chemistry*; John Wiley & Sons, Inc.: Hoboken, NJ, 2007; Vol. *13*, pp 99−132.

(48) Roesky, H. W.; Andruh, M. *Coord. Chem. Rev.* **2003**, *236*, 91−119.

(49) Shetty, A. S.; Zhang, J.; Moore, J. S. *J. Am. Chem. Soc.* **1996**, *118*, 1019−1027.

(50) Chipot, C.; Jaffe, R.; Maigret, B.; Pearlman, D. A.; Kollman, P. A. *J. Am. Chem. Soc.* **1996**, *118*, 11217−11224.

(51) Sinnokrot, M. O.; Valeev, E. F.; Sherrill, C. D. *J. Am. Chem. Soc.* **2002**, *124*, 10887−10893.

(52) Grimme, S. *Angew. Chem., Int. Ed.* **2008**, *47*, 3430−3434.

(53) Hunter, C. A.; Sanders, J. K. M. *J. Am. Chem. Soc.* **1990**, *112*, 5525−5534.

(54) Lundberg, M.; Siegbahn, P. E. M. *J. Chem. Phys.* **2005**, *122*, 224103−9.

(55) Sancho-García, J. C.; Pérez-Jiménez, A. J. *J. Phys. Chem. A* **2008**, *112*, 10325−10332.

(56) Karpfen, A.; Choi, C. H.; Kertesz, M. *J. Phys. Chem. A* **1997**, *101*, 7426−7433.

(57) Knaapila, M.; Lyons, B. P.; Kisko, K.; Foreman, J. P.; Vainio, U.; Mihaylova, M.; Seeck, O. H.; Pålsson, L.-O.; Serimaa, R.; Torkkeli, M.; Monkman, A. P. *J. Phys. Chem. B* **2003**, *107*, 12425−12430.

(58) Riedel, I.; Dyakonov, V. *Phys. Status Solidi A* **2004**, *201*, 1332−1341.

(59) Brédas, J.-L.; Beljonne, D.; Coropceanu, V.; Cornil, J. *Chem. Rev.* **2004**, *104*, 4971−5004.

(60) Scharber, M. C.; Mühlbacher, D.; Koppe, M.; Denk, P.; Waldauf, C.; Heeger, A. J.; Brabec, C. J. *Adv. Mater.* **2006**, *18*, 789−794.

(61) Koster, L. J. A.; Mihailetchi, V. D.; Blom, P. W. M. *Appl. Phys. Lett.* **2006**, *88*, 093511−3.

(62) Mühlbacher, D.; Scharber, M.; Morana, M.; Zhu, Z.; Waller, D.; Gaudiana, R.; Brabec, C. *Adv. Mater.* **2006**, *18*, 2884−2889.

(63) Hou, J.; Chen, H.-Y.; Zhang, S.; Chen, R. I.; Yang, Y.; Wu, Y.; Li, G. *J. Am. Chem. Soc.* **2009**, *131*, 15586−15587.

(64) Peet, J.; Kim, J. Y.; Coates, N. E.; Ma, W. L.; Moses, D.; Heeger, A. J.; Bazan, G. C. *Nat. Mater.* **2007**, *6*, 497−500.

(65) Wang, X.; Perzon, E.; Oswald, F.; Langa, F.; Admassie, S.; Andersson, M. R.; Inganäs, O. *Adv. Funct. Mater.* **2005**, *15*, 1665−1670.

(66) Kohler, B. E.; Woehl, J. C. *J. Chem. Phys.* **1995**, *103*, 6253−6256.

(67) Yaliraki, S. N.; Silbey, R. J. *J. Chem. Phys.* **1996**, *104*, 1245−1253.

(68) Chang, R.; Hsu, J. H.; Fann, W. S.; Liang, K. K.; Chang, C. H.; Hayashi, M.; Yu, J.; Lin, S. H.; Chang, E. C.; Chuang, K. R.; Chen, S. A. *Chem. Phys. Lett.* **2000**, *317*, 142−152.

(69) Rossi, G.; Chance, R. R.; Silbey, R. *J. Chem. Phys.* **1989**, *90*, 7594−7601.

(70) Guo, X.; Ortiz, R. P.; Zheng, Y.; Kim, M.-G.; Zhang, S.; Hu, Y.; Lu, G.; Facchetti, A.; Marks, T. J. *J. Am. Chem. Soc.* **2011**, *133*, 13685−13697.

(71) Shand, M. L.; Chance, R. R.; LePostollec, M.; Schott, M. *Phys. Rev. B* **1982**, *25*, 4431−4436.

(72) He, J.; Crase, J. L.; Wadumethrige, S. H.; Thakur, K.; Dai, L.; Zou, S.; Rathore, R.; Hartley, C. S. *J. Am. Chem. Soc.* **2010**, *132*, 13848−13857.

(73) Holdcroft, S. *Macromolecules* **1991**, *24*, 4834−4838.

Paper IV

APPLIED PHYSICS LETTERS **103**, 213303 (2013)

Conformation sensitive charge transport in conjugated polymers

L. Mattias Andersson,[1,a)] Svante Hedström,[2] and Petter Persson[2]
[1]*Department of Physics, Chemistry and Biology (IFM), Linköping University, Linköping SE-581 83, Sweden*
[2]*Division of Theoretical Chemistry, Lund University, P.O. Box 124, SE-221 00 Lund, Sweden*

(Received 16 October 2013; accepted 3 November 2013; published online 21 November 2013)

Temperature dependent charge carrier mobility measurements using field effect transistors and density functional theory calculations are combined to show how the conformation dependent frontier orbital delocalization influences the hole- and electron mobilities in a donor-acceptor based polymer. A conformationally sensitive lowest unoccupied molecular orbital results in an electron mobility that decreases with increasing temperature above room temperature, while a conformationally stable highest occupied molecular orbital is consistent with a conventional hole mobility behavior and also proposed to be one of the reasons for why the material works well as a hole transporter in amorphous bulk heterojunction solar cells. © *2013 AIP Publishing LLC*. [http://dx.doi.org/10.1063/1.4832075]

Organic semiconductors are rapidly finding their way into more and more applications, and new materials are developed at an ever-increasing rate. One such material, the donor-acceptor polymer poly[2,3-bis-(3-octyloxyphenyl) quinoxaline-5,8-diyl-*alt*-thiophene-2,5-diyl] (TQ1), has been developed for use in organic bulk heterojunction solar cells where it performs admirably with respect to its physical limits.[1] There are hard (material specific) limits on achievable solar cell efficiencies in the form of, e.g., optical band gap and relative donor-acceptor energy level positions. There are also much more commonly encountered soft performance limits, usually related to morphology and phase structure in the form of, e.g., too large phase separation or isolated clusters of one or both of the phases. Only a very small fraction of the multitude of developed materials has come close to the hard efficiency limits.[1,2] Interestingly, fundamentally different morphologies and phase structures have proven to be able to achieve this; poly(3-hexylthiophene) (P3HT) for instance, relies on crystallization,[3] while TQ1 is largely amorphous.[4] Figuring out why certain materials work well, and why others do not, is one of the most rewarding paths to progress. P3HT has been thoroughly investigated and covers the general behavior of crystalline materials well, but there has been considerably less work done on amorphous materials.

To a very large extent, the achieved performance of a specific material system simply reflects the amount of effort spent on synthesis refinement and device optimization. There are, however, certainly differences in how easy the optimization process is for a particular material, and some materials are simply too difficult to be worthwhile. From an application point of view, it is reasonable to believe that easy to optimize materials are more robust and suitable for commercial applications so there are plenty of reasons to consider not only the maximum achievable performance of a material but also how easy it is to get there. Here, temperature dependent charge carrier mobility measurements together with density functional theory (DFT) calculations give insight into some of the fundamental advantages of TQ1. Essentially, this is related to the ability of TQ1 to perform well in an amorphous state, which in turn is linked to the properties of the frontier molecular orbitals and their (in-) sensitivity to conformational changes. These findings can aid in the screening process of new materials and also indicate a possibility for easily fabricated devices with unconventional electronic functions.

Charge transport in conjugated materials occurs in the frontier orbitals, where charges can be delocalized. The degree of delocalization varies, however, and is rarely, if ever, sufficient for ballistic transport. When localization of a charge carrier occurs, activation is necessary for it to continue on its path. Localization can be due to the chemical nature of the molecule, as well as to, e.g., structural, conformational, or packing defects. The soft nature of these materials frequently also causes self-localization of charges due to reorganization. Almost all conjugated materials are dominated by such an activated charge carrier transport. One very important consequence of activated charge transport that is relevant for the present discussion is that the charge carrier mobility in such a system increases with increasing temperature in an Arrhenius-like fashion.

The intimate relationship between the frontier orbital properties and charge transport does, however, make the mobility potentially sensitive to conformational changes and phase transitions since these are in turn known to affect the orbitals.[4,5] Information about the electronic structure of a material can thus aid in the interpretation of experimental charge carrier transport data. One of the most well established ways to calculate the electronic structure is with DFT.[6] DFT is capable of predicting electronic, optical, and structural properties. Due to computational limitations, longer polymer chains are not possible to study, but qualitative explanatory information can be obtained from oligomer calculations with the help of extrapolation techniques that exist for quantitative polymeric predictions. TQ1 has previously been studied with DFT, including frontier orbital analysis, optical absorption profile, and geometrical structure.[7]

As cast TQ1 films have a relatively low field effect transistor (FET) hole mobility, on the order of 10^{-5} cm^2 V^{-1} s^{-1}. In contrast to many other donor-acceptor polymers, it also exhibits an electron mobility, albeit about one order of

[a)]E-mail: matan@ifm.liu.se

magnitude lower than the hole mobility. Annealing above the glass transition temperature has no significant influence on the hole mobility but drastically increases the room temperature electron mobility by almost two orders of magnitude. Figure 1(a) shows the hole and electron mobility as a function of increasing temperature for an as cast film as well as for the same film after annealing above the glass transition temperature. The temperature dependence of the hole mobility is as expected, i.e., the mobility increases with increasing temperature up to the glass transition temperature. Interestingly enough, the electron mobility in the annealed sample does not follow the same trend even though both mobilities are measured simultaneously and on the same device. Further *in-situ* measurements during consecutive temperature scans after sufficient annealing yield identical results within the experimental accuracy. In all cases, it is possible to identify the glass transition temperature as a change in the temperature dependence. Extending the observed temperature range reveals that the electron mobility does behave conventionally at lower temperatures and that both mobilities have similar activation energies, i.e., similar slopes in the Arrhenius representation. This can be seen in, and inferred from, Figure 1(b).

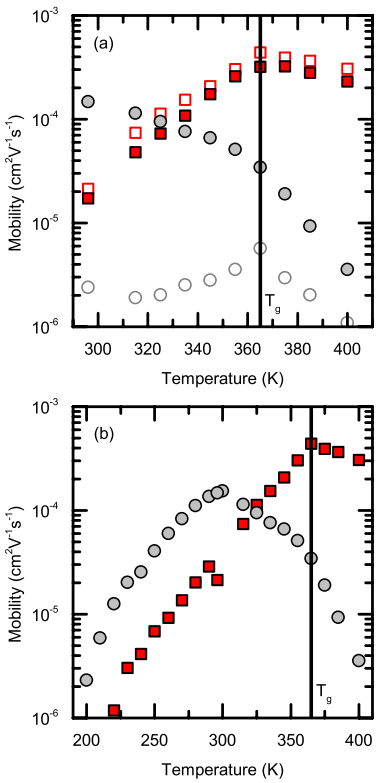

FIG. 1. Hole (squares) and electron (circles) mobility versus temperature for an as cast (open symbols) TQ1 film and the same film after annealing (solid symbols) (a), and mobility versus temperature for an extended temperature range after annealing (b). A vertical line indicates the glass transition temperature in both (a) and (b).

Experimental evidence from, e.g., molecular weight dependent charge transport measurements suggests that the charge transport in this type of amorphous polymer occur predominately along the polymer chains.[4] Extended delocalization along the chain of the frontier molecular orbitals is thus very important for efficient charge transport. Quantum chemical calculations on other donor-acceptor polymers have shown that the highest occupied molecular orbital (HOMO), where hole transport occurs, is well delocalized along the whole chain, while the lowest unoccupied molecular orbital (LUMO) is localized to one of the repeat units.[8] Accordingly, those materials have a decent hole mobility in FETs, but show no evidence of electron transport.[9]

DFT calculations on optimized TQ1 oligomers reveal that both frontier orbitals are delocalized, which is consistent with the ambipolar properties of the material. While high hole mobilities are relatively common in donor-acceptor polymers, high electron mobilities are more unusual. This could possibly be explained by the fact that the LUMO, as is the case for TQ1, tends to be associated with the acceptor unit. In contrast to many other donor-acceptor polymers, the donor unit of TQ1 is small; a single thiophene unit, whereas most other materials have considerably larger donor units. The small size of the thiophene unit does not spatially isolate the acceptor units and allows for an unbroken LUMO across the backbone under favorable circumstances, but only barely; the delocalization of the LUMO is strongly conformation dependent. Figure 2 shows calculated HOMO and LUMO orbitals for partially optimized TQ1 dimers with representative, fixed, dihedral angles between two consecutive quinoxaline units. The TQ1 LUMO displays good delocalization for the more planar structure yielded by the minimum energy interquinoxaline dihedral angle of 53°, as well as those of 133° and 183°, whereas the more twisted dihedral angles of, e.g., 3°, 23°, and 93° effectively break the LUMO delocalization. Although calculations on full films or even complete polymer chains are not possible, the energy minimized structure in vacuum does have a delocalized LUMO and it is reasonable to assume that such a conformation will be more favored in the annealed films compared to the as cast films.

The different temperature dependencies of the hole and electron mobilities seen above room temperature in Figure 1 are thus consistent with the properties of the frontier orbitals. While the HOMO is always delocalized, the delocalization of the LUMO is strongly dependent on the dihedral angle. A higher thermal energy permits the polymer to adopt less energetically favorable conformations, with more twisted and kinked backbones, indicating a predisposition for macroscopic non-uniformity, and a high sensitivity of the electrical properties to conformational changes. Physically, the proposed conformational changes in TQ1 films at increased temperatures is consistent with the fact that they swell by about 4% (determined by ellipsometry) between room temperature and the glass transition temperature. Such a swelling is bound to be associated with some conformational variations, and due to the very strong correlation between conformation and LUMO delocalization it is reasonable to

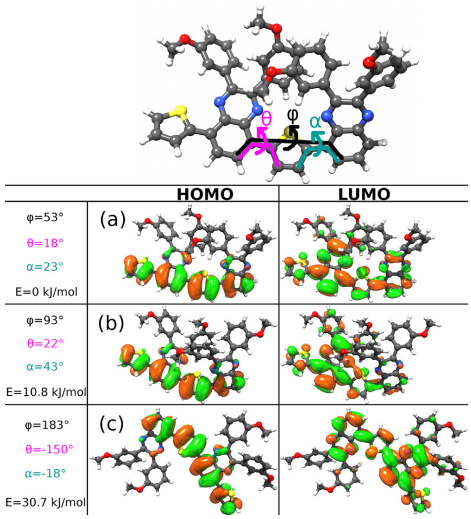

FIG. 2. TQ1 frontier orbitals for the fully optimized TQ1 dimer (a), as well as for two representative cases with imposed interquinoxaline dihedral angles, φ, ((b) and (c)), exhibiting decent, poor, and good LUMO delocalization, respectively. Also shown are the resulting thiophene–quinoxaline dihedral angles θ and α. The total system energy is given relative to the minimum energy conformation. Calculated at the ωB97XD/6-311 + G(2d,p)//6-31G(d,p) level of theory.

conclude that the electron mobility will be (negatively) influenced. It should be noted that it might not be localization *per se* that is the sole cause the observed behavior; spatial LUMO variations will give rise to an increased energetic disorder, which also affects the mobility negatively.

Based on these results, it can be speculated that part of the reason for the successful application of TQ1 in amorphous bulk heterojunction solar cells may be due to the conformational stability of the HOMO delocalization. Because of this stability, even the rather unimpressive hole mobility of TQ1 is capable of high quantum efficiencies and fill factors since the charge transport is relatively homogenous throughout the film and without isolated low-mobility regions. Had the properties of the HOMO and the LUMO been exchanged however, amorphous structures would probably no longer be viable. Frontier orbital delocalization considerations have already been empirically incorporated in some of the best performing polymers, where abundant use of fused rings in their backbones ensures a favorable electronic structure with extensive frontier orbital delocalization.[10] While obviously a possible strategy, the synthesis of such systems is frequently more complex and costly than that of simpler structures. These results show that a forced conformation is not strictly necessary for good charge transport, and that it is possible to find simpler and cheaper materials with the desired frontier orbital properties.

Outside of solar cell applications, there might be new and interesting applications for materials that shift between being dominated by hole or electron mobility at different temperatures. Figure 1(a) shows that in going from room temperature to just below the glass transition temperature in annealed TQ1 films, there is an almost symmetric switch between the magnitudes of the hole- and electron mobilities. One of the drawbacks of organic materials is their stability. By using differential signals from a single material it might, for instance, be possible to mitigate such shortcomings. With rational material design, either frontier orbital's properties should also be possible to tailor for specific needs.

To conclude, differences in the temperature dependence of the hole- and electron mobilities in TQ1 have been linked to conformational dependencies of the frontier orbital properties through DFT calculations. The degree of HOMO delocalization in TQ1 is independent of its conformation, which gives it a stable hole mobility and allows it to function well in amorphous bulk heterojunction solar cells. On the other hand, the LUMO delocalization depends strongly on the conformation, which results in an unconventional electron mobility temperature dependence. Instead of an Arrhenius like increase in electron mobility with increasing temperature it starts to decrease well below the glass transition temperature. This behavior is explained by the conformationally sensitive LUMO delocalization revealed by DFT calculations since higher temperatures induce a higher degree of twisting of the polymer chains. Strongly conformation dependent frontier orbital delocalization is therefore proposed to be detrimental to the efficiency of amorphous bulk heterojunction solar cells, while at the same time being of interest for new applications where temperature dependent variations in the polarity of the dominant carrier type can be exploited.

The authors would like to thank E. Wang and M. R. Andersson for the supply of TQ1. L.M.A. wishes to thank C. Müller and J. Bergqvist for fruitful discussions. NSC and LUNARC are acknowledged for computer resources used. This work was funded by the Swedish Energy Agency and the Swedish Research Council.

[1]E. G. Wang, L. T. Hou, Z. Q. Wang, S. Hellstrom, F. L. Zhang, O. Inganas, and M. R. Andersson, Adv. Mater. **22**(46), 5240 (2010).
[2]P. Schilinsky, C. Waldauf, and C. J. Brabec, Appl. Phys. Lett. **81**(20), 3885 (2002).
[3]C. Muller, T. A. M. Ferenczi, M. Campoy-Quiles, J. M. Frost, D. D. C. Bradley, P. Smith, N. Stingelin-Stutzmann, and J. Nelson, Adv. Mater. **20**(18), 3510 (2008).
[4]L. M. Andersson, Org. Electron. **12**(2), 300 (2011).
[5]C. Muller, J. Bergqvist, K. Vandewal, K. Tvingstedt, A. S. Anselmo, R. Magnusson, M. I. Alonso, E. Moons, H. Arwin, M. Campoy-Quiles, and O. Inganas, J. Mater. Chem. **21**(29), 10676 (2011).
[6]B. Grimm, C. Risko, J. D. Azoulay, J. L. Bredas, and G. C. Bazan, Chem. Sci. **4**(4), 1807 (2013); L. Yang, J. K. Feng, A. M. Ren, and J. Z. Sun, Polymer **47**(4), 1397 (2006); S. S. Zade, N. Zamoshchik, and M. Bendikov, Acc. Chem. Res. **44**(1), 14 (2011).
[7]S. Hedstrom and P. Persson, J. Phys. Chem. C **116**(51), 26700 (2012); R. Kroon, A. Lundin, C. Lindqvist, P. Henriksson, T. T. Steckler, and M. R. Andersson, Polymer **54**(4), 1285 (2013); E. G. Wang, J. Bergqvist, K. Vandewal, Z. F. Ma, L. T. Hou, A. Lundin, S. Himmelberger, A. Salleo, C. Muller, O. Inganas, F. L. Zhang, and M. R. Andersson, Adv. Energy Mater. **3**(6), 806 (2013).
[8]K. G. Jespersen, W. J. D. Beenken, Y. Zaushitsyn, A. Yartsev, M. Andersson, T. Pullerits, and V. Sundstrom, J. Chem. Phys. **121**(24), 12613 (2004).
[9]L. M. Andersson, F. L. Zhang, and O. Inganas, Appl. Phys. Lett. **91**(7), 071108 (2007).
[10]W. W. Li, K. H. Hendriks, W. S. C. Roelofs, Y. Kim, M. M. Wienk, and R. A. J. Janssen, Adv. Mater. **25**(23), 3182 (2013).

Paper V

THE JOURNAL OF PHYSICAL CHEMISTRY C

Article

pubs.acs.org/JPCC

Temperature-Dependent Optical Properties of Flexible Donor−Acceptor Polymers

Svante Hedström,[†] Patrik Henriksson,[‡] Ergang Wang,[‡] Mats R. Andersson,[‡,§] and Petter Persson*[,†]

[†]Division of Theoretical Chemistry, Lund University, P.O. Box 124, S-221 00 Lund, Sweden

[‡]Department of Chemistry and Chemical Engineering, Chalmers University of Technology, S-412 96 Göteborg, Sweden

[§]Ian Wark Research Institute, University of South Australia, Mawson Lakes, South Australia 5095, Australia

● *Supporting Information*

ABSTRACT: Optical properties of five donor−acceptor polymers of interest for light-harvesting in organic photovoltaic devices have been studied experimentally and computationally. Experimentally recorded absorption spectra in solution of the five polymers are shown to be significantly temperature-dependent. The polymers were subjected to a first-principles computational treatment using density functional theory optimizations and excitation calculations. For two of the polymers, APFO-3 and PTI-1, a methodology that accounts for a thermally induced distribution of conformations based on Boltzmann statistics is applied to produce size- and temperature-converged optical results. This provides a deeper understanding of the temperature dependence of optical properties and improves the computational predictions of absorption wavelength and intensity at experimentally accessible temperatures, as compared to results from traditional quantum chemical calculations based on optimized polymers. Together, the combined experimental and computational temperature studies elucidate and quantify the significant influence of structural flexibility on the optical absorption properties of typical donor−acceptor polymers.

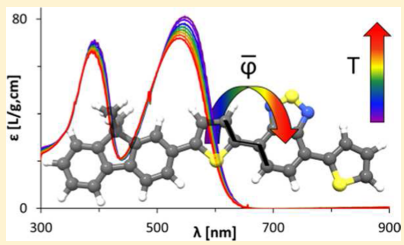

■ INTRODUCTION

Organic photovoltaics (OPVs) are promising as electricity producing devices. They offer a clean, renewable source of energy, and their versatility as compared to silicon solar cells makes them particularly attractive for applications where structural or optical flexibility is required.[1−5] The active layer of an OPV device typically consists of a copolymer of donor−acceptor (D−A) type, blended with a Buckminster-fullerene. While the fullerene accepts and transports electrons, the polymer is mainly responsible for light-absorption and hole-transport. Variation of the chemical composition of the polymer is reflected in its optical properties, offering tunability to the photoresponse. Delocalized π-conjugation in the polymer backbone provides the signature electronic and optical traits of D−A polymers. Completely planar structures would maximize the degree of conjugation, but the presence of single bonds along the backbone induces conformational flexibility, affecting the spectral response. The characterization of the absorption profile is crucial to the performance of solar cells, because the efficient absorption of photons and subsequent charge generation via the photovoltaic effect is the basis of the OPV operation. Thermal stability over time is a challenge in OPVs, and is frequently investigated. The direct temperature dependence of the conformation and resulting optical response, as well as the performance, are not as commonly assessed, although some studies have been made.[6−12]

Many computational studies have been made of polymers intended for use in OPVs.[13−19] Computational methods based on classical mechanics are able to treat entire polymer strands and material blends,[20−22] while quantum chemical calculations are required for quantitative predictions of optical and electronic properties. The computational cost of density functional theory (DFT) calculations increases cubically with system size. Thus, to perform such calculations on D−A polymers within reasonable time, one is typically limited to smaller oligomers of up to around 5−10 repeating units, depending on the size of the repeating unit. Another issue with DFT in its pure (Kohn−Sham) or hybrid (including some exact exchange) form is that it typically underestimates band gaps of conjugated systems, both due to inherent shortcomings with the formalism,[23−27] as well as due to the common omission of descriptions of thermally induced conformational effects. Nevertheless, DFT has successfully been used as a tool for rational design in the development of conjugated polymers,[13,28−31] attributed to the molecular level insight it can provide into the electric and optical properties, crucial for solar cell applications.

Here, we investigate the strong temperature dependence of optical properties of five light-harvesting polymers developed at

Received: November 10, 2014
Revised: March 5, 2015
Published: March 6, 2015

DOI: 10.1021/jp511246n
J. Phys. Chem. C 2015, 119, 6453−6463

Polymer Technology, Chalmers University: APFO-3,[32] BDT-BTz,[13,33] PTI-1,[34] TBDT-BTz, and TQ1,[35] through a combination of experiments and calculations. The chemical structures of the polymers are outlined in Chart 1. APFO-3 and PTI-1 were selected for further computational scrutiny, due to the relatively high performance of these polymers in OPVs, showing power conversion efficiencies of 4.2% and 4.5%, respectively (for the APFO-3 reference, decyl instead of octyl side-chains were used).[36,37] This involves a strategy to predict size- and temperature-converged electronic and optical properties, relying on extrapolations from oligomer calculations together with a correction for thermal effects, influencing structural and optical properties. These calculations result in temperature dependences similar to those of experiments, and accounts for a significant part of the underestimation of calculated band gaps.

Chart 1. Chemical Structures of the Five Investigated Polymers[a]

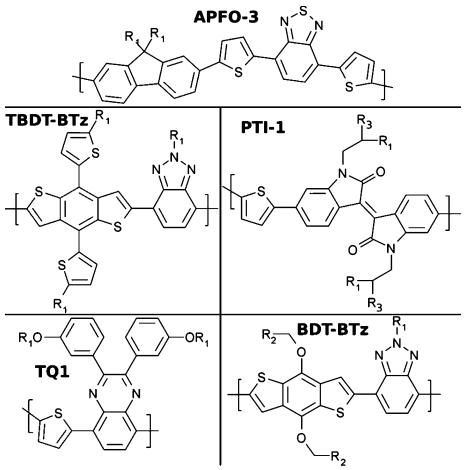

[a]R_1 = 1′-octyl, R_2 = 3′-heptyl, R_3 = 1′-hexyl.

The temperature dependence of optical properties in polymers relates to their conformational flexibility. Thorough experimental and computational scrutiny of these traits in conjunction with the potential energy landscapes that govern the conformational structures provides a deeper understanding of the structure−property relation of polymers in solution. Intermolecular interactions affect polymer films, and although such effects are not explicitly addressed here, a better physical understanding of the intrinsic polymer properties has the potential to aid development of new polymers for more efficient OPV devices.

METHODS

Size Exclusion Chromatography. Size exclusion chromatography (SEC) was performed on a Waters Alliance GPCV2000 with refractive index detector columns: Waters Styragel HT GE × 1, Waters Styragel HMW GE × 2. The eluent used was 1,2,4-trichlorobenzene. The operating temperature was 135 °C, and the dissolution time was 2 h. The concentration of the samples was 0.5 mg mL^{-1}, which were filtered through a 0.45 μm metal filter prior to analysis. The molecular weights were calculated relative to calibration with polystyrene standards.

Temperature-Dependent Optical Characterization. The polymers were dissolved in *ortho*-dichlorobenzene (ODCB) at a concentration of ∼0.02 mg mL^{-1}. The samples were heated to ensure complete dissolution of the polymer. The solutions were then cooled to 3 °C in situ while UV−vis−NIR spectra were recorded on an Agilent 8453 UV−vis spectrophotometer with a temperature control unit. The temperature was then increased to 10 °C, followed by steps of 5 °C up to 70 °C, with spectra being recorded after every increment. The temperature steps were increased manually, with the temperature of the samples measured by a thermometer.

Computational Details. Density functional theory (DFT) optimizations were carried out on oligomers of 1−5 repeating units of PTI-1 and APFO-3. The alkyl side-chains, included in synthesis for solubility, were in the calculations truncated to shorter alkyl groups, depending on branching. These were followed by time-dependent (TD)-DFT calculations of the first five electronic transitions of all oligomers. Further TD-DFT states were calculated on the APFO-3 dimer and PTI-1 trimer, yielding optical properties over the visible region >300 nm. Potential energy surfaces (PES) with the coordinate being the dihedral angle between aryl units were obtained by scanning over dihedral angles in the APFO-3 and the PTI-1 monomers, with the dihedral angle frozen, and all other coordinates relaxed. An ensemble of 10 oligomer samples was constructed for each number of repeating units (1−5), where each sample has a frozen dihedral angle as chosen stochastically but according to the Boltzmann probability, and the remaining coordinates are optimized. This was done for Boltzmann distributions at 293 and 343 K. The total of 200 oligomer sample systems (10 samples per ensemble × 2 temperatures × 5 sizes × 2 polymers) then underwent TD-DFT calculations including the first electronic transitions that correspond to the first absorption peak.

The Gaussian 09 package[38] with the DFT functional/basis set combination PBE0[39]/6-31G(d,p) was used throughout. The common hybrid functional PBE0 was chosen to provide consistent results over a wide range of sizes and geometries, and it is not parametrized for a certain chemistry.

Experimental absorption data were fitted to a Gaussian function in the interval 510−570 nm for APFO-3 to obtain the first peak wavelength without the influence of experimental noise. PTI-1 peak wavelengths were obtained by fitting experimental absorption to six Gaussian functions in the interval 300−800 nm.

RESULTS AND DISCUSSION

Structural Properties. The molecular weights of the investigated light-harvesting polymers, determined by SEC, are reported in Table 1. The D−A polymers consist of inflexible conjugated aryl ring-systems adjoined by more flexible single bonds around which rotations are permitted. APFO-3 has four such ring-systems per repeating unit along the backbone, where the fluorene (F) and two thiophenes (T) act as electron donors, and benzothiadiazole (B) acts as acceptor. The other four polymers have two aryl moieties per repeating unit in the backbone: one donor and one acceptor group. Although maximum conjugation is associated with planarity, the

DOI: 10.1021/jp511246n
J. Phys. Chem. C 2015, 119, 6453−6463

Table 1. Molecular Weights of the Polymers As Determined by SEC, and Optimized C−C−C−C Dihedral Angles of the Central Repeating Unit in Pentamers[a]

polymer	M_w [kDa]	M_n [kDa]	C−C−C−C angle [deg]
APFO-3 (F−T)	15	7	335.5
APFO-3 (T−B)			6.4
PTI-1	132	48	205.3
TBDT-BTz	171	31	
BDT-BTz	21	8	3.5[13]
TQ1	170	56	20.0[13]

[a]Angles for BDT-BTz and TQ1 represent the average out-of-plane angle in optimized trimers, taken from ref 13.

optimized structures are slightly nonplanar due to steric effects such as colliding hydrogens; see Figure S1 in the Supporting Information. The dihedral angles between the ring-systems are listed in Table 1. The optimized APFO-3 F−T angle is similar to the T−isoindigo (I) angle in PTI-1, both corresponding to 25° out-of-plane, due to their large steric hindrance between the H atoms of one six-membered and one five-membered ring. The APFO-3 T−B and the BDT-BTz angles are much smaller, ≤7° due to the absence of colliding H atoms.

Temperature-Dependent Absorption Spectra. The five investigated light-harvesting polymers are found to be strongly thermochromic in solution, evident from Figure 1a−e where the experimental absorption spectra for the five polymers APFO-3, TBDT-BTz, BDT-BTz, PTI-1, and TQ1 are plotted for a number of temperatures between 3 and 70 °C. The first peaks of TBDT-BTz, BDT-BTz, and PTI-1 display distinct double-peak character. Systematic trends are displayed by all polymers in Figure 1: with increasing temperature follows a broadening and weakening of the absorption. This is accompanied by a blue-shift, except for BDT-BTz. The spectral broadening can be qualitatively explained in terms of an entropically induced conformation distribution, where higher temperatures permit a wider range of conformations to be populated, each with slightly different optical response. The blue-shift and weakening of the absorption are also related to the thermally induced conformation distribution at increasing temperatures. Because the most favorable conformations are generally near-planar, and the majority of higher energy conformations are more twisted and kinked, at higher temperatures the polymer ensemble will on average be less planar. This decreases the average degree of conjugation and thus blue-shifts and weakens the absorption.

The experimental peak absorption coefficients (ε_{max}) and peak wavelengths ($\lambda_{max} = hc/E_{abs}$) are listed in Table 2, both for the main peak of all polymers as well as for the shoulder or secondary peak in TBDT-BTz, BDT-BTz, and PTI-1. The temperature dependence is also quantified as the average shifts in ε_{max} and λ_{max} per unit kelvin. The comparatively narrow peaks in TBDT-BTz lead to a greater absorption coefficient loss per unit temperature as compared to the other polymers, and the close proximity of its two peaks makes a reliable assessment difficult.

All polymers in Figure 1 exhibit a stronger ε_{max} and λ_{max} temperature dependence for their low energy peak(s) than for subsequent peaks <500 nm, in agreement with previous studies on conjugated polymers.[12,40−44] The first electronic transition generally exhibits a larger charge-transfer character from donor to acceptor unit, so a small dihedral angle that enhances the conjugation between donor and acceptor has a great effect on this transition. Subsequent transitions display weaker charge-transfer character,[45−47] and are thus less affected by thermally increased dihedral angles between units.

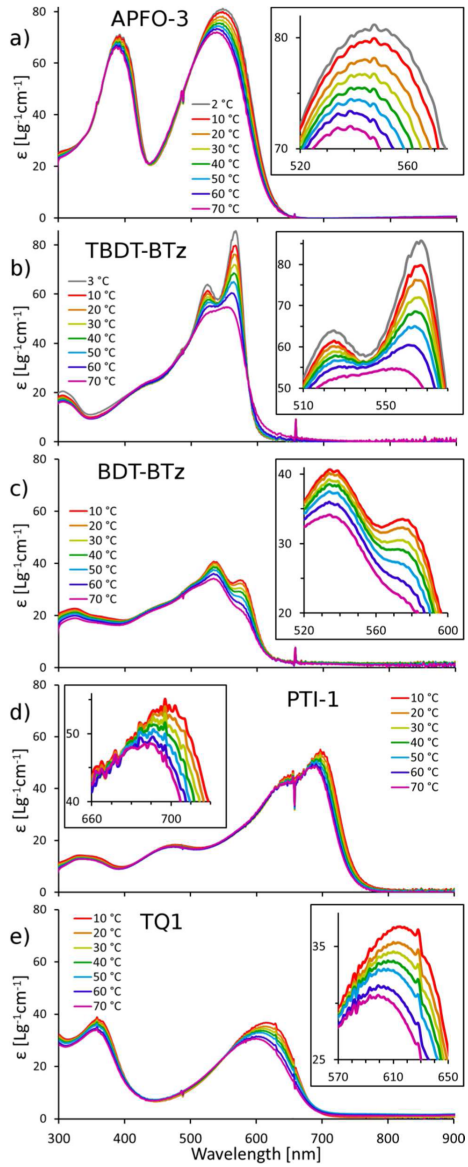

Figure 1. Experimental absorption spectra for APFO-3 (a), TBDT-BTz (b), BDT-BTz (c), PTI-1 (d), and TQ1 (e), at various temperatures. The insets depict the same spectra, zoomed in at the first respective peaks.

DOI: 10.1021/jp511246n
J. Phys. Chem. C 2015, 119, 6453−6463

Table 2. Wavelengths and Absorption Coefficients at Maximum Absorption and at Shoulders at 20 °C, As Well As Changes in ε_{max} and λ_{max} per Unit Temperature

polymer	λ_{max} ($\lambda_{shoulder}$) 20 °C [nm]	peak (shoulder) $\Delta\lambda_{max}/\Delta T$ [nm K^{-1}]	ε_{max} ($\varepsilon_{shoulder}$) 20 °C [L g^{-1} cm^{-1}]	peak (shoulder) $\Delta\varepsilon_{max}/\Delta T$ [L g^{-1} cm^{-1} K^{-1}]
APFO-3	544	−0.15	78	−0.13
TBDT-BTz	564 (525)	−0.21 (0.10)	76 (60)	−0.46 (−0.15)
BDT-BTz	534 (575)	0.00 (−0.09)	40 (32)	−0.11 (−0.15)
PTI-1	697 (645)	−0.15 (−0.12)	54 (46)	−0.10 (−0.04)
TQ1	610	−0.27	35	−0.10

It is difficult to determine the nature of the splitting of the first peaks in TBDT-BTz, BDT-BTz, and PTI-1, apparent in the absorption spectra in Figure 1. The double peak character may be due to two successive vibronic peaks, or due to aggregation where the red-most peak comes from an aggregated specie and the bluer peak corresponds to the single strand absorption. Aggregation peaks are typically red-shifted as compared to the single strand absorption. Their intensity drop upon increasing temperatures is expected to be greater than the single strand peaks, due to dissolution of the aggregates, whereas the thermochromism is expected to be weaker for the aggregation peaks, because the aggregation partly locks its conformation. The almost complete disappearance of the red shoulder in BDT-BTz and the red part of the split peak in TBDT-BTz at higher temperatures leads to them being assigned as aggregation peaks. Subsequent computational treatment further elucidates the nature of the split peak/shoulders in PTI-1, as well as the temperature dependence of the polymers, vide infra.

Electronic and Optical Properties. The first electronic transition in conjugated polymers generally corresponds to the promotion of an electron from HOMO to LUMO. The partial spatial separation of these orbitals as seen in Figure 2 contributes to the greater sensitivity to conformation and thus temperature of the first peaks in Figure 1, as compared to higher energy transitions and peaks with less charge-transfer character. In APFO-3, where donor and acceptor moieties are more spatially separated, LUMO is more localized on the acceptor units, see Figure 2b, whereas HOMO for both polymers (Figure 2a and d) as well as the PTI-1 LUMO (Figure 2e) show more homogeneous delocalization across the trimers. The D−A character of the two polymers is evident from the transition electron density plots (Figure 2c and f), with electrons moving from T−F−T to B in APFO-3, and from T to I in PTI-1. Electron density is also transferred from bonds with more double-bond character to those with more single-bond character. Good agreement between calculated and experimental spectra for the PTI-1 monomer using the B3LYP functional (similar to PBE0 used herein) has previously been reported,[19] but calculations on longer oligomers tend to underestimate the absorption energy.

The calculated absorption spectra are compared to the 20 °C experimental solution spectra in Figure 3a for APFO-3 and Figure 3b for PTI-1, demonstrating the broad spectral coverage and high absorption coefficients of both polymers. Calculated spectra are obtained from TD-DFT calculated transitions subjected to a Gaussian broadening of 3575 cm^{-1} for APFO-3 and 3300 cm^{-1} for PTI-1, which are the widths of the first

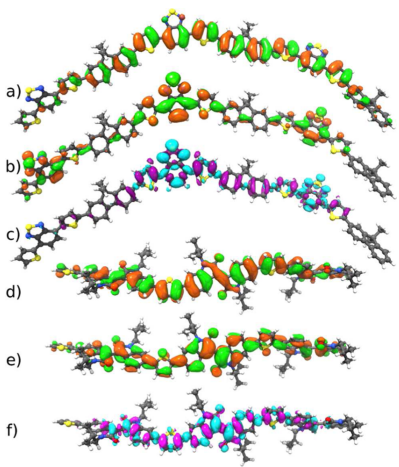

Figure 2. APFO-3 HOMO (a), APFO-3 LUMO (b), APFO-3 first transition electron density difference (c), PTI-1 HOMO (d), PTI-1 LUMO (e), and PTI-1 first transition electron density difference (f), with electrons moving from purple to turquoise upon excitation. Orbital isovalues = 0.015. Density isovalues = 0.0004.

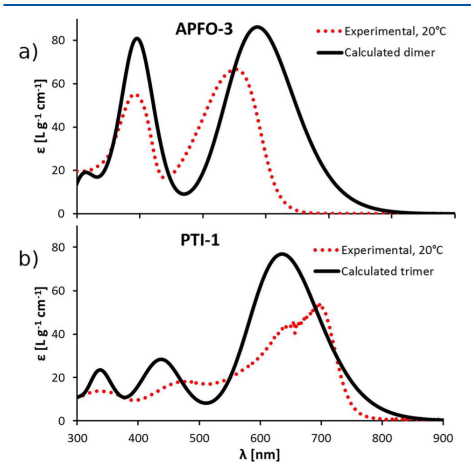

Figure 3. Experimental 20 °C spectra of APFO-3 (a), and PTI-1 (b), as compared to respective calculated spectra of the oligomer size whose spectrum best matches experiment, with an applied Gaussian broadening of the same FWMH as the first corresponding experimental peak.

DOI: 10.1021/jp511246n
J. Phys. Chem. C 2015, 119, 6453−6463

respective experimental peaks; see eq S1 in the Supporting Information for details.

The resulting calculated spectra in Figure 3 differ from the experimental mainly due to three major differences in conditions. First, calculations are limited to smaller oligomers, leading for polymers with a large experimental effective conjugation length to an underestimation of calculated wavelengths (overestimation of E_{abs}), as is the case for the PTI-1 trimer in Figure 3b, as well as for many polymers throughout the literature.[18,48−50] Second, calculations are carried out in the gas phase at 0 K, without the finite temperature effects and neighboring molecules that affect the experimental geometries. The calculated results are thus too ideal, which will lead to unrealistically strong conjugation and thus too long wavelengths and high absorption coefficients. This effect is commonly reported throughout literature,[51−54] and the absorption coefficient overestimation is apparent for both polymers in Figure 3. Third, TD-DFT only calculates the vertical transition, whereas in experiments, unresolved vibronic peaks induce an inhomogeneous broadening toward shorter λ. In consequence, for any polymer, these differences between experimental and computational conditions lead to the existence of an oligomer size for which the three errors cancel out, producing an apparent match of experimental and calculated wavelengths. However, because that oligomer size can only be determined a posteriori, the predictive power of such calculations is limited, and they are best suited as explicatory complements to experiments.

Size-converged polymer properties have been obtained for APFO-3 and PTI-1 from a series of computationally analyzed oligomer properties, by fitting the results to a function of inverse number of repeating units and extrapolating to the polymer limit, in a fashion similar to that of previous studies.[13,55−60] The results are shown in Figure 4a, where the energies of maximum absorption E_{abs} are plotted as a function of inverse oligomer size. The absorption energies are fitted to eq 1, which describes the band gap of a linear chain of orbitals according to the tight binding approximation in theory of solids, also known as a Kuhn fit.[61]

$$E_{abs} = \alpha_{LUMO} - \alpha_{HOMO} - 2(\beta_{LUMO} + \beta_{HOMO}) \cos \frac{\pi}{N+1} \quad (1)$$

$\Delta\alpha$ and $\Sigma\beta$ are used as fitting parameters, and N is one-half the number of rigid ring systems per repeat unit, that is, $N = 2n$ for APFO-3 and $N = n$ for PTI-1.

In Figure 4, PTI-1 exhibits a steeper slope than APFO-3, which is due to the shorter repeating unit of the former. The extrapolation in Figure 4a reveals that the PTI-1 calculations come very close to the experimental first peak E_{abs}. However, due to the aforementioned overidealized conjugation in calculations and lack of higher vibronic transitions in TD-DFT, calculated results extrapolated to the polymer limit should be significantly red-shifted as compared to experiments. This is corroborated by previous studies that consistently show calculated underestimations of E_{abs} of 0.2−0.4 eV,[13,55,62−66] depending on DFT functional. This strongly suggests that the absorption double-peak of PTI-1 is due to aggregation, which has been proposed to be an issue in some isoindigo polymers.[67−71] Thus, the higher energy shoulder at 645 nm (also included in Figure 4a) corresponds to the nonaggregated PTI-1 polymer chains. This is further reinforced by the fact that the shoulder retains most of its intensity at higher temperatures, whereas the red-most peak is weakened, assigned to dissolution of aggregates. Relating the calculations instead to the 645 nm shoulder consequently provides a picture more consistent with other D−A polymer studies.

The peak mass absorption coefficients, proportional to the calculated oscillator strength per molecular weight, display a linear trend when plotted versus inverse oligomer length in Figure 4b; see Supporting Information eqs S2 and S3 for details. This permits an extrapolation analogous to the E_{abs} case, yielding size-converged values, which are compared to experiments. The ε_{calc} values are overestimated for both polymers as compared to experimental values, again due to unrealistically good conjugation in the 0 K, gas-phase calculations.

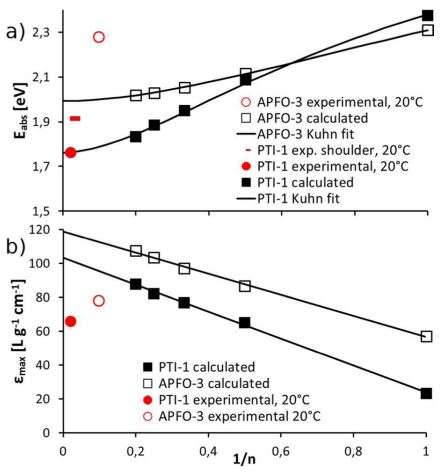

Figure 4. Experimental and calculated optical properties versus inverse number of repeating units for APFO-3 and PTI-1: Absorption energy E_{abs} with Kuhn fits (a), and peak absorption coefficients ε_{max} as calculated according to Supporting Information eq S1 with best linear fits (b).

Temperature Dependence. Calculations for polymers are inherently difficult to evaluate because the conditions in silico are different from those in current experimental methods. While experiments treat long strands of $\gtrsim$10 repeating units at room temperature surrounded by solvent molecules and other polymers, quantum chemical calculations generally involve shorter oligomers at 0 K, with the surrounding normally described by a continuum model solvent. The additional uncertainty stemming from the actual computational method, for example, DFT functional and basis set, further complicates direct comparisons to experiments.

Previous computational studies have to some extent overcome the size-limitation issue and predicted polymeric absorption wavelengths by extrapolating oligomer results according to observed trends,[13,14,72] as done here in Figure 4. We have recently shown that at the same level of theory as used herein (PBE0/6-31g(d,p)), optimized, extrapolated, calculated absorption energies are systematically underestimated by ~0.32 eV as compared to experiments for nine polymers, and the error is assigned mainly to temperature effects, but also

DOI: 10.1021/jp511246n
J. Phys. Chem. C 2015, 119, 6453−6463

limitations in the DFT functional.[13] These results are in agreement with other studies showing 0.2−0.4 eV underestimations, depending on functional.[19,48,49] For the same reasons, extrapolated ε_{calc} values are overestimated. Temperature differences of less than 100 °C have been shown experimentally to shift absorption peaks by up to ∼50 nm.[35,73−75] Thermal variations directly influence structural properties of the polymers, which in turn result in changes in optical properties. Thus, to computationally account for thermally induced optical property variations, it is necessary to scrutinize the geometric properties.

The preferred near-planar conformation of neighboring ring-systems, as mentioned in the Structural Properties, results in four local minima per single bond, corresponding to dihedral angles somewhat above or below 0° or 180°, respectively. These minima are evident in the PES over the dihedral angles, plotted for APFO-3 and PTI-1 in Figure 5a and b. Energy

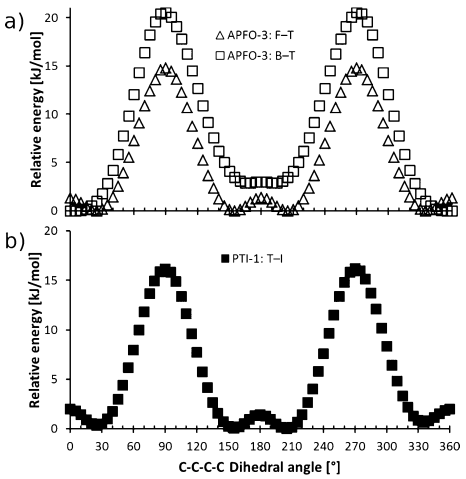

Figure 5. Potential energy surface (PES) scans over the dihedral angles between units in monomers of APFO-3 (a) and PTI-1 (b). All energies are relative to the minimum within the series. Calculated with PBE0/6-31G(d,p).

maxima occur at the lowest degree of conjugation, that is, at dihedral angles of 90° and 270°. The analogous chemistry of F−T and T−I manifests itself as very similar potential energy profiles. The B−T minimum energy angle is practically planar due to the absence of colliding hydrogens between these units. In general, the surfaces exhibit wide and shallow wells, so the polymers are likely to adopt a wide range of dihedral angles at a finite temperature.

Varying the dihedral angles between ring-systems in a conjugated system has a strong effect on optical properties, as shown in Figure 6. The oscillator strength is less sensitive to the F−T angle than the B−T and P−T, because F and T are both part of the donor unit, whereas B−T and P−T correspond to twisting between donor and acceptor units, influencing the first transition that involves distinct charge transfer from donor to acceptor. For B−T and P−T rotations, the oscillator strengths are almost halved upon going from flat 180° dihedral angles to

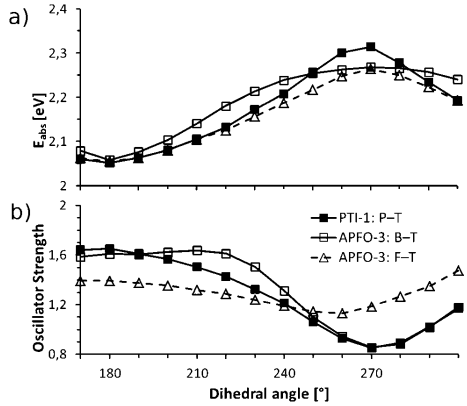

Figure 6. Calculated absorption energy (a), and oscillator strength ∝ molar ε_{max} (b), of the first excitation versus imposed T−I dihedral angle between repeating units in a PTI-1 dimer, as well as for B−T and F−T angles in an APFO-3 dimer, demonstrating the sensitivity to planarity of particularly the excitation intensity.

270°, thus being more strongly affected by backbone twisting than the absorption energies, which vary by ∼0.3 eV depending on twisting.

To compensate for the nonzero temperature conditions in experiments, and produce more accurate calculated spectral properties, we employ a computational methodology based on Boltzmann populations of conformations. The temperature-dependent relative probability P for a polymer chain to adopt a certain dihedral angle is described by a Boltzmann distribution as in eq 2, where ΔE is the energy relative to the minimum energy conformation, R is the ideal gas constant, and T is the temperature in Kelvin.

$$P = e^{-\Delta E/RT} \quad (2)$$

The dihedral angles are selected to follow a thermal distribution, by stochastically sampling the dihedral angles according to their temperature-dependent Boltzmann probability from eq 2, with energies taken from the PES in Figure 5. This is done at 293 and 343 K for both PTI-1 and APFO-3, representing the lower and upper bounds of the temperatures for the experimental absorption spectra. For each oligomer size of one to five repeating units (n = 1−5), 10 sample systems are optimized with thermally distributed dihedral angles imposed. The sampling process is exemplified by the PTI-1 monomer dihedral angles in Figure 7a, which also demonstrates that the angle distribution geometries conform to the T−I PES. Each sample system contains $2 \times n - 1$ angles for PTI-1 and $4 \times n - 1$ angles for APFO-3. Each of the total 50 oligomer structures per polymer is then subjected to TD-DFT calculations to obtain transition wavelengths and oscillator strengths. The spread in dihedral angles and resulting optical properties in the different samples is exemplified with the PTI-1 trimer in Figure 7b, where the minimum, maximum, and average out-of-plane dihedral angles in each sample are plotted, as well as their oscillator strength and E_{abs}. It is apparent that larger average out-of-plane angles correlate with higher absorption energies, whereas the oscillator strengths are negatively correlated to the

DOI: 10.1021/jp511246n
J. Phys. Chem. C 2015, 119, 6453−6463

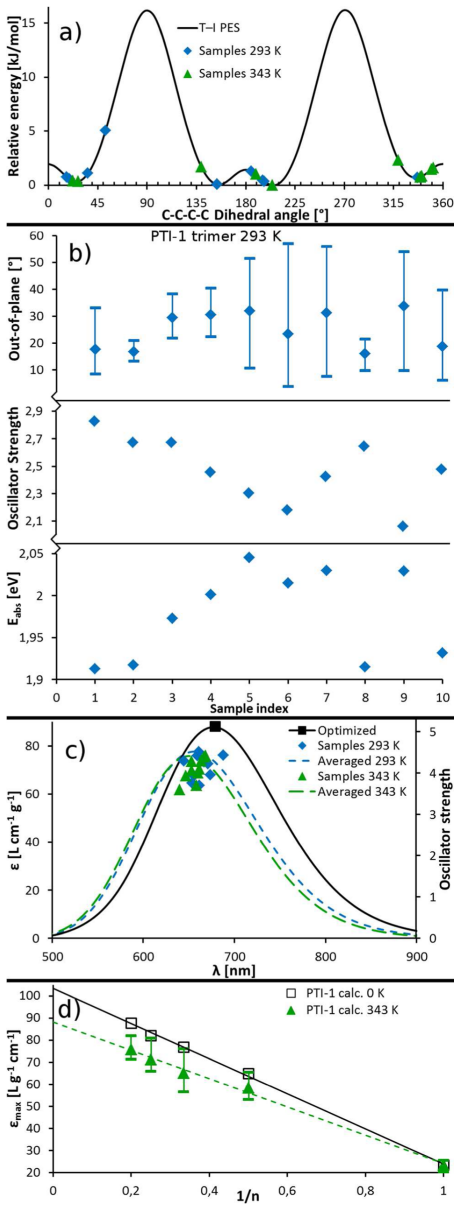

Figure 7. Sampling details. Energies for the 10 PTI-1 monomer samples with dihedral angles as sampled according to their Bolzmann probability at 293 and 343 K (a), as compared to the dihedral PES from Figure 5b. Minimum, maximum, and average out-of-plane dihedral angles in each of the 10 PTI-1 trimer samples, as well as the resulting oscillator strength and absorption energy (b). The first

Figure 7. continued

excitation from the 10 PTI-1 pentamer samples at 293 and 343 K and the resulting averaged spectra, as compared to the optimized pentamer first excitation and corresponding spectrum (c). Average, minimum, and maximum calculated ε_{max} values for PTI-1 oligomer samples n = 1−5 at 343 K, as compared to optimized, 0 K oligomers (d).

maximum angle in the oligomer; see Figures S2 and S3 in the Supporting Information for further details.

For each of the five oligomer sizes, a spectrum averaged over the 10 samples is produced, exemplified by the PTI-1 pentamer in Figure 7c where the blue-shift, broadening, and weakening of the absorption as compared to optimized structures is apparent. From the averaged spectra, peak wavelengths and absorption coefficients are extracted. These temperature-compensated oligomer properties are then extrapolated to experimental polymer sizes with a Kuhn fit for E_{abs} and a linear function for ε_{max}. The extrapolation is exemplified for PTI-1 at 343 K in Figure 7d, where the averaged ε_{max} is put in relation to the largest and smallest sampled ε_{max} for each oligomer size, as well as to the optimized oligomers. The extrapolated peak wavelengths and absorption coefficients as a function of temperature are plotted in Figure 8, with comparisons to

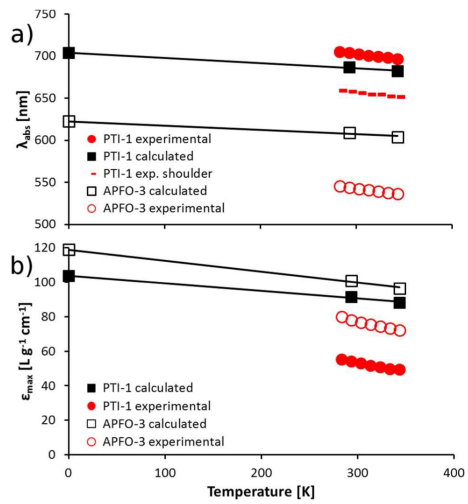

Figure 8. Calculated and experimental peak wavelengths (a) and absorption coefficients (b) as a function of temperature for PTI-1 and for APFO-3 with best linear fits.

experimental absorption measurements. This provides a clear demonstration of the trend in both methods to produce weaker and blue-shifted absorption at higher temperatures.

As described in the previous section, the red-most, intense maximum of PTI-1 in the experimental spectra is attributed to aggregation, whereas the shoulder at slightly higher absorption energy is assigned to the single strand absorption, which consequently corresponds to calculations. Both the aggregation peak and the blue-shifted shoulder are shown in Figure 8a. Neither of the polymer calculations exhibits absolute agreement

DOI: 10.1021/jp511246n
J. Phys. Chem. C 2015, 119, 6453−6463

to experiments, but the computational methodology still improves the results significantly, as compared to fully optimized systems. Our calculations at 0 K show a −0.16 eV error in E_{abs} to 20 °C experiments for PTI-1, and −0.29 eV for APFO-3, which for the latter agrees with our previously reported underestimation of ∼−0.32 eV for nine polymers using the same level of theory.[13] These errors are reduced by 0.04/0.07 eV at 293/343 K for APFO-3 and by 0.04/0.06 eV for PTI-1, with the temperature compensation scheme. The experimental results indicate that increasing the temperature by 100 K would result in a wavelength decrease of 15 and 13 nm for APFO-3 and PTI-1, respectively.

Calculated peak absorption coefficients ε_{max} in Figure 8b are lower in the Boltzmann-weighted stochastic angle calculations than in fully optimized systems, thus closer to experiments. The calculated ε_{max} overestimations are reduced from 50 to 37 and from 41 to 23 L g^{-1} cm^{-1} for PTI-1 and APFO-3, respectively. The improvement from the temperature-compensation is greater for ε_{max} than for λ_{abs}, due to the higher sensitivity of absorption strength to backbone twisting, evident from Figure 6. Both the strengths and the wavelengths of the calculated absorptions reproduce the experimental temperature dependence trends well, as seen in Figure 8.

Many factors contribute to the discrepancies in absolute optical results from standard calculations and experiments. Temperature is one such factor, and by refining the computational description of polymers by including a description of thermal effects as done here, the errors in calculations can be decomposed into quantifiable parts. The remaining discrepancy between experiments and the temperature- and size-compensated calculations is assigned partly to structural imperfections caused by neighboring polymer and solvent molecules, as well as thermally induced geometry distortions and vibration modes other than only the dihedral angles between units. The double-peak nature of the PTI-1 absorption makes assessment of particularly absorption strengths difficult, and a significantly higher experimental ε_{max} of 66 L g^{-1} cm^{-1} has previously been reported for PTI-1 batch with higher molecular weight.[76] This number is in much better agreement with our calculations, indicating that the limited M_W of the PTI-1 batch used in the experiments is part of the reason for the remaining discrepancy between experiment and theory. The choice of quantum chemical method constitutes another potential source of error, both for the calculated PES and for the TD-DFT optical excitations, where standard hybrid DFT functionals such as PBE0 used herein have been reported to overestimate the conjugation and torsional barriers.[27,57,77−81] This suggests that it could be valuable in future studies, beyond the scope of this Article, to use the experimental temperature dependence of polymer batches of more well-defined M_W to better characterize the accuracy of different computational schemes as compared to experiments, for example, considering the influence of the choice of functional, long-range corrections, basis set, solvent interactions, and other structural distortions.

Combined experimental and computational studies of polymers provide detailed information about the conformation−optical property relation, via analysis of exhibited trends in temperature dependence. Solution-based studies provide understanding of the intrinsic polymer properties, such as the energy landscape, which remains an important factor for the polymer conformations adopted also in other aggregation forms, such as films. If the demonstrated temperature sensitivity of the conjugation remains in the film state, it has an impact on the performance of OPV devices, because their operating temperatures can reach up to 60 °C.[82] The larger band gap and weaker absorption at higher temperatures is then detrimental to the device current output. Furthermore, temperature-sensitive frontier orbitals affect the performance because proper alignment of the polymer LUMO versus the fullerene LUMO is crucial for efficient exciton separation, while the HOMO level of the polymer is closely correlated with the V_{OC}. While the charge mobilities should be positively influenced by higher temperatures, electron mobilities in the TQ1 polymer have been shown to decrease above 300 K due to a conformation-sensitive LUMO.[7]

■ CONCLUSIONS

Experimental absorbance measurements of five D−A polymers APFO-3, BDT-BTz, PTI-1, TBDT-BTz, and TQ1 show clear and systematic dependence on temperature. When increasing the temperature gradually from 10 to 70 °C, the absorption strength decreases, and peaks are both blue-shifted and broadened. This is explained in terms of an increase in allowed structural conformations, where polymers at low temperature are limited to the minimum-energy conformation, which generally is associated with good conjugation. More distorted and twisted structures become entropically allowed at higher temperatures, and their weaker conjugation leads to a blue-shift and decreased strength of the absorption.

Standard quantum chemical calculations based on fully optimized geometries do not include thermal effects, influencing the calculated optical properties. Herein, we present results for calculations that account for the multitude of structural conformations that are adopted by polymers under normal temperature conditions. The optical properties are calculated on oligomers with geometries as sampled according to their Boltzmann distribution of dihedral angles between units, followed by extrapolation to the polymer size. This study provides a strategy to obtain temperature- and system size-converged results, considerably improving the computational predictions of optical properties of polymers. This strategy is applied to the polymers APFO-3 and PTI-1 and yields trends in good agreement with experiments regarding blue-shifting, broadening, and weakening of absorption peaks upon temperature increase. The methodology also improves absolute predicted optical properties; PTI-1 peak absorption wavelength is less than 50 nm different from experiments in the entire interval 10−70 °C, and the overestimation of the maximum APFO-3 absorption coefficient at 20 °C is decreased from 52% to 29%.

Consequently, the inclusion of a thermal sampling procedure accounts for the structural flexibility of key low-energy torsional modes for size-converged calculated polymer properties at experimentally relevant temperatures. This is found to provide a computationally efficient way to overcome a significant part of the discrepancy between room-temperature optical properties and calculations based on optimized geometries. It furthermore constitutes a stepping-stone for continued efforts to improve the accuracy of computational polymer predictions, where accounting for additional structurally active modes could be coupled to parallel efforts in identifying the best levels of theory, in terms of DFT functional, long-range corrections, basis sets, and solvent/environment treatment for enhanced description of the potential energy landscape and the optical properties. Finally, improved understanding and quantification of the temperature dependence of conformations at the

DOI: 10.1021/jp511246n
J. Phys. Chem. C 2015, 119, 6453−6463

molecular level and resultant optical properties, as achieved here for representative donor−acceptor polymers, also has broader significance because the intrinsic energy landscapes influence the conformations that these polymers will adopt in a wider set of environments, such as films and OPV devices.

■ ASSOCIATED CONTENT

● Supporting Information

Optimized monomer images of APFO-3 and PTI-1, details on calculated oscillator strength and absorption coefficients, analysis of angle-dependent optical properties, and calculated excitation data. This material is available free of charge via the Internet at http://pubs.acs.org.

■ AUTHOR INFORMATION

Corresponding Author

*Tel.: +46-462223311. Fax: +46-462228648. E-mail: petter.persson@teokem.lu.se.

Notes

The authors declare no competing financial interest.

■ ACKNOWLEDGMENTS

The work was funded by the Swedish research council (VR), the Knut and Alice Wallenberg (KAW) Foundation, and The Swedish Energy Agency (Energimyndigheten). NSC and LUNARC are acknowledged for computer resources used.

■ REFERENCES

(1) Li, G.; Zhu, R.; Yang, Y. Polymer Solar Cells. *Nat. Photonics* **2012**, *6*, 153−161.

(2) Helgesen, M.; Sondergaard, R.; Krebs, F. C. Advanced Materials and Processes for Polymer Solar Cell Devices. *J. Mater. Chem.* **2010**, *20*, 36−60.

(3) Chen, C.-C.; Dou, L.; Zhu, R.; Chung, C.-H.; Song, T.-B.; Zheng, Y. B.; Hawks, S.; Li, G.; Weiss, P. S.; Yang, Y. Visibly Transparent Polymer Solar Cells Produced by Solution Processing. *ACS Nano* **2012**, *6*, 7185−7190.

(4) Nielsen, T. D.; Cruickshank, C.; Foged, S.; Thorsen, J.; Krebs, F. C. Business, Market and Intellectual Property Analysis of Polymer Solar Cells. *Sol. Energy Mater. Sol. Cells* **2010**, *94*, 1553−1571.

(5) Chiechi, R. C.; Havenith, R. W. A.; Hummelen, J. C.; Koster, L. J. A.; Loi, M. A. Modern Plastic Solar Cells: Materials, Mechanisms and Modeling. *Mater. Today* **2013**, *16*, 281−289.

(6) Noriega, R.; Rivnay, J.; Vandewal, K.; Koch, F. P. V.; Stingelin, N.; Smith, P.; Toney, M. F.; Salleo, A. A General Relationship between Disorder, Aggregation and Charge Transport in Conjugated Polymers. *Nat. Mater.* **2013**, *12*, 1038−1044.

(7) Andersson, L. M.; Hedström, S.; Persson, P. Conformation Sensitive Charge Transport in Conjugated Polymers. *Appl. Phys. Lett.* **2013**, *103*, 213303.

(8) Jackson, N. E.; Savoie, B. M.; Kohlstedt, K. L.; Marks, T. J.; Chen, L. X.; Ratner, M. A. Structural and Conformational Dispersion in the Rational Design of Conjugated Polymers. *Macromolecules* **2014**, *47*, 987−992.

(9) Grancini, G.; Maiuri, M.; Fazzi, D.; Petrozza, A.; Egelhaaf, H.-J.; Brida, D.; Cerullo, G.; Lanzani, G. Hot Exciton Dissociation in Polymer Solar Cells. *Nat. Mater.* **2013**, *12*, 29−33.

(10) Sun, Z.; Stafström, S. Dynamics of Exciton Dissociation in Donor-Acceptor Polymer Heterojunctions. *J. Chem. Phys.* **2013**, *138*, 164905.

(11) Costa, T.; Di Paolo, R. E.; Garner, L. E.; Thomas, A. W.; Almeida, J. A. S.; Justino, L. L. G.; Maçanita, A. L.; Bazan, G. C.; Burrows, H. D. Separating Solvent and Conformational Effects on the Photophysics of a Homologous Progression of N-Terminated Phenylenevinylene Oligomers. *J. Phys. Chem. C* **2013**, *117*, 18353−18366.

(12) Salaneck, W. R.; Inganäs, O.; Thémans, B.; Nilsson, J. O.; Sjögren, B.; Österholm, J.-E.; Brédas, J. L.; Svensson, S. Thermochromism in poly(3-hexylthiophene) in the Solid State: A Spectroscopic Study of Temperature-dependent Conformational Defects. *J. Chem. Phys.* **1988**, *89*, 4613−4619.

(13) Hedström, S.; Henriksson, P.; Wang, E.; Andersson, M. R.; Persson, P. Light-Harvesting Capabilities of Donor−acceptor Polymers. *Phys. Chem. Chem. Phys.* **2014**, *16*, 24853−24865.

(14) Hedström, S.; Persson, P. Quantum Chemical Calculations of Side-Group Stacking and Electronic Properties in Thiophene−Quinoxaline Polymers. *J. Phys. Chem. C* **2012**, *116*, 26700−26706.

(15) Song, X.; Hua, W.; Ma, Y.; Wang, C.; Luo, Y. Theoretical Study of Core Excitations of Fullerene-Based Polymer Solar Cell Acceptors. *J. Phys. Chem. C* **2012**, *116*, 23938−23944.

(16) Pandey, L.; Risko, C.; Norton, J. E.; Brédas, J.-L. Donor−Acceptor Copolymers of Relevance for Organic Photovoltaics: A Theoretical Investigation of the Impact of Chemical Structure Modifications on the Electronic and Optical Properties. *Macromolecules* **2012**, *45*, 6405−6414.

(17) Zhang, L.; Pei, K.; Yu, M.; Huang, Y.; Zhao, H.; Zeng, M.; Wang, Y.; Gao, J. Theoretical Investigations on Donor−Acceptor Conjugated Copolymers Based on Naphtho[1,2-c:5,6-c]bis[1,2,5]-thiadiazole for Organic Solar Cell Applications. *J. Phys. Chem. C* **2012**, *116*, 26154−26161.

(18) McCormick, T. M.; Bridges, C. R.; Carrera, E. I.; DiCarmine, P. M.; Gibson, G. L.; Hollinger, J.; Kozycz, L. M.; Seferos, D. S. Conjugated Polymers: Evaluating DFT Methods for More Accurate Orbital Energy Modeling. *Macromolecules* **2013**, *46*, 3879−3886.

(19) Salvatori, P.; Mosconi, E.; Wang, E.; Andersson, M.; Muccini, M.; De Angelis, F. Computational Modeling of Isoindigo-Based Polymers Used in Organic Solar Cells. *J. Phys. Chem. C* **2013**, *117*, 17940−17954.

(20) Müller-Plathe, F. Coarse-Graining in Polymer Simulation: From the Atomistic to the Mesoscopic Scale and Back. *ChemPhysChem* **2002**, *3*, 754−769.

(21) Halverson, J. D.; Lee, W. B.; Grest, G. S.; Grosberg, A. Y.; Kremer, K. Molecular Dynamics Simulation Study of Nonconcatenated Ring Polymers in a Melt. I. Statics. *J. Chem. Phys.* **2011**, *134*, 204904.

(22) Ashrafi Khajeh, A. R.; Shankar, K.; Choi, P. Prediction of the Active Layer Nanomorphology in Polymer Solar Cells Using Molecular Dynamics Simulation. *ACS Appl. Mater. Interfaces* **2013**, *5*, 4617−4624.

(23) Kronik, L.; Stein, T.; Refaely-Abramson, S.; Baer, R. Excitation Gaps of Finite-Sized Systems from Optimally Tuned Range-Separated Hybrid Functionals. *J. Chem. Theory Comput.* **2012**, *8*, 1515−1531.

(24) Sini, G.; Sears, J. S.; Brédas, J.-L. Evaluating the Performance of DFT Functionals in Assessing the Interaction Energy and Ground-State Charge Transfer of Donor/Acceptor Complexes: Tetrathiafulvalene−Tetracyanoquinodimethane (TTF−TCNQ) as a Model Case. *J. Chem. Theory Comput.* **2011**, *7*, 602−609.

(25) Van Gisbergen, S.; Schipper, P.; Gritsenko, O.; Baerends, E.; Snijders, J.; Champagne, B.; Kirtman, B. Electric Field Dependence of the Exchange-Correlation Potential in Molecular Chains. *Phys. Rev. Lett.* **1999**, *83*, 694−697.

(26) Mori-Sánchez, P.; Cohen, A.; Yang, W. Localization and Delocalization Errors in Density Functional Theory and Implications for Band-Gap Prediction. *Phys. Rev. Lett.* **2008**, *100*, 146401.

(27) Janesko, B. G. Comparing Modern Density Functionals for Conjugated Polymer Band Structures: Screened Hybrid, Minnesota, and Rung 3.5 Approximations. *J. Chem. Phys.* **2011**, *134*, 184105.

(28) Kirkpatrick, J.; Nielsen, C. B.; Zhang, W.; Bronstein, H.; Ashraf, R. S.; Heeney, M.; McCulloch, I. A Systematic Approach to the Design Optimization of Light-Absorbing Indenofluorene Polymers for Organic Photovoltaics. *Adv. Energy Mater.* **2012**, *2*, 260−265.

(29) Risko, C.; McGehee, M. D.; Bredas, J.-L. A Quantum-Chemical Perspective into Low Optical-Gap Polymers for Highly-Efficient Organic Solar Cells. *Chem. Sci.* **2011**, *2*, 1200−1218.

DOI: 10.1021/jp511246n
J. Phys. Chem. C 2015, 119, 6453−6463

(30) Mondal, R.; Ko, S.; Norton, J. E.; Miyaki, N.; Becerril, H. A.; Verploegen, E.; Toney, M. F.; Bredas, J.-L.; McGehee, M. D.; Bao, Z. Molecular Design for Improved Photovoltaic Efficiency: Band Gap and Absorption Coefficient Engineering. *J. Mater. Chem.* **2009**, *19*, 7195−7197.
(31) Grimm, B.; Risko, C.; Azoulay, J. D.; Bredas, J.-L.; Bazan, G. C. Structural Dependence of the Optical Properties of Narrow Bandgap Semiconductors with Orthogonal Donor-Acceptor Geometries. *Chem. Sci.* **2013**, *4*, 1807−1819.
(32) Inganäs, O.; Svensson, M.; Zhang, F.; Gadisa, A.; Persson, N. K.; Wang, X.; Andersson, M. R. Low Bandgap Alternating Polyfluorene Copolymers in Plastic Photodiodes and Solar Cells. *Appl. Phys. A: Mater. Sci. Process.* **2004**, *79*, 31−35.
(33) Zhang, Z.; Peng, B.; Liu, B.; Pan, C.; Li, Y.; He, Y.; Zhou, K.; Zou, Y. Copolymers from Benzodithiophene and Benzotriazole: Synthesis and Photovoltaic Applications. *Polym. Chem.* **2010**, *1*, 1441−1447.
(34) Wang, E.; Ma, Z.; Zhang, Z.; Henriksson, P.; Inganäs, O.; Zhang, F.; Andersson, M. R. An Isoindigo-Based Low Band Gap Polymer for Efficient Polymer Solar Cells with High Photo-Voltage. *Chem. Commun.* **2011**, *47*, 4908−4910.
(35) Wang, E.; Hou, L.; Wang, Z.; Hellström, S.; Zhang, F.; Inganäs, O.; Andersson, M. R. An Easily Synthesized Blue Polymer for High-Performance Polymer Solar Cells. *Adv. Mater.* **2010**, *22*, 5240−5244.
(36) Ma, Z.; Wang, E.; Vandewal, K.; Andersson, M. R.; Zhang, F. Enhance Performance of Organic Solar Cells Based on an Isoindigo-Based Copolymer by Balancing Absorption and Miscibility of Electron Acceptor. *Appl. Phys. Lett.* **2011**, *99*, 143302.
(37) Slooff, L. H.; Veenstra, S. C.; Kroon, J. M.; Moet, D. J. D.; Sweelssen, J.; Koetse, M. M. Determining the Internal Quantum Efficiency of Highly Efficient Polymer Solar Cells through Optical Modeling. *Appl. Phys. Lett.* **2007**, *90*, 143506.
(38) Frisch, M.; Trucks, G.; Schlegel, H.; Scuseria, G.; Robb, M.; Cheeseman, J.; Scalmani, G.; Barone, V.; Mennucci, B.; Petersson, G.; et al. *Gaussian 09*, revision A.02; Gaussian, Inc.: Pittsburgh, PA, 2009.
(39) Adamo, C.; Barone, V. Toward Reliable Density Functional Methods without Adjustable Parameters: The PBE0Model. *J. Chem. Phys.* **1999**, *110*, 6158−6170.
(40) Zoombelt, A. P.; Fonrodona, M.; Turbiez, M. G. R.; Wienk, M. M.; Janssen, R. A. J. Synthesis and Photovoltaic Performance of a Series of Small Band Gap Polymers. *J. Mater. Chem.* **2009**, *19*, 5336−5342.
(41) Guo, X.; Watson, M. D. Pyromellitic Diimide-Based Donor−Acceptor Poly(phenylene Ethynylene)s. *Macromolecules* **2011**, *44*, 6711−6716.
(42) Schenning, A. P. H. J.; Kilbinger, A. F. M.; Biscarini, F.; Cavallini, M.; Cooper, H. J.; Derrick, P. J.; Feast, W. J.; Lazzaroni, R.; Leclère, P.; McDonell, L. A.; et al. Supramolecular Organization of A,α′-Disubstituted Sexithiophenes. *J. Am. Chem. Soc.* **2002**, *124*, 1269−1275.
(43) Zoombelt, A. P.; Leenen, M. A. M.; Fonrodona, M.; Nicolas, Y.; Wienk, M. M.; Janssen, R. A. J. The Influence of Side Chains on Solubility and Photovoltaic Performance of Dithiophene−thienopyrazine Small Band Gap Copolymers. *Polymer* **2009**, *50*, 4564−4570.
(44) Qian, D.; Ye, L.; Zhang, M.; Liang, Y.; Li, L.; Huang, Y.; Guo, X.; Zhang, S.; Tan, Z.; Hou, J. Design, Application, and Morphology Study of a New Photovoltaic Polymer with Strong Aggregation in Solution State. *Macromolecules* **2012**, *45*, 9611−9617.
(45) Gieseking, B.; Jäck, B.; Preis, E.; Jung, S.; Forster, M.; Scherf, U.; Deibel, C.; Dyakonov, V. Excitation Dynamics in Low Band Gap Donor−Acceptor Copolymers and Blends. *Adv. Energy Mater.* **2012**, *2*, 1477−1482.
(46) Banerji, N.; Gagnon, E.; Morgantini, P.-Y.; Valouch, S.; Mohebbi, A. R.; Seo, J.-H.; Leclerc, M.; Heeger, A. J. Breaking Down the Problem: Optical Transitions, Electronic Structure, and Photoconductivity in Conjugated Polymer PCDTBT and in Its Separate Building Blocks. *J. Phys. Chem. C* **2012**, *116*, 11456−11469.
(47) Canestraro, C. D.; Rodrigues, P. C.; Marchiori, C. F. N.; Schneider, C. B.; Akcelrud, L.; Koehler, M.; Roman, L. S. The Role of the Double Peaked Absorption Spectrum in the Efficiency of Solar Cells Based on Donor−acceptor−donor Copolymers. *Sol. Energy Mater. Sol. Cells* **2011**, *95*, 2287−2294.
(48) Fazzi, D.; Grancini, G.; Maiuri, M.; Brida, D.; Cerullo, G.; Lanzani, G. Ultrafast Internal Conversion in a Low Band Gap Polymer for Photovoltaics: Experimental and Theoretical Study. *Phys. Chem. Chem. Phys.* **2012**, *14*, 6367−6374.
(49) Huang, Y.; Liu, F.; Guo, X.; Zhang, W.; Gu, Y.; Zhang, J.; Han, C. C.; Russell, T. P.; Hou, J. Manipulating Backbone Structure to Enhance Low Band Gap Polymer Photovoltaic Performance. *Adv. Energy Mater.* **2013**, *3*, 930−937.
(50) Jiang, Y.; Peng, Q.; Gao, X.; Shuai, Z.; Niu, Y.; Lin, S. H. Theoretical Design of Polythienylenevinylene Derivatives for Improvements of Light-Emitting and Photovoltaic Performances. *J. Mater. Chem.* **2012**, *22*, 4491−4501.
(51) Suramitr, S.; Meeto, W.; Wolschann, P.; Hannongbua, S. Understanding on Absorption and Fluorescence Electronic Transitions of Carbazole-Based Conducting Polymers: TD-DFT Approaches. *Theor. Chem. Acc.* **2010**, *125*, 35−44.
(52) Castruita, G.; Garcia, V.; Arias, E.; Moggio, I.; Ziolo, R.; Ponce, A.; Gonzalez, V.; Haley, J. E.; Flikkema, J. L.; Cooper, T. Synthesis, Optical and Structural Properties of Sanidic Liquid Crystal (cholesteryl)benzoate-Ethynylene Oligomers and Polymer. *J. Mater. Chem.* **2012**, *22*, 3770−3780.
(53) Mabrouk, A.; Azazi, A.; Alimi, K. Molecular Structure−property Engineering of Low-Band-Gap Copolymers, Based on Fluorene, for Efficient Bulk Heterojunction Solar Cells: A Density Functional Theory Study. *Polym. Eng. Sci.* **2013**, *53*, 1040−1052.
(54) Henssler, J. T.; Zhang, X.; Matzger, A. J. Thiophene/Thieno[3,2-B]thiophene Co-Oligomers: Fused-Ring Analogues of Sexithiophene. *J. Org. Chem.* **2009**, *74*, 9112−9119.
(55) Gierschner, J.; Cornil, J.; Egelhaaf, H.-J. Optical Bandgaps of Π-Conjugated Organic Materials at the Polymer Limit: Experiment and Theory. *Adv. Mater.* **2007**, *19*, 173−191.
(56) Dkhissi, A.; Ouhib, F.; Chaalane, A.; Hiorns, R. C.; Dagron-Lartigau, C.; Iratcabal, P.; Desbrieres, J.; Pouchan, C. Theoretical and Experimental Study of Low Band Gap Polymers for Organic Solar Cells. *Phys. Chem. Chem. Phys.* **2012**, *14*, 5613−5619.
(57) Zhang, L.; Yu, M.; Zhao, H.; Wang, Y.; Gao, J. Theoretical Investigations on the Electronic and Optical Characteristics of Fused-Ring Homopolymers: Comparison of Oligomer Method and PBC−DFT Method. *Chem. Phys. Lett.* **2013**, *570*, 153−158.
(58) Mike, J. F.; Nalwa, K.; Makowski, A. J.; Putnam, D.; Tomlinson, A. L.; Chaudhary, S.; Jeffries-EL, M. Synthesis, Characterization and Photovoltaic Properties of Poly(thiophenevinylene-Alt-Benzobisoxazole)s. *Phys. Chem. Chem. Phys.* **2011**, *13*, 1338−1344.
(59) Torras, J.; Casanovas, J.; Alemán, C. Reviewing Extrapolation Procedures of the Electronic Properties on the Π-Conjugated Polymer Limit. *J. Phys. Chem. A* **2012**, *116*, 7571−7583.
(60) Wykes, M.; Milián-Medina, B.; Gierschner, J. Computational Engineering of Low Bandgap Copolymers. *Front. Chem.* **2013**, *1*, 35.
(61) Atkins, P.; Friedman, R. *Molecular Quantum Mechanics*, 4th ed.; Oxford University Press: New York, 2005.
(62) Meeto, W.; Suramitr, S.; Vannarat, S.; Hannongbua, S. Structural and Electronic Properties of Poly(fluorene−vinylene) Copolymer and Its Derivatives: Time-Dependent Density Functional Theory Investigation. *Chem. Phys.* **2008**, *349*, 1−8.
(63) Yang, L.; Feng, J.-K.; Liao, Y.; Ren, A.-M. A Theoretical Investigation on the Electronic and Optical Properties of Π-Conjugated Copolymers with an Efficient Electron-Accepting Unit bithieno[3,2-b:2′3′-E]pyridine. *Polymer* **2005**, *46*, 9955−9964.
(64) Hung, Y.-C.; Jiang, J.-C.; Chao, C.-Y.; Su, W.-F.; Lin, S.-T. Theoretical Study on the Correlation between Band Gap, Bandwidth, and Oscillator Strength in Fluorene-Based Donor−Acceptor Conjugated Copolymers. *J. Phys. Chem. B* **2009**, *113*, 8268−8277.
(65) Dutta, T.; Woody, K. B.; Parkin, S. R.; Watson, M. D.; Gierschner, J. Conjugated Polymers with Large Effective Stokes Shift: Benzobisdioxole-Based Poly(phenylene Ethynylene)s. *J. Am. Chem. Soc.* **2009**, *131*, 17321−17327.

DOI: 10.1021/jp511246n
J. Phys. Chem. C 2015, 119, 6453−6463

(66) Mondal, R.; Becerril, H. A.; Verploegen, E.; Kim, D.; Norton, J. E.; Ko, S.; Miyaki, N.; Lee, S.; Toney, M. F.; Bredas, J.-L.; et al. Thiophene-Rich Fused-Aromatic Thienopyrazine Acceptor for Donor-Acceptor Low Band-Gap Polymers for OTFT and Polymer Solar Cell Applications. *J. Mater. Chem.* **2010**, *20*, 5823−5834.
(67) Lei, T.; Cao, Y.; Zhou, X.; Peng, Y.; Bian, J.; Pei, J. Systematic Investigation of Isoindigo-Based Polymeric Field-Effect Transistors: Design Strategy and Impact of Polymer Symmetry and Backbone Curvature. *Chem. Mater.* **2012**, *24*, 1762−1770.
(68) Xu, X.; Cai, P.; Lu, Y.; Choon, N. S.; Chen, J.; Hu, X.; Ong, B. S. Synthesis and Characterization of thieno[3,2-B]thiophene-Isoindigo-Based Copolymers as Electron Donor and Hole Transport Materials for Bulk-Heterojunction Polymer Solar Cells. *J. Polym. Sci., Part A: Polym. Chem.* **2013**, *51*, 424−434.
(69) Shin, J.; Um, H. A.; Lee, D. H.; Lee, T. W.; Cho, M. J.; Choi, D. H. High Mobility Isoindigo-Based Pi-Extended Conjugated Polymers Bearing Di(thienyl)ethylene in Thin-Film Transistors. *Polym. Chem.* **2013**, *4*, 5688−5695.
(70) Zhuang, W.; Bolognesi, M.; Seri, M.; Henriksson, P.; Gedefaw, D.; Kroon, R.; Jarvid, M.; Lundin, A.; Wang, E.; Muccini, M.; et al. Influence of Incorporating Different Electron-Rich Thiophene-Based Units on the Photovoltaic Properties of Isoindigo-Based Conjugated Polymers: An Experimental and DFT Study. *Macromolecules* **2013**, *46*, 8488−8499.
(71) Elsawy, W.; Lee, C.-L.; Cho, S.; Oh, S.-H.; Moon, S.-H.; Elbarbary, A.; Lee, J.-S. Isoindigo-Based Small Molecules for High-Performance Solution-Processed Organic Photovoltaic Devices: The Electron Donating Effect of the Donor Group on Photo-Physical Properties and Device Performance. *Phys. Chem. Chem. Phys.* **2013**, *15*, 15193−15203.
(72) Zade, S. S.; Bendikov, M. From Oligomers to Polymer: Convergence in the HOMO−LUMO Gaps of Conjugated Oligomers. *Org. Lett.* **2006**, *8*, 5243−5246.
(73) Zhou, H.; Yang, L.; Stuart, A. C.; Price, S. C.; Liu, S.; You, W. Development of Fluorinated Benzothiadiazole as a Structural Unit for a Polymer Solar Cell of 7% Efficiency. *Angew. Chem.* **2011**, *123*, 3051−3054.
(74) Bertho, S.; Janssen, G.; Cleij, T. J.; Conings, B.; Moons, W.; Gadisa, A.; D'Haen, J.; Goovaerts, E.; Lutsen, L.; Manca, J.; et al. Effect of Temperature on the Morphological and Photovoltaic Stability of Bulk Heterojunction Polymer:fullerene Solar Cells. *Sol. Energy Mater. Sol. Cells* **2008**, *92*, 753−760.
(75) Yang, C.; Orfino, F. P.; Holdcroft, S. A Phenomenological Model for Predicting Thermochromism of Regioregular and Non-regioregular Poly(3-Alkylthiophenes). *Macromolecules* **1996**, *29*, 6510−6517.
(76) Wang, E.; Ma, Z.; Zhang, Z.; Vandewal, K.; Henriksson, P.; Inganäs, O.; Zhang, F.; Andersson, M. R. An Easily Accessible Isoindigo-Based Polymer for High-Performance Polymer Solar Cells. *J. Am. Chem. Soc.* **2011**, *133*, 14244−14247.
(77) Manninen, V.; Niskanen, M.; Hukka, T. I.; Pasker, F.; Claus, S.; Hoger, S.; Baek, J.; Umeyama, T.; Imahori, H.; Lemmetyinen, H. Conjugated Donor-Acceptor (D-A) Copolymers in Inverted Organic Solar Cells - a Combined Experimental and Modelling Study. *J. Mater. Chem. A* **2013**, *1*, 7451−7462.
(78) Al-Backri, A.; Zólyomi, V.; Lambert, C. J. Electronic Properties of Linear Carbon Chains: Resolving the Controversy. *J. Chem. Phys.* **2014**, *140*, 104306.
(79) Sun, H.; Autschbach, J. Electronic Energy Gaps for Π-Conjugated Oligomers and Polymers Calculated with Density Functional Theory. *J. Chem. Theory Comput.* **2014**, *10*, 1035−1047.
(80) Karpfen, A.; Choi, C. H.; Kertesz, M. Single-Bond Torsional Potentials in Conjugated Systems: A Comparison of Ab Initio and Density Functional Results. *J. Phys. Chem. A* **1997**, *101*, 7426−7433.
(81) Seidl, A.; Görling, A.; Vogl, P.; Majewski, J. A.; Levy, M. Generalized Kohn-Sham Schemes and the Band-Gap Problem. *Phys. Rev. B* **1996**, *53*, 3764−3774.
(82) Katz, E. A.; Faiman, D.; Tuladhar, S. M.; Kroon, J. M.; Wienk, M. M.; Fromherz, T.; Padinger, F.; Brabec, C. J.; Sariciftci, N. S. Temperature Dependence for the Photovoltaic Device Parameters of Polymer-Fullerene Solar Cells under Operating Conditions. *J. Appl. Phys.* **2001**, *90*, 5343−5350.

DOI: 10.1021/jp511246n
J. Phys. Chem. C 2015, 119, 6453−6463

Paper VI

Rational Design of D–A_1–D–A_2 Conjugated Polymers with Superior Spectral Coverage

Svante Hedström,[a] *Qiang Tao,*[b] *Ergang Wang,*[b] *and Petter Persson**[a]
[a]Division of Theoretical Chemistry, Lund University. P. O. Box 124, S-221 00 Lund, Sweden.
[b]Department of Chemistry and Chemical Engineering/Polymer Technology, Chalmers University of Technology, S-412 96 Göteborg, Sweden
*E-mail: petter.persson@teokem.lu.se Telephone: +46-462223311.

Table of contents entry

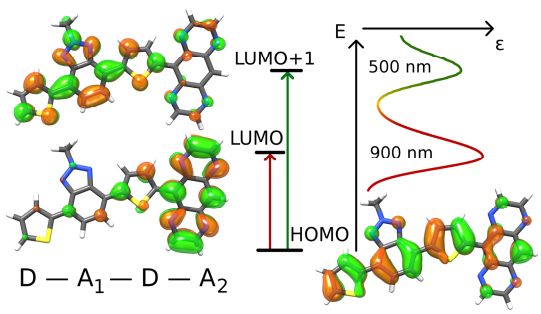

Calculations and experiments elucidate the factors governing the capability of D–A_1–D–A_2 conjugated polymers to offer fundamentally improved spectral coverage due to allowed transitions to both acceptor LUMOs.

Abstract

The spectral coverage of a light-harvesting polymer largely determines the maximum achievable photocurrent in organic photovoltaics, and therefore constitutes a crucial parameter for improving their performance. The D–A_1–D–A_2 copolymer motif is a new and promising design strategy for extending the absorption range by incorporating two acceptor units with complementary photoresponses. The fundamental factors that promote an extended absorption are here determined for three prototype D–A_1–D–A_2 systems through a combination of experimental and computational methods. Systematic quantum chemical calculations are then used to reveal the intrinsic optical properties of ten further D–A_1–D–A_2 polymer candidates. These investigated polymers are all predicted to exhibit intense primary absorption peaks at 615–954 nm, corresponding to charge-transfer (CT) transitions to the stronger acceptor, as well as secondary absorption features at 444–647 nm that originate from CT transitions to the weaker acceptors. Realization of D–A_1–D–A_2 polymers with superior spectral coverage is thereby found to depend critically on the spatial and energetic separation between the two distinct acceptor LUMOs. Two promising D–A_1–D–A_2 copolymer candidates were finally selected for further theoretical and experimental study, and demonstrate superior light-harvesting properties in terms of significantly extended spectral coverage. This demonstrates great potential for enhanced light-harvesting in D–A_1–D–A_2 polymers *via* multiple absorption features compared to traditional D–A polymers.

Introduction

Organic photovoltaics (OPV) offer a clean, renewable source of energy, with a reduced associated cost and complexity of manufacturing compared to silicon p–n junction solar cells. The cell parameter most strongly associated with high efficiency is the short circuit current,[1] which in turn is largely determined by the spectral coverage of the polymer. The donor–acceptor (D–A) motif is the currently dominant polymer category for OPV applications,[2–5] with reported power conversion efficiencies (PCE) up to 10%.[6] The success of D–A polymers for device applications is largely due to their band gaps typically being narrower compared to homopolymers such as polythiophenes, allowing them to absorb a greater part of the solar emission and produce greater photocurrents. The small band gaps are achieved by incorporating one electron-rich (donor) and one electron-poor aryl unit (acceptor) along the backbone, where the donor and acceptor are respectively responsible for elevated highest occupied molecular orbital (HOMO) and deep lowest unoccupied molecular orbital (LUMO) energies

of the copolymer. Electron transitions from HOMO to LUMO, with associated charge-transfer (CT) to the acceptor unit, are responsible for the strong low-energy absorption peak typically present in D–A polymers. Secondary absorption peaks of non-CT, $\pi \rightarrow \pi^*$ character tend to be of wavelengths $\leq$ 400 nm, giving negligible contribution to the photocurrent due to poor overlap with the solar emission spectrum.

D–A polymers constitute an improvement in spectral coverage compared to homopolymers, but further enhancement of OPV photocurrents is still feasible by means of broader effective absorption. This has in part been accomplished by fabrication of tandem solar cells,[7–10] where two subcells using different polymers with complementary absorption profiles together exploit a larger part of the solar emission. These are however considerably more complicated and expensive to manufacture than single junction OPVs. Another strategy for broadening the light-response of OPVs is to blend two D–A polymers into the same bulk heterojunction active layer, fabricating either pure polymer–polymer cells,[11–13] or ternary systems with a fullerene acceptor.[14,15,16] The efficiency of these two types of OPVs is still limited, due to added complexity in controlling *e.g.* morphology and carrier transport.[17,18–20]

Extending the spectral coverage while circumventing the issues with fabrication and morphology associated with tandem, ternary, and polymer–polymer cells, is possible using copolymers with more than one acceptor unit along the backbone, either as random copolymers,[21–24] or less commonly as strictly alternating D–A_1–D–A_2 polymers.[25–32] These are highly promising for OPV applications, we recently reported a 7.0 % PCE for the P3TQTI-F polymer,[33] the most efficient D–A_1–D–A_2 polymer to date. This motif is fundamentally advantageous for the potential of two absorption peaks in the spectral region of strong solar emission.[33,34]

The presence of two peaks in D–A_1–D–A_2 polymers originate from strongly allowed electronic CT transitions to two distinct unoccupied MOs, yielding superior spectral coverage at relevant wavelengths $\geq$ 450 nm, see Figure 1. We recently showed that LUMO and LUMO+1 of D–A_1–D–A_2 polymers agree in shape and energy to the respective LUMOs of corresponding D–A polymers.[33] According to a molecular orbital (MO) argument, the two acceptor LUMOs will interact and mix, forming two polymer LUMOs with larger energy separation. The mixing coefficient λ is proportional to the spatial overlap and the inverse of the energy separation $\Delta E_{LUMO,A}$ of the non-interacting acceptor LUMOs, as outlined in Equation 1.[35]

$$\lambda_{LUMO-LUMO} \cong \frac{k\langle \varphi_{LUMO,A_1} | \varphi_{LUMO,A_2} \rangle}{E_{LUMO,A_2} - E_{LUMO,A_1}} \propto \frac{e^{-\beta R(A_1 - A_2)}}{\Delta E_{LUMO,A}} \qquad (1)$$

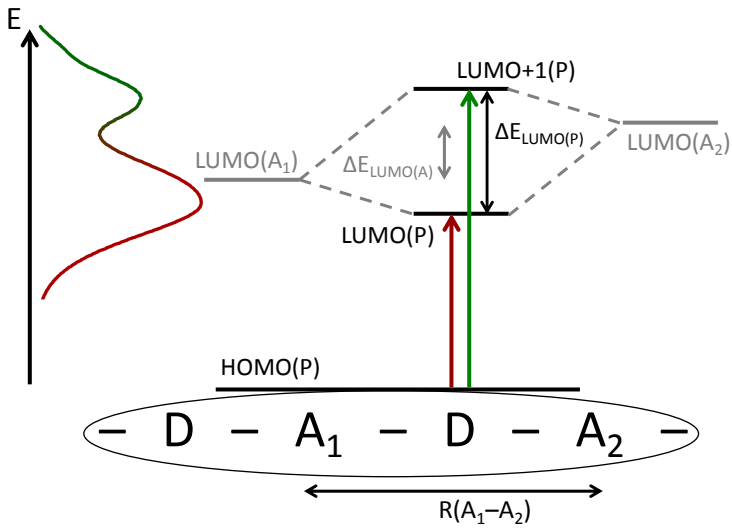

Figure 1. Schematic description of the energy levels involved in D–A_1–D–A_2 polymers. While the HOMO is typically delocalized across the backbone, the two acceptor LUMOs interact, forming the copolymer LUMO and LUMO+1 with slightly altered energies but largely retained character. Improved spectral coverage is obtained if electronic transitions to both polymer LUMO (red) and LUMO+1 (green) are allowed.

The development of new D–A_1–D–A_2 designs with improved light-harvesting properties requires better insight into the special optical features of D–A_1–D–A_2 polymers, in combination with screening of more new candidate systems, typically relying on time-consuming synthetic and experimental characterization work. Light-harvesting traits of polymers such as the intensity and energy of excitations, the resulting spectra, as well as structural and electronic properties, *e.g.* molecular orbitals can however all be accurately and efficiently calculated using density functional theory (DFT).[36–40] While calculations have traditionally served as an explanatory tool for experimental findings, they can also be exploited to guide the pursuit of polymer candidates with superior spectral properties.[36]

In this article, we use DFT calculations to explore the fundamental properties of the new class of D–A_1–D–A_2 copolymers, providing guidelines to the ongoing development of new and efficient light-harvesting polymers. The electronic and optical properties of 15 such copolymers are scrutinized based on extrapolations of oligomer calculations to the polymer limit. First, we examine three previously reported D–A_1–D–A_2 polymers and their qualitatively different spectral responses, where good agreement between calculations and reported experimental data serves as validation of the computational methodology. Second, we present and study 10 new D–A_1–D–A_2 polymer designs, focusing on the structure–property relation with respect to substantial absorptivity over a wide spectral region, and a molecular scale insight into the relevant orbitals that govern the electronic transitions. Finally, two promising D–A_1–D–A_2 polymers are subjected to

extended experimental and computational investigation, confirming our strategy to broaden the spectral response by two allowed low-energy excitations, having profound implications for the photocurrents and efficiencies of OPVs.

Methods

Computational details

All calculations were made with the Gaussian 09 program package,[41] at the DFT PBE0[42]/6-31g(d,p) level of theory. Monomer and dimer model systems of D–A_1–D–A_2 polymers were fully optimized, and a time-dependent (TD)-DFT scheme was applied to the minimum energy conformations, calculating the transition wavelengths (λ) and oscillator strengths (f) of the oligomers. D–A polymers underwent the same treatment, for oligomers of 1–2 repeating units for PTI-1, 1–3 repeating units for P3TPhQ and PTPzQ, and 1, 3, and 4 repeating units for PTBTz and PTBT. Calculated UV/vis absorption spectra were simulated for all oligomers by applying an inhomogeneous Gaussian shape broadening, with a 4800 cm^{-1} FWHM broadening towards higher frequencies and 3200 cm^{-1} towards lower, and exploiting the relation between the dimensionless f and mass extinction coefficients (ε), as outlined in Equation 2,[43] where m_e and q_e are the electron mass and charge, ε_0 is the vacuum permittivity, N_A is the Avogadro number, ν is the photon frequency, and M is the molecular mass.

$$f = \frac{4ln(10)m_e c\varepsilon_0 M}{N_A q_e^2} \times \int \varepsilon(\nu) d\nu \qquad (2)$$

The calculated oligomer first peak E_{abs}=hc/ λ and ε_{max} were plotted *vs.* the inverse number of repeating units (1/n), and the best linear fits were extrapolated to 1/n→0, *i.e.* infinite polymer length, as described in the literature.[36,44–46] Although the PBE0 functional has been used successfully for studies of conjugated polymers,[36,47,48,49] being a standard hybrid DFT functional it tends to overestimate the conjugation and planarity, and consequently also the absorption λ and ε. We have recently introduced an empirical correction that compensates for this systematic overestimation.[36] The correction is based on the extrapolated first peak E_{abs} and ε_{max} which are respectively blue-shifted by +0.32 eV and downscaled by a factor of 1.6, as per Equation 3.

$$\varepsilon_{corr}\left(E_{abs,corr}\right) = \frac{\varepsilon_{extrapol}\left(E_{abs,extrapol} + 0.32\ eV\right)}{1.6} \qquad (3)$$

The oligomer size (1 or 2 repeating units for D–A_1–D–A_2 polymers, 2, 3, or 4 for D–A polymers) whose uncorrected, calculated first peak E_{abs} best agrees with the

extrapolated and corrected $E_{abs,corr}$, had its spectrum parallel-shifted to that its first peak matches $E_{abs,corr}$, and scaled to match $\varepsilon_{max,corr}$. For the D–A_1–D–A_2 polymers whose extrapolated E_{abs} falls between the calculated mono- and dimer spectra, the procedure was done for both sizes, and the average of the two spectra was used. The $PC_{71}BM$ absorption spectrum was calculated at the TD-PBE0/6-31g(d,p)//PBE0/6-31g(d,p) level, applying a homogenous Gaussian broadening of 3000 cm^{-1}.

Material characterization

^{1}H NMR (400 MHz) and ^{13}C NMR (100 MHz) spectra were acquired using a Varian Inova 400 MHz NMR spectrometer. Tetramethylsilane was used as an internal reference with deuterated chloroform as the solvent. Size exclusion chromatography (SEC) was performed on an Agilent PL-GPC 220 Integrated High Temperature GPC/SEC System with refractive index and viscometer detectors. The columns are 3 PLgel 10 µm MIXED-B LS 300×7.5 mm columns. The eluent was 1,2,4-trichlorobenzene. The working temperature was 150 °C. The molecular weights were calculated according to relative calibration with polystyrene standards. UV-Vis absorption spectra were measured with a Perkin Elmer Lambda 900 UV-Vis-NIR absorption spectrometer.

Results

Acceptor unit strength

The copolymer LUMO energy is crucial for solar cell performance, since its offset *vs.* the fullerene LUMO energy provides a driving force for charge transfer at the polymer–fullerene interface, and also because it partly determines the optical band gap of the copolymer. The copolymer LUMO is mainly determined by the acceptor unit, whose LUMO energy thus roughly indicates the strength of the acceptor. D–A_1–D–A_2 polymers rely on their two acceptors having different strength, so that their spectral responses complement each other. In total, we use eight different two-acceptor combinations of seven different acceptor units. These are benzo[1,2-c;4,5-c′]bis[1,2,5]thiadiazole (BBT), 2,1,3-benzothiadiazole (BT), 2-alkyl-benzo[d][1,2,3]triazole (BTz), 2,5-dialkyl-1,4-diketopyrrolo[3,4-c]pyrrole (DPP), N,N′-dialkyl-isoindigo (II), 2,3-bis-(3-alkoxyphenyl)quinoxaline (PhQ), pyrazino[2,3-g]quinoxaline (PzQ). Their molecular structures are shown in Chart 1, together with thiophene (T) which acts as donor in all polymers, either as a single unit, as bithiophene (2T), or as terthiophene (3T). Probing donors with

varying lengths is important, since these act not only as electron donators, but also spatial separators between the acceptors.

Chart 1. Structures of the studied donor unit (T) and the 7 acceptor units.

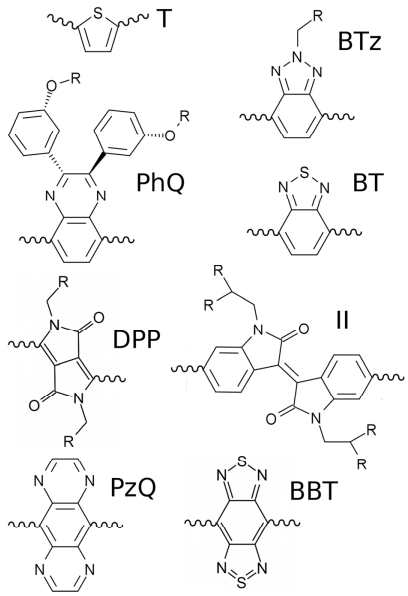

The calculated HOMO and LUMO energies of the isolated acceptor units used in this study are presented in Table 1 together with peak wavelengths (λ_{max}) in solution for typical D–A polymers incorporating the respective acceptors. Calculated $E_{LUMO,A}$ are in good trend-wise agreement with the calculated λ_{max}, even though the copolymer HOMO energies also affect the band gap. DPP induces longer λ_{max} in copolymers than indicated by its LUMO energy. This is partly due to the absence of steric hindrance from hydrogen atoms when DPP is coupled to thiophene-like donors, leading to more planar copolymer backbones, and partly because of the high HOMO energy of DPP. The LUMO of BTz is stabilized when substituted with electron withdrawing fluorine atoms, often decreasing the copolymer band gap. This band gap reduction is not apparent in all cases, since fluorination typically also lowers the copolymer HOMO energy.[25,50–52]

Table 1. The calculated HOMO and LUMO energies of the acceptors as single molecules. Peak absorption wavelengths in solution for typical D–A polymers incorporating the respective acceptor units. Sorted by increasing LUMO energy, approximately corresponding to decreasing acceptor strength.

Acceptor	HOMO [eV]	LUMO [eV]	λ_{max} range [nm]
BBT	-6.48	-3.44	850–1320[46,53,54]
PzQ	-6.80	-2.74	650–870[36,54,55]
II	-5.79	-2.59	550–720[56–58]
BT	-6.91	-2.21	480–700[59–61]
DPP	-5.70	-2.02	570–830[62,63]
PhQ	-6.08	-1.77	490–620[64–66]
BTzF	-6.76	-1.35	530–610[50,67–69]
BTz	-6.39	-1.04	400–580[50,70,71]

Origin of dual peak absorption in D–A_1–D–A_2 copolymers

Of the few reported strictly alternating D–A_1–D–A_2 polymers, some exhibit two absorption peaks $\gtrsim$ 450 nm,[30,31,32] whereas others show photoresponses similar to D–A polymers, with only one resolved low energy peak.[26–28,30,29,72] However, no detailed information regarding these spectral features, rationalized from the nature of the electronic transitions, has been reported. To gain insight into the molecular level structure–property relation with respect to dual absorption potential, three D–A_1–D–A_2 polymers from the literature were chosen for computational scrutiny: PBBTDPP[30] with two distinct low-energy peaks, as well as PTQTI[26,25] and PBTDPP,[30] each with only one resolved experimental peak. DFT and TD-DFT was used to explore how the electronic structure and optical properties of conjugated polymers are affected by including two acceptor units with distinct electronic traits.

Calculated absorption spectra were obtained from extrapolations of calculated mono- and dimer transitions, using the previously developed empirical correction, given in Equation 3.[36] For all three polymers, the agreement in relative peak heights and peak wavelengths is excellent, as seen in Figure 2a and b. The experimental absorption coefficients for PBTDPP and PBBTDPP have not been reported, and for PTQTI they are slightly lower compared to calculations. The qualitative and quantitative agreement serves as a validation of our computational methodology, and encourages its application in the continued investigation of the optical traits of the polymers.

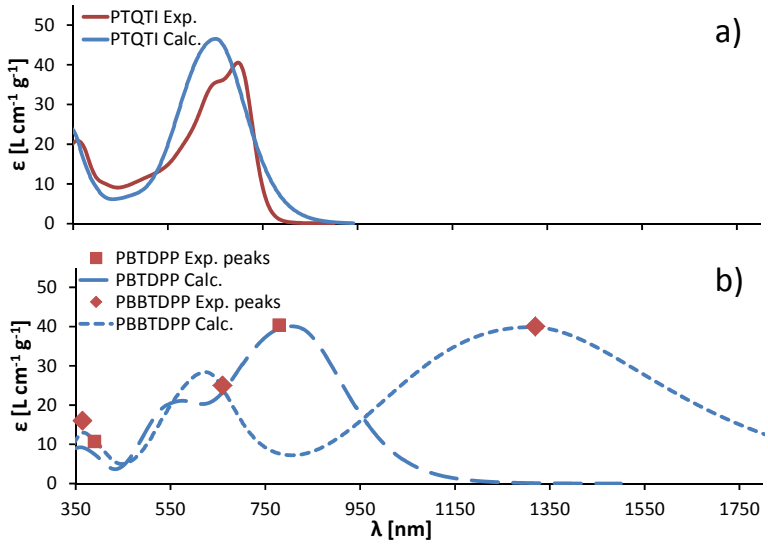

Figure 2. Calculated and experimental absorption spectrum for PTQTI (a). Calculated spectrum of PBTDPP and PBBTDPP, with experimental peak positions as taken from literature,[30] and normalized to the same first peak ε_{max} as the calculations (b). Calculated spectra are obtained as per Equation 3.

The first (lowest energy) calculated absorption peak positions for the three D–A_1–D–A_2 polymers are mainly governed by the stronger acceptor, falling within the λ_{max} range of typical corresponding D–A polymers, as listed in Table 1. Furthermore, the second peak at 624 nm for PBBTDPP and the shoulder at ~570 nm for PBTDPP both coincide with the peak wavelengths displayed by DPP-containing D–A polymers (see Table 1), indicating a direct link between the weaker acceptor in D–A_1–D–A_2 polymers and the second absorption feature. In the PTQTI spectrum however, only one discernable peak appears.

To elucidate the reasons for the qualitatively different spectral profiles of the three D–A_1–D–A_2 polymers, their calculated electronic transitions were examined on the mono- and dimer levels. Monomer excitation data is presented, see Table 2, since orbitals and transitions are of more pure character in smaller systems, being therefore easier to analyze, although oligomers of two repeating units often are more representative of experimental polymers, and in better quantitative agreement. All monomers exhibit an intense first transition of mainly HOMO→LUMO character, whereas the HOMO→LUMO+1 transition is very weak for PTQTI but strongly allowed for PBTDPP and PBBTDPP. Excitations $\lesssim$ 450 nm are typically of non-CT, $\pi\rightarrow\pi^*$ character, and are not significant for solar cell performance since the solar emission lacks intensity at such short wavelengths.

Table 2. Wavelengths, oscillator strengths and dominant orbital contributions of relevant calculated transitions for the three D–A_1–D–A_2 polymers, as calculated for the monomers.[a]

PTQTI			PBTDPP			PBBTDPP		
λ_{abs} [nm]	f	Orbitals	λ_{abs} [nm]	f	Orbitals	λ_{abs} [nm]	f	Orbitals
582.4	1.03	H→L	660.0	1.10	H→L	1070	0.66	H→L
494.1	0.09	H→L+1	538.3	0.62	H→L+1	573.9	1.02	H→L+1
347.0	0.24	H-4→L+1	378.8	0.14	H-2→L	398.2	0.16	H→L+3
341.5	0.15	H→L+3	336.0	0.18	H-2→L+1	347.1	0.24	H-2→L+1

[a]H=HOMO, L=LUMO.

The HOMO, LUMO, and LUMO+1 orbitals of the three D–A_1–D–A_2 monomers are depicted in Figure 3 and their energies are listed in Table S1 in the ESI. In all cases, the HOMO is delocalized across the backbone, promoting the important hole-mobility through the polymer phase. The LUMO on the other hand, is more localized on the stronger acceptor, analogous to the typical behavior of D–A polymers,[36,73–75] and the LUMO+1 orbitals are denser on the weaker acceptors. The dimers (not shown) display qualitatively identical orbital distributions over the respective acceptors, although their orbital energies differ from the monomers. The partial localization of LUMO and LUMO+1 on the respective acceptors is most pronounced for PBBTDPP where the difference in acceptor strength $\Delta E_{LUMO,A}$=-1.42 eV is largest. PTQTI and particularly PBTDPP have smaller $\Delta E_{LUMO,A}$ of -0.82, -0.19 eV respectively, which in accordance with Equation 1 enhances the LUMO(A_1)–LUMO(A_2) interactions, and consequently results in more mixed and delocalized LUMO and LUMO+1 orbitals. Thus, the two absorption peaks for PBBTDPP correspond to CT transitions to the LUMOs of the two respective acceptors. The PBTDPP absorption is analogous, though the similar strength of its two acceptors leads to the second absorption feature being unresolved, appearing only as a shoulder in the spectrum in Figure 2. Table 2 demonstrates that PTQTI has a HOMO→LUMO+1 transition of negligible intensity, despite its $\Delta E_{LUMO,A}$ being larger than that of PBTDPP, resulting in a single absorption peak.

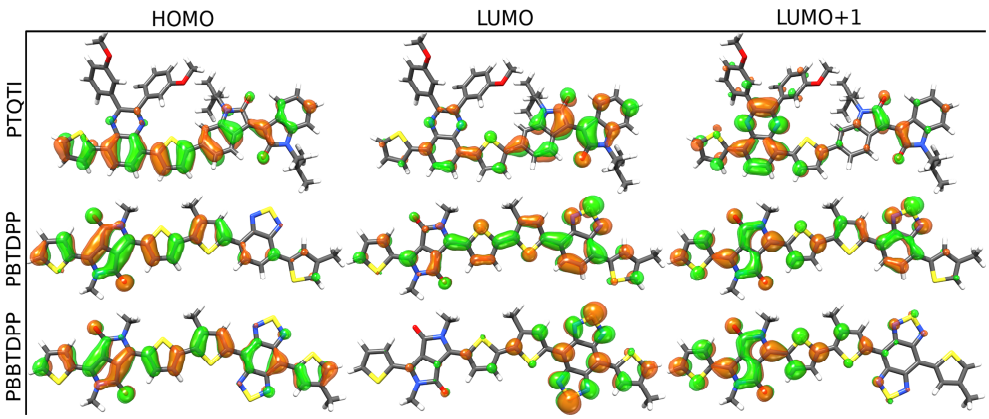

Figure 3. Frontier orbitals for the monomers of PTQTI, PBTDPP, and PBBTDPP. Isovalue=0.025.

Systematic screening of new D–A_1–D–A_2 copolymer designs

Chart 2. The structures of the 10 computational D–A_1–D–A_2 polymers. The donor (D) is either thiophene (T, n=1) or terthiophene (3T, n=3). R is an arbitrary alkyl side-chain.

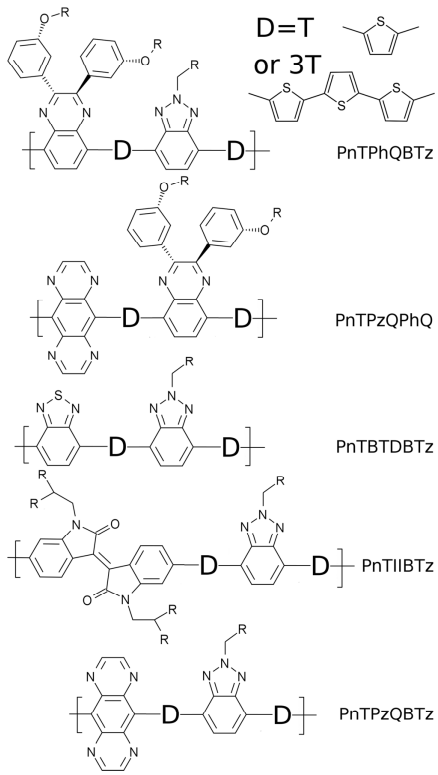

In this section, systematic computational scrutiny of a larger set of D–A_1–D–A_2 polymers is used to elucidate the factors that determine the potential for increased spectral coverage of this type of polymers, and to provide computational guidance for promising D–A_1–D–A_2 structural designs. To this end, an extended set of ten copolymers were selected, in five distinct two-acceptor combinations with different resulting $\Delta E_{LUMO,A}$. The acceptors are separated by one or three thiophene donor units, to permit probing of the effect of spatial acceptor separation R(A_1–A_2). The weak BTz acceptor was used in eight of the ten polymers, expecting it to induce an absorption contribution complementary to that of the stronger acceptors PhQ, BT, II, and PzQ. The structures of the ten D–A_1–D–A_2 polymers are presented in Chart 2.

The absorption spectra of the polymers are presented in Figure 4, as obtained through extrapolations from mono- and dimer calculations, employing Equation 3. The polymers were modeled without long alkyl chains in the DFT calculations, but to estimate the mass extinction coefficients ε, an arbitrary side-chain mass was added, equal to a side-chain ratio of 33 wt% for all polymers. The spectra of the ten D–A_1–D–A_2 copolymers show large variations in shape, peak wavelength, maximum extinction coefficient, and resulting spectral coverage. In all cases, the polymers with one thiophene unit in the donor segments exhibit longer first peak λ_{max} than the corresponding polymer with 3T-donors. This trend is qualitatively understood from the distance dependent LUMO(A_1)–LUMO(A_2) interactions described by Equation 1 and Figure 1, where a shorter donor induces a lower LUMO(polymer). This accounts also for the secondary peak/shoulders being considerably blueshifted, due to higher LUMO+1 conferred by a shorter donor segment.

The four polymers containing the very strong PzQ acceptor demonstrate very long λ_{max} of 866–954 nm, constituting a slight redshift compared to the typical absorption of D–PzQ polymers as listed in Table 1, which is attributed to that we omit phenyl side groups while they are normally included in synthesis of this acceptor. The first peak ε_{max} of the polymers with PzQ are however limited to around 40–50 $Lg^{-1}cm^{-1}$. Also PTBTBTz, PTPhQBTz, and P3TPhQBTz exhibit first peak λ_{max} (730, 681, and 643 nm respectively) longer than D–A polymers with those respective strongest acceptors: BT and PhQ. The 1st peak ε_{max} appears insensitive to the number of thiophenes, amounting to around 50, 65, 65, and 40 $Lg^{-1}cm^{-1}$ for PnTPzQBTz, PnTIIBTz, PnTBTBTz, and PnTPzQPhQ, respectively. Only when PhQ is the stronger acceptor does the addition of two thiophenes noticeably increase 1st peak ε_{max}: from 32 to 49 $Lg^{-1}cm^{-1}$.

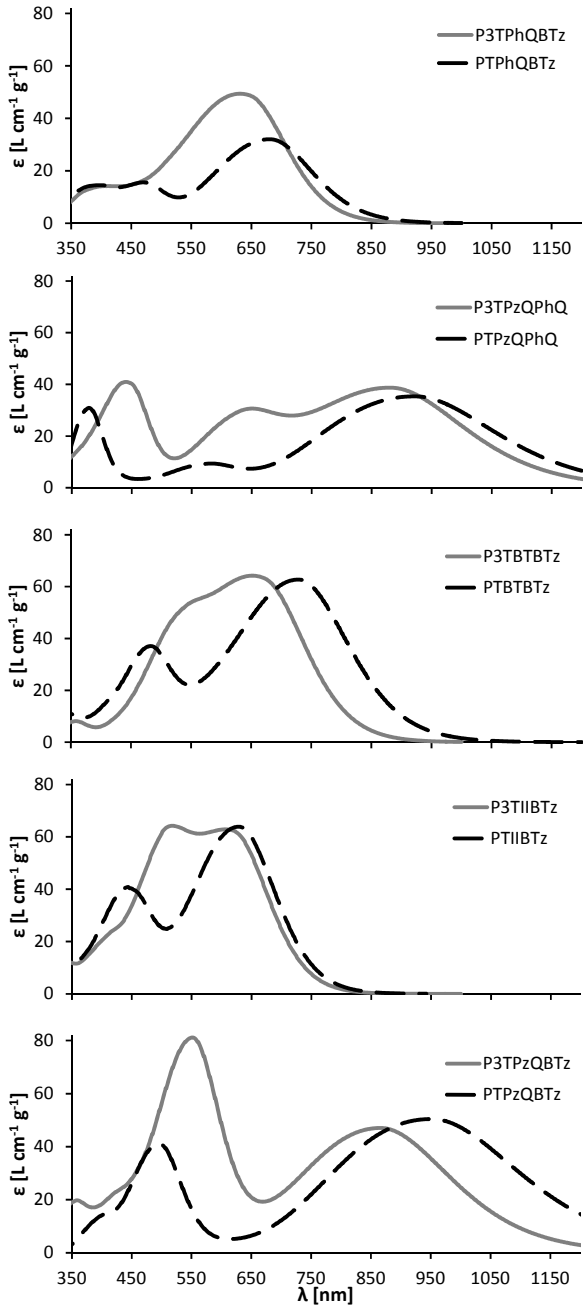

Figure 4. Absorption spectra of the 10 computationally studied D–A_1–D–A_2 polymers, as calculated with TD-DFT, employing the empirical correction based on Equation 3.

All polymer spectra in Figure 4 show some secondary spectral features $\gtrsim$ 450 nm, though their intensities and wavelengths vary greatly, and for P3TBTBTz, and

P3TPhQBTz they appear only as unresolved shoulders to the 1st peak. The secondary absorption peaks/shoulders exhibit a clear redshift when extending the donor segments, again relating to Equation 1. The origin of the secondary absorption features is elucidated in Table 3, where the first two transitions with non-negligible intensity for all monomers are listed. It is obvious that the first peaks for all polymers arise due to HOMO→LUMO transitions, whereas the second transitions are of dominantly HOMO→LUMO+1 character, validating the $D–A_1–D–A_2$ design strategy. Note that the 3T donor polymers at the monomer level give lower energy transitions compared to those with the shorter T donors, which is simply due to their longer repeating unit. For the extrapolated values the opposite is observed: the longer donor induces a slight blueshift, apparent in Figure 4.

Table 3. Monomer transitions responsible for the first two spectral features in polymers, with dominant orbital contributions.[a]

PTPhQBTz			**P3TPhQBTz**		
λ [nm]	f	Orbitals	λ [nm]	f	Orbitals
491.6	0.63	H→L	578.1	1.78	H→L
408.8	0.39	H→L+1	503.5	0.60	H→L+1
PTPzQPhQ			**P3TPzQPhQ**		
623.5	0.43	H→L	813.6	0.97	H→L
483.1	0.16	H→L+1	592.8	0.45	H→L+1
PTBTBTz			**P3TBTBTz**		
507.2	0.66	H→L	631.1	1.55	H→L
408.6	0.54	H→L+1	517.2	1.12	H→L+1
PTIIBTz			**P3TIIBTz**		
572.3	0.96	H→L	646.1	1.66	H→L
426.4	0.77	H→L+1	513.1	1.09	H→L+1
PTPzQBTz			**P3TPzQBTz**		
644.3	0.48	H→L	800.2	0.90	H→L
413.1	0.33	H→L+1	523.6	1.52	H→L+1

[a]H=HOMO, L=LUMO.

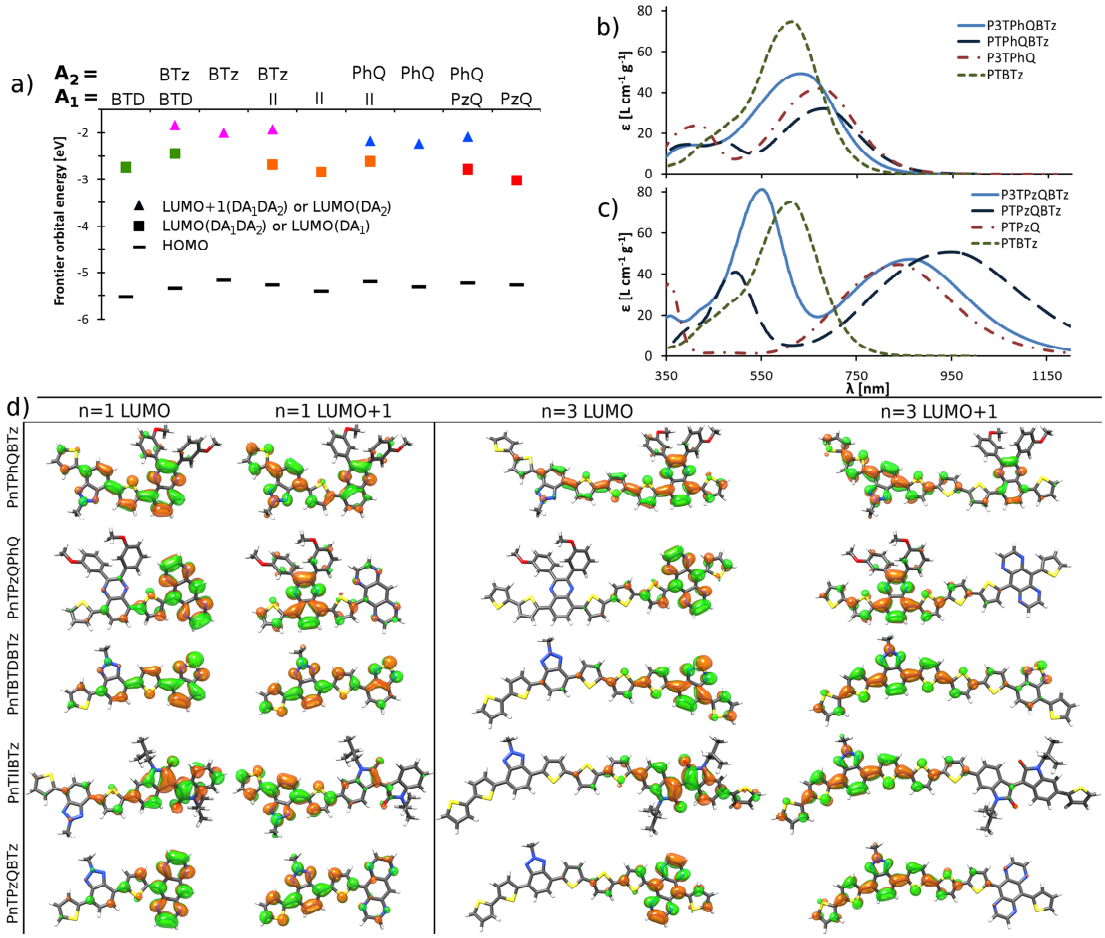

Figure 5. Calculated frontier orbital energies of a few representative D–A_1–D–A_2 polymers (one repeating unit) compared to the corresponding D–A polymers with a T donor and A_1 or A_2 (two repeating units), demonstrating the agreement between D–A LUMO to the corresponding D–A_1–D–A_2 LUMO or LUMO+1 (a). Calculated spectra of PnTPhQBTz (b) and PnTPzQBTz (c) compared to their corresponding D–A polymer calculated spectra. LUMO and LUMO+1 of the 10 computational D–A_1–D–A_2 polymers, sorted by increasing $\Delta E_{LUMO,A}$ (d). LUMO is densest on the stronger acceptor, and LUMO+1 on the weaker acceptor, but the localization is dependent on donor length and $\Delta E_{LUMO,A}$. Orbital isovalue=0.025.

As evident from Table 3, the two first, relatively intense excitations in all cases mostly correspond to transitions from HOMO to LUMO and LUMO+1 respectively. The delocalized HOMOs (see Figure S2 in the ESI) promotes good hole transport through the polymers. The HOMO, LUMO, and LUMO+1 energies are listed in Table S1 in the ESI. In agreement with our previous study,[33] each D–A_1–D–A_2 LUMO and LUMO+1 matches the corresponding D–A copolymer

LUMO both in energy (Figure 5a) and in localization (Figure 5d). All polymers exhibit LUMOs mostly situated on the stronger acceptor (right hand side in Figure 5d), and LUMO+1s on the weaker acceptors. However, in analogy to Figure 3, the localization of these orbitals on the respective acceptors is only partial, appearing more localized for longer donors and larger $\Delta E_{LUMO,A}$ (further down in Figure 5d). This is consistent with the basic molecular orbital argument outlined in Equation 1 and Figure 1, that the LUMOs of the two acceptor units interact, forming the LUMO and LUMO+1 of the copolymers/oligomers. This LUMO(A_1)–LUMO(A_2) mixing is more pronounced for small spatial and energetic separations of the constituent orbitals. So for *e.g.* P3TPzQBTz, being the extreme case of large spatial and energetic separation of the two acceptor LUMOs, the copolymer LUMO and LUMO+1 almost exclusively resemble the respective PzQ and BTz LUMOs. In PTPhQBTz conversely, the copolymer LUMO and LUMO+1 have significant character of both PhQ and BTz LUMO, due to the prominent LUMO(A_1)–LUMO(A_2) mixing afforded by a short donor and small $\Delta E_{LUMO,A}$.

The maximum absorption coefficients ε_{max} of the second absorption feature vary greatly, from 81 $Lg^{-1}cm^{-1}$ for P3TPzQBTz to 9 $Lg^{-1}cm^{-1}$ for PTPzQPhQ, appearing positively influenced by donor length and also qualitatively correlating to $\Delta E_{LUMO,A}$, see spectra in Figure 4 and listed ε_{max} in Table 4. This is rationalized from an analogy between the D–A_1 and D–A_2 parts and an excitonic J-dimer. With sufficiently strong excited state interaction, the total excited state wave functions $\Psi(S_1)$ and $\Psi(S_2)$, with corresponding transition dipole moments $M(S_1)$ and $M(S_2)$ are described by Equation 4, where ψ_1 and ψ_2 are the wave functions of the non-interacting excitonic parts with transition dipole moments μ_1 and μ_2, respectively.[76]

$$\Psi(S_1) = \frac{1}{\sqrt{2}}(\psi_1^*\psi_2 + \psi_1\psi_2^*) \quad M(S_1) = \frac{1}{\sqrt{2}}(\mu_1 + \mu_2) \qquad (4)$$

$$\Psi(S_2) = \frac{1}{\sqrt{2}}(\psi_1^*\psi_2 - \psi_1\psi_2^*) \quad M(S_2) = \frac{1}{\sqrt{2}}(\mu_1 - \mu_2)$$

With increasing interaction between the D–A_1 and D–A_2 excitonic parts, the transition to S_1 is strengthened and S_2 is weakened, since the transition dipoles μ_1 and μ_2 are approximately parallel along the polymer backbone. If conversely the excitonic interaction is small, the D–A_1 and D–A_2 absorb more independently of each other, and the D–A_1–D–A_2 spectrum resembles a combination of the corresponding D–A polymer spectra. This is visualized in Figure 5b and 5c where the calculated spectra of PnTPhQBTz and PnTPzQBTz are compared to their corresponding D–A polymers: PTPzQ, P3TPhQ, and PTBTz, showing a clear resemblance for P3TPzQBTz whose excitonic interaction is minimal (large R(A_1–A_2) and $\Delta E_{LUMO,A}$). These D–A polymers display large calculated absorption coefficients since they are based on the same small side-group ratio of 33 wt% as the D–A_1–D–A_2 polymers. The remaining three D–A_1–D–A_2 spectra are compared to their corresponding D–A polymers in Figure S3 in the ESI. The very small

$\Delta E_{LUMO,A}$ in PnTPzQPhQ and PnTPhQBTz result in such strong excitonic interaction and small calculated second $\varepsilon_{max} \leq 28$ $Lg^{-1}cm^{-1}$, that this secondary absorption feature is likely to be indistinguishable in experimental spectra, similar to the case for PTQTI in Figure 2a.

Table 4. Wavelengths (λ) and absorption coefficients (ε), of the 1st (peak) and 2nd (peak or shoulder) calculated absorption features, as well as difference in LUMO energy between the two acceptors ($\Delta E_{LUMO,A}$).

	PnTPhQBTz	PnTPzQPhQ	PnTBTBTz	PnTIIBTz	PnTPzQBTz
n=1 λ_1 [nm]	681	924	730	630	954
n=3 λ_1 [nm]	643	882	667	618	866
n=1 λ_2 [nm]	467	580	483	444	496
n=3 λ_2 [nm]	552	647	532	517	550
n=1 ε_1 [$Lg^{-1}cm^{-1}$]	32.4	35.6	63.6	64.6	50.9
n=3 ε_1 [$Lg^{-1}cm^{-1}$]	51.4	39.6	67.8	67.5	47.3
n=1 ε_2 [$Lg^{-1}cm^{-1}$]	15.9	9.1	36.1	41.2	41.1
n=3 ε_2 [$Lg^{-1}cm^{-1}$]	14.1	28.1	51.4	59.2	81.2
$\Delta E_{LUMO,A}$ [eV]	0.73	0.97	1.17	1.55	1.70

The light-harvesting capabilities of polymers in OPVs are reflected by the resulting device external quantum efficiency (EQE) which depends on the active layer (polymer + fullerene) absorbance *A*. The integration of the EQE with the solar emission spectrum gives the current of the cell. The calculated solution mass absorption coefficients of the polymer ε(poly) and of the fullerene ε($PC_{71}BM$) can be used for a rough estimation of the theoretical short circuit current J_{SC}, using a number of assumptions: film thickness d=100 nm, film densities ρ=1 g cm^{-3}, a 1:1 polymer:$PC_{71}BM$ mass ratio, full reflectivity of the bottom electrode yielding two optical passes through the active layer, and an internal quantum efficiency IQE=100% for all polymers, *i.e.* absorbed photons produce one charge each. In addition, the transition dipole moments are assumed to be perfectly parallel to the backbones of the polymers, which during spin-coating become parallel to the surface of the film. This increases the polymer absorption by a factor 1.5 compared to an 3D-isotropic solution.[77–79] Using these assumptions, the calculated solution absorption coefficients ε are transformed to film EQE according to Equation 5, and integrated with the AM 1.5 solar spectral photon flux $\Phi_{e\lambda}$ [s^{-1} m^{-2} nm^{-1}], providing an approximate estimation of J_{SC}. This permits a valuable qualitative comparison of the light-harvesting potential between polymers, although the approximations are too rough for quantitative predictions, neglecting *e.g.* effects of optical interference, internal reflection, diffuse scattering, and crystallinity.[80]

$$J_{SC}^{theo} = q_e \int_0^{\infty} \Phi_{e\lambda}^{sol} EQE \, d\lambda \approx q_e \int_0^{\infty} \Phi_{e\lambda}^{sol} (1 - 10^{-A}) \, d\lambda$$
$$\approx q_e \sum_{\lambda=350}^{2000} \Phi_{e\lambda}^{sol} \left(1 - 10^{-\frac{2d\rho\left(1.5\varepsilon(poly)+\varepsilon(PC71BM)\right)}{2}}\right) \quad (5)$$

The theoretical J_{SC} as calculated for the thirteen D–A_1–D–A_2 polymers in this and the previous section are listed in Table 5.The polymers with 3T donors yield greater theoretical J_{SC}s than the T donor polymers for most acceptor combinations, since their secondary peaks/shoulders absorb more strongly and at longer λ where the solar emission is more intense. Only in PnTBTBTz does the appreciable 1st peak redshift with the shorter T donor lead to larger estimated currents than the 3T case. Of the ten computationally modelled polymers, P3TPzQBTz exhibits the greatest theoretical J_{SC}. However, the very strong PzQ acceptor usually causes unfavorably low copolymer LUMO energies, hampering the driving force for electron transfer to the fullerene, thus limiting the device IQE, J_{SC}, and fill factor (FF).[81–84] For the same reasons of having too low LUMO energy, PBBTDPP is discarded for OPV applications. The PnTBTBTz, PnTIIBTz, and PBTDPP polymers accordingly emerge as D–A_1–D–A_2 polymer candidates with excellent spectral coverage and concomitant driving force for charge separation at the fullerene/polymer interface.

Table 5. Theoretical J_{SC} of the D–A_1–D–A_2 polymer, obtained according to Equation 5. For the sake of fair comparison, PTQTI, PBTDPP, and PBBTDPP were here assumed to have the same side-chain ratio of 33 wt% as the 10 computationally modelled polymers.

	$J_{SC,theo}$ [mA/cm^2]	
Polymer	**(n=1)**	**(n=3)**
PnTPhQBTz	14.8	16.9
PnTPzQPhQ	21.2	27.3
PnTBTBTz	24.2	21.2
PnTIIBTz	18.2	18.3
PnTPzQBTz	27.9	30.4
PTQTI	15.4	
PBTDPP	28.0	
PBBTDPP	35.8	

Proof of concept –Two D–A_1–D–A_2 polymers with superior spectral coverage

Proceeding from the knowledge obtained from the systematic computational investigation in the previous section, two promising D–A_1–D–A_2 polymers P3TQTIF and PTIIBTzF were selected for further experimental and theoretical examination. Their structures are presented in Chart 3. They both employ isoindigo as the stronger acceptor, chosen for its good spectral and electronic properties, with LUMO energies suitably aligned to PCBM LUMO.[57,56,85–88] P3TQTIF was recently synthesized and exhibits a PCE of over 7%, attributed in part to its broad absorption.[33] PTIIBTzF is here synthesized for the first time. It is a fluorinated variation of one of the best light-harvesters from the previous section. Fluorination of BTz has previously been shown to improve the performance of D–A polymers with this acceptor,[50,67,68,89] due to a lowering of the HOMO/LUMO levels, but also to an increase in absorption strength.

Chart 3. Chemical structures of P3TQTIF and PTIIBTzF. R_1=1'-octyl, R_2=1'-hexyl, R_3=5'-undecyl.

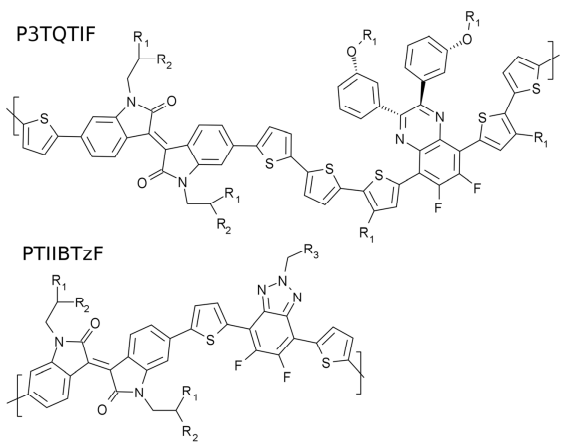

The experimental solution spectra for the two D–A_1–D–A_2 polymers are compared to the computationally predicted spectra in Figure 6a and 6b, as calculated with TD-DFT and applying Equation 3. Similarly to Figure 2, the calculated predictions in Figure 6 show good agreement with experiments concerning both relative and absolute peak intensities, as well as peak wavelengths. For both polymers, the calculated predictions overestimate the ε_{max} and E_{abs} slightly. While P3TQTIF displays only one resolved absorption feature ≥ 450 nm, the spectrum of PTIIBTzF reveals a pronounced secondary peak at ~450 nm. PTIIBTzF exhibits a calculated ε_{max} practically identical to the non-fluorinated PTIIBTz: 55 $Lg^{-1}cm^{-1}$ if using the experimental side-chain mass, and 63 $Lg^{-1}cm^{-1}$ if assuming 33 wt% side-chains as in the previous section. The calculated first peak λ_{max} blue-shifts by 19

nm upon fluorination, which is rationalized from the placement of the fluorine atoms on the BTz acceptor where LUMO has negligible density, leading to greater stabilization of HOMO than of LUMO. The second peak λ_{max} is redshifted with fluorination due to a stabilization of LUMO+1.

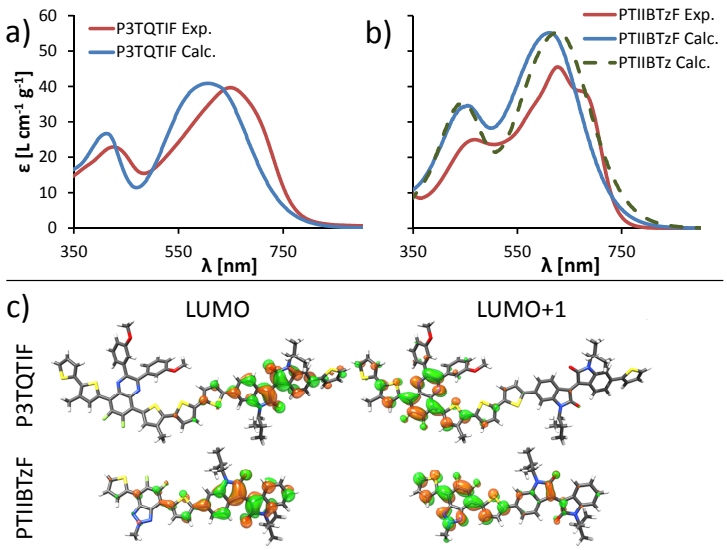

Figure 6. Absorption spectra, experimental and as calculated, of P3TQTIF (a), and PTIIBTzF, compared its non-fluorinated variant PTIIBTz (b). Monomer LUMO and LUMO+1 of both P3TQTIF and PTIIBTzF, partly localized on the respective stronger and weaker acceptors (c). Orbital isovalue=0.025.

The electronic transitions for P3TQTIF and PTIIBTzF were calculated with TD-DFT for both mono- and dimers. The monomer results are presented in Table 6, due to the more pure orbital and transition characteristics of these smaller systems compared to dimers. Table 6 reveals a behavior analogous to that of the 10 polymers from the previous section: the two strongest low energy excitations are of respectively HOMO→LUMO and HOMO→LUMO+1 character. Copolymer LUMO and LUMO+1 again correspond mainly to the LUMOs of the respective acceptors, see Figure 6c. See Table S1 in the ESI for orbital energies, and Figure S4 in the ESI for the HOMO and LUMO+2 orbitals.

Table 6. Wavelengths, oscillator strengths and dominant orbital contributions of the four strongest calculated transitions for P3TQTIF and PTIIBTzF monomers.[a]

P3TQTIF			PTIIBTzF		
λ_{abs} [nm]	f	Orbitals	λ_{abs} [nm]	f	Orbitals
643	1.57	H→L	558	0.93	H→L
558	0.43	H→L+1	462	0.26	H-2→L
539	0.15	H-1→L	423	0.63	H→L+1
421	0.95	H→L+2	302	0.14	H→L+2

[a]H=HOMO, L=LUMO.

In PTIIBTzF the transitions to LUMO and LUMO+1 are responsible for the two respective absorption peaks, as demonstrated in Table 6 and Figure 6c. For P3TQTIF however, the absorption peak at ~400 nm in P3TQTIF is a non-CT, $\pi \rightarrow \pi^*$ transition, analogous to the typical case for D–A polymers. The HOMO→LUMO+1 transition in P3TQTIF is too weak and too close in wavelength to the stronger HOMO→LUMO transition for it to be resolved as a secondary peak or even a discernable shoulder. However, this CT transition to PhQ is the reason for the particularly wide absorption peak as seen here in Figure 6a and as previously reported for P3TQTIF, thus contributing to its total light-harvesting capability and the resulting excellent J_{SC} and good PCE of 15.5 mA/cm^2 and 7.0 %.[33] This demonstrates that the D–A_1–D–A_2 motif can be advantageous even when the two absorption features in the low-energy region are not resolved. The theoretical J_{SC}s based on calculated solution spectra, introduced in Equation 5, amount to 14.6 and 17.2 mA/cm^2 for P3TQTIF and PTIIBTzF respectively, assuming 33 wt% side-chains. This rough estimate is for P3TQTIF slightly lower than the experimental J_{SC}, mainly assigned to the ~40 nm underestimation of its calculated absorption apparent in Figure 6a.

P3TQTIF exhibits better spectral coverage than most D–A polymers. But the fact that it is poorer than for many of the D–A_1–D–A_2 polymers studied here, and yet produces an impressive experimental J_{SC} of 15.5 mA/cm^2, is very encouraging for the continued development of new D–A_1–D–A_2 polymers. For example, BTz combined with BT or II acceptors constitute copolymer designs which here are predicted to display superior spectral coverage compared to existing polymers.

Conclusions

The D–A_1–D–A_2 motif for conjugated polymers is attractive for organic photovoltaic (OPV) purposes, already having achieved a 7% PCE in bulk heterojunction solar cells.[33] Their advantage over D–A polymers resides in their potential for enhanced spectral coverage facilitated by employing two acceptors

with complementary absorption properties. However, the molecular electronic structure governing the optical properties of D–A_1–D–A_2 has not previously been studied in a systematic way. We here use a DFT-based computational strategy to assess the electronic and optical traits of 15 D–A_1–D–A_2 copolymer candidates, with careful comparison to selected experimental spectra warranting the validity of the calculations.

All polymers show intense primary absorption peaks originating from electronic transitions HOMO→LUMO, where LUMO mainly corresponds to the LUMO of the stronger acceptor. Copolymer LUMO+1 predominantly displays character of the weaker acceptor LUMO, and electronic transitions to this orbital are responsible for additional absorption features ~450–650 nm. The intensity and wavelength of these secondary features are shown to be strongly dependent on the respective acceptor LUMOs' separation in space ($R(A_1–A_2)$) and energy ($\Delta E_{LUMO,A}$). This is rationalized from a MO argument: the two acceptor LUMOs interact and mix, forming the copolymer LUMO and LUMO+1, where the degree of mixing is proportional to $e^{-R(A-A)}/\Delta E_{LUMO,A}$, affecting the λ_{max} splitting between the 1st and 2nd absorption peaks. The second peak/shoulder intensity is positively influenced by a small LUMO(A_1)–LUMO(A_2) interaction, to the point where for weak interactions, the absorption profile of the D–A_1–D–A_2 polymer appears similar to a combination of the corresponding two D–A polymer spectra. For the strong LUMO–LUMO mixing cases conversely, the first transition dominates and the addition of the second acceptor loses its effect on the optical response of the polymer. Consequently, copolymers with the weak BTz acceptor and an adequately strong acceptor such as II or BT display excellent spectral coverage *via* dual peak absorption, and are expected to result in efficient OPVs, in particular if combined with a spatially separating donor segment such as terthiophene.

In a broader perspective, strictly alternating D–A_1–D–A_2 polymers are still uncommon, although the motif has proven its ability to yield efficient solar cells due to an enhanced spectral coverage with potential for additional absorption features $\gtrsim$ 450 nm, where the solar emission is intense. These features derive from optically allowed charge-transfer transitions to the LUMO+1 of the copolymers, an excitation which normally is forbidden in D–A polymers. The D–A_1–D–A_2 concept thus constitutes a fundamentally advantageous fourth strategy to extend the spectral coverage of polymer solar cells, beyond tandem, ternary, or polymer–polymer solar cells. We demonstrate the usefulness of quantum chemical calculations, offering deeper insight into the structure–property relation with respect to the choice of acceptors and donor, and the resulting optical and electronic properties of copolymers. The accuracy of the calculations is furthermore demonstrated to approach the level required for quantitative prediction of absorption spectra. Our computational approach serves to guide the development of new D–A_1–D–A_2 polymers with superior light-harvesting capabilities. Specifically, we advise the design of copolymers with three key parameters: 1) a similarly strong intrinsic absorptivity of D–A_1 and D–A_2, and a

weak LUMO(A_1)–LUMO(A_2) interaction as achieved by 2) extended donor segments and 3) substantial difference in LUMO energy between the two acceptors. The success of this approach for rational design of polymers with superior spectral coverage was, to conclude, demonstrated through the proof-of-concept synthesis and characterization of two new D–A_1–D–A_2 polymers with excellent light-harvesting capabilities.

Electronic supplementary information

Electronic supplementary information (ESI) available: D–A_1–D–A_2 planarity and calculated frontier orbital energies. Correlation between acceptor unit LUMO energies, copolymer LUMO energies, and second absorption peak/shoulder intensity. LUMO+2 for P3TQTIF and PTIIBTzF. Synthesis details for PTIIBTzF.

Acknowledgements

The work was funded by the Swedish research council (VR), the Knut and Alice Wallenberg (KAW) Foundation, and The Swedish Energy Agency (Energimyndigheten). NSC and LUNARC are acknowledged for computer resources used.

References

(1) Jackson, N. E.; Savoie, B. M.; Marks, T. J.; Chen, L. X.; Ratner, M. A. *J. Phys. Chem. Lett.* **2015**, *6* (1), 77.

(2) Wang, E.; Mammo, W.; Andersson, M. R. *Adv. Mater.* **2014**, *26* (12), 1801.

(3) Li, Y. *Acc. Chem. Res.* **2012**, *45* (5), 723.

(4) Li, G.; Zhu, R.; Yang, Y. *Nat. Photonics* **2012**, *6* (3), 153.

(5) Zhou, H.; Yang, L.; You, W. *Macromolecules* **2012**, *45* (2), 607.

(6) Liu, Y.; Zhao, J.; Li, Z.; Mu, C.; Ma, W.; Hu, H.; Jiang, K.; Lin, H.; Ade, H.; Yan, H. *Nat. Commun.* **2014**, *5*.

(7) You, J.; Dou, L.; Yoshimura, K.; Kato, T.; Ohya, K.; Moriarty, T.; Emery, K.; Chen, C.-C.; Gao, J.; Li, G.; Yang, Y. *Nat. Commun.* **2013**, *4*, 1446.

(8) Kim, J. Y.; Lee, K.; Coates, N. E.; Moses, D.; Nguyen, T.-Q.; Dante, M.; Heeger, A. J. *Science* **2007**, *317* (5835), 222.

(9) Tang, Z.; George, Z.; Ma, Z.; Bergqvist, J.; Tvingstedt, K.; Vandewal, K.; Wang, E.; Andersson, L. M.; Andersson, M. R.; Zhang, F.; Inganäs, O. *Adv. Energy Mater.* **2012**, *2* (12), 1467.

(10) Li, W.; Furlan, A.; Hendriks, K. H.; Wienk, M. M.; Janssen, R. A. J. *J. Am. Chem. Soc.* **2013**, *135* (15), 5529.

(11) Zhou, E.; Cong, J.; Wei, Q.; Tajima, K.; Yang, C.; Hashimoto, K. *Angew. Chem. Int. Ed.* **2011**, *50* (12), 2799.

(12) Li, W.; Roelofs, W. S. C.; Turbiez, M.; Wienk, M. M.; Janssen, R. A. J. *Adv. Mater.* **2014**, *26* (20), 3304.

(13) Zhou, Y.; Kurosawa, T.; Ma, W.; Guo, Y.; Fang, L.; Vandewal, K.; Diao, Y.; Wang, C.; Yan, Q.; Reinspach, J.; Mei, J.; Appleton, A. L.; Koleilat, G. I.; Gao, Y.; Mannsfeld, S. C. B.; Salleo, A.; Ade, H.; Zhao, D.; Bao, Z. *Adv. Mater.* **2014**, *26* (22), 3767.

(14) Khlyabich, P. P.; Burkhart, B.; Thompson, B. C. *J. Am. Chem. Soc.* **2012**, *134* (22), 9074.

(15) Lu, L.; Xu, T.; Chen, W.; Landry, E. S.; Yu, L. *Nat. Photonics* **2014**, *8* (9), 716.

(16) Gu, Y.; Wang, C.; Liu, F.; Chen, J.; Dyck, O. E.; Duscher, G.; Russell, T. P. *Energy Environ. Sci.* **2014**, *7* (11), 3782.

(17) Goubard, F.; Wantz, G. *Polym. Int.* **2014**, *63* (8), 1362.

(18) Ameri, T.; Khoram, P.; Min, J.; Brabec, C. J. *Adv. Mater.* **2013**, *25* (31), 4245.

(19) Facchetti, A. *Mater. Today* **2013**, *16* (4), 123.

(20) McNeill, C. R. *Energy Environ. Sci.* **2012**, *5* (2), 5653.

(21) Burkhart, B.; Khlyabich, P. P.; Thompson, B. C. *ACS Macro Lett.* **2012**, *1* (6), 660.

(22) Tamilavan, V.; Roh, K. H.; Agneeswari, R.; Lee, D. Y.; Cho, S.; Jin, Y.; Park, S. H.; Hyun, M. H. *J. Mater. Chem. A* **2014**, *2*, 20126.

(23) Jiang, J.-M.; Chen, H.-C.; Lin, H.-K.; Yu, C.-M.; Lan, S.-C.; Liu, C.-M.; Wei, K.-H. *Polym. Chem.* **2013**, *4* (20), 5321.

(24) Jung, J. W.; Liu, F.; Russell, T. P.; Jo, W. H. *Energy Environ. Sci.* **2013**, *6* (11), 3301.

(25) Dang, D.; Chen, W.; Yang, R.; Zhu, W.; Mammo, W.; Wang, E. *Chem. Commun.* **2013**, *49* (81), 9335.

(26) Sun, W.; Ma, Z.; Dang, D.; Zhu, W.; Andersson, M. R.; Zhang, F.; Wang, E. *J. Mater. Chem. A* **2013**, *1* (37), 11141.

(27) Kronemeijer, A. J.; Gili, E.; Shahid, M.; Rivnay, J.; Salleo, A.; Heeney, M.; Sirringhaus, H. *Adv. Mater.* **2012**, *24* (12), 1558.

(28) Sonar, P.; Singh, S. P.; Li, Y.; Soh, M. S.; Dodabalapur, A. *Adv. Mater.* **2010**, *22* (47), 5409.

(29) Albert-Seifried, S.; Ko, D.-H.; Huttner, S.; Kanimozhi, C.; Patil, S.; Friend, R. H. *Phys. Chem. Chem. Phys.* **2014**, *16* (14), 6743.

(30) Yuen, J. D.; Fan, J.; Seifter, J.; Lim, B.; Hufschmid, R.; Heeger, A. J.; Wudl, F. *J. Am. Chem. Soc.* **2011**, *133* (51), 20799.

(31) Subramaniyan, S.; Kim, F. S.; Ren, G.; Li, H.; Jenekhe, S. A. *Macromolecules* **2012**, *45* (22), 9029.

(32) Balan, B.; Vijayakumar, C.; Saeki, A.; Koizumi, Y.; Seki, S. *Macromolecules* **2012**, *45* (6), 2709.

(33) Tao, Q.; Xia, Y.; Xu, X.; Hedström, S.; Bäcke, O.; James, D. I.; Persson, P.; Olsson, E.; Inganäs, O.; Hou, L.; Zhu, W.; Wang, E. *Macromolecules* **2015**, *48* (4), 1009.

(34) Kang, T. E.; Kim, K.-H.; Kim, B. J. *J. Mater. Chem. A* **2014**, *2* (37), 15252.

(35) Rauk, A. *Orbital Interaction Theory of Organic Chemistry*; Wiley: New York, 2004.

(36) Hedström, S.; Henriksson, P.; Wang, E.; Andersson, M. R.; Persson, P. *Phys. Chem. Chem. Phys.* **2014**, *16* (45), 24853.

(37) Hedström, S.; Persson, P. *J. Phys. Chem. C* **2012**, *116* (51), 26700.

(38) Jackson, N. E.; Savoie, B. M.; Kohlstedt, K. L.; Marks, T. J.; Chen, L. X.; Ratner, M. A. *Macromolecules* **2014**, *47* (3), 987.

(39) Mothy, S.; Guillaume, M.; Idé, J.; Castet, F.; Ducasse, L.; Cornil, J.; Beljonne, D. *J. Phys. Chem. Lett.* **2012**, *3* (17), 2374.

(40) Ma, H.; Qin, T.; Troisi, A. *J. Chem. Theory Comput.* **2014**, *10* (3), 1272.

(41) Frisch, M.; Trucks, G.; Schlegel, H.; Scuseria, G.; Robb, M.; Cheeseman, J.; Scalmani, G.; Barone, V.; Mennucci, B.; Petersson, G.; Nakatsuji, H.; Caricato, M.; Li, X.; Hratchian, H.; Izmaylov, A.; Bloino, J.; Zheng, G.; Sonnenberg, J.; Hada, M.; Ehara, M.; Toyota, K.; Fukuda, R.; Hasegawa, J.; Ishida, M.; Nakajima, T.; Honda, Y.; Kitao, O.; Nakai, H.; Vreven, T.; Montgomery, J.; Peralta, J.; Ogliaro, F.; Bearpark, M.; Heyd, J.; Brothers, E.; Kudin, K.; Staroverov, V.; Kobayashi, R.; Normand, J.; Raghavachari, K.; Rendell, A.; Burant, J.; Iyengar, S.; Tomasi, J.; Cossi, M.; Rega, N.; Millam, J.; Klene, M.; Knox, J.; Cross, J.; Bakken, V.; Adamo, C.; Jaramillo, J.; Gomperts, R.; Stratmann, R.; Yazyev, O.; Austin, A.; Cammi, R.; Pomelli, C.; Ochterski, J.; Martin, R.; Morokuma, K.; Zakrzewski, V.; Voth, G.; Salvador, P.; Dannenberg, J.; Dapprich, S.; Daniels, A.; Farkas; Foresman, J.; Ortiz, J.; Cioslowski, J.; Fox, D. Gaussian 09, Revision A.02, 2009.

(42) Adamo, C.; Barone, V. *J. Chem. Phys.* **1999**, *110* (13), 6158.

(43) Atkins, P.; Friedman, R. *Molecular Quantum Mechanics*, 4th ed.; Oxford University Press: New York, 2005.

(44) Cornil, J.; Gueli, I.; Dkhissi, A.; Sancho-Garcia, J. C.; Hennebicq, E.; Calbert, J. P.; Lemaur, V.; Beljonne, D.; Bredas, J. L. *J. Chem. Phys.* **2003**, *118* (14), 6615.

(45) Ford, W. K.; Duke, C. B.; Salaneck, W. R. *J. Chem. Phys.* **1982**, *77* (10), 5030.

(46) Steckler, T. T.; Zhang, X.; Hwang, J.; Honeyager, R.; Ohira, S.; Zhang, X.-H.; Grant, A.; Ellinger, S.; Odom, S. A.; Sweat, D.; Tanner, D. B.; Rinzler, A. G.; Barlow, S.; Brédas, J.-L.; Kippelen, B.; Marder, S. R.; Reynolds, J. R. *J. Am. Chem. Soc.* **2009**, *131* (8), 2824.

(47) Tao, J.; Tretiak, S.; Zhu, J.-X. *Phys. Rev. B* **2009**, *80* (23), 235110.

(48) Hu, B.; Zhang, J. *Polymer* **2009**, *50* (25), 6172.

(49) Hedström, S.; Henriksson, P.; Wang, E.; Andersson, M. R.; Persson, P. *J. Phys. Chem. C* **2015**, *119*, 6453.

(50) Price, S. C.; Stuart, A. C.; Yang, L.; Zhou, H.; You, W. *J. Am. Chem. Soc.* **2011**, *133* (12), 4625.

(51) Zhang, Y.; Chien, S.-C.; Chen, K.-S.; Yip, H.-L.; Sun, Y.; Davies, J. A.; Chen, F.-C.; Jen, A. K.-Y. *Chem. Commun.* **2011**, *47* (39), 11026.

(52) Son, H. J.; Wang, W.; Xu, T.; Liang, Y.; Wu, Y.; Li, G.; Yu, L. *J. Am. Chem. Soc.* **2011**, *133* (6), 1885.

(53) Yuen, J. D.; Kumar, R.; Zakhidov, D.; Seifter, J.; Lim, B.; Heeger, A. J.; Wudl, F. *Adv. Mater.* **2011**, *23* (33), 3780.

(54) Dexter Tam, T. L.; Salim, T.; Li, H.; Zhou, F.; Mhaisalkar, S. G.; Su, H.; Lam, Y. M.; Grimsdale, A. C. *J. Mater. Chem.* **2012**, *22* (35), 18528.

(55) Schulz, G. L.; Mastalerz, M.; Ma, C.-Q.; Wienk, M.; Janssen, R.; Bäuerle, P. *Macromolecules* **2013**, *46* (6), 2141.

(56) Stalder, R.; Mei, J.; Reynolds, J. R. *Macromolecules* **2010**, *43* (20), 8348.

(57) Wang, E.; Ma, Z.; Zhang, Z.; Vandewal, K.; Henriksson, P.; Inganäs, O.; Zhang, F.; Andersson, M. R. *J. Am. Chem. Soc.* **2011**, *133* (36), 14244.

(58) Lei, T.; Cao, Y.; Zhou, X.; Peng, Y.; Bian, J.; Pei, J. *Chem. Mater.* **2012**, *24* (10), 1762.

(59) Zhou, H.; Yang, L.; Xiao, S.; Liu, S.; You, W. *Macromolecules* **2010**, *43* (2), 811.

(60) Beaujuge, P. M.; Amb, C. M.; Reynolds, J. R. *Acc. Chem. Res.* **2010**, *43* (11), 1396.

(61) Gibson, G. L.; McCormick, T. M.; Seferos, D. S. *J. Am. Chem. Soc.* **2011**, *134* (1), 539.

(62) Chan, W. K.; Chen, Y.; Peng, Z.; Yu, L. *J. Am. Chem. Soc.* **1993**, *115* (25), 11735.

(63) Hendriks, K. H.; Heintges, G. H. L.; Gevaerts, V. S.; Wienk, M. M.; Janssen, R. A. J. *Angew. Chem. Int. Ed.* **2013**, *52* (32), 8341.

(64) Lee, Y.; Nam, Y. M.; Jo, W. H. *J. Mater. Chem.* **2011**, *21* (24), 8583.

(65) Dang, D.; Chen, W.; Himmelberger, S.; Tao, Q.; Lundin, A.; Yang, R.; Zhu, W.; Salleo, A.; Müller, C.; Wang, E. *Adv. Energy Mater.* **2014**, *4*, 1400680.

(66) Xu, X.; Li, Z.; Backe, O.; Bini, K.; James, D. I.; Olsson, E.; Andersson, M. R.; Wang, E. *J. Mater. Chem. A* **2014**, *2*, 18988.

(67) Min, J.; Zhang, Z.-G.; Zhang, S.; Li, Y. *Chem. Mater.* **2012**, *24* (16), 3247.

(68) Min, J.; Zhang, Z.-G.; Zhang, M.; Li, Y. *Polym. Chem.* **2013**, *4* (5), 1467.

(69) Uy, R. L.; Yan, L.; Li, W.; You, W. *Macromolecules* **2014**, *47* (7), 2289.

(70) Tanimoto, A.; Yamamoto, T. *Macromolecules* **2006**, *39* (10), 3546.

(71) Akbaşoğlu, N.; Balan, A.; Baran, D.; Cirpan, A.; Toppare, L. *J. Polym. Sci. Polym. Chem.* **2010**, *48* (23), 5603.

(72) Hendriks, K. H.; Heintges, G. H. L.; Wienk, M. M.; Janssen, R. A. J. *J. Mater. Chem. A* **2014**, *2* (42), 17899.

(73) Salvatori, P.; Mosconi, E.; Wang, E.; Andersson, M.; Muccini, M.; De Angelis, F. *J. Phys. Chem. C* **2013**, *117* (35), 17940.

(74) Ma, Z.; Wang, E.; Jarvid, M. E.; Henriksson, P.; Inganäs, O.; Zhang, F.; Andersson, M. R. *J. Mater. Chem.* **2012**, *22* (5), 2306.

(75) Schroeder, B. C.; Huang, Z.; Ashraf, R. S.; Smith, J.; D'Angelo, P.; Watkins, S. E.; Anthopoulos, T. D.; Durrant, J. R.; McCulloch, I. *Adv. Funct. Mater.* **2012**, *22* (8), 1663.

(76) Lanzani, G. *The Photophysics behind Photovoltaics and Photonics*; Wiley: New York, 2012.

(77) Campoy-Quiles, M.; Alonso, M. I.; Bradley, D. D. C.; Richter, L. J. *Adv. Funct. Mater.* **2014**, *24* (15), 2116.

(78) Campoy-Quiles, M.; Etchegoin, P. G.; Bradley, D. D. C. *Phys. Rev. B* **2005**, *72* (4), 045209.

(79) Marshall, G. M.; Lopinski, G. P.; Bensebaa, F.; Dubowski, J. J. *Langmuir* **2009**, *25* (23), 13561.

(80) Burkhard, G. F.; Hoke, E. T.; McGehee, M. D. *Adv. Mater.* **2010**, *22* (30), 3293.

(81) Peng, Q.; Liu, X.; Qin, Y.; Xu, J.; Li, M.; Dai, L. *J. Mater. Chem.* **2011**, *21* (21), 7714.

(82) Zhang, F.; Bijleveld, J.; Perzon, E.; Tvingstedt, K.; Barrau, S.; Inganäs, O.; Andersson, M. R. *J. Mater. Chem.* **2008**, *18* (45), 5468.

(83) Yi Zhou; Gedefaw, D. A.; Hellström, S.; Krätschmer, I.; Zhang, F.; Mammo, W.; Inganäs, O.; Andersson, M. R. *IEEE J. Sel. Top. Quantum Electron.* **2010**, *16* (6), 1565.

(84) Hellström, S.; Zhang, F.; Inganäs, O.; Andersson, M. R. *Dalton Trans.* **2009**, No. 45, 10032.

(85) Fang, L.; Zhou, Y.; Yao, Y.-X.; Diao, Y.; Lee, W.-Y.; Appleton, A. L.; Allen, R.; Reinspach, J.; Mannsfeld, S. C. B.; Bao, Z. *Chem. Mater.* **2013**, *25* (24), 4874.

(86) Ma, Z.; Sun, W.; Himmelberger, S.; Vandewal, K.; Tang, Z.; Bergqvist, J.; Salleo, A.; Andreasen, J. W.; Inganäs, O.; Andersson, M. R.; Muller, C.; Zhang, F.; Wang, E. *Energy Environ. Sci.* **2014**, *7* (1), 361.

(87) Deng, Y.; Liu, J.; Wang, J.; Liu, L.; Li, W.; Tian, H.; Zhang, X.; Xie, Z.; Geng, Y.; Wang, F. *Adv. Mater.* **2014**, *26* (3), 471.

(88) Stalder, R.; Mei, J.; Graham, K. R.; Estrada, L. A.; Reynolds, J. R. *Chem. Mater.* **2013**, *26* (1), 664.

(89) Pasker, F. M.; Klein, M. F. G.; Sanyal, M.; Barrena, E.; Lemmer, U.; Colsmann, A.; Höger, S. *J. Polym. Sci. Polym. Chem.* **2011**, *49* (23), 5001.

Paper VII

Reprinted with permission from Macromolecules, **2015**, *48* (4), 1009–1016.

Macromolecules

Article

pubs.acs.org/Macromolecules

D−A_1−D−A_2 Copolymers with Extended Donor Segments for Efficient Polymer Solar Cells

Qiang Tao,[†,‡] Yuxin Xia,[∥] Xiaofeng Xu,[‡] Svante Hedström,[⊥] Olof Bäcke,[§] David I. James,[‡] Petter Persson,[⊥] Eva Olsson,[§] Olle Inganäs,[∥] Lintao Hou,*[,#] Weiguo Zhu,*[,†] and Ergang Wang*[,‡]

[†]Key Lab of Environment-Friendly Chemistry and Application in Ministry of Education, College of Chemistry, Xiangtan University, Xiangtan 411105, China

[‡]Department of Chemistry and Chemical Engineering/Polymer Technology and [§]Department of Applied Physics, Chalmers University of Technology, SE-412 96 Göteborg, Sweden

[∥]Biomolecular and Organic Electronics, IFM, Linköping University, SE-581 83 Linköping, Sweden

[⊥]Division of Theoretical Chemistry, Lund University, P.O. Box 124, SE-221 00 Lund, Sweden

[#]Siyuan Laboratory, Department of Physics, Jinan University, Guangzhou 510632, China

● *Supporting Information*

ABSTRACT: Typically a donor−acceptor (D−A) design strategy is used for engineering the bandgap of polymers for solar cells. However, in this work, a series of alternating D−A_1−D−A_2 copolymers P*n*TQTI(F) were synthesized and characterized with oligothiophenes (*n*T, *n* = 1, 2, 3) as the donor and two electron-deficient moieties, quinoxaline and isoindigo, as the acceptors in the repeating unit. We have studied the influence of the donor segments with different numbers of thiophene units and the effect of the addition of fluorine to the quinoxaline unit of the D−A_1−D−A_2 polymers. The photophysical, electrochemical, and photovoltaic properties of the polymers were examined via a range of techniques and related to theoretical simulations. On increasing the length of the donor thiophene units, broader absorption spectra were observed in addition to a sequential increase in HOMO levels, while the LUMO levels displayed very small variations. The addition of fluorine to the quinoxaline unit not only decreased the HOMO levels of the resulting polymers but also enhanced the absorption coefficients. A superior photovoltaic performance was observed for the P3TQTI-F-based device with a power conversion efficiency (PCE) of 7.0%, which is the highest efficiency for alternating D−A_1−D−A_2 polymers reported to date. The structure−property correlations of the P*n*TQTI(F) polymers demonstrate that varying of the length of the donor segments is a valuable method for designing high-performance D−A_1−D−A_2 copolymers and highlight the promising nature of D−A_1−D−A_2 copolymers for efficient bulk-heterojunction solar cells.

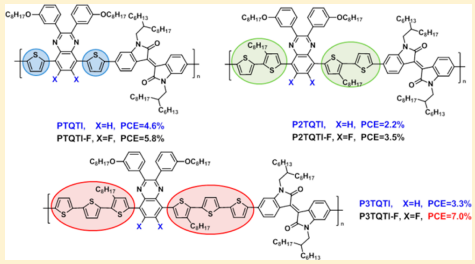

■ INTRODUCTION

Conjugated polymers have gained much attention due to their potential for use in flexible, lightweight, and low-cost solar energy harvesting devices.[1−5] The recent significant increase in power conversion efficiency (PCE) of polymer/fullerene polymer solar cells (PSCs) largely originates from the successful development of new electron-donor polymers.[6−11] Conjugated donor−acceptor copolymers, combining an electron-donating (D) and an electron-withdrawing (A) moiety, are particularly promising candidates now.[12−15] D−A copolymers can facilitate the fine-tuning of absorption bands, charge transporting properties, and HOMO/LUMO levels via tailoring the D−A interaction and π-electron delocalization. To date, a number of successful electron-withdrawing units have been identified, such as 2,1,3-benzothiadiazole (BT),[16,17] quinoxaline,[18−20] pyrrolo[3,4-*c*]pyrrole-1,4-dione (DPP),[21,22] thieno[3,4-*c*]pyrrole-4,6-dione (TPD),[23−25] and isoindigo.[26−34] In our previous work, we found that quinoxaline is an easily synthesized and weak acceptor for high-performance D−A copolymers.[19,35−37] The polymer TQ1 shows promising photophysical properties with a broad absorption spectrum and an optical bandgap of 1.7 eV. The HOMO and LUMO levels are located in a suitable position matching well with that of [6,6]-phenyl-C_{71}-butyric acid methyl ester ($PC_{71}BM$) and result in a high open-circuit voltage (V_{oc}) of 0.9 V. Another promising polymer series we focused on are polymers based on an isoindigo acceptor unit, with the LUMO levels of the isoindigo-based polymers being mainly localized on the isoindigo unit, while their HOMO levels could be easily tuned via the judicious selection of electron-donating

Received: October 27, 2014
Revised: January 23, 2015
Published: February 9, 2015

DOI: 10.1021/ma502186g
Macromolecules 2015, 48, 1009−1016

Scheme 1. Synthetic Routes of the Polymers P2TQTI(F) and P3TQTI(F) and the Structures of the Six Copolymers

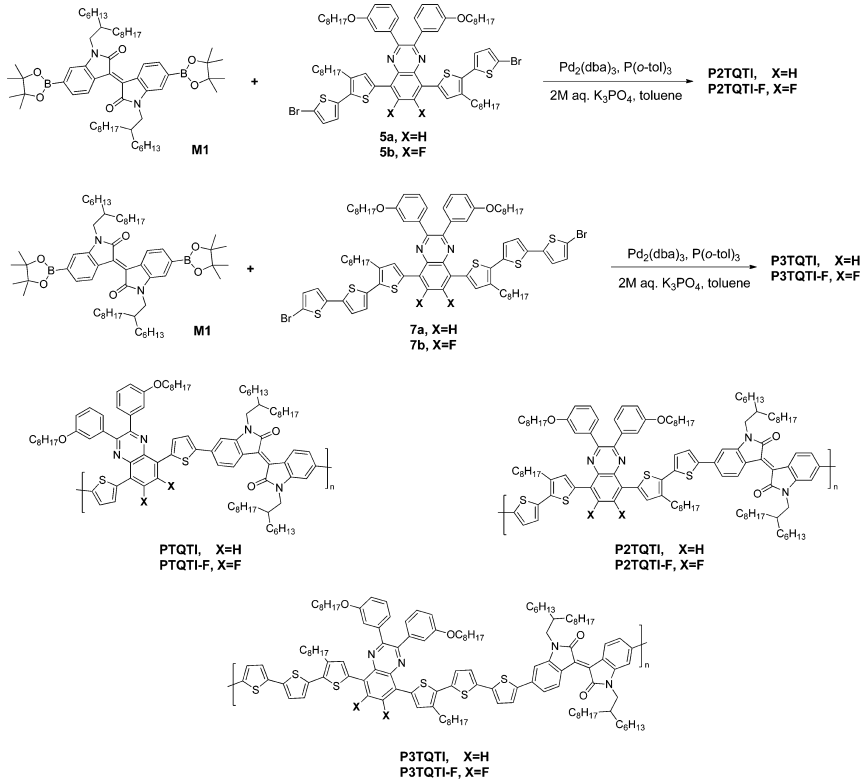

units.[31,32,38−40] However, the normal D−A copolymers synthesized present two absorption bands, which are not very broad. To combine the advantages of two chromophores and extend the absorption spectrum, a new class of D−A_1−D−A_2 copolymers containing two electron-deficient moieties as the acceptors was developed.[41−43] The first comparative study between the D−A_1−D−A_2 alternating copolymers and the corresponding D−A_1 and D−A_2 polymers was reported in our previous work.[44] We synthesized an alternating D−A_1−D−A_2 polymer PTQTI via incorporating two electron-withdrawing moieties (quinoxaline and isoindigo) with thiophenes as the electron-donating units. The polymer PTQTI showed a broader absorption spectrum than the corresponding D−A polymer TQ1[19] and PTI-1[31] as well as an enhanced photovoltaic performance with a PCE over 5.0%. A further enhanced PCE of 6.3% was achieved via attaching two fluorine atoms on the quinoxaline unit to afford the polymer PTQTI-F.[45] This previous work demonstrates that the D−A_1−D−A_2 polymer design strategy is very promising for producing highly efficient polymers for solar cells.

Another effective method for varying the bandgap of D−A copolymers is to tailor the length of the donor segment along the main chain. Recently, we systematically studied a series of benzo[1,2-*b*:3,4-*b*′]dithiophene (BDT)−isoindigo polymers, which revealed that extending the length of the thiophene donor section can enhance the absorption intensity in the high-energy band of the copolymers, resulting in higher short-circuit current density (J_{sc}) being obtained.[39] We have also studied the influence of the length of the oligothiophene building blocks on the photovoltaic properties of the thiophene−isoindigo polymers (P*n*TI). This demonstrated that the length of the oligothiophene donor segment can manipulate the LUMO to LUMO offset between the polymer and fullerene to give an appropriate driving force for charge separation and also attain an optimal morphology to achieve a high efficiency of 6.9%.[40]

Inspired by the previous work above, here we intend to make a direct comparison and explore the influence of the variation of donor length on the properties of D−A_1−D−A_2 polymers. To this end, we have synthesized four D−A_1−D−A_2 copolymers based on quinoxaline and isoindigo. Taking into account our previously developed polymers PTQTI and PTQTI-F,[45] we can compare the characteristics of the six copolymers, as the number of thiophene segments between the two electron-withdrawing moieties are varied from one to three. Two fluorine atoms were included on the weaker quinoxaline acceptor in the polymer PTQTI-F, P2TQTI-F, and P3TQTI-F in anticipation of obtaining a low-lying HOMO and an enhanced V_{oc}[46−51] (Scheme 1). For the polymer P2TQTI-

DOI: 10.1021/ma502186g
Macromolecules 2015, 48, 1009−1016

Table 1. Molecular Weights and Optical Properties of the Six Copolymers

	molecular weight[a]		solution in *o*DCB			film		
polymer	M_n (kDa)	PDI	λ_{abs} (nm)	ε_{max}[b] (L g^{-1} cm^{-1})	fwhm[c] (nm)	λ_{abs} (nm)	λ_{onset} (nm)	E_g^{opt}[d] (eV)
PTQTI	76.0	3.7	698	40.6	149	642	815	1.52
PTQTI-F	57.6	3.0	691	47.2	142	628	749	1.66
P2TQTI	25.1	4.3	655	26.4	235	667	818	1.52
P2TQTI-F	37.2	2.2	673	37.9	180	705	814	1.52
P3TQTI	19.5	2.4	642	32.3	215	646	790	1.57
P3TQTI-F	32.7	2.8	648	39.0	206	650	794	1.56

[a]Determined by GPC with 1,2,4-trichlorobenzene at 150 °C. [b]Measured from the peak at long wavelength. [c]Full width at half-maximum. [d]Band gap estimated from optical absorption band edge of the film.

(F) and P3TQTI(F), octyl side chains were incorporated on the thiophene units to ensure that the copolymers were soluble. The UV−vis absorption, electrochemical properties, film morphology, and photovoltaic performances of the copolymers were evaluated in relation to theoretical simulations. Using a conventional device structure, the polymer P3TQTI-F attains a promising PCE of 6.4%. An enhanced PCE of 7.0% was achieved after the active layer was treated with methanol. The results indicate that the length of thiophene segments directly influences the photovoltaic performance of the D−A_1−D−A_2 copolymers based on quinoxaline and isoindigo.

■ RESULTS AND DISCUSSION

Material Synthesis. The synthetic routes of the four polymers P2TQTI(F) and P3TQTI(F) are shown in Scheme 1. The synthesis of the monomer **M1** is described in our previous work.[44] The preparations of the other monomers and polymers are described in the Supporting Information. The four polymers were prepared via a modified Suzuki reaction using a $Pd_2(dba)_3$ catalyst and P(*o*-tol)$_3$ ligand in refluxing toluene. Further purification was carried out by Soxhlet extraction and column chromatography. All the polymers are readily soluble in organic solvents like chloroform, toluene, and *o*-dichlorobenzene (*o*DCB). The molecular weights of the polymers were determined by size exclusion chromatography (SEC). The molecular weights (M_n) and polydispersity index (PDI) are listed in Table 1. The polymers P2TQTI(F) and P3TQTI(F) exhibit decreased solubility, resulting in lower number-average molecular weight (M_n), when compared to the polymers PTQTI(F). The polymer P2TQTI shows a fairly large polydispersity index (PDI) of 4.3, which means the less uniform polymer main chains vary over a wide range of molecular masses. When fluorine atoms were attached to the quinoxaline unit, P2TQTI-F and P3TQTI-F achieve higher molecular weights compared to their non-fluorinated analogues. However, PTQTI-F does not follow this trend.

Optical and Electrochemical Properties. The normalized UV−vis absorption spectra of the six copolymers in *o*DCB solutions and thin films spin-coated on quartz plates are shown in Figure 1. The absorption maxima wavelength in solutions and in films, the optical band gap deduced from the film absorption onsets, and the maximum absorption coefficients in solution are summarized in Table 1. All of the copolymers show relatively broad absorptions, while increased donor length uniformly broadens the absorption (except for P2TQTI, which presents an extraordinary broad absorption band); see Table 1 for full width at half-maximum (fwhm) absorption peak widths. The low-energy absorption bands (600−750 nm) are blue-shifted as the number of thiophene units increases. This is consistent with DFT calculations that show a larger average

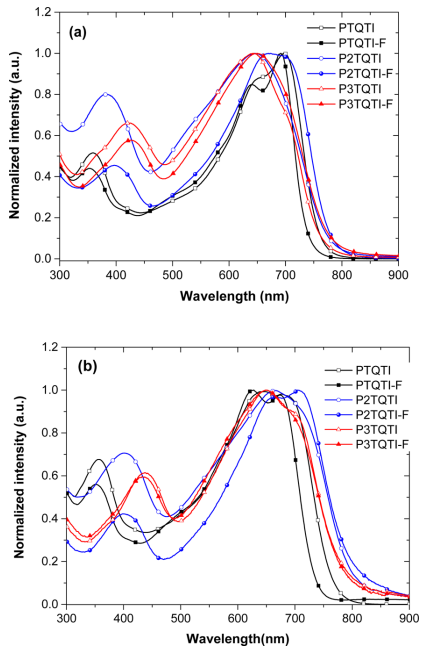

Figure 1. Normalized UV−vis absorption spectra of the copolymers (a) in *o*DCB solution and (b) in the solid state.

dihedral angle with longer donor segments; for details see the next section and Supporting Information Table S1. With increasing numbers of thiophene rings, the absorption bands in the high-energy region (350−450 nm) are red-shifted in both the solutions and films. The red-shifts of these bands are explained by their correspondence to an electronic transition that is more localized on the thiophene segments, which with an increasing number of units exhibit a smaller $\pi-\pi^*$ band gap.[52,53] To gain insight into the light harvesting ability of the polymers, the absorption coefficients at the absorption maxima for the six polymers were measured in dilute *o*DCB solutions. This shows that the fluorinated polymers exhibit higher absorption coefficients compared to their non-fluorinated counterparts. The polymer P2TQTI shows the lowest maximum extinction coefficient compared to the other polymers. In thin films, the absorption onsets of the polymers

DOI: 10.1021/ma502186g
Macromolecules 2015, 48, 1009−1016

P2TQTI(F) and P3TQTI(F) have a small red-shift compared to polymers PTQTI(F). It is noted that the fluorinated quinoxaline-containing polymer PTQTI-F shows a clear blue-shift compared to the non-fluorinated polymer PTQTI, while no similar phenomena are observed in P2TQTI(F) and P3TQTI(F).

The electrochemical properties of the copolymer thin films were characterized by cyclic voltammetry (CV). The HOMO and LUMO positions were derived from the onset of oxidation (E_{ox}) and reduction potentials (E_{red}) of the CV curves. All potentials were calibrated with the standard ferrocene/ferrocenium redox couple. According to the equations HOMO = $-(E_{ox} + 5.13)$ eV and LUMO = $-(E_{red} + 5.13)$ eV, the respective HOMO and LUMO energies (versus vacuum) are summarized in Figure 2b, where they are

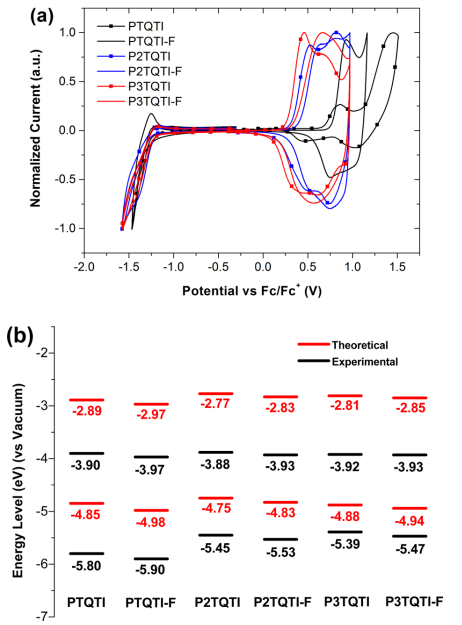

Figure 2. (a) Cyclic voltammetry (CV) plots of the six copolymers. (b) Experimental and calculated HOMO and LUMO energy levels.

compared to the monomer orbital energies as calculated with DFT. The HOMO levels of the fluorinated polymers P*n*TQTI-F are ~0.1 eV lower than that of the corresponding non-fluorinated polymers due to the electron-withdrawing nature of the fluorine atoms; thus, higher V_{oc} can be expected from fluorinated copolymers. It is noted that as the length of the donor segments are extended, the HOMO levels of the polymers increase while the LUMO levels remain unchanged, which agrees with our previous studies.[8,40]

Theoretical Simulation. To further understand the photophysical properties of the six copolymers investigated in this work, density functional theory (DFT) calculations were performed using the Gaussian 09 program package with the hybrid PBE0 correlation[54] functional and the 6-31G(d,p) basis set. Oligomers of one and two repeating units were optimized. Long alkyl side chains were truncated to shorter methyl or isopropyl groups to reduce computational time consumption. The calculated HOMO, LUMO, and LUMO+1 monomer frontier orbitals are depicted in Figure 3. The corresponding calculated orbital energies are reported in Table S1 along with the average out-of-plane dihedral angles.

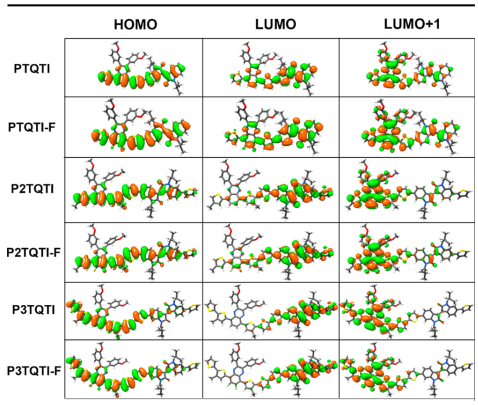

Figure 3. Calculated frontier orbitals of the copolymers with one repeating unit (isovalue = 0.015).

The calculated orbital energies are consistently overestimated compared to the experimental values due to limitations in Koopman's theorem, i.e., DFT producing nonrelaxed orbitals. However, the trendwise agreement is excellent, which is demonstrated by the practically constant LUMO energies and the clear linear relationship between calculated and experimental HOMO energies as plotted in Figure S1. All the six polymers exhibit similar LUMO levels around −3.9 eV, suggesting that the LUMO levels are basically determined by the isoindigo units, confirmed by the localization of LUMO on this, the stronger acceptor, as shown in Figure 3. The LUMOs on P*n*TQTI(F) appear very similar in shape[55] and energy[31] to the LUMOs of the D−A polymer PTI-1. The LUMO+1 conversely are in all cases more localized on the weaker acceptor quinoxaline, agreeing in shape[56] and energy[19] with the LUMO of the corresponding D−A polymer TQ1. The localization of LUMO on isoindigo and LUMO+1 on quinoxaline becomes more pronounced with longer donor segments due to increased spatial separation of the acceptor units. The HOMOs are delocalized over the backbones for the six copolymers.

Photovoltaic Properties. To evaluate the photovoltaic performances of the six copolymers, bulk-heterojunction (BHJ) solar cells with a conventional device structure ITO/PEDOT:PSS/Polymer:PCBM/LiF/Al were prepared and evaluated under an illumination of AM1.5G simulated solar light at 100 mW/cm^2. The optimized results were obtained by varying polymer:PCBM weight ratios, active layer thicknesses, and additives. Device parameters of the PSCs are summarized in Table 2. $PC_{61}BM$ was used as the acceptor instead of $PC_{71}BM$ for the polymer PTQTI(F)-based devices, which exhibited favorable morphologies and superior PCEs.[44,45] In the case of the polymers P2TQTI(F) and P3TQTI(F), the use

DOI: 10.1021/ma502186g
Macromolecules 2015, 48, 1009−1016

Table 2. Photovoltaic Parameters of the Polymer Solar Cells

polymer	ratio[a]	d^b (nm)	V_{oc} (V)	J_{sc} (mA/cm^2)	FF	PCE (%) best/av[c]
PTQTI	1:1	100	0.81	10.4	0.54	4.6/4.4
PTQTI-F	1:1	100	0.92	11.2	0.54	5.5/5.4
PTQTI-F[d]	1:1	100	0.93	12.1	0.51	5.8/5.6
P2TQTI	1:1.5	84	0.68	7.9	0.40	2.2/2.0
P2TQTI-F	1:1.5	84	0.71	8.8	0.56	3.5/3.4
P3TQTI	1:1.5	88	0.56	11.8	0.49	3.3/3.1
P3TQTI-F	1:1.5	102	0.67	14.8	0.64	6.4/6.3
P3TQTI-F[d]	1:1.5	100	0.67	15.5	0.67	7.0/6.8

[a]Polymer:PCBM weight ratio. [b]Active layer thickness (d). [c]Average values calculated from five devices. [d]The surface of active layer was washed with methanol.

of $PC_{71}BM$ can further improve the photovoltaic performance compared to $PC_{61}BM$. The processing solvent was *o*DCB with 2.5 vol % of 1,8-diiodooctane (DIO) as the additive. The optimal active layer thickness is around 100 nm for all the polymer:PCBM blend layers. The $J-V$ curves of the PSCs based on the polymers are shown in Figure 4a. Device

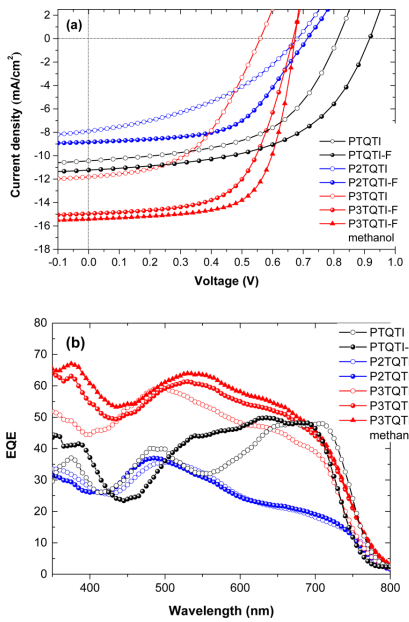

Figure 4. (a) Current density−voltage characteristics of the six polymer:PCBM solar cells. (b) Corresponding external quantum efficiency (EQE) spectra measured under illumination of monochromatic light.

performance of the OPV material often has batch to batch variations and is also very sensitive to device fabrication conditions. For a more reliable comparison, all the devices based on these six copolymers were fabricated under the same processing conditions, which can minimize unnecessary deviations. In this case, the two previously developed polymers PTQTI[44] and PTQTI-F[45] display PCEs of 4.6% and 5.5%, respectively. Compared to the non-fluorinated polymers, all of the fluorinated polymers exhibit an enhanced V_{oc}, which is ascribed to the observed trend in HOMO levels. A direct correlation between an increased number of thiophene units and a decreased V_{oc} is recorded for both the fluorinated and non-fluorinated copolymers, which can be explained by an increase in HOMO levels as the number of electron-donating units increases. The lower J_{sc} limits the PCE of the P2TQTI:$PC_{71}BM$-based device, which is possibly due to its lower absorption coefficient and larger molecular weight polydispersity. Compared to PTQTI-F, the P3TQTI-F polymer exhibits a lower V_{oc} but shows a greater J_{sc} and fill factor (FF), which thus enables it to have a superior PCE of 6.4%, partly due to its broader absorption spectrum. To further optimize the device performance, the surface of the active layer was washed with methanol. Solvent treatment of the interface is an effective method for enhancing the device parameters.[57,58] The simple solvent-fluxing process allows the formation of a graded BHJ film (donor enriched at the anode and acceptor enriched at the cathode side), which is proposed to facilitate charge extraction and to reduce charge recombination.[59] The efficiency enhancement via the methanol treatment is not obvious for the four polymers PTQTI, P2TQTI(F), and P3TQTI. The polymer PTQTI-F shows a slightly enhanced PCE of 5.8%, while the best performing device for the polymer P3TQTI-F exhibits a PCE of 7.0% with an unchanged V_{oc} and an enhanced J_{sc} and FF. Moreover, it is interesting to note that when the experimental V_{oc} of the polymers was plotted as a function of the calculated HOMO levels (in Figure S1), a strong linear correlation was found. Although there are a number of factors besides HOMO levels that can influence V_{oc}, the linear correlation observed could be valuable for simulation studies.

To investigate the accuracy of the J_{sc} from the $J-V$ measurements, the corresponding external quantum efficiencies (EQEs) of the PSCs were measured under the illumination of monochromatic light. All the J_{sc} calculated from integrating the EQE with an AM 1.5G reference spectrum agree well with the J_{sc} obtained from the $J-V$ measurements. As shown in Figure 4b, the polymers P3TQTI(F) exhibit much higher EQE values above 50% in the broad range of 400−700 nm, compared to those of polymer PTQTI(F) and P2TQTI(F). After being washed with methanol, the corresponding P3TQTI-F device shows a slightly higher EQE value, which is consistent with the $J-V$ results.

Film Morphology. In order to understand the effect of the active layer morphology on the device performance, the morphologies of all the polymer:PCBM blend films were studied by atomic force microscopy (AFM) and transmission electron microscopy (TEM). AFM measurements were carried out to study the surface morphology of the D/A blend layers, as shown in Figure S. The polymers PTQTI(F), P2TQTI, and P3TQTI(F) form continuous phase-segregated morphologies of the D/A components with a root-mean-square (RMS) roughness of between 0.9 and 1.8 nm, which depict uniform and smooth surfaces. On the contrary, the polymer P2TQTI-F exhibits larger phase segregation and a much rougher surface with an RMS value of 3.6 nm. The poor miscibility of the D/A components may give rise to this nonoptimal nanostructure, which in turn limits the photocurrent of the corresponding devices. After washing the surface of the P3TQTI-F:$PC_{71}BM$ blend layer, the RMS roughness slightly increases from 0.9 to

DOI: 10.1021/ma502186g
Macromolecules 2015, 48, 1009−1016

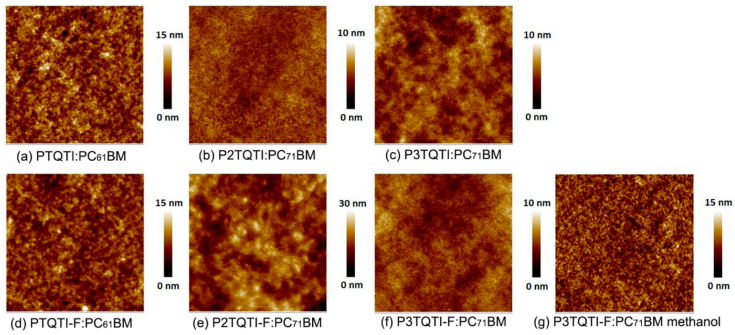

Figure 5. AFM topography ($5 \times 5\ \mu m^2$) of optimized polymer:PCBM blended layers.

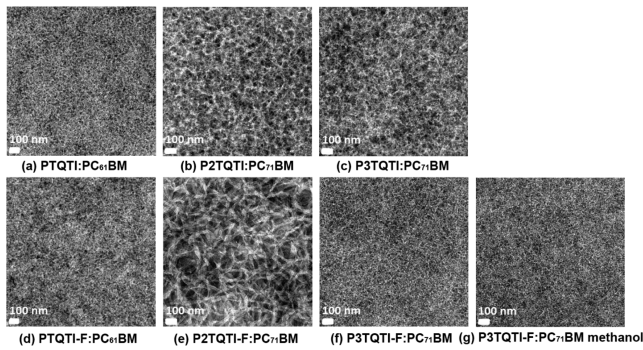

Figure 6. TEM bright-field images of optimized polymer:PCBM blended layers.

1.3 nm, as the methanol enables the development of short fibrils close to the surface.[55]

To probe the morphology throughout the active layers, TEM was carried out to investigate the real-space structures of the polymer:PCBM blends. Figure 6 shows dark and light regions representing PCBM and polymer domains, respectively. The TEM images from the films of PTQTI, PTQTI-F, and P3TQTI-F present finer features, indicating better miscibility and smaller phase separation between the polymer and the PCBM. On the contrary, the images from films of the other three polymers P2TQTI, P2TQTI-F, and P3TQTI show larger fibers bundles corresponding to the polymer domains. The large polymer domains exceed the exciton diffusion length (10 nm) and thus increases geminate recombination and reduce photocurrent.[60] The lowest performance of P2TQTI can be attributed to the synergy between its low absorption coefficient and nonoptimal morphology. The TEM image of the P2TQTI-F blend film shows a clear fibril structure of 30−40 nm in width due to polymer aggregation.[61] This is consistent with the observed low EQE values and low J_{sc} of the three copolymer-based PSCs. On the other hand, the optimal nanostructure of the film from P3TQTI-F and the high absorption coefficient and broad absorption spectrum grant this polymer an impressive J_{sc} of 15.5 mA/cm^2 with a decent FF of 0.67, which enables a PCE of up to 7.0% to be attained. There is no observable change in the TEM images of P3TQTI-F: $PC_{71}BM$ with or without methanol treatment, indicating that the methanol treatment only modifies the surface of the D/A blend layer and has no effect on the morphology of the bulk.

■ CONCLUSION

In summary, a series of D−A_1−D−A_2 copolymers based on quinoxaline/fluorinated quinoxaline and isoindigo with varying lengths of the electron-donating segments were synthesized and characterized. It was found that the addition of fluorine to the quinoxaline unit can not only decrease the HOMO levels of the polymers giving higher V_{oc}s but also enhance the absorption coefficients, which is beneficial for attaining higher J_{sc}s. The PSCs based on the polymer P2TQTI(F) and P3TQTI(F) with extended donor segments have lower V_{oc}s compared to the polymer PTQTI(F) with shorter donor segments. An optimal nanostructure, high absorption coefficient, and broad absorption spectrum of the polymer P3TQTI-F result in an impressive J_{sc} of 15.5 mA/cm^2 and a PCE of up to 7.0%. To our knowledge, this is the highest efficiency reported for an alternating D−A_1−D−A_2 copolymer in conventional BHJ PSCs. With this comparative study, the structure−property correlations of the P*n*TQTI(F) polymers demonstrate that varying the length of the donor segments is rational for designing high-performance D−A_1−D−A_2 copolymers. This design strategy is expected to be valuable for further enhancing

DOI: 10.1021/ma502186g
Macromolecules 2015, 48, 1009−1016

the photovoltaic performance of other D−A_1−D−A_2 copolymer systems.

■ ASSOCIATED CONTENT

● Supporting Information

Experimental details for monomers and polymers synthesis and characterization, polymer solar cell fabrication, and theoretical simulation results. This material is available free of charge via the Internet at http://pubs.acs.org.

■ AUTHOR INFORMATION

Corresponding Authors

*E-mail: thlt@jnu.edu.cn (L.H.).
*E-mail: zhuwg18@126.com (W.Z.).
*E-mail: ergang@chalmers.se (E.W.).

Author Contributions

Q.T. and Y.X. contributed equally to this work.

Notes

The authors declare no competing financial interest.

■ ACKNOWLEDGMENTS

We thank the Swedish Research Council, the Swedish Energy Agency, and the EU projects SUNFLOWER-"SUstainable Novel FLexible Organic Watts Efficiently Reliable" (FP7-ICT-2011-7, Grant 287594) and the National Natural Science Foundation of China (Grant 21172187) for financial support.

■ REFERENCES

(1) Chen, C.-C.; Dou, L.; Zhu, R.; Chung, C.-H.; Song, T.-B.; Zheng, Y. B.; Hawks, S.; Li, G.; Weiss, P. S.; Yang, Y. *ACS Nano* **2012**, *6*, 7185−7190.

(2) Krebs, F. C.; Espinosa, N.; Hösel, M.; Søndergaard, R. R.; Jørgensen, M. *Adv. Mater.* **2014**, *26*, 29−39.

(3) Espinosa, N.; Hosel, M.; Jorgensen, M.; Krebs, F. C. *Energy Environ. Sci.* **2014**, *7*, 855−866.

(4) Heeger, A. J. *Adv. Mater.* **2014**, *26*, 10−28.

(5) Zhan, X.; Zhu, D. *Polym. Chem.* **2010**, *1*, 409−419.

(6) He, Z.; Zhong, C.; Su, S.; Xu, M.; Wu, H.; Cao, Y. *Nat. Photonics* **2012**, *6*, 591−595.

(7) Dou, L.; Chen, C.-C.; Yoshimura, K.; Ohya, K.; Chang, W.-H.; Gao, J.; Liu, Y.; Richard, E.; Yang, Y. *Macromolecules* **2013**, *46*, 3384−3390.

(8) Dang, D.; Chen, W.; Himmelberger, S.; Tao, Q.; Lundin, A.; Yang, R.; Zhu, W.; Salleo, A.; Müller, C.; Wang, E. *Adv. Energy Mater.* **2014**, *4*, 1400680.

(9) Nguyen, T. L.; Choi, H.; Ko, S. J.; Uddin, M. A.; Walker, B.; Yum, S.; Jeong, J. E.; Yun, M. H.; Shin, T. J.; Hwang, S.; Kim, J. Y.; Woo, H. Y. *Energy Environ. Sci.* **2014**, *7*, 3040−3051.

(10) Cui, C.; Wong, W.-Y.; Li, Y. *Energy Environ. Sci.* **2014**, *7*, 2276−2284.

(11) Chen, Z.; Cai, P.; Chen, J.; Liu, X.; Zhang, L.; Lan, L.; Peng, J.; Ma, Y.; Cao, Y. *Adv. Mater.* **2014**, *26*, 2586−2591.

(12) Chen, J.; Cao, Y. *Acc. Chem. Res.* **2009**, *42*, 1709−1718.

(13) Cheng, Y.-J.; Yang, S.-H.; Hsu, C.-S. *Chem. Rev.* **2009**, *109*, 5868−5923.

(14) Zhou, H.; Yang, L.; You, W. *Macromolecules* **2012**, *45*, 607−632.

(15) Lu, L.; Yu, L. *Adv. Mater.* **2014**, *26*, 4413−4430.

(16) Svensson, M.; Zhang, F.; Veenstra, S. C.; Verhees, W. J. H.; Hummelen, J. C.; Kroon, J. M.; Inganäs, O.; Andersson, M. R. *Adv. Mater.* **2003**, *15*, 988−991.

(17) Wang, E.; Wang, L.; Lan, L.; Luo, C.; Zhuang, W.; Peng, J.; Cao, Y. *Appl. Phys. Lett.* **2008**, *92*, 033307.

(18) Zhang, Y.; Zou, J.; Yip, H.-L.; Chen, K.-S.; Davies, J. A.; Sun, Y.; Jen, A. K. Y. *Macromolecules* **2011**, *44*, 4752−4758.

(19) Wang, E.; Hou, L.; Wang, Z.; Hellström, S.; Zhang, F.; Inganäs, O.; Andersson, M. R. *Adv. Mater.* **2010**, *22*, 5240−5244.

(20) Zhan, X.; Liu, Y.; Wu, X.; Wang, S.; Zhu, D. *Macromolecules* **2002**, *35*, 2529−2537.

(21) Wienk, M. M.; Turbiez, M.; Gilot, J.; Janssen, R. A. J. *Adv. Mater.* **2008**, *20*, 2556−2560.

(22) Bijleveld, J. C.; Gevaerts, V. S.; Di Nuzzo, D.; Turbiez, M.; Mathijssen, S. G. J.; de Leeuw, D. M.; Wienk, M. M.; Janssen, R. A. J. *Adv. Mater.* **2010**, *22*, E242−E246.

(23) Zou, Y.; Najari, A.; Berrouard, P.; Beaupré, S.; Réda Aïch, B.; Tao, Y.; Leclerc, M. *J. Am. Chem. Soc.* **2010**, *132*, 5330−5331.

(24) Piliego, C.; Holcombe, T. W.; Douglas, J. D.; Woo, C. H.; Beaujuge, P. M.; Fréchet, J. M. J. *J. Am. Chem. Soc.* **2010**, *132*, 7595−7597.

(25) Zhang, Y.; Hau, S. K.; Yip, H.-L.; Sun, Y.; Acton, O.; Jen, A. K. Y. *Chem. Mater.* **2010**, *22*, 2696−2698.

(26) Stalder, R.; Mei, J.; Reynolds, J. R. *Macromolecules* **2010**, *43*, 8348−8352.

(27) Lei, T.; Wang, J.-Y.; Pei, J. *Acc. Chem. Res.* **2014**, *47*, 1117−1126.

(28) Robb, M. J.; Ku, S.-Y.; Brunetti, F. G.; Hawker, C. J. *J. Polym. Sci., Part A: Polym. Chem.* **2013**, *51*, 1263−1271.

(29) Chen, M. S.; Niskala, J. R.; Unruh, D. A.; Chu, C. K.; Lee, O. P.; Fréchet, J. M. J. *Chem. Mater.* **2013**, *25*, 4088−4096.

(30) Wang, E.; Mammo, W.; Andersson, M. R. *Adv. Mater.* **2014**, *26*, 1801−1826.

(31) Wang, E.; Ma, Z.; Zhang, Z.; Henriksson, P.; Inganas, O.; Zhang, F.; Andersson, M. R. *Chem. Commun.* **2011**, *47*, 4908−4910.

(32) Wang, E.; Ma, Z.; Zhang, Z.; Vandewal, K.; Henriksson, P.; Inganäs, O.; Zhang, F.; Andersson, M. R. *J. Am. Chem. Soc.* **2011**, *133*, 14244−14247.

(33) Xu, X.; Cai, P.; Lu, Y.; Choon, N. S.; Chen, J.; Hu, X.; Ong, B. S. *J. Polym. Sci., Part A: Polym. Chem.* **2013**, *51*, 424−434.

(34) Ma, Z.; Wang, E.; Vandewal, K.; Andersson, M. R.; Zhang, F. *Appl. Phys. Lett.* **2011**, *99*, 143302.

(35) Hou, L.; Wang, E.; Bergqvist, J.; Andersson, B. V.; Wang, Z.; Müller, C.; Campoy-Quiles, M.; Andersson, M. R.; Zhang, F.; Inganäs, O. *Adv. Funct. Mater.* **2011**, *21*, 3169−3175.

(36) Wang, E.; Bergqvist, J.; Vandewal, K.; Ma, Z.; Hou, L.; Lundin, A.; Himmelberger, S.; Salleo, A.; Müller, C.; Inganäs, O.; Zhang, F.; Andersson, M. R. *Adv. Energy Mater.* **2013**, *3*, 806−814.

(37) Ma, Z.; Tang, Z.; Wang, E.; Andersson, M. R.; Inganäs, O.; Zhang, F. *J. Phys. Chem. C* **2012**, *116*, 24462−24468.

(38) Ma, Z.; Wang, E.; Jarvid, M. E.; Henriksson, P.; Inganas, O.; Zhang, F.; Andersson, M. R. *J. Mater. Chem.* **2012**, *22*, 2306−2314.

(39) Ma, Z.; Dang, D.; Tang, Z.; Gedefaw, D.; Bergqvist, J.; Zhu, W.; Mammo, W.; Andersson, M. R.; Inganäs, O.; Zhang, F.; Wang, E. *Adv. Energy Mater.* **2014**, *4*, 1301455.

(40) Ma, Z.; Sun, W.; Himmelberger, S.; Vandewal, K.; Tang, Z.; Bergqvist, J.; Salleo, A.; Andreasen, J. W.; Inganas, O.; Andersson, M. R.; Muller, C.; Zhang, F.; Wang, E. *Energy Environ. Sci.* **2014**, *7*, 361−369.

(41) Yuen, J. D.; Fan, J.; Seifter, J.; Lim, B.; Hufschmid, R.; Heeger, A. J.; Wudl, F. *J. Am. Chem. Soc.* **2011**, *133*, 20799−20807.

(42) Subramaniyan, S.; Kim, F. S.; Ren, G.; Li, H.; Jenekhe, S. A. *Macromolecules* **2012**, *45*, 9029−9037.

(43) Shi, Q.; Fan, H.; Liu, Y.; Hu, W.; Li, Y.; Zhan, X. *J. Phys. Chem. C* **2010**, *114*, 16843−16848.

(44) Sun, W.; Ma, Z.; Dang, D.; Zhu, W.; Andersson, M. R.; Zhang, F.; Wang, E. *J. Mater. Chem. A* **2013**, *1*, 11141−11144.

(45) Dang, D.; Chen, W.; Yang, R.; Zhu, W.; Mammo, W.; Wang, E. *Chem. Commun.* **2013**, *49*, 9335−9337.

(46) Liang, Y.; Feng, D.; Wu, Y.; Tsai, S.-T.; Li, G.; Ray, C.; Yu, L. *J. Am. Chem. Soc.* **2009**, *131*, 7792−7799.

(47) Zhou, H.; Yang, L.; Stuart, A. C.; Price, S. C.; Liu, S.; You, W. *Angew. Chem., Int. Ed.* **2011**, *50*, 2995−2998.

(48) Price, S. C.; Stuart, A. C.; Yang, L.; Zhou, H.; You, W. *J. Am. Chem. Soc.* **2011**, *133*, 4625−4631.

DOI: 10.1021/ma502186g
Macromolecules 2015, 48, 1009−1016

(49) Albrecht, S.; Janietz, S.; Schindler, W.; Frisch, J.; Kurpiers, J.; Kniepert, J.; Inal, S.; Pingel, P.; Fostiropoulos, K.; Koch, N.; Neher, D. *J. Am. Chem. Soc.* **2012**, *134*, 14932−14944.
(50) Min, J.; Zhang, Z.-G.; Zhang, S.; Li, Y. *Chem. Mater.* **2012**, *24*, 3247−3254.
(51) Peng, Q.; Liu, X.; Su, D.; Fu, G.; Xu, J.; Dai, L. *Adv. Mater.* **2011**, *23*, 4554−4558.
(52) Brédas, J.-L.; Norton, J. E.; Cornil, J.; Coropceanu, V. *Acc. Chem. Res.* **2009**, *42*, 1691−1699.
(53) Beaujuge, P. M.; Amb, C. M.; Reynolds, J. R. *Acc. Chem. Res.* **2010**, *43*, 1396−1407.
(54) Adamo, C.; Barone, V. *J. Chem. Phys.* **1999**, *110*, 6158−6170.
(55) Salvatori, P.; Mosconi, E.; Wang, E.; Andersson, M.; Muccini, M.; De Angelis, F. *J. Phys. Chem. C* **2013**, *117*, 17940−17954.
(56) Hedström, S.; Persson, P. *J. Phys. Chem. C* **2012**, *116*, 26700−26706.
(57) Seo, J. H.; Gutacker, A.; Sun, Y.; Wu, H.; Huang, F.; Cao, Y.; Scherf, U.; Heeger, A. J.; Bazan, G. C. *J. Am. Chem. Soc.* **2011**, *133*, 8416−8419.
(58) Zhou, H.; Zhang, Y.; Seifter, J.; Collins, S. D.; Luo, C.; Bazan, G. C.; Nguyen, T.-Q.; Heeger, A. J. *Adv. Mater.* **2013**, *25*, 1646−1652.
(59) Xiao, Z.; Yuan, Y.; Yang, B.; VanDerslice, J.; Chen, J.; Dyck, O.; Duscher, G.; Huang, J. *Adv. Mater.* **2014**, *26*, 3068−3075.
(60) Pal, S. K.; Kesti, T.; Maiti, M.; Zhang, F.; Inganäs, O.; Hellström, S.; Andersson, M. R.; Oswald, F.; Langa, F.; Österman, T.; Pascher, T.; Yartsev, A.; Sundström, V. *J. Am. Chem. Soc.* **2010**, *132*, 12440−12451.
(61) Haugeneder, A.; Neges, M.; Kallinger, C.; Spirkl, W.; Lemmer, U.; Feldmann, J.; Scherf, U.; Harth, E.; Gügel, A.; Müllen, K. *Phys. Rev. B* **1999**, *59*, 15346−15351.

DOI: 10.1021/ma502186g
Macromolecules 2015, 48, 1009−1016